JÜLICH
FORSCHUNGSZENTRUM

Institut für Kernphysik
COSY

SPIN@COSY: Looking Inside a Spin Resonance

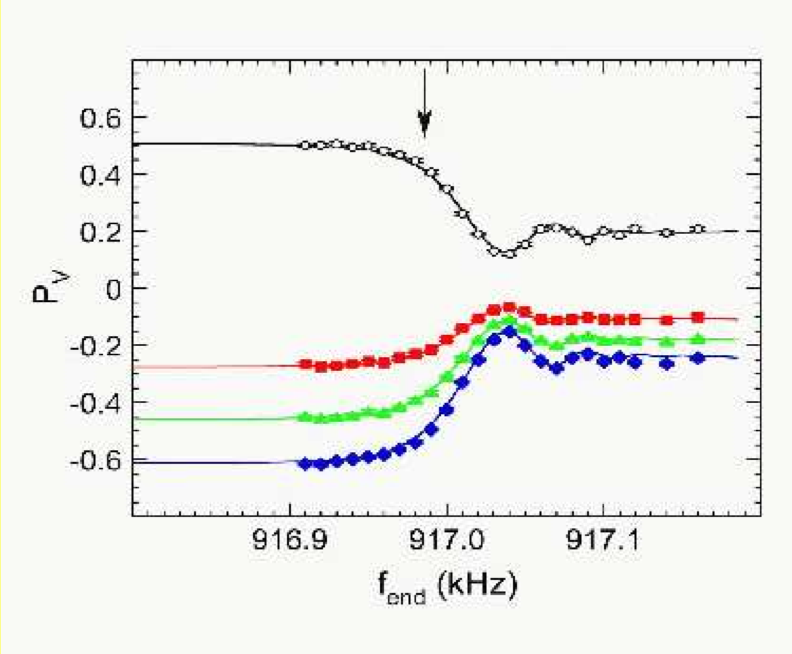

ANNUAL REPORT 2007

Jül-4262

Annual Report 2007

Institut für Kernphysik / COSY

Cover picture:

The SPIN@COSY polarized beam team found striking new results while studying the spin-manipulation of polarized deuterons at COSY. The newly developed Chao formalism (the first generalization of the Froissart-Stora formula) was used to calculate in detail what might happen in a new type of experiment, where a 1 MHz RF-magnet's frequency is swept by a fixed range of 400 Hz, while its end-frequency f_{end} is stepped through many different values near and inside a spin resonance. The calculations predicted that, if the resonance strength of the magnet was not strong enough to fully flip the spin, then there would be large oscillations in the final polarization. The figure shows four measured vertical vector polarization states (P_{V}) (black: $+1$, red: $-1/3$, green: $-2/3$, blue: -1) of 1.85 GeV/c stored deuterons plotted *vs.* the end frequency of the 400 Hz sweep. The calculations (solid lines) predict the oscillations very well, indicating that the experimental results confirm the validity of the Chao formalism. Precise values were obtained for the resonance frequency $f_{\mathrm{R}} = 916985.3 \pm 0.5$ Hz, the frequency spread $\delta p_{\Delta p} = 23 \pm 1$ Hz (FWHM), and the strength $\varepsilon = (1.060 \pm 0.005) \cdot 10^{-5}$. The arrow shows the center of the resonance.

Preface

On November 7/8, 2007 the kick-off event and a symposium on physics at the future FAIR facility took place at GSI-Darmstadt, during which the start of the project was officially announced. This important milestone strongly influences the activities of the IKP. As in previous years, the institute continued its vigorous engagement for the High Energy Storage Ring (HESR) as well as the PANDA and PAX experiments. IKP is in charge of all major HESR components, among them the ion optical design of the ring, the rf systems, the beam-diagnostics and magnets, as well as stochastic cooling. IKP has also taken on central responsibilities for the PANDA central charged particle tracking and vertexing, the PANDA frozen pellet target, as well as establishing a method to achieve a high degree of antiproton polarization for PAX. After the launching of the FAIR project these activities are now continuing to be vigorously pursued.

After the HGF Midterm Review in September, the committee expressed strong support for the theory group and was impressed by the stable operation of COSY and by the developments for the HESR. The ongoing physics program at ANKE was very positively acknowledged as well as progress with WASA, and the new proposal on ”Strangeness Physics at COSY-TOF”.

The inaugural meeting of the Virtual Institute “Spin and strong QCD” (Spokesperson: Ulf-G. Meißner) took place on November 30, 2007 at the IKP. The experimental as well as theoretical research of this Virtual Institute — with participating institutions IKP, GSI, Universities Bern, Bonn, Cracow, Torino, INFN Ferrara — is focused on three of the most important aspects of non-perturbative strong interactions with a direct connection to the hadron physics programs at COSY, PANDA and PAX at FAIR: Hadron spectroscopy, symmetry tests and polarization.

The experimental work at IKP is focused around the COSY accelerator complex:

- The WASA detector at an internal target station of COSY has been completely installed. A first experiment on the $pp \rightarrow pp\eta$ reaction has successfully been carried out.
- A first double polarization experiment took place at ANKE (polarized deuteron beam on polarized proton target with a storage cell). The ANKE collaboration also made a first attempt to precisely determine the η-mass by accurately measuring the beam energy of polarized deuterons with a spin-flip technique.
- The Spin@COSY polarized beam team found new striking results while studying the spin manipulation of polarized deuterons (see cover page). A new model, called Chao matrix formalism, that describes the beam polarization behavior inside a spin resonance was verified in detail and effectually applied for the first time at COSY. The result will also help to understand the behavior of polarized beams at other machines and someday also of antiproton beams at FAIR.
- The PAX collaboration has continued its test measurements at COSY to further investigate the possibilities to effectively produce polarized antiprotons for a later upgrade of the HESR.
- The number of COSY users has increased to more than 400. In the coming years new groups will carry out measurements at COSY, *e.g.* the EDM collaboration with preparatory studies aiming at the measurement of the deuteron’s electric dipole moment.

- During the two months summer shut down necessary repairs at cyclotron were accomplished, a barrier bucket cavity and a RF solenoid were installed. The PISA set-up was removed from the ring tunnel and will be send to IMP-Lanzhou, China.

Outstanding results from the theory group are:

- A novel method for the extraction of scattering phases and mixing angles from lattice simulations has been applied to nucleon-nucleon scattering.
- A new Regge model for pion photoproduction at energies above 3 GeV has been developed in order to extract high-lying Baryon resonances.
- It has been demonstrated that the decay properties of the $X(3872) \to \bar{D}D\pi$ and $\to J/\psi\pi\pi$ only allow for an interpretation as a virtual state.
- We have shown that it is possible to extract the neutron-neutron scattering length with an accuracy of $\delta a_{nn} = \pm 0.1$ fm from the differential cross section of the $\gamma d \to \pi^+ nn$ reaction.

Besides the regular physics program at the COSY accelerator, components and prototypes designed and built for HESR are being examined at COSY. New and important steps can be recorded:

- Substantial progress has been made in developing new pickup structures for stochastic cooling at the HESR. With funding of the EU project "DIRAC secondary beams" a prototype tank has been constructed and successfully tested at COSY.
- A prototype barrier bucket cavity came successfully into operation at COSY. This device is foreseen at the HESR to compensate the indispensable strong mean energy loss due to the beam-target interaction.
- The development of a 2 MeV electron cooler for COSY has continued. The new electron cooling system is proposed to further boost the luminosity even with strong heating effects of high-density internal targets. The 2 MeV electron cooler is best qualified to explore new essential features of the high energy electron cooler for the HESR.
- The HESR ring lattice was completely redesigned with normal conducting magnets and stochastic cooling properties were studied in this new lattice version.

We are looking forward to the constitution of the FAIR GmbH and we hope for investment money in order to prepare and build the accelerator HESR and detector components of PANDA and PAX as planned.

Finally we would like to express our sincere gratitude to the colleagues of the infrastructure of the Research Center in particular JSC, ZAT and ZEL. Our special thanks go to the surrounding universities and national research centers and our CANU community. We acknowledge the continuous support by the Helmholtz society, the board of management of the Research Center, by the COSY-FFE program and, in particular, by Dr. Sebastian M. Schmidt who became the new director of the research area "Key technologies and structure of matter" on 1 November 2007.

Jülich, March 2008 Rudolf Maier

Contents

1 Experimental Hadron Physics

Production of ϕ-mesons in *pA* collisions*

M. Hartmann, Yu. Kiselev[1], V. Koptev[2]

One of the goals of the experiment on ϕ meson production in *pA* collisions is to determine the ϕ properties in nuclear matter at normal density [1]. According to theoretical predictions the ϕ meson modification in mass is small and the main medium effect is a significant increase of its width up to an order of magnitude compared to the free (vacuum) value of 4.4 MeV.

The experiment was carried out at an initial proton energy of 2.83 GeV with the ANKE spectrometer in February/March 2007. Two data sets were obtained in parallel. The first contains K^+K^- correlations with hardware K^+ selection using the delayed veto technique and the absolute measurements of K^+K^- TOF difference. In the second set triple K^+, K^- and p,d,T(^{3}H) or ^{3}He correlations were measured using only the TOF technique. The measurements were performed with four strip targets: C, Cu, Ag and Au. Up to now only the first data set with K^+K^- correlations has been analyzed. K^+K^- invariant mass spectra look similar for all four targets. As an example the spectrum for the Au target is presented in Fig. 1.

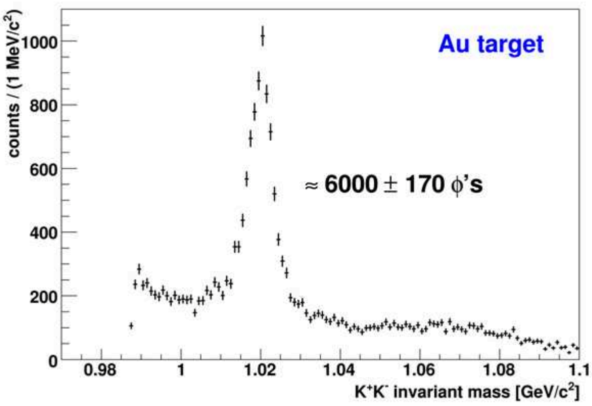

Fig. 1: Invariant mass distribution for K^+K^- pairs from *p*Au collisions.

The numbers of selected K^+K^- pairs in the ϕ peaks for the C, Cu, Ag and Au targets are given in Table 1.

Table 1: Estimated number of detected ϕ-mesons in the data set of two particle K^+K^- correlations.

solid strip targets	C	Cu	Ag	Au
detected ϕ's	6700	5000	5000	6000

The ϕ positions and the widths (taking into account our resolution) coincide within 0.5 MeV with the vacuum values since ϕ mesons are reconstructed from almost undistorted K^+ and K^- mesons from ϕ's decaying outside the nuclear volume. Information about a modification of the ϕ width can be obtained from the *A*-dependence of the additional nuclear ϕ absorption as compared to that from quasi-free ϕ*N* inelastic reactions on the nucleons. To obtain this *A*-dependence the data on ϕ production were normalized to fluxes of π^+ mesons with momenta of 500 ± 25 MeV/c for angles $\leq 4°$ simultaneously measured for each target. The production cross sections of these π^+ mesons are proportional to $A^{2/3}$ within 2%. The preliminary ratios of these normalized ϕ yields from Cu, Ag and Au to the yield from C-target are given in the Table 2; they reasonably coincide with the ones predicted in [2].

Table 2: Preliminary ratios of ϕ yields from Cu, Ag and Au to the yield from C-target.

	C/C	Cu/C	Ag/C	Au/C
ratio	1	0.46	0.39	0.29

Final ratios will be given after the corrections of the detection efficiencies and acceptances are done. First simulations indicate that the ϕ-meson acceptance on the Au target is around 14% smaller compared to C. The input distributions for the simulations where generated using a microscopic transport code for nuclear collisions (JAM) [3]. We also plan to check our π^+ normalization with π^- mesons which have been detected in parallel. Finally also the absolute values of the cross sections for ϕ meson production will be determined.

A first look on the triple coincidence data shows that by detecting one forward going proton in coincidence with the K^+K^-, the π^+ normalized Au/C ϕ production ratio decreases by a factor two relative to the Au/C ratio given in Table 2. This effect can be explained by the additional distortion of the outgoing protons.

References:

[1] M. Hartmann, Yu.Kiselev *et al.*, COSY Proposal **No. 147**;
[2] V.K Magas *et al.*, Phys. Rev. C **71**, 065202 (2005).
[3] Y. Nara, url:"http://quark.phy.bnl.gov/ ynara/jam/".

[1] Institut for Theoretical and Experimental Physics, 117218 Moscow, Russia
[2] High Energy Physiks Department, Petersburg Nuclear Institut, 188350 Gatchina, Russia
* Supported by DFG

Φ meson production in near–threshold proton–nucleus reactions. Target mass dependence*

E.Ya. Paryev[1], M. Hartmann, Yu. Kiselev[2]

Studies of modification of the ϕ meson spectral function at finite baryon density through its production and decay in pion–nucleus [1], proton–nucleus [2–5] and photon–nucleus [6–10] reactions have received considerable interest in recent years. Because, on the one hand, the ϕ meson (in contrast to the ρ and ω mesons) does not overlap with other light resonances in the mass spectrum and, on the other hand, the reactions on ordinary nuclei with elementary probes are less complicated compared to heavy–ion collisions especially in the near–threshold energy regime where a small number of possible channels for meson production contributes, one may hope to get from these studies a more clear precursor signals for partial restoration of chiral symmetry–the fundamental symmetry of QCD in the limit of massless quarks– and thus to test this prominent feature of QCD as well as to extract valuable information on the nucleon strangeness content [4, 7] and on the kaon in-medium properties [1–4]. As is expected [11–14], the mass shift of the ϕ meson in nuclear matter is small, whereas its total in-medium width is appreciably increased compared to the vacuum value ($\Gamma_\phi = 4.45$ MeV). The nontraditional possibility to learn about this width has been considered in [2,3, 8–10]. As a measure for the in-medium broadening of the ϕ meson the A-dependence of its production cross section in nuclei in proton– and photon–induced reactions has been employed in these works. The A-dependence is governed by the absorption of the ϕ meson flux in nuclear matter, which in turn is determined, in particular, by the ϕ in-medium width.

Following the above method and using nuclear spectral function approach [4] for incoherent primary proton–nucleon ($pp \to pp\phi$, $pn \to pn\phi$, $pn \to d\phi$) and secondary pion–nucleon ($\pi^+ n \to \phi p$, $\pi^0 p \to \phi p$, $\pi^0 n \to \phi n$, $\pi^- p \to \phi n$) production processes, we studied the inclusive ϕ meson production in the interaction of 2.83 GeV protons with nuclei. In particular, the A-dependences of the absolute and relative ϕ meson yields were investigated within the different scenarios for its in-medium width as well as for the cross section ratio $\sigma_{pn\to pn\phi}/\sigma_{pp\to pp\phi}$. Our model calculations took into account the acceptance window of the ANKE facility used in a recent experiment [15] performed at COSY. They show (see Fig. 1) that: i) the pion–nucleon production channels contribute distinctly to the ϕ creation in heavy nuclei in the chosen kinematics and, hence, have to be taken into consideration on close examination of the dependences of the ϕ meson yields on the target mass number with the aim to get information on its width in the medium; ii) the experimentally unknown ratio $\sigma_{pn\to pn\phi}/\sigma_{pp\to pp\phi}$ has a weak effect on the A-dependence of the relative ϕ meson production cross section at incident energy of present interest, whereas it is found to be appreciably sensitive to the ϕ in-medium width, which means that this relative observable can indeed be useful to help determine the above width from the direct comparison the results of our calculations with the future data from the ANKE-at-COSY experiment [15].

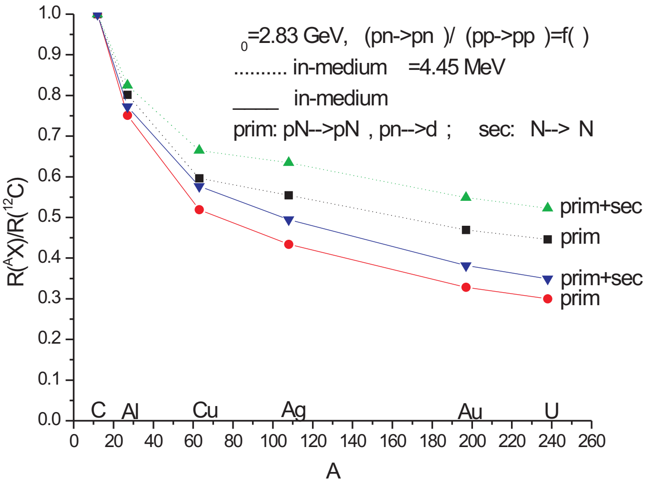

Fig. 1: Ratio $R(^AX)/R(^{12}C)$=$(\sigma_{pA\to\phi X}/A)/(\sigma_{p^{12}C\to\phi X}/12)$, where $\sigma_{pA\to\phi X}$ is the nuclear cross section for ϕ production from proton–nucleus collisions in the ANKE acceptance window: 0.6 GeV/c $\le p_\phi \le$ 1.8 GeV/c and $0^\circ \le \theta_\phi \le 8^\circ$, as a function of the target mass number for initial energy of 2.83 GeV as well as for the cross section ratio $\sigma_{pn\to pn\phi}/\sigma_{pp\to pp\phi}$ in the excess-energy-dependent form $f(\varepsilon)$ taken from [16] calculated within the different scenarios for the ϕ meson production mechanism and for its in-medium width. The dotted lines with symbols "prim" and "prim+sec" by them are calculations, respectively, for the one-step and one- plus two-step ϕ creation mechanisms for the free ϕ width. The solid lines denote the same as the dotted lines, but it is supposed that the ϕ in-medium width is calculated following strictly [4].

References:

[1] Ye. S. Golubeva, L. A. Kondratyuk, W. Cassing, Nucl. Phys. A **625**, 832 (1997).

[2] H. W. Barz and M. Zetenyi, Phys. Rev. C **69**, 024605 (2004).

[3] V. K. Magas, L. Roca, E. Oset, Phys. Rev. C **71**, 065202 (2005).

[4] E. Ya. Paryev, Eur. Phys. J. A **23**, 453 (2005).

[5] R. Muto *et al.*, nucl-ex/0511019.

[6] E. Oset *et al.*, Phys. Lett. B **508**, 237 (2001).

[7] P. Muehlich, T. Falter, C. Greiner, *et al.*, Phys. Rev. C **67**, 024605 (2003).

[8] D. Cabrera *et al.*, Nucl. Phys. A **733**, 130 (2004).

[9] P. Muehlich and U. Mosel, nucl-th/0510078.

[10] T. Ishikawa *et al.*, Phys. Lett. B **608**, 215 (2005).

[11] T. Hatsuda and S. H. Lee, Phys. Rev. C **46**, R34 (1992).

[12] E. Oset and A. Ramos, Nucl. Phys. A **679**, 616 (2001).

[13] D. Cabrera and M. J. Vicente Vacas, Phys. Rev. C **67**, 045203 (2003).

[14] F. Klingl, T. Waas, W. Weise, Phys. Lett. B **431**, 254 (1998).

[15] M. Hartmann, Yu. Kiselev, *et al.*, ANKE–COSY proposal #147 (2005).

[16] L. P. Kaptari and B. Kämpfer, Eur. Phys. J. A **23**, 291 (2005).

[1] Moscow State University, 119992 Moscow, Russia
[2] Institut for Theoretical and Experimental Physics, 117218 Moscow, Russia
* Supported by DFG

Lineshape of the $\Lambda(1405)$ Hyperon Measured Through its $\Sigma^0\pi^0$ Decay

I.Zychor[a] for the ANKE Collaboration

Although a four–star resonance [1], and known already for many years, the dynamics of the $\Lambda(1405)$ are still not fully understood. Within the quark model it can be explained as a P–wave q^3 baryon. It is also widely discussed as a candidate for a $\bar{K}N$ molecular state, or for one with a more intrinsic $q^4\bar{q}$ pentaquark structure. If the $\Lambda(1405)$ is a dynamically generated resonance produced *via* $\bar{K}N$ rescattering within a coupled–channel formalism, it may consist of two overlapping $I = 0$ states. Its decay spectrum would then depend upon the production reaction. Due to the opening of the $\bar{K}N$ channels, the $\Lambda(1405)$ lineshape is not represented satisfactorily by a Breit–Wigner resonance. Nevertheless, if the $\Lambda(1405)$ were a single quantum state, as in the quark model or molecular pictures, its lineshape should be independent of the production method.

Recent theoretical investigations based on chiral dynamics predict two poles for the $\Lambda(1405)$, one with a mass 1390 MeV/c^2 and a width of about 130 MeV/c^2 coupling strongly to $\pi\Sigma$ states and the other one with a mass around 1425 MeV/c^2 and a width of about 30 MeV/c^2 coupling mostly to $\bar{K}N$ states [2].

We report on measurements done with the ANKE spectrometer at COSY-Jülich. The reaction $pp \to pK^+Y^{0*}$ has been studied at a beam momentum of 3.65 GeV/c to investigate the production of excited hyperon resonances Y^{0*} decaying via $\Sigma^0\pi^0$. In case of $\Lambda(1405)$ production in pp collisions there are two protons, one positively charged kaon and negatively charged pion in the final state: $pp \to pK^+\Lambda(1405) \to pK^+\Sigma^0\pi^0 \to pK^+\Lambda\gamma\pi^0 \to pK^+p\pi^-\pi^0\gamma$. At ANKE those particles are measured with *different* parts of the detection system.

In Fig. 1 the simplified decay scheme of excited neutral resonances with masses below 1432 MeV/c^2 demonstrates the differences between $\Sigma^0(1385)$ and $\Lambda(1405)$ utilised in the present analysis.

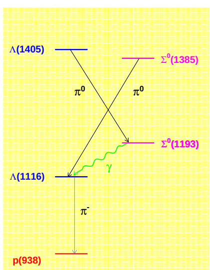

Fig. 1: Simplified decay scheme for the $\Lambda(1405)$ and $\Sigma^0(1385)$ hyperon resonances

The $(\Sigma\pi)^0$ invariant–mass distributions have been previously studied in two hydrogen bubble chamber experiments. Thomas *et al.* [3] found $\sim$400 $\Sigma^+\pi^-$ or $\Sigma^-\pi^+$ events corresponding to the $\pi^-p \to K^0\Lambda(1405) \to K^0(\Sigma\pi)^0$ reaction at a beam momentum of 1.69 GeV/c. Hemingway [4] used a 4.2 GeV/c kaon beam to investigate $K^-p \to \Sigma^+(1660)\pi^- \to \Lambda(1405)\pi^+\pi^- \to (\Sigma^+\pi^-)\pi^+\pi^-$ and measured 1106 events.

In Fig. 2 our experimental points correspond to the background–subtracted lineshape of the $\Lambda(1405)$ [5]. They are compared to the results of Thomas and Hemingway. Despite the very different production mechanisms, the three distributions have consistent shapes.

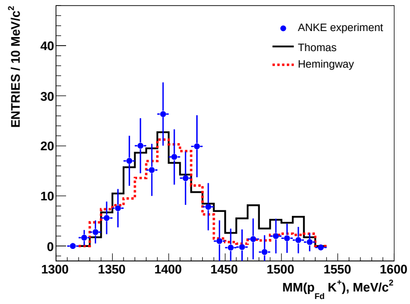

Fig. 2: The background–subtracted lineshape of the $\Lambda(1405)$ decaying into $\Sigma^0\pi^0$ (points) compared to $\pi^-p \to K^0(\Sigma\pi)^0$ (black–solid line) and $K^-p \to \pi^+\pi^-\Sigma^+\pi^-$ (red–dotted line) data.

This might suggest that, if there are two states present in this region, then the reaction mechanisms in the three cases are preferentially populating the same one. It should, however, be noted that by identifying a particular reaction mechanism, the proponents of the two–state solution can describe the shape of the distribution that we have found [6].

In Table 1 the information that is relevant for the evaluation of the total cross section is given.

Table 1: Total cross section for the production of the $\Sigma^0(1385)$ and $\Lambda(1405)$ resonances in the 3.65 GeV/c $pp \to pK^+Y^0$ reaction

	$\Sigma^0(1385)$	$\Lambda(1405)$
number of events	170 ± 26	156 ± 23
acceptance	2.0×10^{-6}	4.4×10^{-6}
combined BR (%)	56	21
luminosity (pb^{-1})	69 ± 10	69 ± 10
detection efficiency (%)	55 ± 11	55 ± 11
cross section (μb)	4.0 $\pm 1.0_{stat}$ $\pm 1.6_{syst}$	4.5 $\pm 0.9_{stat}$ $\pm 1.8_{syst}$

References:

[1] W.-M. Yao *et al.*, J. Phys. G **33**, 1 (2006), but see also the minireview in D.E. Groom *et al.*, Eur. Phys. J. C **15**, 1 (2000).
[2] V.K. Magas, E. Oset and A. Ramos, Phys. Rev. Lett. **95**, 052301 (2005).
[3] D.W. Thomas, *et al.*, Nucl. Phys. B **56**, 15 (1973).
[4] R.J. Hemingway, Nucl. Phys. B **253**, 742 (1984).
[5] I. Zychor *et al.*, Phys. Lett. B **660** (2008) 167.
[6] L.S. Geng and E. Oset, arXiv:0707.3343 [hep-ph].

[a] The Andrzej Sołtan Institute for Nuclear Studies,Świerk,Poland

Investigation of the ^{3}He η Final State in dp-Reactions at ANKE*

T. Rausmann[1], A. Khoukaz[1], T. Mersmann[1], M. Mielke[1], M. Papenbrock[1] and A. Täschner[1] for the ANKE-Collaboration

The existence of η-mesic nuclei is still an open issue of research. To investigate the possibility of the formation of such bound systems, production measurements with one η meson and one light nucleus in the final state are of great interest. By studying the final state interaction at low excess energies, information about the poles of the η-nucleus system can be gained. The latter one is closely related to the properties of such a possible bound state and has to be determined with high precision. In this context the reaction d+p$\rightarrow$ ^{3}He+η is of high interest. Since already close to threshold there are significant contributions from higher partial waves, a carefull investigation of differential cross sections from threshold up to higher excess energies is desirable. However, available data sets at higher excess energies expose clear discrepancies [1]. Due to this a complete theoretical description of the excitation function from threshold up to higher excess energies is currently not possible. A single data sample with minimized systematic uncertainties over the whole energy range could help to solve this problem.

Therefore, the reaction d+p$\rightarrow$ ^{3}He+η has been investigated using the ANKE spectrometer from threshold up to an excess energy of Q = 60 MeV [2]. To allow for detailed investigation on the final state interaction of the ^{3}He-η system, the very near threshold region has been studies using a continuously ramped accelerator beam at excess energies ranging from below threshold (Q = -5.1 MeV) up to Q = +11.3 MeV [3]. Furthermore, in order to investigate the energy dependence of the total and differential cross sections up to higher excess energies with minimal systematic uncertainties, additional measurements have been performed at fixed excess energies of Q = 20, 40 and 60 MeV.

To select events of the reaction channel of interest the ^{3}He nuclei are detected using the ANKE forward detector and the production of η-mesons is identified via the missing mass technique. For the reconstruction of the momenta of the ^{3}He nuclei via the magnetic spectrometer the information of the three drift- and multi-wire proportional chambers are used.

The particle identification is achieved by the energy loss versus momentum method (ΔE/p) for the three segmented scintillation walls. A simultaneous cut on the expected region for ^{3}He nuclei in the (ΔE/p) plot in the three scintillation walls allows for a clear identification of the ^{3}He band.

The extraction of the η signal from the missing mass spectrum is done by fiting simulations of the background reactions to the real data and to substract them from the data (Fig.1). Possible background reactions in this energy range are the two-pion production (red line), the three-pion production (green line), the four-pion production and misidentified protons from the deuteron breakup reaction (purple line). This method has also been used for the different angular bins (Fig. 2).

After the fine tuning of the background description total as well as differential cross sections will be determined for the excess energies of Q = 20, 40 and 60 MeV. Together with the results from the already analyzed continous ramp data [3] this will form a complete differential and total cross section sample from treshold up to 60 MeV excess energy for the d+p$\rightarrow$ ^{3}He+η reaction.

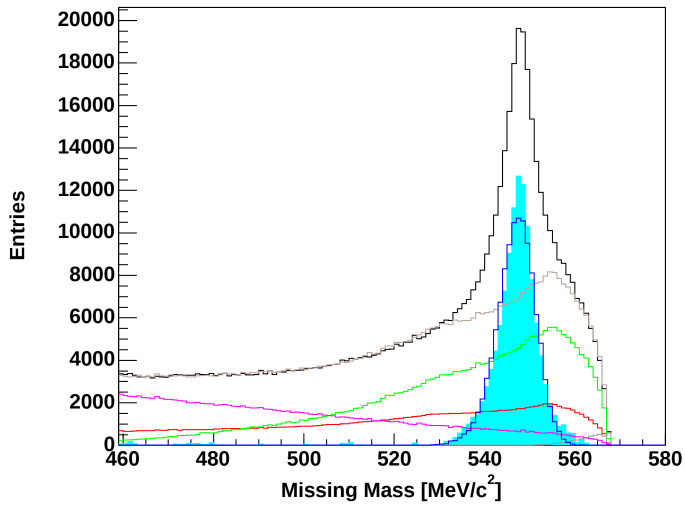

Fig. 1: Preliminary missing mass plot (black line) at an excess energy of Q = 20 MeV with the different background reactions. The background reactions are added (grey line) and then subtracted from the data to get the η signal (bright blue). This is compared with the simulated η signal (dark blue line).

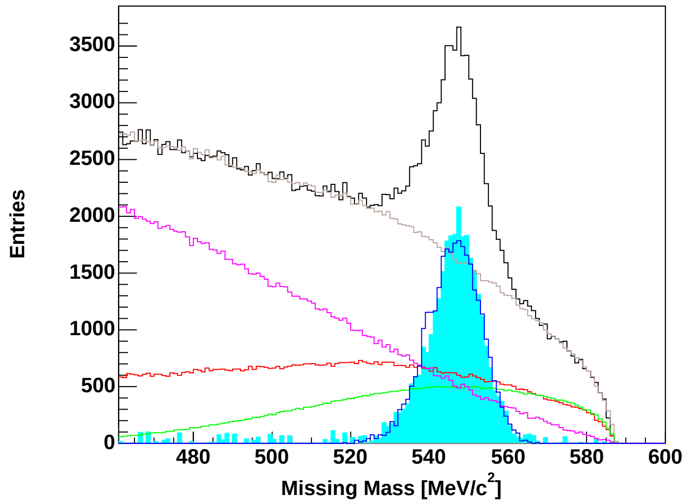

Fig. 2: Preliminary missing mass plot at an excess energy of Q = 40 MeV for 0.8 $\leq$ cos(θ)$\leq$ 1.0.

References:

[1] A. Sibirtsev et al., Eur.Phys.J. A22 (2004).
[2] A. Khoukaz, T. Mersmann, *Investigation of the ^{3}He η final state in the reaction d+p$\rightarrow$ ^{3}He+η at ANKE*, COSY-Proposal, 2004
[3] T. Mersmann et al., PRL 98,242301(2007).

[1] Institut für Kernphysik Westfälische Wilhelms-Universität, 48149 Münster, Germany
* Supported by FZ-Jülich FFE

Spin observables of the reaction $pd \to {}^3He\eta$ and quasi-bound ${}^3He-\eta$ pole

Yu. N. Uzikov[a]

Strong enhancement of the cross section of the $pd \to {}^3He\eta$ reaction near the threshold can be explained assuming presence of a quasi-bound ${}^3He-\eta$ state [1]. According to recent unpolarized measurement at COSY [2], the pole corresponding to the ${}^3He-\eta$ quasi-bound (or anti-bound) state, if it really exists, is located on the excitation energy plane at the point $Q_0 = [(-0.30 \pm 0.15_{stat} \pm 0.04_{syst}) \pm \imath(0.21 \pm 0.29_{stat} \pm 0.06_{syst}]$ MeV. As was noted in [4], the presence of the pole in the s-wave amplitude of this reaction must lead to fast variation not only in its magnitude, but also in the phase. The latter provides a new criterion for identification of the pole. The specific phase behaviour comes from the following analytical form of the s-wave amplitude near the pole:

$$f(p_\eta) = \frac{\xi}{p_\eta - ip_0}, \qquad (1)$$

where p_η is the (real) c.m.s. momentum of the η-meson, p_0 is the (complex) pole point directly related to the energy Q_0, and ξ is a smooth function of p_η. On the other hand, p-waves are expected to exhibit non-pole behaviour. Using the available unpolarized data [2, 3], the authors of Ref.[4] found some non-direct indications of this specific phase behaviour of the s-wave amplitudes near the threshold. It is important to validate this interpretation by direct measurement of energy dependence of the s-wave amplitudes, which requires polarization experiments. Some of spin observables were discussed in Ref.[4] under certain approximations and with restriction mainly to collinear kinematics.

We discuss here [5] polarization measurements in general case. The full transition operator of the reaction $pd \to {}^3He\eta$ can be written as

$$\hat{F} = A\boldsymbol{\varepsilon}\cdot\hat{\mathbf{p}}_p + iB[\boldsymbol{\varepsilon}\times\boldsymbol{\sigma}]\cdot\hat{\mathbf{p}}_p + C\boldsymbol{\varepsilon}\cdot\mathbf{p}_\eta + iD[\boldsymbol{\varepsilon}\times\boldsymbol{\sigma}]\cdot\mathbf{p}_\eta + iE(\boldsymbol{\varepsilon}\cdot\mathbf{n})(\boldsymbol{\sigma}\cdot\hat{\mathbf{p}}_p) + iF(\boldsymbol{\varepsilon}\cdot\mathbf{n})(\boldsymbol{\sigma}\cdot\mathbf{p}_\eta), \qquad (2)$$

where $\boldsymbol{\sigma}$ is the Pauli matrix, $\boldsymbol{\varepsilon}$ is the polarization vector of the deuteron, $\hat{\mathbf{p}}_p$ is the unit vector along the proton beam direction, $\mathbf{p}_p$ and $\mathbf{p}_\eta$ are the cms momenta of the proton and the $\eta-$meson, respectively, and $\mathbf{n} = [\mathbf{p}_\eta \times \hat{\mathbf{p}}_p]$. We choose the coordinate system with the axes OZ $\uparrow\uparrow$ $\mathbf{p}_p$, OY $\uparrow\uparrow$ $\mathbf{n}$, OX $\uparrow\uparrow$ $[\mathbf{n}\times\hat{\mathbf{p}}_p]$. As compared to Ref.[4], we consider two additional terms, E and F, both of the non-s-wave type. The s-wave amplitudes are contained in the terms A and B only. The terms C, D and E are p-wave ones, and the last term F in Eq. (2) corresponds to the d-wave (and higher partial waves) in the final state.

We derived a full set of spin observables for this reaction in model independent way. It was shown that in collinear kinematics the complete polarization experiment suggests only four measurements. However, one cannot separate s- and p-wave amplitudes in collinear regime. We considered two different cases beyond collinear kinematics. (i) In the case of four spin amplitudes (A, B, C, and D), four observables $d\sigma_0$, A_{yy}, A_{xx} and $K_x^{x'}(p)$ completely determine moduli of the amplitudes. Here $K_x^{x'}(p)$ is the coefficient of polarization transfer from the proton to the ${}^3He$. In order to determine relative phases of the amplitudes, one needs ten observables (including spin transfer coefficients) and three of them can be measured roughly. On the contrary, knowledge of only analyzing powers and spin-correlation coefficients in the initial state does not allow one to determine moduli of the amplitudes independently of their phases and suggests performing 14 accurate measurements to get all four amplitudes. (ii) In the case of five independent amplitudes (A, B, C, D, E), measurement of spin transfer coefficients also simplifies considerably the complete polarization experiment. In this case five observables $d\sigma_0$, A_{yy}, A_{xx}, $K_x^{x'}(p)$ and $K_z^{z'}(p)$ determine five moduli of the amplitudes.

Furthermore, for the general case of six spin amplitudes the complete polarization experiment is found to be too cumbersome and practically unrealizable. In view of this complexity, we suggest to measure those spin observables which allow one to single out the pole dependence given by Eq. (1) for the s-wave amplitudes. We found two sets of such observables: $C_{z,x}$, $K_x^{z'}(d)$, $C_{z,yz}$, $K_{yz}^{z'}$ and $C_{x,z}$, $K_z^{x'}(d)$, $C_{x,xy}$, $K_{xy}^{x'}$. Here $K_i^{j'}(d)$ is the polarization transfer from the proton to the final deuteron. We show that measurement of these observables provides knowledge of energy dependence of the s-wave amplitudes near the threshold and could allow one to determine the signs of the real and imaginary parts of the pole point p_0 in Eq. (1) in the complex momentum plane. In its turn, this will allow one to determine whether the ${}^3He-\eta$ state is quasi-bound or anti-bound.

[a] Joint Institute for Nuclear Research, Dubna, Russia

References:

[1] C. Wilkin, Phys. Rev. C **47** (1993) R938.
[2] T. Mersmann et al. Phys. Rev. Lett. **9**8 (2007) 242301.
[3] J. Smyrski et al. Phys. Lett. **6**49 (2007) 258.
[4] C. Wilkin et al., Phys. Lett. **B 654** (2007) 92.
[5] Yu.N. Uzikov, Nucl. Phys. A **801** (2008) 114.

Study of the ABC effect in the reaction d+p→^{3}He+π^++π^- close to the η-production threshold at ANKE*

M. Mielke[1], A. Khoukaz[1], P. Goslawski[1] T. Mersmann[1], M. Papenbrock[1],
T. Rausmann[1] and A. Täschner[1] for the ANKE-Collaboration

Double pionic fusion of protons and deuterons is known to be correlated with a large enhancement at low values of the two pion invariant mass distribution. The origin of this phenomenon, called ABC effect, is not yet completly understood and hence a subject of current research [1]. A dp scattering experiment, conducted in 2005 at ANKE to investigate the ^{3}Heη final state interaction [2], offered excellent conditions to additionally study the ABC effect in the reaction d+p→^{3}He+π^++π^-.

The data presented here were obtained at a fixed beam momentum of 3.224 GeV/c. The coincident detection of ^{3}He nuclei in the forward detector and π^- mesons in the negative detector of the ANKE experimental setup allows for a complete reconstruction of events resulting from the reaction channel of interest using the missing mass technique. Identification of ^{3}He nuclei was performed as described in [3]. Particles detected by the negative system in coincidence with a ^{3}He nucleus in the forward system can, at the used beam energy, only be pions or leptonic background. The selection of two pion events is done via a missing mass analysis (for details see [4]). Due to limitations in the geometrical ANKE acceptance, the results shown in this report contain events with a ^{3}He-scattering angle that fullfils the condition $\cos\left(\vartheta^{CMS}\right) < -0.7$.

Figure 1 displays the resulting preliminary invariant mass distribution $M_{\pi^+\pi^-}$ after acceptance correction. The uncertanties correspond purly to statistical errors. For comparison phase space calculations are given by the shaded area. As expected the ABC effect manifests itself in a pronounced enhancement at low values of $M_{\pi^+\pi^-}$. According to [1] a possible explanation of the ABC effect is an excitation of two Δ resonances which undergo a strong attractive final state interaction and decay each into a nucleon and a pion. As a consequence one should expect Δ resonance peaks in both $M_{^3He\pi}$ spectra. As it can be seen in figure 2 the ANKE data show such a behaviour. However, it is obvious that the distributions differ from each other. This hints towards at least partly unequal excitation of the two Δ states, which would be an indication for different production mechanisms. To examine this aspect in more detail, both preliminary $M_{^3He\pi}$ spectra were subtracted from each other bin by bin. The result, visible in figure 3, reveals a significant shift to higher invariant masses for the combination ^{3}Heπ^+. This behaviour might be caused by N* excitations, decaying through Δ into a nucleon and two pions. Due to different isospin coefficients for Δ^{++} and Δ^0 excitations, a larger number of Δ baryons should in this case be found in $M_{^3He\pi^+}$ compared to $M_{^3He\pi^-}$. Hence the tail of the Δ to higher masses leads to the observed enhancement of $M_{^3He\pi^+}$ above the maximum of the Δ resonance peak. The further investigation of this effect is currently in progress at ANKE and is expected to lead to an important step towards an understanding of the ABC anomaly.

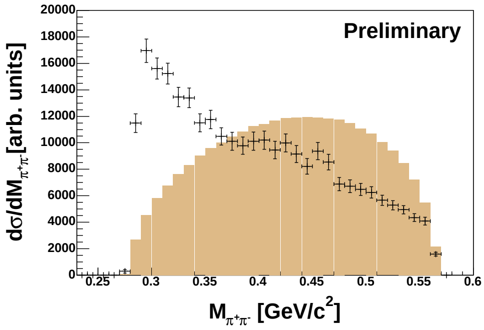

Fig. 1: Invariant mass spectrum $M_{\pi^+\pi^-}$ of the two pion system compared to phase space calculations, represented by the shaded area. Both distributions are corrected for the geometrical acceptance of ANKE.

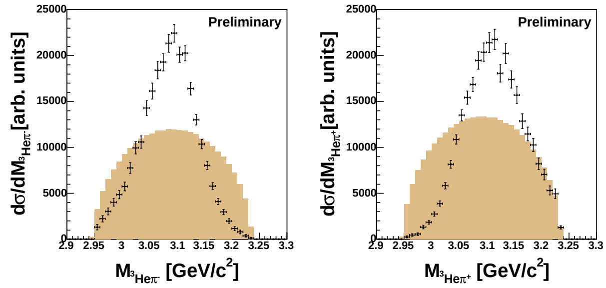

Fig. 2: Invariant mass spectra $M_{^3He\pi^-}$ (left) and $M_{^3He\pi^+}$ (right), corrected for the geometrical acceptance of ANKE and compared to phase space calculations.

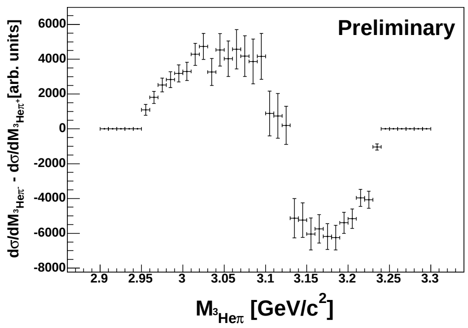

Fig. 3: Difference spectrum of the $M_{^3He\pi^-}$ and $M_{^3He\pi^+}$ distributions.

References:

[1] M. Bashkanov et al., *Phys. Lett.* **B 637**, *223 (2006)*

[2] A. Khoukaz, T. Mersmann, *Investigation of the ^{3}Heη Final State in the Reaction d+p→^{3}He+η at ANKE, COSY-Proposal 137, 2004*

[3] T. Rausmann et al.,ibidem, *Investigation of the η^{3}He Final State in dp-Reactions at ANKE*

[4] M. Mielke et al., *Annual Report, Forschungszentrum Jülich, 2006*

[1] Institut für Kernphysik Westfälische Wilhelms-Universität, 48149 Münster, Germany

* Supported by FZ-Jülich FFE

Luminosity determination for the dd → αK^+K^- reaction with ANKE

X. Yuan [1,2] for the ANKE collaboration

An attempt to measureme the $dd \to \alpha f_0 \to \alpha K^+K^-$ process at maximum COSY beam momentum of $p_d = 3.7$ GeV/c has been made using the magnetic ANKE spectrometer. In order to determine the $dd \to \alpha K^+K^-$ cross section $\sigma_{\alpha K^+K^-}$, one has to determine the integrated luminosity $L_{\rm int}$ during the measurement. In our experiment elastically and quasi-elastically scattered deuterons, which were recorded simultaneously with the αK^+K^- events, have been used for this purpose.

Figure 1 shows the result of a Monte-Carlo simulation on the ANKE acceptance for $dd \to dX$ events at our beam momentum $p_d = 3.7$ GeV/c. Deuterons in the angular interval $\theta = 5^\circ \dots 7^\circ$ and $\phi = -20^\circ \dots +20^\circ$, where the ANKE acceptance A_d amounts to 100%, have been selected for luminosity determination. In that angular-momentum bin, the differential cross section $\mathrm{d}\sigma(dX)/\mathrm{d}\Omega\mathrm{d}p$ of the scattered deuterons is sizable and smooth.

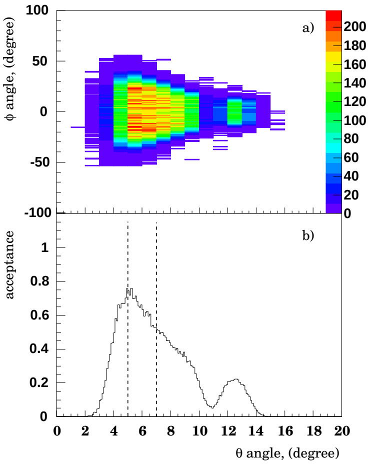

Fig. 1: Monte-Carlo simulation for $dd \to dX$ events in the ANKE acceptance at $p_d = 3.7$ GeV/c. a) Distribution of the events in the polar and azimuthal angles θ and φ. b) Projection on the polar angle. The dashed lines show the θ range that has been used for the luminosity determination.

The differential cross section $\mathrm{d}\sigma(dX)/\mathrm{d}\Omega$ of dd quasi-elastic scattering has been measured at an angle of $\theta = 103$ mrad (5.9°) for beam momenta $p_d = 4.3$, 6.3, 8.9 GeV/c [2], and in the small-angle Coulomb-interference region $\theta = 16.5\dots70.5$ mrad for $p_d = 1.69$ GeV/c [3]. For the latter data $\mathrm{d}\sigma(dX)/\mathrm{d}\Omega$ at 103 mrad can be extrapolated by a fit, shown in Fig. 2 (l.h.s.), with a parameterization that can be found in Ref. [3]. This extrapolated value is shown in Fig. 2 (r.h.s.) together with the cross sections at the higher beam momenta $p_d = 4.3$, 6.3, 8.9 GeV/c [2]. We then make an interpolation for $p_d = 3.7$ GeV/c, using different shapes of the fit function, see Fig. 2. From these fits the differential cross section is deduced to be 30 mb/sr, the error is estimated to be ±10 mb/sr.

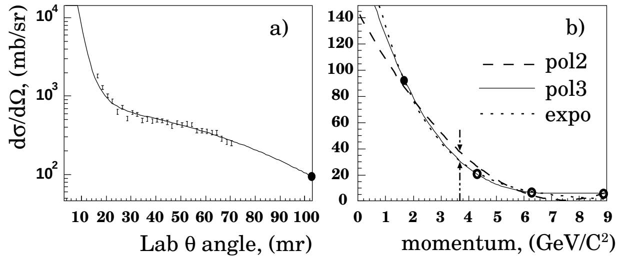

Fig. 2: a) Differential cross section for quasi-elastic deuterons at $p_d = 1.69$ GeV/c [2]. The error bars represent the statistical uncertainties of the data. The line is a fit to the data using a parameterization from Ref. [3]. The black bullet corresponds to the extrapolated cross section at 103 mrad. b) Measured (open bullets) and extrapolated (solid) differential cross section for $p_d = 1.69$, 4.3, 6.3, 8.9 GeV/c. Three different functions have been fitted to the data in order to interpolate to the p_d value of our experiment (indicated by arrows).

The average efficiency ε to identify the deuterons and reconstruct their trajectories in the above mentioned angular-momentum criterion and momentum cut amounts to 92%. Using that number, the number of detected deuterons $N_{\rm exp}$ and

$$L_{\rm int} = \frac{N_{\rm exp}}{\varepsilon \cdot A_d \cdot \frac{\mathrm{d}\sigma(dX)}{\mathrm{d}\Omega}}$$

the luminosity has been determined for each of the ∼ 350 experimental runs individually. Starting with Run # 100 (where we changed the on-line trigger conditions) the experimental conditions were more or less constant. The integrated luminosity over all runs has been determined to $L_{\rm int} = 2.5\,\mathrm{pb}^{-1}$. This corresponds to an average value of $L = [2.6 \pm 0.1(\mathrm{stat}) \pm 0.8(\mathrm{syst}) \pm 0.3(\mathrm{syst})] \times 10^{31}\,\mathrm{s}^{-1}\mathrm{cm}^{-2}$. The systematic error is mainly from the $dd \to dX$ cross section estimate and the uncertainty of the θ angle reconstruction.

References:

[1] L. S. Azhgirey et al., *Nucl. Phys.* **A 305**, 397 (1978).
[2] L. M. C. Dutton et al., *Nucl. Phys.* **B 78**, 484 (1974).

[1] Institute of Mordern Physics, Chinese Acedemy of Sciences, Lanzhou, P.R. China
[2] Graduate University, Chinese Acedemy of Sciences, Beijing, P.R. China

Luminosity determination for $\vec{d}\,p \to (pp)n$ charge-exchange reaction*

D. Chiladze[a,b], S. Dymov[c], A. Kacharava, F. Rathmann, and C. Wilkin[d] for the ANKE collaboration

In order to extract the differential cross section for the $dp \to (pp)n$ charge–exchange breakup reaction [1], the absolute luminosity must be determined. The measurement of the luminosity has been done using the dp elastic scattering reaction. For this purpose only the data sample with the unpolarized beam from the polarized source were used. For the normalization of ANKE data, the KEK results has been used, where the dp total, elastic, inelastic, and differential cross sections have been measured at 10 different beam momenta in the range of p_d = 2.0-3.7 GeV/c and in the angular interval of $\theta^d_{lab} = 4^\circ \div 15^\circ$ [2]. There were no measurements exactly at our momentum p_d = 2.4 GeV/c, therefore we used the KEK data for 2.26 GeV/c and 2.46 GeV/c to extract the cross–section for our beam energy in the assumption of linear approximation (see Fig. 1).

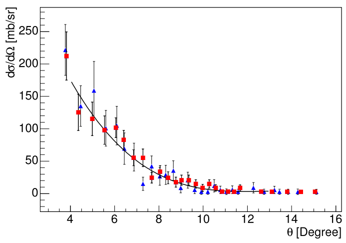

Fig. 1: Thr KEK results for dp elastic cross section [2]: blue triangels are data for p_d = 2.26 GeV/c and red squares are for p_d = 2.46 GeV/c. The solid line is the fit of all data points.

In this experiment we have used only the forward detection (FD) system (three MWPC's and scintillation hodoscope) of the ANKE spectrometer and system was able to detect deuterons in the forward direction for polar angles from 5° to 10°. The dp-elastic process has high cross section and is clearly seen in the one dimensional momentum distribution (Fig 2). The elastic momentum peak is well separated from the other processes. After selecting the peak region in the momentum distribution, the produced missing mass of the selected events clearly sits on the proton mass with almost no background (see Fig. 2).

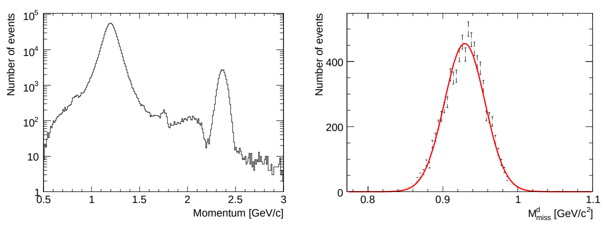

Fig. 2: Identification of the dp elastic reaction at ANKE. Left panel: momentum distribution for single track events; right panel: the deuteron missing mass spectra

For the acceptance calculation of the reaction the data sample of the identifyied events has been divided into the deuteron polar angle bins of 0.5°. After that for each polar angular range, the detector solid angle calculated. Typical spectra for the azimuthal angular distributions are shown in Fig. 3. Finally for each slice of the polar angle the geometrical acceptance was calculated in the following way:

$$A_i = \Omega_i^{det} = \Delta\phi_i[cos\theta_i - cos(\theta_i + 0.5^\circ)], \qquad (1)$$

where Ω_i^{det} is the solid angle element of the FD system.

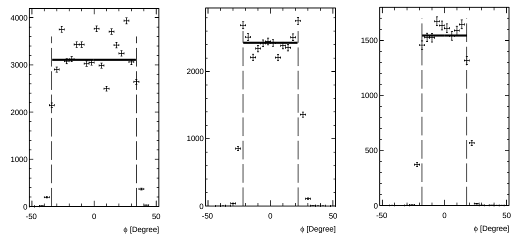

Fig. 3: Typical histograms to define the detector edges in the azimuthal direction for several polar angle bins (from left to right: $\theta = 5.5^\circ - 6.0^\circ$, $7.0^\circ - 7.5^\circ$, $8.0^\circ - 8.5^\circ$.

In these histograms the events are already corrected for the MWPC's efficiencies (around 99%). The number of events where also corrected by the prescaling factor of the FD trigger and by the total DAQ efficiency factor (around 75%).

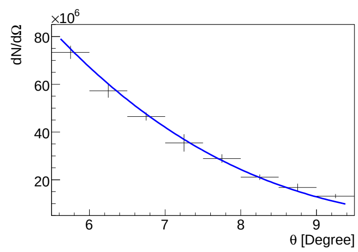

Fig. 4: Acceptance corrected angular distribution for deuterons. The solid line is the fit function find from the Fig.1.

Finally, using the acceptance corrected dp count rates and fitting our angular distribution (see Fig.3) by the one parameter function derived from the KEK differential cross section data, the luminosity for the different polar angular bins was determined and the results has been found consistent. The integrated luminosity for whole beam time is: $L_{int} = (9 \pm 0.04) \times 10^6$ mb^{-1}, which gives the average luminosity of $L = 671 \pm 3$ mb^{-1} sec^{-1}.

References:

[1] D. Chiladze et al. Phys. Lett. B637 (2006) 170.
[2] N. Katayama et al. Nucl. Phys. A438 (1985) 685.

[a] IKP FZJ, Germany
[b] HEPI Tbilisi State University, Georgia
[c] Erlangen University, Germany
[d] University College London, U.K.
* supported by COSY–FFE programm (COSY-080)

Proton beam polarization measurement with the ANKE vertex detector at 45 MeV

S. Barsov[a], G. Macharashvili[b,c], S. Merzliakov[c], D. Oellers[d], F. Rathmann[d], R. Schleichert[d], and S. Trusov[e]

The ANKE Silicon Tracking Telescopes (STT) were successfully applied to measure the polarization of a proton beam circulating inside the COSY ring at the injection energy of 45 MeV. The polarization was determined from the left-right asymmetry of the proton-deuteron elastic scattering on the deuterium cluster jet target at ANKE. Scattered particles were detected by two STTs installed inside the vacuum near the cluster jet to the left and to the right of the beam direction. A detailed description of the telescope parameters is given in Ref.[1].

Each of telescopes consisted of three double-sided strip detectors. Counting from the beam, the first and the second detectors had a thickness of 300 μm, while the third one was of 5 mm thickness. The first detectors were placed as close to the target as 30 mm. In this configuration each of telescopes covered the angular ranges of $45^o < \vartheta < 108^o$ and $\Delta\phi \simeq 50^o$ for scattering polar and azimuthal angles, respectively. All the detectors delivered both a hit energy loss and the position information, so that the track of a particle detected in, at least, the 1^{st} and the 2^{nd} detector was reconstructed.

The pd elastic scattering was identified by the detection of recoil deuterons. The $(\Delta E_1, \Delta E_2)$ plot for particles detected in the 1^{st} and in the 2^{nd} detectors of one STT (see Fig. 1) demonstrates the clear separation of the deuteron and the proton bands. The same type of separation was obtained for the other STT as well. It provided a reliable identification for most of the deuterons, excluding the overlap of the two bands.

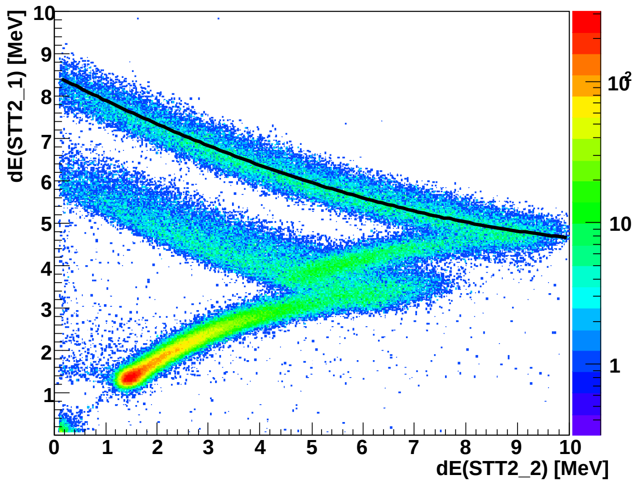

Fig. 1: Deposited energy correlation in the 1^{st} and the 2^{nd} detectors. The upper band corresponds to deuterons and the lower one to protons. Clear particle separation is possible. The solid line on the deuteron band shows the most probable deposited energies.

The relative alignment of detectors was checked using events when both particles, proton and deuteron, from the pd elastic scattering were simultaneously detected in both STTs. The Fig. 2 shows the distribution over the azimuthal angle between two tracks found in different STTs. Brown peaks correspond to events where the deuteron was identified in the given STT. These peaks are quite clean and well centered around 180^o. Their widths of $\simeq 6^o$ (FWHM) are in a good agreement with a result of Monte-Carlo simulations and mainly determined by the multiple scattering of deuterons in the 1^{st} detectors. The same distributions obtained without the deuteron selection demonstrate significant tails due to the deuteron break-up process into a three-nucleon final state.

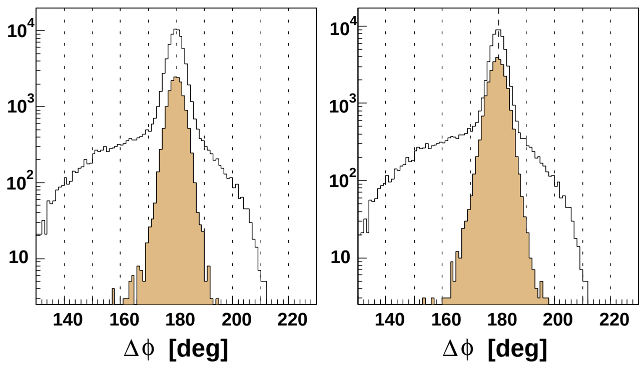

Fig. 2: Two track azimuthal angle differences for the 1^{st} (*left panel*) and the 2^{nd} (*right panel*) STTs. In yellow the selected elastic pd scattering events are shown. The background corresponds to the three-body final state (deuteron break-up process) with two protons detected.

For up and down polarized beams we calculated the asymmetry using the geometric means of the counts of the STTsin the $\vartheta \pm \Delta\vartheta$ interval. The angle ϑ corresponds to deuteron scattering angle in lab. system. The asymmetry is calculated using

$$\varepsilon(\vartheta) = \frac{\sqrt{L_1 L_2} - \sqrt{R_1 R_2}}{\sqrt{L_1 L_2} + \sqrt{R_1 R_2}} = P_B \langle cos\phi \rangle A_y(\vartheta), \quad (1)$$

where $L_{1(2)}$ corresponds to the counts of STT-1(2) located to the left with respect to the beam polarization vector, and $R_{1(2)}$ is the same for STT-1(2) located to the right with respect to the beam polarization vector. As has been noted above, in the ANKE target system, the STT-1 is placed at positive x -coordinate and the STT-2 symmetrically at negative x -coordinate. P_B denotes the absolute value of the beam polarization being measured. We assume that polarization modules are the same for beam up and down polarizations. $A_y(\vartheta)$ is the analyzing power in elastic *pd* scattering at 45 MeV taken from Ref.[2] The calculation of the expression (1), used for asymmetry, eliminates the difference of the two telescopes accepted solid angles, efficiencies, and the difference of the luminosities for up and down polarized beams at first order. This guarantees that the false asymmetry enters only in second order [3].

For the analyzing power approximation, as well as for the obtained asymmetry data, we used a parabola in the following form,

$$\varepsilon(\vartheta) = a(\vartheta - \vartheta_o)[1 + b(\vartheta - \vartheta_o)] \tag{2}$$

where a, b, and ϑ_o are the fit parameters. At first we fitted Eq(2) to the experimental data taken from [2]. Then the parameters b and ϑ_o were fixed and the same function has been used to fit the measured asymmetry points. So, we defined one single parameter a' for our data. The fit curves are shown in Fig. 3, in red for asymmetry and in blue for the experimental analyzing power data. Substituting these two fitted functions in Eq(1) with different a and a' values we obtain

$$P_B = \frac{a'}{a}\langle cos\phi\rangle^{-1} = 0.431 \pm 0.014. \tag{3}$$

It has to be stressed that the statistical uncertainty is dominated by the fit procedure, and not directly by the event sample.

The STT detectors demonstrate quite good performance to identify protons and deuterons and to measure reliably the spin asymmetry in case of polarized beam. Nevertheless, the long-time stability and the stability control methods have to be studied carefully.

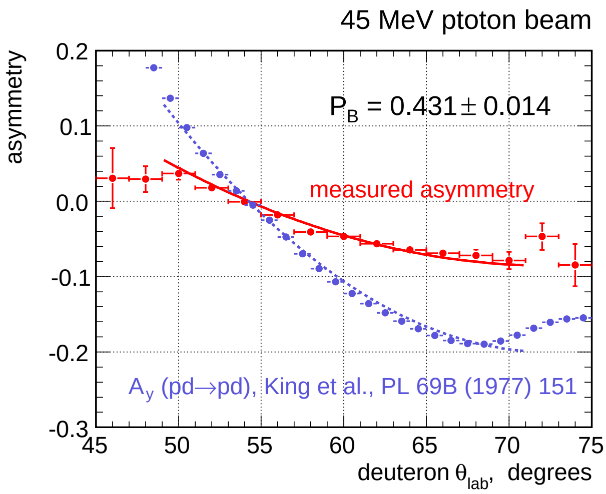

Fig. 3: Measured asymmetry of *pd* -elastic scattering (in red) and the experimental data on A_y (in blue), used for the beam polarization determination, are taken from [2]. The experimental data points are smoothed by spline.

References:

[1] A. Mussgiller, Ph.D. thesis, Univ. of Cologne (2006).
[2] N.S.P King *et al.*, Phys. Lett **69 B** (1977) 151.
[3] G.G. Ohlsen and P.W. Keaton, Jr. NIM, **109** (1973) 41.

[a] PNPI, Gatchina, Russia
[b] Tbilisi State University, Tbilisi, Georgia
[c] JINR, Dubna, Russia
[d] IKP, FZ-Juelich, Germany
[e] INP MSU, Dubna, Russia, FZ-Rossendorf, Germany

Determination of the ANKE detector coordinates

Yu. Valdau[1,2] for the ANKE collaboration

Knowledge about detector position is very important for the data analysis. Tracking detectors are suited to provide information about track with precision better than 1 mm, thus determine momentum resolution. Therefore, it is very important to know chamber positions to a good accuracy.

In August 2007 a precision measurements of ANKE detector positions has been done for several settings of the D2 spectrometric magnet. In these measurements coordinates of the 10 points on the ANKE detectors have been determined in arbitrary coordinate system. Each set of measurements contains information about coordinates of the rod installed at the top of the D2 magnet. Position of the rod with respect to the center of the ANKE coordinate system, which coincides with the center of the D2 chamber, is precisely known. Thus, coordinates of the rod are used for recalculation of the measured detector coordinates to the ANKE coordinate system.

In August 2007 new positive stop side chamber (SdMWPC2) support system has been implemented. From this time ANKE stop chamber is rotating around the axis which is fixed with respect to the D2 magnet at the low momentum side. The high momentum side of the chamber support is fixed on the Fd platform such that it keeps constant distance between FdMWPC2 (second forward multi-wire proportional chamber) and SdMWPC2. New forward detector (Fd) support system is designed such that all the Fd detector rotating around one point, and parameters of this rotation are determined by the position of the D2 magnet, which is set by the linear drive (LA1). The linear drive shift determines distance between COSY beam axis and the center of ANKE D2 magnet in X direction. Thus, new ANKE detectors support system makes detector coordinates predictable on the basis of information provided by COSY (See Fig. 1).

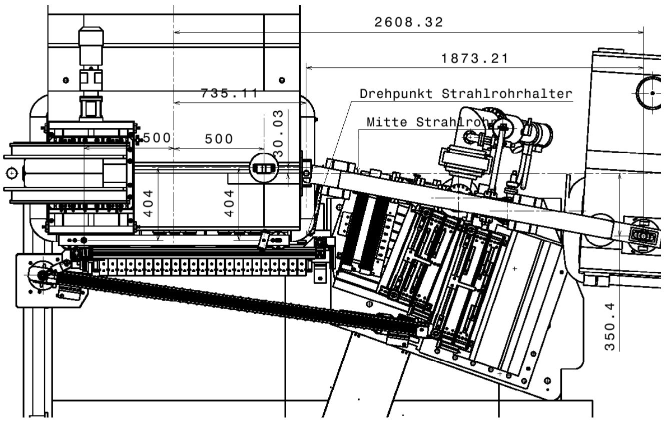

Fig. 1: Sketch of the ANKE detector system.

A simple C++ code has been developed to determine detector coordinates for any linear-drive position [1]. This program use user selected set of the measured points to produce output detector coordinates for any linear drive position. Output contains detector coordinates in form used in both old and new ANKE analysis codes.

The analysis of the all data shows internal consistency of the measurements at different positions of linear drive. Sizes of the detectors as well as distances between them remain constant within a precision of roughly 0.1 mm (see Table 1). However, geometrical sizes of chambers extracted from all the measurements differ from ones extracted from the drawings. This leads to the systematic shift of the detector positions, which has been determined using calibration reactions.

Detector	S_{meas}	σ_{meas}	S_{known}
Rod	1000.14	0.0866	1000
SdMWPC2	2126.67	0.101	2125
FdMWDC1	361.123	0.058	360
FdMWPC2	472.531	0.038	472
FdMWPC3	594.035	0.073	592

Table 1: Comparison between measured and known sizes of the detectors. All dimensions are in millimeters.

LA1	Δ_{dc1}	Δ_{pc2}	Δ_{pc3}
278.9	0.75	1.37	0
274.2	0.94	1.47	0
266.1	0.59	1.27	0
263.1	0.59	1.27	0
258.2	0.75	1.47	0

Table 2: Systematic shift of the chamber positions determined from the experimental data as a function of the linear drive position. All dimensions are in millimeters.

The results of the Fd detector position calibration using pp elastic scattering for different LA1 is presented in Table 2. Systematic shift in the X coordinate for the first and second chambers has been implemented on the basis of the information about reconstructed track. Difference between values of shifts for different energies is of the oder of the measurement uncertainty.

Analysis of the precision measurements of the ANKE detector positions has been done. It is shown that the measurements are internally consistent. On the basis of this measurements a program has been developed which allows to determine the detector positions for any settings of spectrometric magnet.

References:

[1] http://ankecvs.ikp.kfa-juelich.de/forum/viewtopic.php?t=107

1 High Energy Physics Department, Petersburg Nuclear Physics Institute, 188350 Gatchina, Russia

2 Institut für Kernphysik, Forschungszentrum Jülich, 52425 Jülich, Germany

High statistics investigation of the reaction $pp \to K^+\Lambda p$ with COSY-TOF

W. Eyrich, L. Kober, M. Krapp, A. Lehmann, C. Pizzolotto, W. Schroeder, and A. Teufel
Physikalisches Institut, Universität Erlangen-Nürnberg,
for the COSY-TOF-Collaboration

The experiment COSY-TOF is a wide angle, non magnetic spectrometer with an inner detector system, which is optimized for strangeness production measurements. This system with small beam holes as well as the outer detector system covers the full angular range of the reaction products and allows the complete reconstruction of $pp \to KYp$ events, including a precise measurement of the delayed decay of the hyperon $Y = \Lambda, \Sigma^+, \Sigma^0$.

The reaction $pp \to K^+\Lambda p$ has been investigated at several beam momenta from close to threshold up to nearly the COSY-limit. Dalitz plots, extracted at beam momenta between 2.5 GeV/c and 3.3 GeV/c corresponding to sample sizes between about 5.000 and 30.000 events show strong deviations from phase space [1,2,3]. Using a parametrization of Sibirtsev [4], which includes the resonances $N^*(1650)$, $N^*(1710)$, $N^*(1720)$ and the $p\Lambda$-final state interaction, shows a strong energy dependent contribution of the various resonances. Moreover in the whole energy range there is a significant influence of the $p\Lambda$-final state interaction.

To study the resonance parameters in more detail and to search for unknown resonances, much larger event samples are needed. For the first time such a sample, consisting of more than 300.000 fully reconstructed $pp \to K^+\Lambda p$ events, is now available at a beam momentum of 3.06 GeV/c.

The corresponding preliminary Dalitz plot is shown in Fig.1. Again a striking deviation from phase space is observed which is caused by the strong influence of N^* resonances and the $p\Lambda$-final state interaction and which is in agreement with the former results.

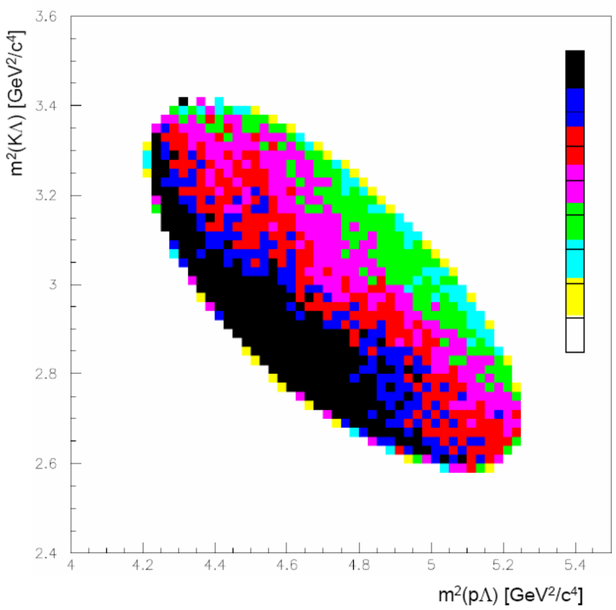

Fig. 1: Preliminary Dalitz plot of the reaction $pp \to K^+\Lambda p$ for a beam momentum of p_{beam} = 3.06 GeV/c. The sample contains about 320.000 events covering the full phase space.

In Fig.2 the reconstructed mass of the Λp-subsystem is shown. On top of a smooth distribution an enhancement is observed at the $\Sigma^0 p$ mass. Indications of such an enhancement had already been observed in the former measurements, but could not be unambiguously identified due to lacking statistical precision. The origin of the observed peak might be a channel coupling of the Λ and the Σ^0 channel (cusp effect), which was already addressed interpreting semi-inclusive data from a measurement performed at Saclay [5].

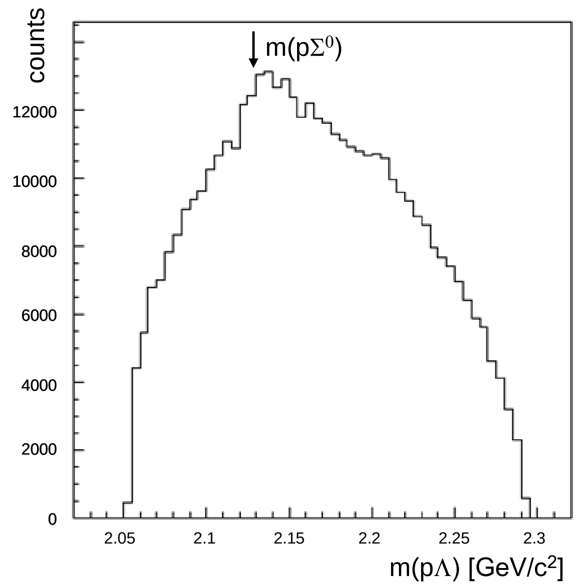

Fig. 2: Preliminary mass distribution of the Λp-subsystem for a beam momentum of 3.06 GeV/c.

The ongoing investigation of the actual data will concentrate in the next steps on detailed analyses of the Dalitz plot using the model of Sibirtsev to investigate with high precision the contributing resonances and their parameters and to search for additional resonances. In a further step other differential observables as the angular distributions in the various systems will be included. Moreover a partial wave analyses is planned. Work on this has already been started for the former COSY-TOF data by Anisovich et al. [6].

In the near future TOF will concentrate on the use of a polarized proton beam which will give access to additional observables. Furthermore existing data from the channel $pp \to K^0\Sigma^+p$ will be included as well as first hyperon production data which were taken using a liquid D_2 target to investigate the reaction $pn \to K^0\Lambda p$.

References:

[1] COSY-TOF coll., Phys. Lett. B 420 (1998) 217
[2] COSY-TOF coll., Phys. Lett. B 632 (2006) 27
[3] COSY Annual report, 2005, p. 47
[4] A. Sibirtsev, private communication, 2002, 2005
[5] R. Siebert, et al., Nucl. Phys. A 567 (1994) 819
[6] A.V. Anisovich et al., arXiv:hep-ph/0703216

$pn\pi^+$ Production in pp Collisions at 0.95 GeV/c

E. Doroshkevich[a], H. Clement[a], A. Erhardt[a], K. Ehrhardt[a] and G.J. Wagner[a] for the COSY-TOF Collaboration

We report on a high-statistics measurement of the differential cross sections at a beam momentum of 0.95 GeV/c (corresponding to T_p =397 MeV) for the reaction $pp \to pn\pi^+$. The reaction $pp \to pp\pi^0$ stemming from the same run has been published already [1].

By use of the central calorimeter the COSY-TOF setup is capable of providing a reliable particle identification on the basis of the ΔE-E technique for charged particles. Whereas the calorimeter provides the residual energy information, the Quirl is used as ΔE detector by using its time-of-flight (relative to the start detector) information, since it is superior to the ΔE information of the Quirl [1]. Neutrons are recognized by their signal in the calorimeter in combination with no signal in the Quirl.

In this way the different single pion production channels could be well separated. The results for the $d\pi^+$ channel agree with well-known previous results [2]. For the $pp\pi^0$ channel, which for the first time has been measured over the full phase space at this incident energy, significant deviations from previous investigations were obtained for angular distributions as well as for invariant mass spectra [1].

Due to the need for π^+ detection, the $pn\pi^+$ data do not cover the full phase space, however, still a large fraction of it. Contrary to the observation in the $pp\pi^0$ channel the Dalitz plots in this channel are not flat. The $p\pi^+$ and $n\pi^+$ invariant mass distributions rather peak at the highest available invariant masses signaling a strong Δ excitation in this channel.

The efficiency and acceptance corrected invariant mass M_{pn} and $M_{p\pi^+}$ distributions are shown in Fig.1. The effect of a Migdal-Watson type pn Final State Interaction (FSI) [3] is shown by the dashed curve. Inclusion of the Δ excitation gives the full curves. The dotted curves show the result, if we use the FSI prescription according to Ref. [4]. From these calculations it gets obvious that Δ excitation plays a dominant role in this reaction channel.

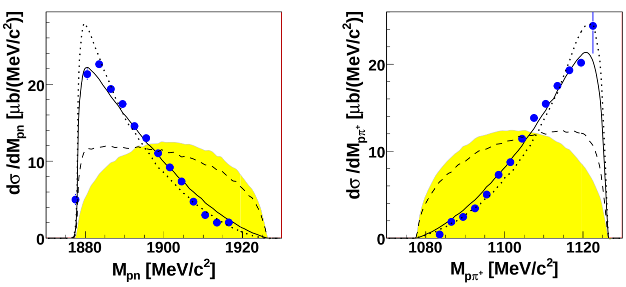

Fig. 1: M_{pn}, $M_{p\pi^+}$ invariant mass distributions in comparison with phase-space distribution (hatched area), pn-FSI (dashed) according to Ref.[3] and ansatz including also the Δ excitation (full lines). Using the pn-FSI according to the prescription of Ref. [4] together with the Δ excitation result in the dotted curves.

As an example for the angular dependence of the differential cross sections we show in Fig.2 the pion angular distributions observed in $pn\pi^+$ and $d\pi^+$ channels. Whereas the proton angular distributions are rather flat in both $pp\pi^0$ and $pn\pi^+$ channels, the pion angular distributions are markedly different in both channels. In case of $pp\pi^0$ we find an angular dependence with maximum cross section at $\Theta^{CM} = 90°$.

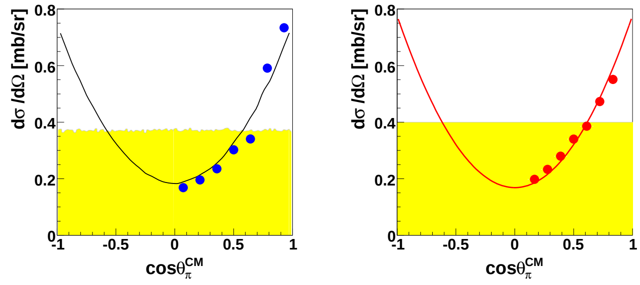

Fig. 2: Angular distributions of pions (overall CM system) for the $pp \to pn\pi^+$ (left) (normalized by factor $\sigma_{d\pi^+}/\sigma_{pn\pi^+}$) and $pp \to d\pi^+$ reactions. Data of this work and Ref. [1] are shown by full circles, the fit to the data assuming a $3cos^2\Theta^{CM}+1$ dependence by solid lines (curve for $d\pi^+$ is from SAID [2], which is very close to a $3cos^2\Theta^{CM}+1$ dependence). The hatched areas denote the flat phase space distributions.

In case of the $pn\pi^+$ channel we find a very strong angular dependence with a cross section minimum at $\Theta^{CM} = 90°$ and with an angular dependence, which is exactly that of a Δ excitation in the πN s-channel, i.e., $3cos^2\Theta^{CM}+1$.

This dependence is also observed in the $pp \to d\pi^+$ reaction over a wide energy region from threshold up to T_p = 800 MeV combined with a resonance-like energy-dependence, which in phase-shift analyses is traced back to the resonant ^1D_2P partial wave in this reaction. This partial wave constituting a s-channel resonance of a $N\Delta$ configuration dominates the $d\pi^+$ channel cross section over the full energy range - see also the discussion on this matter in [5].

Since the $pn\pi^+$ channel shows the same characteristic angular dependence as the $d\pi^+$ channel, we conclude that the breakup channel obviously is also dominated by this partial wave featuring a dibaryonic $N\Delta$ s-channel resonance, at least in the energy regime around $T_p \approx 400$ MeV.

References:

[1] S. Abd El-Samad et al., Eur.Phys.J.**A30** 443 (2006)
[2] R. A. Arndt et al., Phys. Rev. **C48** 1926 (1993)
[3] M. Schepkin, O. Zabronsky, H. Clement, Z. Phys.**A345** 407 (1993)
[4] C. Hanhart, Phys. Rep. **397**, 155 (2004) and priv. comm.
[5] H.Clement et al.,Progr.Part.Nucl.Phys.(2008),in press [doi:10.1016/jinpp.2007.12.032]

[a] Physikalisches Institut Tübingen Universität Tübingen 72076 Tübingen Germany

A new algorithm for the walk correction of the COSY-TOF time of flight measurement

E. Roderburg
for the COSY-TOF Collaboration

1.) Walk effect and time of flight measurement

The signals of the start and stop scintillators, which provide the time of flight of the particles detected in the TOF detector, are processed with leading edge discriminators [1] and digitised with TDCs with a binning of 100 ps. The stop scintillators are operated with XP2020 tubes with about -2000 V supply voltage, resulting in signal heights at the input of the discriminators in the order of 1 V. Especially for the spiral shaped quirl and ring scintillators the pulse-height varies up to a factor of 8 due to the different light losses in these scintillators (Fig. 1).

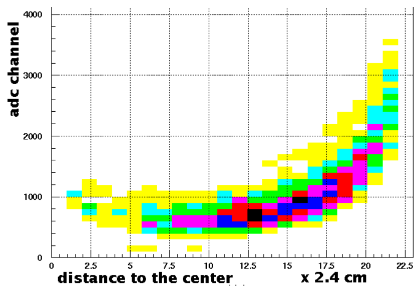

Fig. 1: Signal amplitude measured with an integrating ADC in dependence on the track location in a quirl spiral element

The signal rise-time at the discriminator input of 1 - 5 ns is mainly caused by transmitting the signals through 50m long coaxial cables. The threshold of the discriminators is set to 20 - 50 mV. These conditions produce a walk effect, which can be larger than 4 ns. In order to exploit the capability of the TOF spectrometer to reconstruct the missing mass of one neutral particle, a time resolution of of $\sigma = 0.2 - 0.3 ns$ is required. Therefore the walk effect has to be corrected with a precision of better than 0.1 ns.

2.) Method

The method of walk calibration with particle tracks, which is described in the following, is valid for a set of two scintillators of the same geometry, arranged back to back.

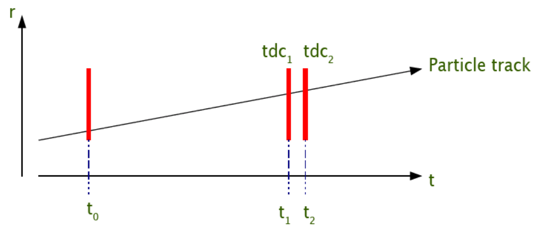

Fig. 2: Scheme of the arrangement of start and stop scintillators

Given the points in time t_0 of a particle track passing the start scintillator and t_1, t_2 for passing two stop scintillators sc1 and sc2 respectively, as defined in Fig. 2 the measured tdc values are given by:

$$tdc_1 = t_1 + T_{os}(sc_1) + T_{walk}(sc_1) + T_{lp}(sc_1(r_1)) - t_0 \quad (1)$$
$$tdc_2 = t_2 + T_{os}(sc_2) + T_{walk}(sc_2) + T_{lp}(sc_2(r_2)) - t_0 \quad (2)$$

r_1, r_2 : radial coordinates of intersection of the track with scintillator sc_1 and sc_2

T_{os} : time offset for each channel given by the cable length, photomultiplier tube parameters, etc. This offset is constant for all particle tracks

T_{walk} : walk effect. This time is dependent on the signal rise-time from 0 to the value of the discriminator threshold. It is different for each particle track.

T_{lp} : time of the light propagation in the scintillator. This time is dependent on the coordinate r of the particle track at the scintillator and on the scintillator geometry .

Exploiting the conditions of identical geometry and of the close back to back arrangement of the scintillators the following relations are approximately valid:

$$r_1 = r_2 \quad (3)$$
$$T_{lp}(sc_1(r_1)) = T_{lp}(sc_2(r_2)) \quad (4)$$
$$t_1 = t_2 \quad (5)$$

Therefore the difference of both tdc values is only dependent on the time of the walk effects and on the sum of the offsets, which does not vary with different particle tracks:

$$tdc_2 - tdc_1 = T_{walk}(sc_2) - T_{walk}(sc_1) + T_{os} \quad (6)$$

The walk effect is dependent on the signal rise-time from 0 to the value of the discriminator threshold. This rise-time is approximately inversely proportional to the integrated signal, which is measured with an ADC. For large amplitudes, the time walk approaches a value close to 0. This effect is applied in a first step of calibrating the walk of the scintillator 2, utilising only events, which have a large amplitude in scintillator 1 (larger than a given limit ADC_{limit}):

$$tdc_2 - tdc_1 = T_{walk}(ADC_2) - T_{walk}(ADC_1 > ADC_{limit}) + T_{os} \quad (7)$$

Equation (7) represents the walk of scintillator 2 measured as the tdc differences of both scintillators in dependence on the ADC of scintillator 2. The data are parametrised with the following formula:

$$T_{walk}[ns] = \frac{A}{(ADC) + B} + D \cdot log(ADC) + C \quad (8)$$

After the correction of the time measurement of scintillator 2 with formula (8) the walk of scintillator 1 can be calibrated according to

$$tdc_{2_{walk-corrected}} - tdc_1 = -T_{walk}(ADC_1) + T_{os} \quad (9)$$

This procedure of walk calibration by the difference of the tdc of two scintillators, one of which is pre-calibrated, can be iterated in several steps. Experimentally it is found, that after 4 iterations the solution for the calibration is stable.

3.) Results

The result of the walk correction for one quirl spiral element is shown in Fig. 3. As this element is overlapped by 23 spirals of the second quirl layer, the tdc information of these 23 spirals was first corrected to have the same offset.

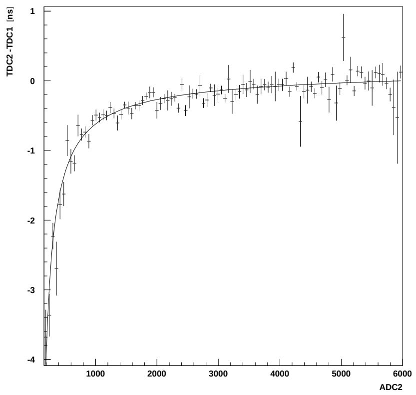

Fig. 3: Profile of the dependence on the tdc difference on the pulse-height of scintillator 2. The curve is a fit to this data with the function given in formula (8)

The walk calibration is applied on data, which were taken to measure the analysing power of $\vec{p}p \rightarrow pp\eta$ [2] The quality of the walk calibration can be tested by calculating the time difference of two detector layers. Events are selected, which have a multiplicity of exactly 2 charged tracks and a missing mass in the region of 0.5 GeV/c^2. With these constraints proton tracks with velocities of $\beta = 0.5 - 0.8$ are dominating. The combined time resolution of the quirl left and right plane results to $\sigma = 0.25ns$ (upper part in Fig. 4). The resolution of the straight quirl layer can be measured with the time difference of the averaged values of the left and right layer to the straight layer (lower part of Fig. 4). With 0.25 ns resolution of the sum of the spiral layers, the resolution of the straight layer is 0.18 ns.

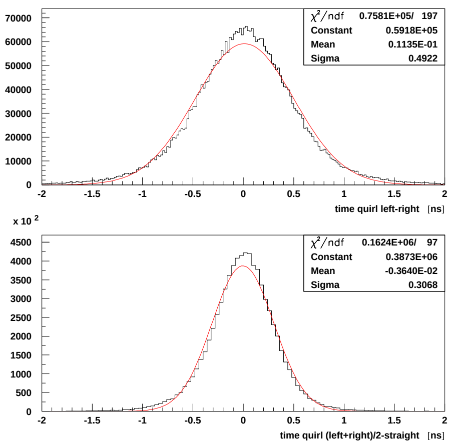

Fig. 4: Time resolution of the quirl layers measured with protons in the range of $\beta = 0.5 - 0.8$. The smooth curve shows a gauss fit to the data, the parameter of this fit are given in the inlet

For the ring counter the time resolution is for the spiral layers $\sigma = 0.31ns$ and for the straight layer $\sigma = 0.24ns$ (Fig. 5).

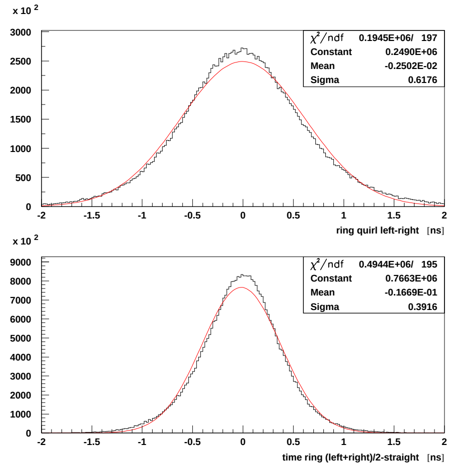

Fig. 5: Time resolution of the ring layers measured with protons in the range of $\beta = 0.5 - 0.8$. The smooth curve shows a gauss fit to the data, the parameter of this fit are given in the inlet

The missing mass distribution of these events is shown in Fig. 6. The mass resolution of the η particle is 0.7% at an excess energy of 58 MeV.

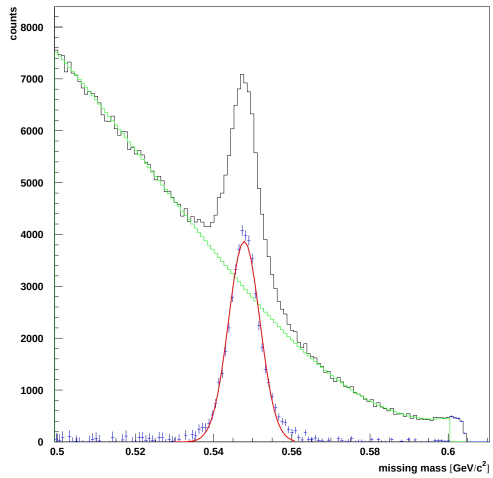

Fig. 6: Missing mass distribution of two track events. The green curve is a fit to the multi-pion background events, the red curve is the difference to the data, a gauss-fit to this distribution gives a σ of 4 MeV/c^2.

References:

[1] A new sixteen channel leading-edge discriminator for time-of-flight experiments at COSY
Jochmann, M.; Fub, S.; Mueller, K.D.; Reinartz, R.; Nuclear Science Symposium and Medical Imaging Conference, 1992.

[2] E. Roderburg and P. Zupranski, COSY Proposal 41.4.

Status report on the analysis of the $\eta \to 3\pi^\circ$ decay with WASA-at-COSY.

P.Vlasov, for the WASA-at-COSY Collaboration

The isospin violating $\eta \to 3\pi^\circ$ decay mode occurs due to the $m_d - m_u$ quark mass difference and allows the possibility of precise tests of QCD predictions. The theoretical and experimental efforts on the investigation of the η-meson decays show the importance of the accurate treatment of final state interactions. In lowest order, the Dalitz Plot of the $\eta \to 3\pi^\circ$ decay should be uniformly populated because the final state particles are identical. However, including a strong π-π interaction treated to higher orders results in a small nonuniformity of the Dalitz plot [1][2][3]. Due to the 3 identical particles in the final state the Dalitz plot can be shown in symmetrized form, which is represented by the variables

$$x = (T_{\pi_2} - T_{\pi_3})/\sqrt{3} \qquad y = \bar{T} - T_{\pi_1} \tag{1}$$

(See Fig.1), where T_i is the kinetic energy of the i-th pion and $\bar{T}$ is the mean kinetic energy of the pions. The transformation into a one-dimensional distribution in terms of the radial density z

$$z = 6\sum_{i=1}^{3}(E_{\pi_i} - m_\eta/3)^2/(m_\eta - m_{\pi^\circ})^2 \tag{2}$$

allows the linear parametrization of the decay amplitude

$$|A_{\eta\to 3\pi^\circ}(z)|^2 \sim 1 + 2\alpha z, \tag{3}$$

where the slope parameter α is a measure of the Dalitz plot nonuniformity and z is the distance from the center of the $\eta \to 3\pi^\circ$ Dalitz plot normalized to its maximum allowed value.

In the first experiment with WASA-at-COSY[4] in April 2007, a measurement of $\eta \to 3\pi^0$ decay has been performed focusing on a high statistics analysis of the Dalitz plot of the $\eta \to 3\pi^0$ decay. The η mesons have been produced in proton-proton interactions at a beam kinetic energy of 1.4 GeV. At the trigger level, events with two tracks in the Forward Detector and energy deposit in the Central Detector exceeding a certain threshold were accepted. In addition, a veto on charged particles in the Central Detector was required.

The $\eta \to 3\pi^\circ$ decay channel with subsequent decays of the pions into two photons was identified by selecting six clusters detected in the calorimeter. The conditions provide a clean data sample in which the remaining dominant background contribution from direct $3\pi^\circ$ production is estimated to be below 10%.

To select correct π° candidates out of the six reconstructed photons all fifteen possible combinations of the three photon pairs were considered. The three pairs which give a minimum χ^2

$$\chi_j^2 = \sum_{i}^{3} \frac{(m^j_{\pi_i^\circ} - m_{\pi^\circ_{PDG}})^2}{\sigma^2_{m_{\pi^\circ}}} \qquad j = 1,2,3,...15 \tag{4}$$

(where $m^j_{\pi_i^\circ}$ is the invariant mass of the i^{th} $\gamma\gamma$ pair, $\sigma_{m_{\pi^\circ}}$ is the resolution of reconstructed π° mass and $m_{\pi^\circ_{PDG}} = 0.13498\ GeV$) have been chosen. The hypothesis of the $\eta \to 3\pi^\circ$ reaction was used to constrain the kinematic variables of the reconstructed $\eta \to 3\pi^\circ$ system using kinematic fit procedures.

In Figure 1, the preliminary experimental Dalitz plot is presented. Using Monte-Carlo tools, the acceptance correction has been applied and a preliminary value for the slope parameter has been obtained by a linear fit of the acceptance corrected radial density distribution (see Figure 2). The preliminary value is $\alpha = -0.033 \pm 0.012(stat)$.

Only half of the data has been analyzed and reconstruction algorithms are still under development. Eventually we expect a statistical improvement by a factor 3. Systematic uncertainties are under investigation.

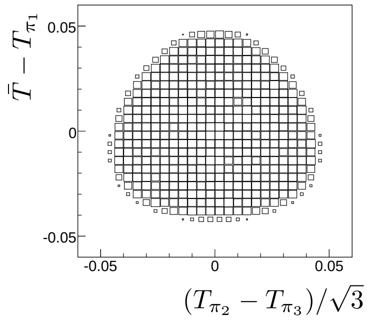

Fig. 1: Efficiency corrected Dalitz plot of the $\eta \to 3\pi^\circ$ decay.

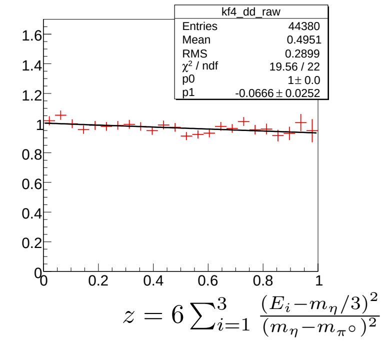

Fig. 2: Preliminary result for the slope parameter α extracted from acceptance corrected radial density distribution.

References:

[1] J. Gasser and H. Leutwyler, Nucl. Phys. B **250** (1985) 539.

[2] J. Kambor, C. Wiesendanger and D. Wyler, Nucl. Phys. B **465** (1996) 215.

[3] B. Borasoy and R. Nissler, Eur. Phys. J. A **26** (2005) 383.

[4] H. H. Adam *et al.* [WASA-at-COSY Collaboration], arXiv:nucl-ex/0411038.

First signals of charged η decays at WASA-at-COSY

C. F. Redmer for the WASA-at-COSY collaboration

The Plastic Scintillator Barrel (PSB) and the Mini Drift Chamber (MDC) in combination with a superconducting solenoid make the WASA-at-COSY detection setup [1] capable of investigating charged decays of the η-meson.

During the first production run of WASA-at-COSY in April 2007, dedicated to neutral decay channels of the η meson, especially $\eta \longrightarrow 3\pi^0$, it was possible to take first data on charged decays albeit with highly prescaled triggers.

From these data, the most abundant channels, $\eta \longrightarrow \pi^+\pi^-\pi^0$ and $\eta \longrightarrow \pi^+\pi^-\gamma$, have been investigated in an exploratory analysis, based on the idea of an online monitoring used in CELSIUS/WASA [2]. It is independent of the information provided by the MDC and can thus be performed even before the tracker is calibrated. As a drawback, only missing mass distributions are obtained.

From the events of interest two tracks within a certain time limit are demanded in the Forward Detector (FD). They are candidates for the outgoing protons of the reaction. To identify them as protons, the ΔE-E–method is applied in the Forward Range Hodoscope.

For the decay $\eta \longrightarrow \pi^+\pi^-\pi^0$ two tracks from charged particles and at least two tracks from neutral particles are required in the Central Detector (CD). In this analysis, a track in the CD is first of all a cluster in the calorimeter. A coincident signal from an element of the PSB, which is geometrically overlapping with the cluster, distinguishes between neutral and charged hits. All hits in the CD should be correlated in time with the tracks in the FD.

From the neutral hits those two are selected, which provide the best combination for a π^0 within an energy range defined by the resolution of the calorimeter. By higher numbers of neutral clusters in the first steps of event selection the possibility of cluster split-offs is taken into account.

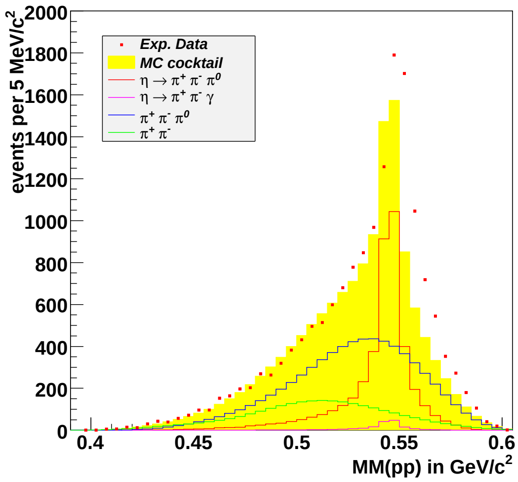

Fig. 1: Missing mass spectrum of two protons after applying cuts for the selection of $\eta \longrightarrow \pi^+\pi^-\pi^0$, fitted with MC distributions

The final criterion for event selection is the missing mass of the selected protons and photons. It is connected to the invariant mass of the two charged pions from the η decay and consequently at least twice the pion rest mass. Therefore, a cut is applied, to select only events with calculated missing masses larger than 300 MeV. Fig. 1 shows the missing mass spectrum of the two protons as a result of the performed event selection. Only 7% of the data taken in April 2007 have been analyzed. Extrapolated from this fraction about 6×10^4 events of the decay $\eta \longrightarrow \pi^+\pi^-\pi^0$ can be expected in the complete data set. Fig. 1 also shows first tests to describe the result by Monte-Carlo (MC) distributions. Deviations at higher missing masses may be artefacts at this exploratory stage. The ongoing analysis using the MDC should improve the situation.

In case of the decay $\eta \longrightarrow \pi^+\pi^-\gamma$, events of interest are selected in a very similar way as for $\eta \longrightarrow \pi^+\pi^-\pi^0$. The only difference is the selection of neutral hits. Only those events are accepted which have only one neutral hit and where the deposited energy affiliated with this track is larger than 150 MeV.

This cut suppresses a large part of the phase space but, as

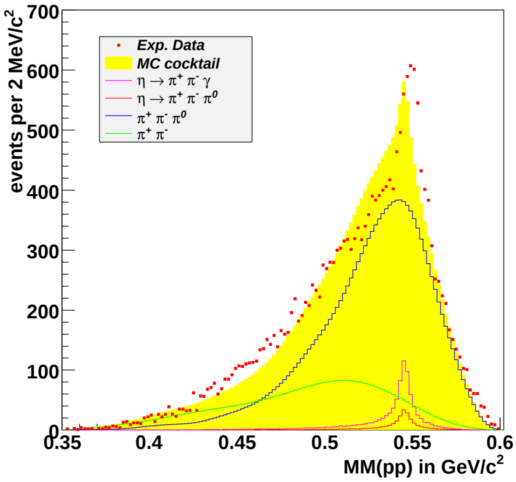

Fig. 2: Missing mass spectrum of two protons after applying cuts for the selection of $\eta \longrightarrow \pi^+\pi^-\gamma$, fitted with MC distributions

Fig. 2 shows, contributions of $\eta \longrightarrow \pi^+\pi^-\pi^0$ can be suppressed effectively. A complete analysis of $\eta \longrightarrow \pi^+\pi^-\gamma$ will be performed in the near future, with the help of the MDC information.

References:

[1] H.-H. Adam et al, Proposal for the Wide Angle Shower Apparatus (WASA) at COSY-Jülich, COSY Proposal (2004), e-Print arXiv: nucl-ex/0411038

[2] M. Jacewicz, Measurement of the reaction $pp \longrightarrow pp\pi^+\pi^-\pi^0$ with CELSIUS/WASA at 1.36 GeV, PhD thesis, University of Uppsala (2004)

η' hadronic decays with WASA-at-COSY

B.R. Jany[a,b]
for the WASA-at-COSY Collaboration

The η' meson belongs to the lightest nonet of the pseudoscalar mesons. The isospin conserving hadronic decays of the η' into three mesons $\eta' \to \pi\pi\eta$ are responsible for more than half of the total decay width (65.3% [1]). Studying the decays gives insight into the fundamental symmetries of QCD and the dynamics of the decay itself by investigating final state interaction [2, 3]. The experimental database is rather scarce [4, 5, 6, 7], with a maximum of ten thousand events only.
The newly commissioned WASA-at-COSY detector setup [8] is well suited to study all decay products and has a large acceptance.
During the commissioning, a 45 hour data run has been taken for η' production, with a proton beam momentum of 3.35GeV/c, and a trigger on the $pp \to ppX$ system. Due to large contamination of beam – rest gas interactions – the data were only searched for the very selective decay channel $\eta' \to \pi^0\pi^0\eta \to 5\pi^0 \to 10\gamma$. The result of the exploratory analysis is shown in Fig. 1, where the reconstructed invariant mass of the ten photons versus the missing mass of two protons is shown. The enhancement at the η' mass might be considered as a first evidence for the signal. More details of the analysis can be found in [9].

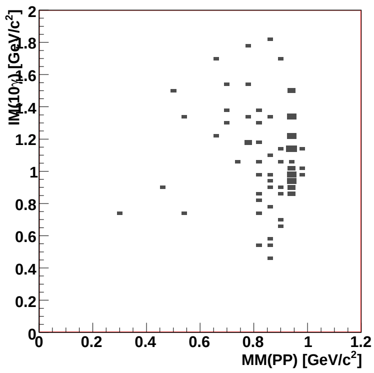

Fig. 1: Invariant mass of 10γ versus missing mass of two protons, the enhancement at η' mass is seen.

Detailed Monte-Carlo studies have also been performed, using dedicated GEANT3 based simulation, to estimate the background contributions from different reaction channels. The result for the 10γ final state is presented in Fig. 2 and Tab. 1. Background estimates for the case $\eta' \to \pi^0\pi^0\eta \to 6\gamma$ are given in Fig. 3 and Tab. 2.
We are looking forward to the first systematical studies of η' decays feasibility in pp collisions, according to the accepted proposal COSY-184 – „Feasibility Studies for η' Decays", in spring 2008.

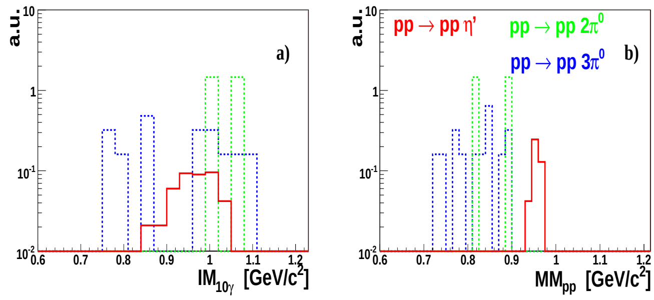

Fig. 2: Monte-Carlo simulations for the $pp \to pp\eta' \to pp10\gamma$ reaction and for the background channels, a) invariant mass of ten photons, b) missing mass of two protons.

Background reaction	N_B/N_S
$pp \to pp2\pi^0$	< 3.3
$pp \to pp3\pi^0$	< 0.37

Table 1: Number of background events for one $pp \to pp\eta' \to pp10\gamma$ event for missing mass range 0.9 – 1.0GeV, based on Fig. 2.

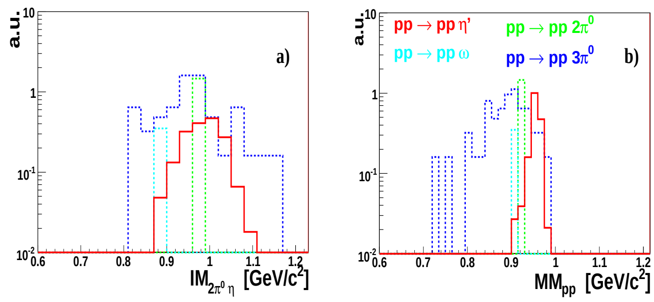

Fig. 3: Monte-Carlo simulations for the $pp \to pp\eta' \to pp6\gamma$ reaction and for the background channels, a) invariant mass of six photons, b) missing mass of two protons.

Background reaction	N_B/N_S
$pp \to pp2\pi^0$	< 0.83
$pp \to pp3\pi^0$	2.14 ± 0.46
$pp \to pp\omega$	< 0.20

Table 2: Number of background events for one $pp \to pp\eta' \to pp6\gamma$ event for missing mass range 0.9 – 1.0GeV, based on Fig. 3.

References:

[1] W. M. Yao, et al., *J. Phys.* **G33**, 1–1232 (2006).
[2] B. Borasoy and R. Nissler, *Eur. Phys. J.* **A26**, 383–398 (2005), `hep-ph/0510384`.
[3] B.R. Jany, *AIP Conf. Proc.* **950**, 209–212 (2007), `nucl-ex/07092834`.
[4] G. R. Kalbfleisch, *Phys. Rev.* **D10**, 916 (1974).
[5] D. Alde, et al., *Z. Phys.* **C36**, 603–609 (1987).
[6] R. A. Briere, et al., *Phys. Rev. Lett.* **84**, 26–30 (2000).
[7] V. Dorofeev, et al. (2006), `hep-ph/0607044`.
[8] H. H. Adam, et al. (2004), `nucl-ex/0411038`.
[9] D. Duniec and B.R. Jany, *AIP Conf. Proc.* **950**, 213–215 (2007).

[a] Institut für Kernphysik, Forschungszentrum Jülich

[b] Nuclear Physics Department, Jagiellonian University, PL-30059 Kraków, Poland

Pion production in $dd \to AN\pi$ with WASA-at-COSY

P. Podkopał [1,2]

One of the key experiments of the physics program of WASA-at-COSY is the determination of the p-wave contributions to the Charge-Symmetry-Breaking amplitude in the reaction $dd \to \alpha\pi^0$ at 1.2 GeV/c beam momentum [1]. As a first step towards this measurements the Charge Symmetry Conserving reactions $dd \to {}^3\mathrm{He}n\pi^0$, $dd \to {}^3\mathrm{He}p\pi^-$ were choosen. For an overall theoretical analysis of CSB [2] reactions in terms of Chiral Perturbation Theory these reactions channels are an important supplement. In addition, the background characteristics for 1.2 GeV/c deuterons on a deuteron pellet target using a large acceptance detector system like WASA-at-COSY are unknown and the small cross section of $dd \to \alpha\pi^0$ (a few pb) requires a thorough preparation.
The first step in identification of both reactions was to select events which contain one charged track in the forward detector (FD). Hits belonging to the track should have both time and energy information within allowed limits. Since most of ^{3}He are stopped before the third layer of the FTH detector, subsequent layer of the FRH detector was used as veto. The comparison of energy loss of particles detected in FD allows to separate ^{3}He from deuterons and protons (see Fig. 1).
Using a cut around the ^{3}He "banana" and requiring two neutral clusters measured in calorimeter in coincidence, we can unambiguously identify $dd \to {}^3\mathrm{He}n\pi^0$. In Fig. 2 (left side) the invariant mass of two neutral clusters is presented, a nearby background free at π^0 mass.

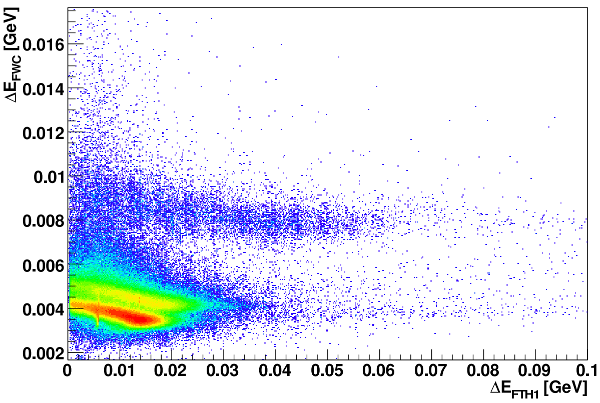

Fig. 1: Energy loss of forward going particles in FWC (scintillator detector) versus first layer of FTH (scintillator detector) without energy deposit in the second layer.

To minimise the background contribution a proper threshold on energy sum trigger was applied, as well as time matching between CD (clusters) and FD (tracks).
The identification of $dd \to {}^3\mathrm{He}p\pi^-$ is done using combined information from FD and CD detectors. Using the selected ^{3}He particles in the same way as it was described above, we can look for events with two charged tracks in CD. The particles in the central detector can be distinguished by comparing the momentum (obtained from Mini Drift Chamber) with the energy deposition in the Plastic Scintillator Barrel (PSB). In Fig. 3 (right panel) the $\triangle E - P$ identification method is shown, bands belonging to protons and pions are visible. Using MDC, four-vectors of p and π^- can be reconstructed. This information in connection with the known beam momentum allows to calculate missing mass of ^{3}He (see Fig. 2, right panel).

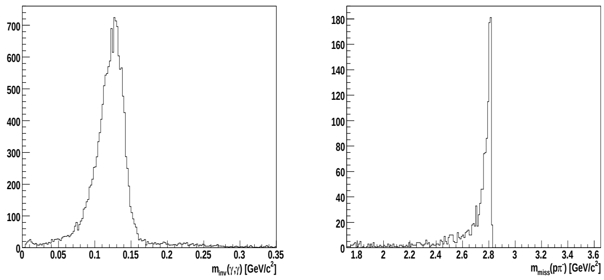

Fig. 2: Invariant mass of two gammas (left) and missing mass obtained from two measured particles in CD detector (right)

These first analysis steps show clearly that using WASA-at-COSY we are able to identify $dd \to {}^3\mathrm{He}n\pi^0$ and $dd \to {}^3\mathrm{He}p\pi^-$. For the first reaction around seven percent of data was analyzed, for the second fifteen percent. This implies, the collected amount of data is enough to calculate cross sections with good statistics.

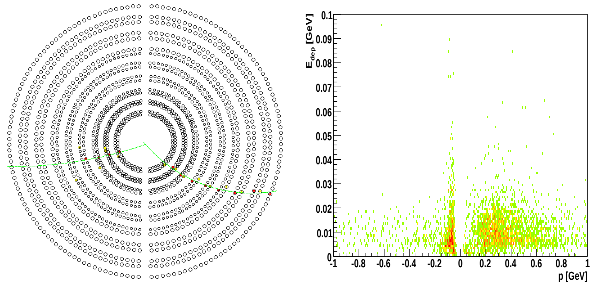

Fig. 3: Two tracks corresponding to p and π^- (left); energy deposited in PSB detector as a function of signed momentum taken from MDC (right)

References:

[1] COSY-Proposal - 173: "Charge Symmetry Breaking in $dd \to \alpha\pi^0$ ", Spokespersons: V.Hejny, A. Megiera
[2] G.A. Miller, B.M.K. Nefkens, and I. Šlaus, Phys. Rept. **194**, 1 (1990).

[1] Institut für Kernphysik, Forschungszentrum Jülich
[2] Nuclear Physics Department, Jagiellonian University, Cracow, Poland

Identification of pions and electrons using the WASA–at–COSY facility

M. Janusz[1,2], A. Kupść[3], C.F. Redmer[2], L. Yurev[2,4]

The WASA detector [1] is divided into a forward (FD) and a central (CD) part. Charged particles from decays of the produced meson have to be identified and their momenta should be precisely measured. The reconstruction is based on the information from the CD componentes: Mini Drift Chamber (MDC), Plastic Scintillator Barrel (PSB) and Scintillator Electromagnetic Calorimeter (SEC).
Data collected during the first production run for the $pp \to pp\eta$ reaction (April/May 2007) have been used to test different methods of identification of charged pions and electrons. The decays $\eta \to \pi^+\pi^-e^+e^-$, $\eta \to \pi^+\pi^-\gamma$ and $\eta \to e^+e^-e^+e^-$ are presently analysed A data sample with two tracks in the FD consistent with protons and with two or more tracks in the MDC has been selected. The MDC inside the solenoidal field provides the curvature of tracks (leading to the determination of the momentum) and sign of the electric charge of the particles. Only events where the charge is balanced are processed. An example event with four tracks is shown on the single event display for the MDC detector in Fig. 1.

In a first step identification electron-positron pairs could be identifiedd reliably by requiring a small opening angle between two tracks of particles with opposite charges. The method is motivated by the fact that electrons and positrons are mostly created in conversions of virtual or real photons and their momenta are mostly parallel.

Electrons and pions are separated by a correlation plot of the deposited energy in PSB (ΔE) or in the SEC (E) as a function of the reconstructed momentum from the MDC (p). Figs. 2,3 present the experimental $\Delta E - p$ and $E - p$ plots respectively. The separation between particles of opposite charge is obvious. With both methods pions and electrons are clearly separated. Theseparticle identification methods are now beeing applied in the analysis of charged η decay channel.

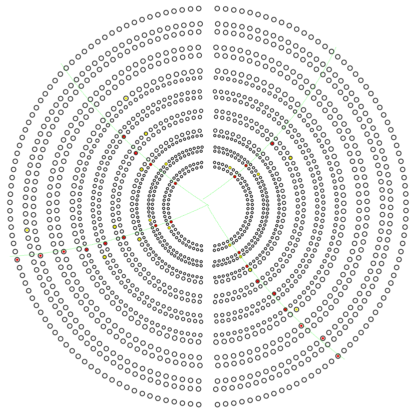

Fig. 1: Event with four charged tracks reconstructed in the MDC. The solid lines indicate tracks recognized by reconstruction algorithm, full dots denote MDC hit tubes.

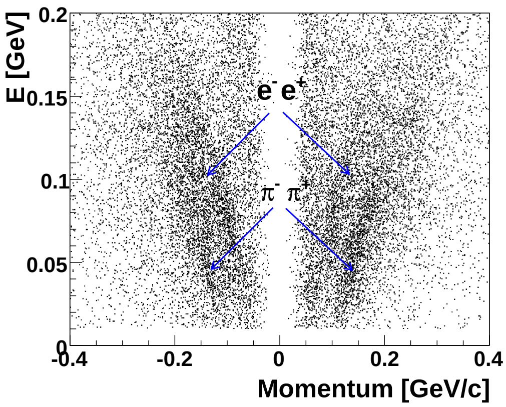

Fig. 2: The E-p identification method using SEC and MDC.

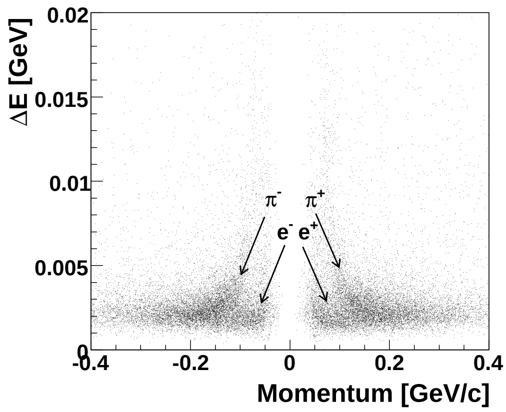

Fig. 3: The $\Delta E - p$ identification method using PSB and MDC.

References:

[1] J. Zabierowski et al., Phys. Scripta, **T99**, 159, (2002).

[1] Institute of Physics, Jagellonian University, PL 30-059 Cracow, Poland
[2] Institute für Kernphysik, Forschungszentrum Jülich
[3] Department of Physics and Astronomy, Uppsala University, SE-75120 , Uppsala, Sweden
[4] Dzhelepov Laboratory of Nuclear Problems, JINR, RU 141980 Dubna, Russia

Forward tracker calibration for the WASA–at-COSY experiment

M. Janusz[1,2], M. Jacewicz[4], L. Yurev[2,3]

The analysis of the first data taken with WASA–at–COSY Forward Proportional Chamber (FPC) [1] is presented. Data were recorded at a beam energy of 400 MeV proton scatterted elastically. Here we present results of the drift distance determination of the FPC operated with newly designed electronics [2, 3].
The common start time (T_0) of the signal which, varies from event to event is related directly to the trigger condition. It depends on the number of elements and planes involved in the trigger logic [4]. The reference time can be expressed by following equation:

$$T_0 = T_{tof} + T_{scint} + T_{offset} \tag{1}$$

where T_{tof} is the time–of–flight of registered particles, the T_{scint} is the light propagation in the scintillator counters and T_{offset} denotes the time delay due to the used electonics and cables.
During data collection the FPC delivers time records corresponding to the drift time. Simultaneously a lot of random coincidence signals are coming in the same time interval. Therfore, as a first step we clean the event bank and record only hits orginating from protons and pions penetrating the tracker.

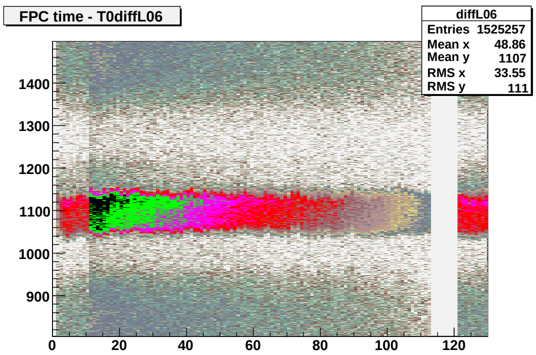

Fig. 1: The time difference ΔT between T_{FPC} and T_{FTH} (y–axis) versus straw number of the seventh layer of the FPC tracker (x–axis).

All time spectra are shifted in respect to each other due to individual delays of readout electronic and signal cables. Time offsets have been found for each straw individually. The method of finding is realized by fitting a function in the form presented below:

$$f(x) = P_1 \cdot e^{\frac{1}{2}\left(\frac{(x-P_1)}{P_2}\cdot\frac{(x-P_1)}{P_2}\right)} \tag{2}$$

The offset–corrected raw time spectrum is shown in Fig. 1.
At this stage of the calibration it is possible to determine the hit region with the accuracy of the straw dimension. This method is called binary mode of the chamber operation.
In order to determine the relation between the drift time and the distance to the wire, corrected time spectra are integrated in the drift time region to evaluate the drift velocity and finally calculate drift distance. Due to the used gas mixture[1] the drift distance is a linear function of the drift time, so linear regression permits to extract the drift velocity. This method can be used as a first approximation of the drift–time–to–drift–distance relation in the analysis procedure. Results prepared for all planes separately[2] are summarized in the table below.

Calibration results		
layer	velocity [cm/ns] 1st half	2nd half
1*	0	0
2*	0	0
3	0.033829	0.031993
4	0.032995	0.031557
5	0.045872	0.032384
6	0.045390	0.032051
7	0.033997	0.034857
8	0.033881	0.034915

* layers were not in the operation during the April/May production run

The missing mass technique needs a precise track reconstruction. This fact requires a good description of the region with non linear electric field – close to the cathode and the anode wire. Precise determination of the drift distance is performed by the interpolating discrete drift–to–distance function event by event. The radial distribution obtained by the presented way is shown in Fig. 2.

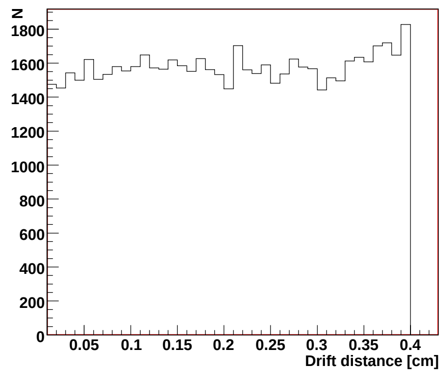

Fig. 2: Distribution of the drift distance obtained by the interpolation method.

Finally the calibration of the time–to–distance relation provides correction for the position of hit obtained in binary mode and final reconstruction of the track. An example of the iterative reconstruction is presented in Fig. 3.

[1]80% Ethane and 20% Argon
[2]Since the drift time is common in for all straws and lies in the range of 100 - 150 ns the summarized drift time of full half–planes is used for the the drift distance evaluation.

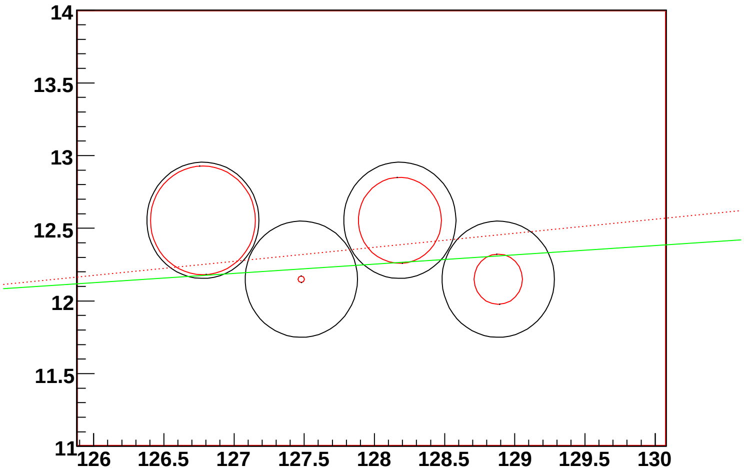

Fig. 3: The event display designed for the FPC chamber. Red circles depict the drift distance. Lines: red – presents preliminary fit, green – final fit results.

References:

[1] J. Zabierowski et al., Phys. Scripta, **T99**, 159, (2002).
[2] H. Kleines et al., IEEE Trans. Nucl. Sci **53**, 893 (2006).
[3] http://www-hep.phys.cmu.edu/cms
[4] M. Bashkanov – private communication (2008).

[1] Institute of Physics, Jagellonian University, PL 30-059 Cracow, Poland
[2] Institute für Kernphysik, Forschungszentrum Jülich
[3] Dzhelepov Laboratory of Nuclear Problems, JINR, RU 141980 Dubna, Russia
[4] Department of Physics and Astronomy, Uppsala University, SE-75120, Uppsala, Sweden

Mini Drift Chamber calibration at the WASA-at-COSY facility

L. Yurev[1,2], M. Jacewicz[3] for the WASA-at-COSY collaboration

The Mini Drift Chamber provides track coordinate information from charged particles in the central part of WASA. It consists of 1738 straw tubes with different diameter. Calibration of the MDC is based on the drift time measurement in each tube to determine the *time-to-distance* relation. The MDC calibration procedure must be performed for stable operational conditions (high voltage, thresholds on electronics, gas mixture) and redone in case of changes. The time is measured relatively to the trigger signal which may vary event by event. Therefore, only events from one trigger were selected, corresponding to one charged particle in the PS and one charged in the first plane of the FRH from elastic proton-proton scattering at 600 MeV.

Time alignment in the MDC. The first step of the MDC calibration is to align the initial time in all tubes[1]. Time is measured with a TDC-F1[1] individually for each tube[2]. It means there are 1738 different cables and electronic delays. These time offsets are determined by individually fitting raw spectra from the TDCs with Fermi functions:

$$f(x) = P_3 + \frac{P_2}{1 + e^{\frac{x - P_0}{P_1}}} \quad (1)$$

The greatest value among 20% from maximum of time spectra and P_3 is selected as an individual time offset.

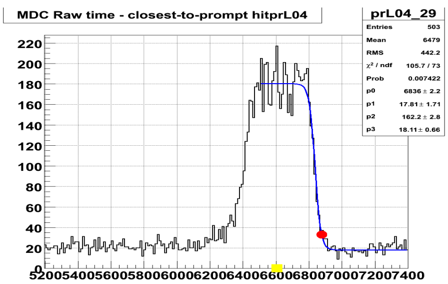

Fig. 1: "Raw" time spectra in one MDC tube fitted with Fermi function. The time corresponding to the wire position is marked in red. Maximum point of time spectra is marked in yellow.

A corresponding table is filled with the acquired time offsets and raw time values are corrected for each tube.

Time-distance parameters. The second procedure in the calibration is the extraction of time-distance parameters, which implies transformation of drift time into drift distance inside the tube. There are three groups of straws with the same tube diameter, but 17 layers. The time-distance parameters were obtained individually for each MDC layer. The time-distance relation in a drift tube depends on the gas mixture, $Ar + 20\% C_2H_6$ was used to achieve high electron multiplication with relatively low voltage applied to the wire. Another feature of this gas mixture is its "linearity" - it provides a homogeneous drift velocity along the radius of tube. Therefore, in the first order, only one parameter contributes to the time-distance relation, the drift velocity.

[1] H.Kleines et al., IEEE. Trans.Nucl.Sci.53(2006) p.893-897

[2] The time is measured in common stop mode, so the time axis is inverted in the raw time spectra

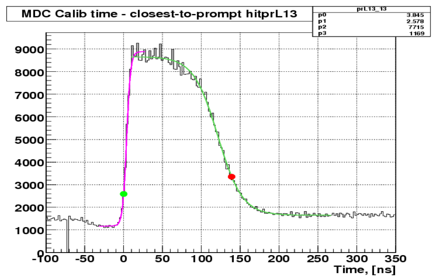

Fig. 2: A wire position is marked in green, a wall position is marked in red.

There are two general steps:

• Subtraction of the background and integration of the time spectra afterwards for getting drift function. The time spectra for individual layers is determined assuming all tubes within the layer to have the same drift function. Fermi and reversed Fermi functions were used for fitting time spectra. At this stage the aligned time was already used, that means time offsets were applied to each tube in order to reduce edge fluctuations of the drift region - especially a wire position. Supposed limits of drift region are marked in the Fig.2: green is a wire position and red - a wall position.

• Fitting of integrated spectra - drift function - takes place in the supposed drift region with a straight line(Fig.3). As can be seen from Fig.3, the drift function is linear in the wide range even for tubes with 8 mm diameter, a deviation occurs only in region very close to the wall of the tube due to inefficiency of a tube by itself. Finally, two tables with constants

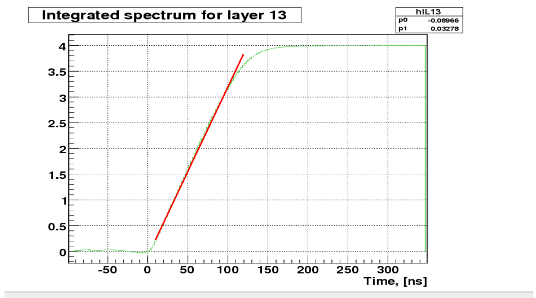

Fig. 3: Drift function for the tubes with 8 mm diameter is green line and linear fit is marked in red.

provide the calibration of the MDC: individual time offsets for each tube and time-distance parameters for each layer.

References:

[1] M. Jacewicz, "Measurement of the Reaction $pp \rightarrow pp\pi^+\pi^-\pi^0$ with CELSIUS/WASA at 1.36 GeV"

[1] Joint Institute for Nuclear Research, Dubna, Russia
[2] Institut für Kernphysik, Forschungszentrum Jülich, Germany
[3] Department of Nuclear and Particle Physics, Uppsala University, Sweden

Investigation of pp Elastic scattering for a luminosity measurement

Neha Kiritkumar Shah*

In any experiment it is essential to determine the luminosity as an essential ingredient in the study of excitation functions. To determine the time integrated luminosity in the WASA experiment at COSY for the proton on proton run, we propose to utilize the available data on the elastic scattering of protons.
To clean up the data, one can ensure the following physical constraints, for an elastic collision between two particles of equal mass:

$$|\phi_1 - \phi_2| = \pi \qquad (1)$$

$$tan\Theta_{1,lab} * tan\Theta_{2,lab} = \frac{1}{{\gamma_{cm}}^2} \qquad (2)$$

Equation (1) is the co-planarity condition and equation (2) is known as kinematical correlation. The Lorentz factor γ_{cm} describes the movement of the laboratory system with respect to the center of mass systems and can be written as

$$\gamma_{cm} = \sqrt{1 + \frac{T_{lab}}{2m}} \qquad (3)$$

where T_{lab} is the kinetic energy of the incident beam and m is the rest mass of the beam particle. For a proton beam with beam energy T_{lab}=1.4 GeV.

Beam kinetic energy	T_{lab} = 1.4 GeV
Total energy in CM	$\sqrt{s}$ = 2.4844 GeV
Lorentz Factor	γ_{cm} = 1.3215
Symmetric angle	$\Theta_{sym} = 37.12°$

TABLE I: Kinematical parameters characterizing the pp elastic scattering.

Θ_{sym} is the symmetric angle, where both protons have the same laboratory scattering angle.

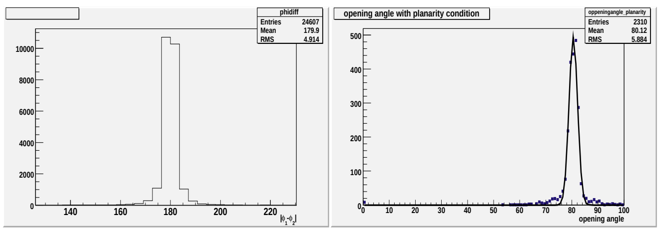

(a) **(b)**

FIG. 1: (a) Co-planarity distribution for data and (b) opening angle with co-planarity condition for data

The pp elastic scattering has been measured in several experiments at COSY, IUCF, and SATURNE [3]. The EDDA experiment at COSY has contributed substantially to several observables of the pp elastic scattering and is compiled in a comprehensive database called SAID[1].

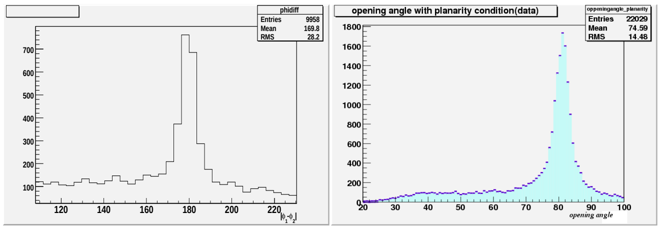

(a) **(b)**

FIG. 2: (a) Co-planarity distribution for data and (b) opening angle with the co-planarity condition for data

Monte Carlo simulations of the pp elastic scattering events(10K) are generated by using event generator. The pp elastic scattering events are selected with the condition that we have one charged track in the Forward Detector(FD) and one charged track in the Central Detector(CD)[2, 3]. The opening angle and co-planarity distribution are plotted for the simulated data(Figure 1). The co-planarity distribution peaks as expected, peaks at the value of 180° (Figure 1(a)). By using the co-planarity cut set to three $\sigma(\sigma = 2.4°)$ around the mean value(= 180°), opening angle between two charged tracks is plotted in Figure 1(b). The co-planarity distribution and opening angle(with the same co-planarity cut as in simulation) are plotted for raw data taken in April 2007 in Figure 2.
We are now in the process of fitting the background to determine the yield of the pp elastic scattering. Once this is done using the earlier measurements we can determine the luminosity.

References

[1] R. A. Arndt, I. I. Strakovsky and R. L. Workman, Nucleon nucleon elastic scattering to 3-GeV, Phys. Rev. C 62, 034005 (2000).

[2] H.-H. Adam et al, Proposal for the Wide Angle Shower Apparatus (WASA) at COSY-Juelich,COSY Proposal(2004), e-Print arXiv:nucl-ex/0411038.

[3] Levent Demiroers, Investigating Interactions of Deutrons and Protons with the Hydrogen Pellet Target of the CELSIUS/WASA experiment, Dissertation thesis, University of Hamburg.

* Indian Institute of Technology Bombay, Mumbai, India

e^+e^- Identification for the Reaction $pp \to pp\eta \to pp\gamma e^+e^-$

H. Bhatt*

We intend to investigate the transition form factor of the η meson by looking at the decay $\eta \to \gamma\gamma^* \to \gamma e^+e^-$. The invariant mass of the lepton pairs is equal to the four momentum transfer squared ($q_l^2 = m_{l^+l^-}^2$). This channel can serve as a probe of spatial structure of the region of interaction.

The q^2 dependence of the transition form factor in the Vector Dominance Model[1] is given by

$$F^{VDM}(q^2) = \sum_V \frac{g'_{PV\gamma}}{2g_{V\gamma}} \frac{M_V^2}{M_V^2 - q^2}$$

Where $g_{V\gamma}$ are SU(3) symmetric coupling of vector mesons to the photon and $g'_{PV\gamma}$ are SU(3) symmetric coupling of vector mesons to psuedoscalar meson and photon. The slope parameter at small q^2 can be obtained by taking the derivative of the above equation with respect to q^2:

$$\frac{dF(q^2)}{dq^2}\Big|_{q^2=0} = \frac{1}{\Lambda^2}$$

The VDM model predicts Λ_η = 0.75 GeV. The following tables gives the value of Λ_η as measured by different experiments .

Experiment	Λ_η
CLEO	0.774 ± 0.011 GeV [2]
IHEP	0.72 ± 0.09 GeV [3]
TPC-2γ	0.70 ± 0.08 GeV [4]
CELLO	0.84 ± 0.06 GeV [5]

TABLE I: Experimental results for the pole mass Λ_η

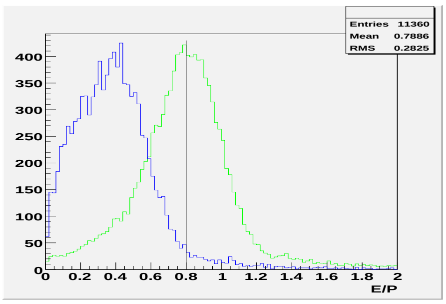

FIG. 1: E/P ratio for leptons ($\eta \to e^+e^-\gamma$, green) and pions ($\eta \to \pi^+\pi^-\gamma$, blue) from simulations.

To analyze the rare decay channel $\eta \to e^+e^-\gamma$ ($\Gamma_{e^+e^-\gamma}/\Gamma_{tot} = (6.0 \pm 0.8) \times 10^{-3}$), charged particle identification is necessary. In simulation studies, we have used the ΔE $-$ P method for identification of charged particle which do not stop in the MDC. 50K Monte Carlo events are generated using the Pluto event generator. In the analysis, events are selected with two oppositely charged tracks and one neutral hit in the Central Detector (CD) and two charged tracks in the Forward Detector (FD). In the data, similar reactions, $\eta \to \pi^+\pi^-\gamma$ and $\eta \to \pi^+\pi^-\pi^0$ also satisfy the same conditions with larger branching ratio ($\Gamma_{\pi^+\pi^-\gamma}/\Gamma_{tot} = (4.69 \pm 0.10) \times 10^{-2}$). Therefore, we need to distinguish the leptons from pions.

We have generated E/P ratio plots, i.e. the ratio of energy loss in the electromagnetic calorimeter (SEC) to the momentum reconstructed from the track curvature in the central drift chamber (MDC), for both charged decay channels in Fig 1. Here, we can see that for leptons the E/P ratio peaks around 0.8 and for pions the E/P ratio peaks around 0.4. Here we are using the events which have E/P > 0.8, we are able to separate the pions from the leptons. Similarly, an opening angle cut on angles $< 20^0$ is applied to select electrons, as discussed in [6].

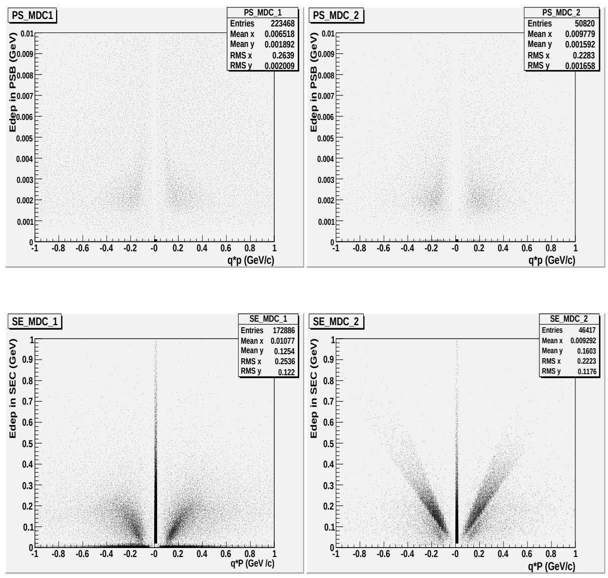

(a) **(b)**

FIG. 2: The ΔE $-$ P method for PSB (top) and SEC (bottom) for data taken in April 2007(a) for small opening angle less than 20^0 and (b) for E/P grater than 0.8.

In fig. 2 we have plotted the energy deposited in the PSB (Plastic Scintillator Barrel) and calorimeter given as a function of momentum from MDC for data taken in April 2007. Here a positive (negative) momentum corresponds to positively (negatively) charged particles.

In fig. 2(a), those events are selected which have less than 20^0 opening angle and in fig. 2(b), those events are selected which

Simulations for a Feasibility Study of the Reaction $pp \to pp\eta \to pp\pi^0\gamma\gamma$ with WASA at COSY

K. Chandwani*

Quantum Chromodynamics (QCD), the accepted theory for strong interactions based on quark and gluon degrees of freedom, is not calculable at low energy. Chiral Perturbation Theory (χPTh), an effective field theory of QCD, where the baryons and mesons are effective degrees of freedom is used in this energy regime of low momentum transfer. In the non perturbative regime of QCD, where effective field theories have to be used, χPTh is the most successful. It therefore becomes imperative to test this theory to higher precision.

The measurement of the branching ratio for $\eta \to \pi^0\gamma\gamma$ is a precision test of χPTh as the leading order and next to leading order do not contribute to it. The first sizeable contribution comes from $O(p^6)$ and therefore the measurement provides a stringent test for the theory. There have been a number of experiments to measure the BR of the decay channel $\eta \to \pi^0\gamma\gamma$ with contradictory results because of the orders of magnitude larger backgrounds coming from other decay channels (Table 1).

Experiments	BR ($\eta \to \pi^0\gamma\gamma$)
GAMS-2000	$(7.1 \pm 1.4) \times 10^{-4}$ [1]
Crystal Ball	$(3.5 \pm 0.7_{stat} \pm 0.6_{syst}) \times 10^{-4}$ [2]
KLOE	$(8.4 \pm 2.7_{stat} + 1.4_{syst}) \times 10^{-5}$ [3]

Table 1: Experimental Measurements

The situation is equally uncertain on the theoretical front. This is primarily because there are 96 terms which contribute at order p^6. The calculation of these terms is not straightforward.

Thus there is an urgent need to improve the accuracy of the BR measurements and to provide more restrictive constraints for theory by also measuring the distributions of particles from the decay.

Here we present first simulation results concerning the feasibility for the proposed study with the WASA detector, using the reaction $pp \to pp\eta \to pp\pi^0\gamma\gamma$ at COSY. The essential difficulty in the identification of this decay is due to the channel $pp \to pp2\pi^0$ which has a cross section of 250 μb. To optimize the cuts, we have analyzed Monte Carlo data (1 million events) for the decay $\eta \to \pi^0\gamma\gamma$ and the background channel $pp \to pp2\pi^0$ at a beam energy of 1.4 GeV.

To reduce the contribution of the $2\pi^0$ channel in our study, we use the following cuts

1. The missing Energy of the system $pp \to pp\pi^0\gamma\gamma$ has to be in the range of -0.2 to 0.2 GeV.

2. Sum of the kinetic Energy of two out going protons has to be in the range of -0.3 to 0.8.

3. The two photons not forming a π^0 have their invariant mass different from the π^0 invariant mass by $(M_{\gamma\gamma} - M_{\pi^0}) > 0.04$ GeV.

4. Cut on the missing mass of two scattered protons in the range of the η mass, $0.530 < MM_{pp} < 0.560$ to get η events.

The results are shown in Figures 1 and 2. Here the invariant mass spectra and missing mass spectra from MC are scaled according to cross section. We are now investigating how to increase the signal to background ratio further.

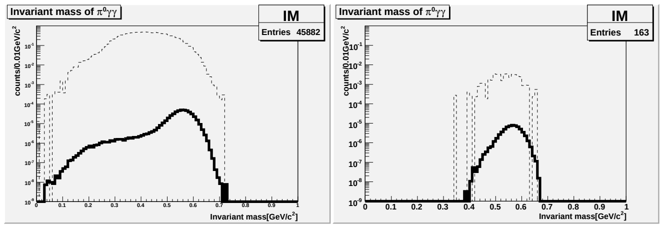

(a) (b)

Figure 1: Invariant Mass of $\pi^0\gamma\gamma$ in the Central Detector (a) without cut (b) with cuts from 1 to 4. Dashed line: $pp \to pp2\pi^0$ and solid line: $\eta \to \pi^0\gamma\gamma$.

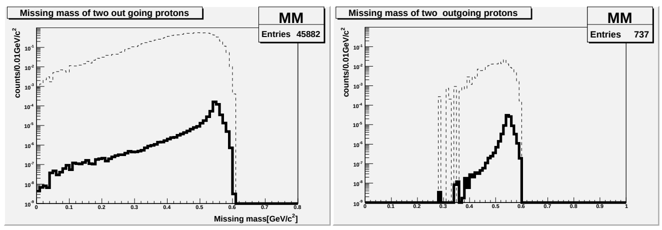

(a) (b)

Figure 2: Missing Mass of the two outgoing protons in the Forward Detector (a) without cut (b) with cuts from 1 to 3. Dashed line: decay $pp \to pp2\pi^0$ and solid line: $\eta \to \pi^0\gamma\gamma$.

References

[1] D. Alde et al., Z. Phys. C 25 (1984) 225.
[2] Prakhov et al., Phys. Rev. C 72 (2005) 025201.
[3] B. Di Mico et al., Acta Phys. Slov. 56 (2006) 403.

* IIT Bombay, India

Preparations of studies of the analysing power for the $\vec{p}p \to pp\eta$ reaction with WASA-at-COSY

M. Hodana[1,2], A. Kupść[3], P. Moskal[1,2] for the WASA-at-COSY Collaboration

In this report we give an account of the preparations of the measurement of the analysing power for the $\vec{p}p \to pp\eta$ reaction. We intend to carry out the measurement using the azimuthally symmetric WASA detector and the vertically polarized beam of COSY. The aim of the planned investigations is the determination of the interference terms contribution to the partial waves. Some of the terms are inaccessible from the spin averaged observables. Decomposition of the amplitude of the $pp \to pp\eta$ reaction into partial waves contributions is mandatory for an unambiguous understanding of the production process independent of the theoretical paradigm.

In the first step we have examined the geometrical acceptance of the WASA detector for the $pp \to pp\eta$ reaction as a function of the polar and azimuthal angles of the η meson emission in the reaction center-of-mass system. Calculations has been made for excess energies in the range from 10 to 400 MeV with the use of the GENBOD program for the generation of particles momenta. At present we consider only the decay of the η meson into two gamma quanta, which provides a conservative estimate of the measurement possibilities. The protons from the $pp \to pp\eta$ reaction will be registered in the Forward Detector (polar angles 2.5° to 18°) and the photons from the decay will be detected in the electromagnetic calorimeter (polar angles 20° to 169°). The acceptance for two excess energies are presented in Fig. 1. The simulations shows full coverage of the θ-ϕ space in the whole range of the excess energies. To study the asymmetries as a function of the $\cos\theta$, we divide the range into ten bins and assume the avarage luminosity of $10^{31} cm^{-2}s^{-1}$ and a beam polarisation of 0.8. We estimate that data from a one day run at each energy are sufficient to reach a statistical accuracy of the asymmetry better than ± 0.01 for each angular bin.

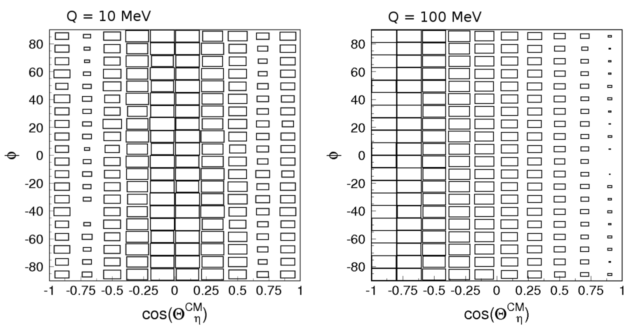

Fig. 1: Geometrical acceptance of the WASA apparatus for measurements of the $pp \to pp\eta \to pp\gamma\gamma$ reaction at excess energies of 10 MeV (left) and 100 MeV (right) for the η meson production.

At present we are working on the identification of sources of the systematic errors and the estimations of their influence on the measured asymmetries. Due to the azimuthal symmetry of the detector and the possibility of the spin flipping of the COSY beam most of the uncertainties will be suppressed by using the geometrical mean from the production yields, normalised to the efficiency and luminosity, obtained with the different spin orientations:

$$N_- = \sqrt{\frac{N\uparrow_R}{\epsilon_R L^\uparrow}\frac{N\downarrow_L}{\epsilon_L L^\downarrow}}, \quad N_+ = \sqrt{\frac{N\uparrow_L}{\epsilon_L L^\uparrow}\frac{N\downarrow_R}{\epsilon_R L^\downarrow}}, \qquad (1)$$

which are used for the determination of the analysing power according to the formula:

$$A_y(\theta) = \frac{1}{P cos\phi}\frac{N_+(\theta,\phi) - N_-(\theta,\phi)}{N_+(\theta,\phi) + N_-(\theta,\phi)}, \qquad (2)$$

where P denotes the beam polarization and N_+ and N_- are production yields of the η mesons obtained using the Madison convention (see Fig. 2)[1]. The background free production yields N_L and N_R will be established from the proton-proton missing mass spectra reconstructed for each of the angular bins separately. Determination of

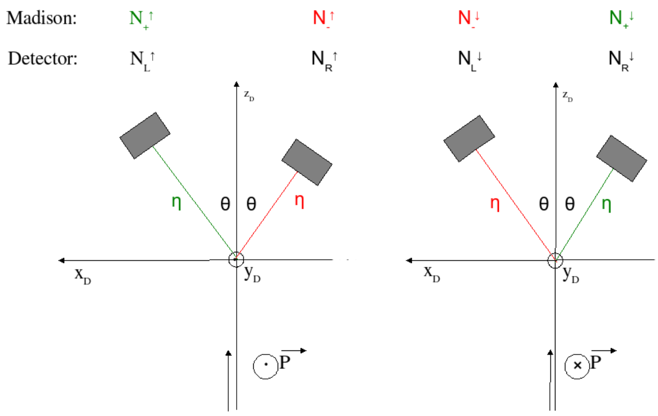

Fig. 2: Illustration of the Madison convention. A given event contributes to the N_+ yield if the vector product of the beam and the η meson momenta is parallel to the polarisation vector, and to N_- if it is antiparallel.

the beam polarisation and the control of the systematic uncertainties will be done by the concurrent measurement of the well known asymmetries e.g. for the proton proton elastic scattering.

We conclude that the features of the WASA detector: axial symmetry and large acceptance together with the possibility to flip spin polarization of the COSY beam will allow to achieve a two orders of magnitude better accuracy for the analysing power than the previous measurements [2].

References:

[1] Conference Proceedings: "Polarisation Phenomena in Nuclear Reactions", University of Wisconsin Press, Madison (1971) pp. XXV.

[2] R. Czyzykiewicz et al., Phys. Rev. Lett. **98** (2007) 122003.

[1] Institute of Physics, Jagellonian University
[2] Institute of Nuclear Physics, Research Center Jülich
[3] Department of Physics and Astronomy, Uppsala University

Estimate of the multimeson background for measurement of the η' decays with WASA-at-COSY

M. Zieliński[a], A. Kupść[b], P. Moskal[a]

The η' mesons for the rare decay studies with the WASA detector will be produced in the $pp \to pp\eta'$ reaction near the threshold. The identification of the $pp \to pp\eta'$ process will be performed by means of the missing mass of the two outgoing protons measured in the Forward Range Hodoscope (FRH). One of the sources of the background originates from multimeson (mainly 2π and 3π) production. For the decay channels with similar particles in the final state this background is crucial for the determination of systematical and statistical uncertainty. The background will appear as a continuum under the η' peak in the missing mass distribution.
The upper limit of the background can be estimated using the COSY-11 measurements of the $pp \to ppX$ reaction near the threshold for the production of the η' meson [1]. We have extracted differential cross section $\rho_B \equiv \left.\frac{d\sigma_B}{dm}\right|_{m=m_{\eta'}}$ for the production of the multimeson system with the invariant mass corresponding to the mass of the η' meson according to the formula:

$$\rho_B = \frac{N_B}{N_S}\frac{\sigma^{tot}_{\eta'}}{\Delta m}, \qquad (1)$$

where N_B number of measured background events, N_S number of registered $pp \to pp\eta'$ events, $\sigma^{tot}_{\eta'}$ is the total cross section for the η' meson production and Δm is the width of the signal. Table 1 shows the derived values of the ρ_B as a function of Q (center-of-mass excess energy for the $pp \to pp\eta'$ reaction), with corresponding statistical and systematical errors [2].

Q [MeV]	ρ_B [nb/MeV]	$\Delta\rho_B(stat)$ [nb/MeV]	$\Delta\rho_B(syst)$ [nb/MeV]
1.53	1.04	0.14	0.2
4.10	7.0	1.1	1.1
5.80	13.4	1.2	2.0
7.60	18.2	1.6	2.8
9.42	32.3	3.6	4.9
10.98	32.7	3.2	4.9
14.21	60	11	9.0
15.50	85	2.4	13
23.64	117	17	17
46.60	322	16	48

Table 1: Differential cross section for multipion production extracted form the COSY-11 data [1]

A satisfactory description of the Q dependence of ρ_B was obtained by a function of the following form:

$$\rho_B(Q) = \alpha(Q/Q_0)^\beta \qquad (2)$$

where Q_0=1 MeV and the parameters α and β were estimated to be $\alpha = 0.64 \pm 0.14$ nb/MeV and $\beta = 1.662 \pm 0.081$. The extracted values of ρ_B with the superimposed fit are shown in Fig. 1.
The established differential cross section can be treated as an upper limit for the expected background from $pp \to pp\pi^+\pi^-\pi^0$ for the η' decay into $\pi^+\pi^-\pi^0$. The signal to background ratio expected for the WASA detector could be then

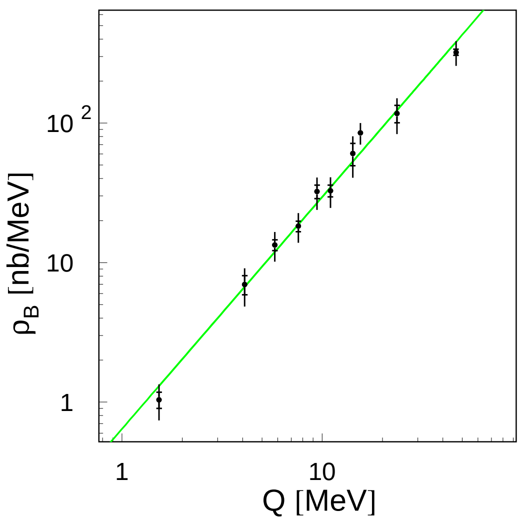

Fig. 1: Inclusive differential cross section for multipion production derived from the COSY-11 data [1]. Line – the function (2) fitted to the data.

calculated from ρ_B using formula (1) by replacing Δm by the WASA detector missing mass resolution and the cross section $\sigma^{tot}_{\eta'}$ by the product $\sigma^{tot}_{\eta'} \times BR(\eta' \to \pi^+\pi^-\pi^0)$.
By that means we can compute values of the expected continuum background as a function of the excess energy near the η' threshold. The value is an important ingredient for the preparation of the η' meson decays experiments at WASA-at-COSY and the estimates of the expected uncertainties and necessary duration of the experiments [3].

References:

[1] A. Khoukaz et al., Eur. Phys. J. **A20** (2004) 344;
P. Moskal et al., Phys. Rev. Lett. **80** (1998) 3202;
P. Moskal et al., Phys. Lett. **B 474** (2000) 416;
F. Hibou et al., Phys. Lett. **B 438** (1998) 41.

[2] M. Zieliński, Diploma Thesis, JU Cracow 2008, in preparation.

[3] M. Zieliński, et al., contribution in this report.

[a] Institute of Physics, Jagellonian University, 30-059 Cracow, Poland
[b] Department of Physics and Astronomy, Uppsala University, 75121 Uppsala, Sweden

Feasibility studies of the measurement of $BR(\eta' \to \pi^+\pi^-\pi^0)$ with WASA-at-COSY

M. Zieliński[a], P. Moskal[a], A. Kupść[b]

Studies of rare decays of the η and η' mesons are one of the most important goals of the WASA-at-COSY physics program. For example decay $\eta' \to \pi^+\pi^-\pi^0$ was pointed out as an accurate way of extracting the quark mass difference [1]. The process is possible only by isospin-violating interaction due to $(m_d - m_u)$ term in the QCD Lagrangian and as a consequence the decay width is proportional to $(m_d - m_u)^2$. The decay has been never observed and only an upper limit of 5% (90% CL) for the branching ratio has been reported [2]. Recent calculations based on chiral unitary approach predict the branching ratio to be about 1% [3].

An attempt to observe the decay will be made with the WASA-at-COSY facility. The η' mesons will be produced in two proton collisions via the $pp \to pp\eta'$ reaction. Due to huge background from direct production of three pions the experimental conditions must be carefully optimized. WASA detector is designed to work with maximum luminosity of $10^{32}\text{cm}^{-2}\text{s}^{-1}$. After what taking into account the detection and reconstruction efficiencies this leads to about 10^6 η' mesons tagged per day.

In order to find the optimum beam momentum for the measurement of the branching ratio (BR) for the $\eta' \to \pi^+\pi^-\pi^0$ decay we have studied the relative statistical uncertainty as a function of the excess energy (Q):

$$\frac{\sigma(BR)}{BR}(Q) = \frac{\sqrt{N_S + N_B}}{N_S}, \qquad (1)$$

where the N_S denotes the number of the signal events and the N_B indicates the number of the background events.

The values of N_S were estimated based on the known total cross section energy dependence for the $pp \to pp\eta'$ reaction and the assumptions for the BR based on the theoretical predictions. The values for N_B were extracted from the COSY-11 measurements [4]. The direct three pion production and the $\eta' \to \pi^+\pi^-\pi^0$ decay will be reconstructed with the best precision by using missing mass of the two outgoing protons measured in the forward detector. We have assumed that the kinetic energies of the protons will be extracted using energy loss method in the layers of the Forward Range Hodoscope and the directions are determined using the Forward Proportional Chambers. The momentum resolution of the COSY beam, extensions of the interaction region, the detection efficiency and the proton-proton final state interactions are also taken into account.

An example calculation of the branching ratio accuracy have been conducted assuming a one week experiment with luminosity L=$10^{32}\text{cm}^{-2}\text{s}^{-1}$ and five values of $BR(\eta' \to \pi^+\pi^-\pi^0)$: 5%, 2%, 1%, 0.75% and 0.5%. The Q dependence of $\sigma(BR)/BR$ is shown in Fig. 1. As expected the relative accuracy nearly scales with the value of the assumed branching ratio. The optimum accuracy is achieved for the excess energies between 60 and 90 MeV, independent of the BR magnitude.

The statistical uncertainty of the branching ratio will improve with time as $1/\sqrt{t}$. The dependence for the beam momentum of p_{beam}=3.45 GeV/c corresponding to the excess energy Q=75 MeV is shown in Fig. 2. The plot shows that for the BR equal 0.5% a relative accuracy of 10% would require two months of beamtime.

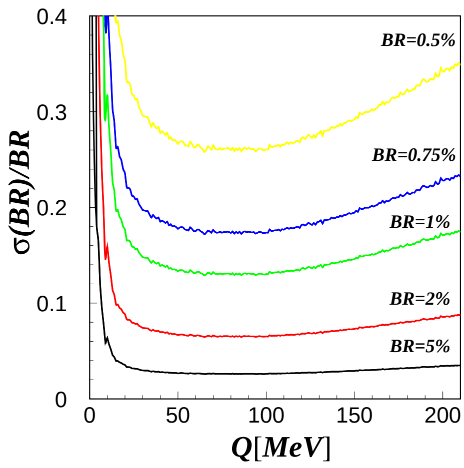

Fig. 1: The relative accuracy of the BR as a function of the excess energy Q for the $pp \to pp\eta'$ reaction. The results for the five values for BR are shown.

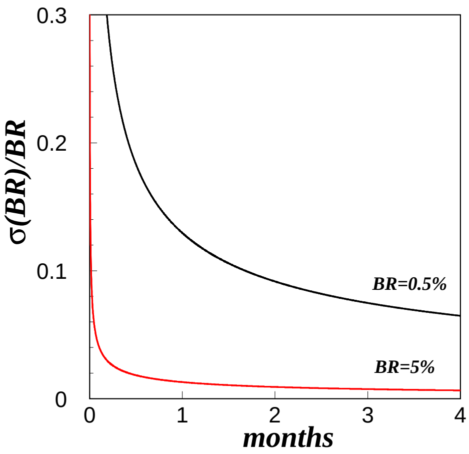

Fig. 2: The branching ratio accuracy as a function of measurement time in months.

An additional source of background, not discussed here, comes from other decays of η' involving similar particles: $\eta' \to \pi^+\pi^-\eta$ and $\eta' \to \omega\gamma$. This background can not be suppressed using the missing mass method.

References:

[1] D. Gross, et al., Phys. Rev. **D19** (1979) 2188;
H. Leutwyler, Phys. Lett. **B378** (1996) 313.

[2] A. Rittenberg, LBNL (1969), UCRL-18863, http://repositories.cdlib.org/lbnl/UCRL-18863.

[3] B. Borasoy, U. G. Meissner and R. Nissler, Phys. Lett. **B643** (2006) 41.

[4] M. Zieliński, et al., contribution in this report.

[a] Institute of Physics, Jagellonian University, 30-059 Cracow, Poland
[b] Department of Physics and Astronomy, Uppsala University, 75121 Uppsala, Sweden

Feasibility studies for the $\eta \to \pi^+\pi^-e^+e^-$ decay on behalf of WASA–at–COSY collaboration

M. Janusz[1,2], A. Kupść[3]

The decay of the η meson into $\pi^+\pi^-e^+e^-$ provides a unique test of CP symmetry in flavor conserving interactions. In the Standard Model (SM) the decay proceeds via direct emission of a virtual photon. A violation of the CP symmetry would lead to an asymmetry in the dihedral angle (ϕ) of the pion and lepton system [1, 2]. The effect would be analogous to that observed recently in K_L decays [3, 4]. The asymmetry is caused by the interference between direct and radiative emission of the virtual photon. The measure of CP violation is provided by the asymmetry A [5]:

$$A = \frac{N(0^\circ < \phi < 90^\circ) - N(90^\circ < \phi < 180^\circ)}{N(0^\circ < \phi < 180^\circ)}. \qquad (1)$$

In the SM the angular distribution $d\Gamma/d\phi$ can be expressed as ([5]):

$$\frac{d\Gamma}{d\phi} \propto 1 + 2\cos^2\phi. \qquad (2)$$

The distribution is given by the solid line in Fig. 1 where also the reconstructed distribution of the Monte Carlo simulated data is shown, indicating a flat detector efficiency over the whole ϕ range.

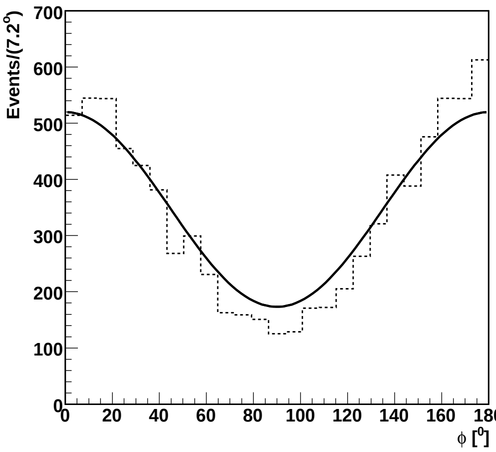

Fig. 1: Distribution of the dihedral angle ϕ angle: SM prediction (solid line), and WASA detector response (dashed line). The distributions are normalized to the same area.

The resolution in the ϕ angle is about 10° (FWHM) and constant (Fig. 2). For small asymmetries, i.e $N(0^\circ < \phi < 90^\circ) \approx N(90^\circ < \phi < 180^\circ)$ the statistical error can be approximated by:

$$\Delta A = \frac{\sqrt{N_S + N_B}}{N_S}. \qquad (3)$$

where $N_S = N(0^\circ < \phi < 90^\circ) + N(90^\circ < \phi < 180^\circ)$ and N_B are numbers of the signal and the background events after final selection, respectively. The overall acceptance and reconstruction efficiency is about 10%. A conservative estimate of the background leads to a relation $N_B \approx N_S$. From the theory it is important to probe the values of the asymmetry $A \leq 0.01$, what would require a data sample of $2{\times}10^4$ $\eta \to \pi^+\pi^-e^+e^-$ decays.

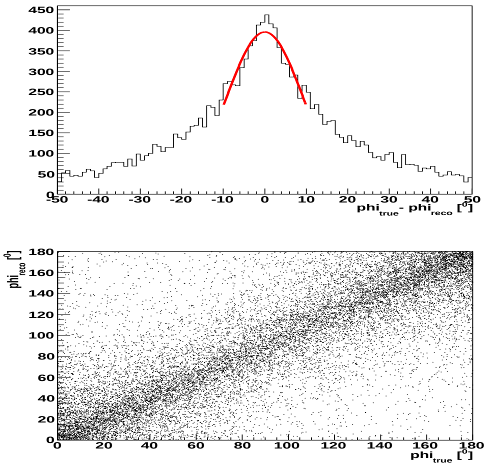

Fig. 2: Upper panel: resolution in the ϕ angle; lower: simulated (true) ϕ angle vs reconstructed.

The decay can also provide information about the transition Form Factor (FF), which can be extracted from the distribution of the dilepton invariant mass (q). The FF is usually parametrized by a single pole formula: $FF(q^2) = \Lambda^2/(\Lambda^2 - q^2)$. For the decay $\eta \to \pi^+\pi^-e^+e^-$ the q value is restricted to the range $4m_e < q^2 < m_\eta - 2m_\pi$. The statistical uncertainty of the slope parameter Λ was extracted from Monte Carlo data samples of $\eta \to \pi^+\pi^-e^+e^-$ decays generated with Λ set to 0.77 GeV. The accuracy of Λ can be parametrized as:

$$\Delta\Lambda = C\frac{\sqrt{N_S + N_B}}{N_S}. \qquad (4)$$

where $C \approx 20$ GeV. In order to get e.g. $\Delta\Lambda = 0.1$ GeV a data sample of more than 10^5 collected events is required.

References:

[1] D.-N. Gao, Mod. Phys. Lett. **A17**, 1583-1588 (2002).
[2] C. Q. Geng, J. N. Ng, and T. H.Wu, Mod. Phys. Lett. **A17**, 1489-1498 (2002).
[3] A. Lai, et al.(NA48 Collaboration), Eur. Phys. J. **C30** C30, 33-49 (2003).
[4] E. Abonzaid et al.(KTeV Collaboration), Phys. Rev. Lett. **96** 101801 (2006).
[5] H. Chew, Nuovo Cim. **26**, 1109 (1962).

[1] Institute of Physics, Jagellonian University, PL 30–059 Cracow, Poland
[2] Institut für Kernphysik, Forschungszentrum Jülich
[3] Department of Physics and Astronomy, Uppsala University SE–75120, Uppsala, Sweden

Feasibility studies on $pp \to pK^+\Lambda(1405)$ with WASA-at-COSY

W. Węglorz [1,2] for the WASA-at-COSY collaboration

One open question in hadron physics is the nature of the hyperon resonsance $\Lambda(1405)$. In order to gain further insight it is important to exclusively study its decay channels and separate it from neighbouring, overlapping resonances (mainly $\Sigma(1385)$). Recently, the neutral decay $\Lambda(1405) \to \pi^0\Sigma^0$ in the reaction $pp \to pK^+\Lambda(1405)$ was measured at COSY by the ANKE collaboration (see [1] and references therein).

The newly available WASA-at-COSY installation with its close to 4π geometrical acceptance for charged and neutral particles provides the opportunity to actively identify all the decay channels of the $\Lambda(1405)$. However, different to the ANKE setup no positive strangeness identification is available and, thus, the background situation might be more severe, which requires detailed feasibility studies.

As a first channel, the decay $\Lambda(1405) \to \pi^0\Sigma^0 \to (\gamma\gamma)_{\pi^0}(p\pi^-\gamma)_{\Sigma^0}$ has been chosen and Monte Carlo simulations have been carried out for the reaction $pp \to pK^+\Lambda(1405)$ at a beam momentum of 3.35 MeV/c. For the simulation all $\Lambda(1405)$ decay channels and the background reactions $pp \to pp\pi^+\pi^-\pi^0$, $pp \to pp\eta$, $pp \to pp\omega$, were taken into account. Although the final states of the latter reactions differ from the neutral $\Lambda(1405)$ decay mode, missidentified particles in the detector combined with high cross sections and large acceptance make these reactions contributing significantly to background.

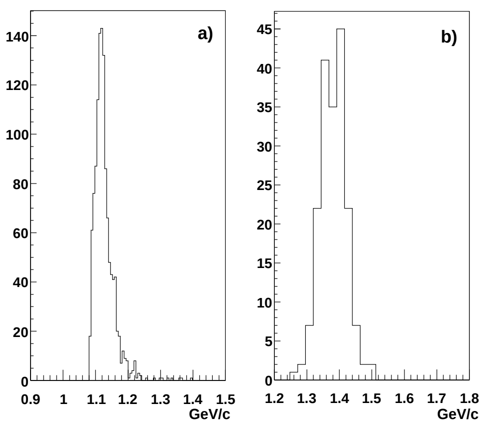

Fig. 1: Invariant masses of a) $\Lambda(1115)$ with combinatoric background, b) $\Lambda(1405)$.

At the current stage of analysis, the conditions for the identification of the reaction channel were the following: 3 charged tracks (two protons and one K^+) in the forward detector of WASA and 3 neutral tracks (3 photons) and one negatively charged track (π^-) in the central detector. Due to the missing kaon identification the K^+ and the two protons are treated equally in the first step of the analysis. They have to be combined with the three photons and the π^- in order to match the decay kinematics by means of missing mass and invariant mass. An example of the reconstructed invariant masses of the Λ ground state and the $\Lambda(1405)$ is shown in Fig 1. In order to select cleanly reconstructed events, the cuts currently in use are quite strong. Thus, for the neutral decay chain of the $\Lambda(1405)$ given above a geometrical acceptance of 24% has been obtained, but the total reconstruction efficiency is currently only at the level of 0.2%. The reconstructed invariant mass of $\Lambda(1405)$ together with the main background reactions is shown in Fig 2.

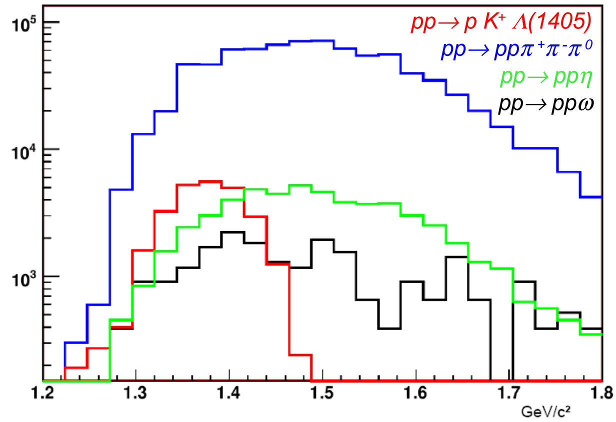

Fig. 2: Reconstructed invariant mass of $\Lambda(1405)$ with main background reactions.

Fig 2. shows that the current background suppression had to be improved by at least one order of magnitude. Further possibilities are under investigation. Since the new readout electronics provide quite precise time information, one option might be using time-of-flight in the forward detector for proton - K^+ separation. Further background discrimination will be introduced based on the analysis of the decay vertex of the Lamda ground state. For this tracking capabilities of the Mini Drift Chamber will be used. The corresponding reconstruction algorithms are under development. First results show that cutting on minimum vertex displacements of 2 cm is required for a substantial background reduction, which is within the scope of the MDC.

The aim is to finish the feasibility study until May 2008. At that time a beam time concerning η' decays at the same beam momentum will be carried out, which will allow to test the results.

References:

[1] I. Zychor, "Lineshape of the Lamda(1405) hyperon measured through its Sigma0pi0 decay", this Annual Report

[1] Institute of Physics, University of Silesia, 40-007 Katowice, Poland

[2] Institut für Kernphysik, Forschungszentrum Jülich

Scintillator series tests for the WASA Forward Trigger Hodoscope renewal

C. Pauly

The Forward Trigger Hodoscope, FTH, is an essential component of the WASA Forward Detector (FD) [1, 2]. It consists out of 96 individual plastic scintillator elements of 5mm thickness. The scintillators are arranged in one straight layer (48 elements) and two layers of counterrotating Archimedian-spiral shaped elements. The FTH provides fast signals on the charged particle multiplicity in the FD for the first level trigger, and is also used in the offline track reconstruction. Future trigger developments aim for a complete real time scattering angle reconstruction of individual tracks. This information, combined with the deposited energy information of successive detector layers, will allow to determine the missing mass of forward going particles on trigger level, and thus provides very efficient meson tagging. To suppress ambiguities when more than one particle track is in the FD (e.g. the two protons in the reaction $pp \rightarrow pp\,\eta$) simultaneous particle detection in all three FTH layers is essential and requires a high and homogeneous detection efficiency.

The present FTH detector was already in use for many years in the CELSIUS/WASA setup and suffered severe performance degration due to aging effects and radiation damage (see ref. [3]). Therefore the renewal of all plastic scintillator elements was initiated in 2006.

In order to control the quality of the new scintillator elements prior to installation a small test stand was set up, allowing the light output and uniformity of individual scintillator elements to be compared. The elements are tested inside a light-tight box with fixed light guide and multiplier assembly, allowing for tests even prior to wrapping the elements. For simplicity only a loose coupling to the light guide is used with a fixed mechanical alignment. Initial tests proved the good reproducibility of the light coupling of better than 10 %.

A collimated ^{90}Sr source positioned above the test scintillator is used to radiate the test elements at certain well defined positions, mechanically combined with a thin trigger scintillator below the test scintillator as shown in Fig. 1. The analog signal of the test scintillator multiplier readout is amplified using an integrating amplifier to suppress any dependence on the exact shape of the analog signal (which may vary with the position along the scintillator), and evaluated using a digital oscilloscope. The discriminated signal of the trigger scintillator located below the test scintillator is used to trigger the oscilloscope so that only high energy electrons from the source which fully transverse the test scintillator can contribute to the measurement. Use of a digital oscilloscope provides the possibility to automatically average and measure the signal amplitude; it eliminates the need for a full data acquisition system and thus allows for very quick and efficient measurements with sufficient accuracy.

A digitally controlled high-voltage supply ensures that the gain is reproducable for both PM tubes. A LED light pulser, coupled to the light guide via light fiber is used to monitor and control the long-term gain stability. A sketch of the setup can be seen in Fig. 1.

Using this setup, the first 20 scintillator spiral elements where tested directly after element wrapping, prior to gluing to their individual light guides. Results of this first test are shown in Fig. 2. The black lines show a comparison of the absolute light output of all individual elements as a function of the source position along the scintillator. All elements show a fairly uniform behavior, with a clear increase of light output close to the far end of the scintillator which is a typical and well known feature of this scintillator shape. The observed spread of light output can be partly explained by the varying scintillator thickness in the order of $\pm$ 10%. The highlighted curves in Fig. 2 show two measurements of the same scintillator separated several weeks. Their good agreement demonstrates the reproducibility of the measurement.

The new scintillator elements show a much higher and more uniform light output compared to the old elements presently installed in the WASA detector; their installation will significantly improve the performance of the FTH.

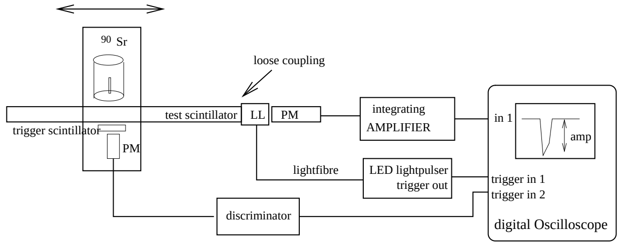

Fig. 1: *Schematic overview of the test setup consisting of the test scintillator, trigger scintillator, and readout electronics.*

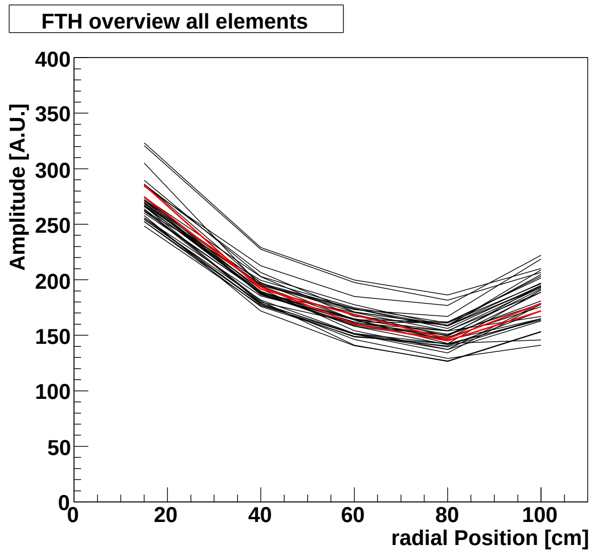

Fig. 2: *Comparison of light output as function of the position of the ^{90}Sr source for all tested scintillator elements.*

References:

[1] H-H. Adam et al., Proposal for the Wide Angle Shower Apparatus (WASA) at COSY-Jülich - “WASA-at-COSY”, nucl-ex 0411038.

[2] J.Zabierowski et al., The CELSIUS/WASA Detector Facility, T99 159-168 (2002).

[3] C. Pauly, ”In-beam efficiency study of the WASA trigger hodoscope”, IKP annual report 2006.

The renewal of the WASA Plastic Scintillator Barrel

P. Podkopał [1,2] and T. Smoliński [1,2]

The Plastic Scintillator Barrel (PSB) consists of a cylindrical part formed by 48 bars and two end caps of 48 trapezoidal elements each. The detector is placed inside the solenoid and surrounds the mini drift chamber (MDC). The purpose of this detector is twofold, it provides fast signals for the first level trigger logic (for separating neutral and charged tracks) and analog signals for particle identification. PID can be achieved either via the ΔE-E or the ΔE-p technique, using the corresponding information from calorimeter and MDC, respectively[1].

Prior to the installation at COSY, all elements had been tested with a ^{207}Bi source. The results of the study[2] had shown, that in the central part of the detector the light attenuation length for elements in use was mostly close to 50 cm whereas in case of spare elements it was around 200 cm. Moreover, during calibration of the PSB it turned out that for some scintillators the minimum ionizing particles are very close to noise level, although the voltage applied to the photomultiplier was at maximum. This situation made it necessary to lower the threshold, which however implied less clean trigger conditions. As a consequence of both results, the decision has been taken to exchange the central part of the PSB detector.

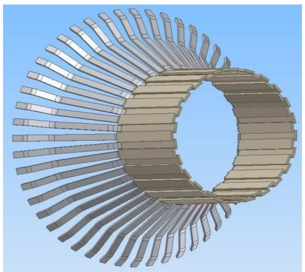

Fig. 1: View of PSC (central part of Plastic Scintillator Barrel) detector.

The scintillators were wrapped first in aluminium foil (13 μm thick) and then protected by a 50 μm thick tedlar foil. Each element was attached to an acrylic light guide wrapped in 13 μm aluminium foil and 220 μm thick polyester tape. All counters are equipped with two optical fibres to inject the signals from the light pulser system. In order to check the performance of the new elements, laboratory tests with ^{207}Bi were carried out to extract the attenuation length. The radioactive source emits monochromatic electrons via electron capture with energy lines at E_{e^-} = 0.481 MeV, E_{e^-} = 0.975 MeV and E_{e^-} = 1.047 MeV. It was positioned along each scintillator at five equally shifted points. Signals from the counters were then split into two branches. One branch was used to construct the trigger via a threshold discriminator while the second branch after amplification was delayed in order to compensate the time for trigger generation. After digitization the data were ready for analysis. Each spectrum was fitted (see Fig. 2) using the sum of an exponential function and two Gaussians for background and signal, respectively. Using the fit parameters, the dependence of the loss of light along the scintillator was extracted. The light attenuation (Fig. 3, left) can be derived by fitting an exponential function. It has been found that the light attenuation for the new elements is around 200 cm. In comparison with the results obtained for the old scintillators a significant difference of around factor was observed i.e. the length after which the light intensity is reduced by factor e^{-1} is four times larger in case of the new elements. In Fig. 3 (right plot) the relative energy resolution for E_{e^-} = 1.047 MeV is presented as a function of the irradiation position. In addition in Fig. 2 peak stemming from E_{e^-} = 0.481 MeV can be observed. This peak was not visible for old elements due to cracks and other damages caused by radiation.

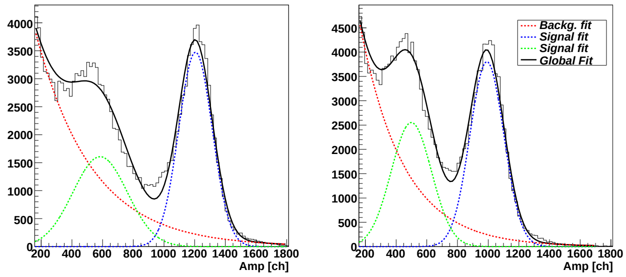

Fig. 2: Peak position for source location closest to the photomultiplier and at the edge of the element (left and right, respectively)

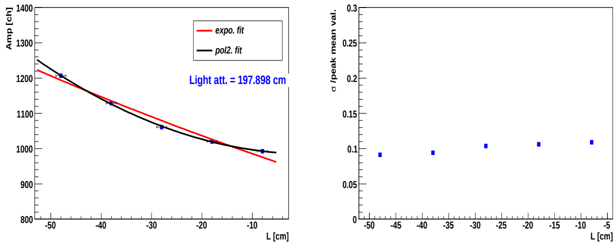

Fig. 3: Light intensity as a function of position (left) and relative energy resolution (right).

References:

[1] M.Jacewicz, Measurement of $pp \rightarrow pp\pi^+\pi^-\pi^0$ with CELSIUS/WASA at 1.36 GeV, PhD thesis, Uppsala University (2004).

[2] I.Keshelashvili, M. Mittag, Test of the WASA Plastic Scintillator Barrel, contribution to Annual Report 2006.

[1] Institut für Kernphysik, Forschungszentrum Jülich

[2] Nuclear Physics Department, Jagiellonian University, Cracow, Poland

New Forward Window Hodoscope for WASA

A.Pricking[a,b], M.Bashkanov[a], J. Bisplinghof[b], H.Clement[a], E. Doroshkevich[a], F. Hinterberger[b], O. Khakimova[a], F. Kren[a], T. Skorodko[a] and G. J.Wagner[a] for the WASA-at-COSY Collaboration

In order to run at highest possible luminosities WASA has been upgraded by a new Forward Window Hodoscope. It covers the conical exit window of the cylinder symmetric scattering chamber towards the Forward Detector assembly and possseses a much increased granularity. Since it will be used in future also for trigger purposes and as time-of-flight start detector, the light collection had to be optimized with the additional condition to keep the detection efficiency as homogeneous as possible over the full hodoscope area. Further geometrical constraints were given by the very restrictive space available in the respective area of the WASA setup. The new Forward Window Hodoscope has been installed during the COSY shutdown period in August 2007 and is used since then in the experimental runs at WASA.

The previous Forward Window Counter (FWC) consisted of 12 5 mm thick radially segmented plastic scintillator pieces forming a cone at the WASA scattering window. Due to the restricted space at the place of installation the big 2” XP 2020 readout photomultiplier tubes could only be installed far above and below the FWC detector resulting in long light paths and complicated shapes of the lightguides. For this reason the light output efficiency was relatively small and - in particular - strongly position dependent. i.e. causing a strong non-uniformity in dependence of the scattering angles Θ and ϕ. [2].

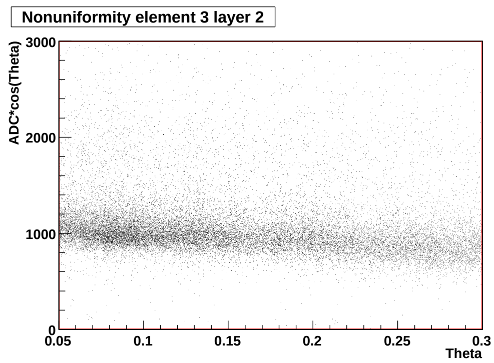

Fig. 1: Nonuniformity of an element in 2nd layer of the new FWC. Note that the light collection efficiency near the tip (left) is slightly increased due to the well-known geometrical focussing there.

The new detector is made out of 3 mm plastic scintillator material BC-400. It is 48-fold segmented and composed of two layers à 24 elements. The first layer is of conical shape like the old detector and placed just as close as possible at the forward scattering window. The second layer is planar and shifted in ϕ direction by half an element. This geometry provides a complete coverage of the forward area without holes. In addition the 48-fold granularity coincides with the 48-fold granularity of the Forward Trigger Hodoscope FTH [1]. The increased segmentation in combination with the use of thinner scintillator material allowed now to use small 1” photomultipiers XP 3112, which enabled a construction of a fully radially symmetric detector - thus providing also a fully radially symmetric acceptance and efficiency.

In order to optimize light output and timing performance adiabatic (twisted) lightguides have been designed and constructed. Each of these adiabatic lightguides consists of 7 twisted stripes of plexiglas.

In the commissioning and experimental runs following the detector installation in August 2007 the performance of the new FWC could be tested. As a result it is found that the new detector fulfills all its design values or even exceeds them as demonstrated in the examples displayed in Figs. 1 - 3.

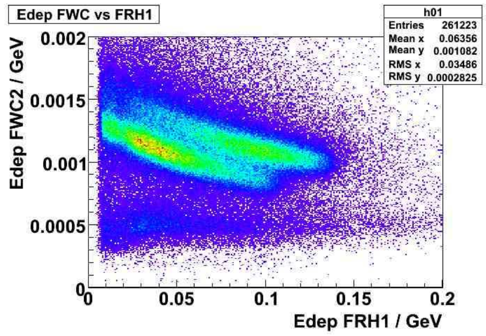

Fig. 2: ΔE-E plot of the energy deposited in FWC1 versus the energy deposited in FRH1. The bands for detected protons and deuterons appear clearly separated.

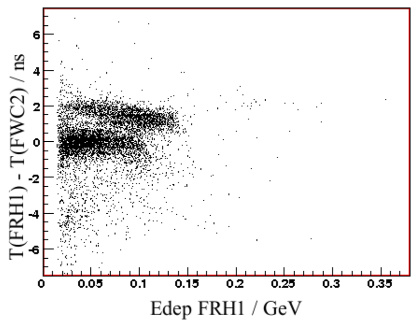

Fig. 3: Plot of the Time-of-flight between FWC2 and FRH1 versus the energy deposited in FRH1. The particle bands appear again well separated.

References:

[1] WASA Collaboration, e-Print Archive: nucl-ex/0411038

[2] O.Messner, Design and Setup of the Window Counter for the new WASA 4π Detector at CELSIUS, Diploma Thesis, 1999 Tübingen

[a] Physikalisches Institut Tübingen Universität Tübingen 72076 Tübingen Germany

[b] Helmholtz-Institut für Strahlenphysik Rheinisches Friedrich-Wilhelms Universität Bonn 53115 Bonn Germany

The WASA-at-COSY pellet target*

A. Winnemöller[1], G. D'Orsaneo[2], G. D'Orsaneo[3], A. Khoukaz[1], N. Milke[1], P. Pistel[3], T. Rausmann[1], D. Spölgen[2], and A. Täschner[1]

The WASA pellet target is the first and up to now only pellet target running in an internal beam accelerator experiment [1,2]. After its dismounting from the CELSIUS ring in Uppsala and the later installation at the COSY ring in summer 2006, all scheduled aims were achieved. Since that time three commissioning runs and three beam times have been accomplished successfully.

The quality of the glass nozzles is of prime importance for the target performance. Therefore, a facility for the production of nozzles has been established in 2007 at the ZAT of the FZ Jülich. Two very powerful microscopes (Zeiss Axiovert 40 MAT and Zeiss SteREO Discovery.V12) have been acquired in order to improve the production performance. These microscopes with large magnifications allow to produce nozzles with certain inner diameters with high accuracy by cutting the tip of the nozzle at well defined positions. The vacuum injection capillaries, which separates the triple point chamber (p~60mbar) from vacuum (p~10^{-3}mbar) are produced with the same devices. The production takes place under very clean conditions in order to avoid any impurities inside of the nozzles, which would lead to irreversible blocking (fig. 1). Since the first produced nozzles showed a tendency to block, detailed studies have been performed in order to improve their operation time.

Fig. 1: Photography of the tip of a blocked nozzle. The conical inner opening channel has a minimum diameter of 12 µm at its end (right hand side) and is blocked by particles.

In fig. 1 a photography of a blocked nozzle is shown. The objects had a diameter of more than 12µm, therefore they could not leave the nozzle and accumulated at its tip. Since the objects are larger than the pores of a special sinter filter at the gas input side of the nozzle, a transport from outside the nozzle to the tip is not possible. Instead they must have been present or produced during the production process. However, due to the very clean conditions at the production site a contamination with dust or other impurities could be excluded. After careful investigations it was found that the objects blocking the nozzles were debris from the above mentioned sinter filters. The cylindrical stainless steel filters have a diameter of approx. 1.6mm and a pore size of 2µm. Further investigation of the filters showed that their surface was very crumbly (fig. 2, left hand side) so that particles could easily detach. Due to the different expansion coefficients of the glass and the filter material strong forces are applied to the filters during the production. Additionally, the piezo that oscillates the nozzle during operation of the target applies a force. To prevent the production of such perturbing particles, the previously used filters (GKN) were replaced by ones from an other company (MOTT) with a slightly different shape (fig. 2, right hand side). Furthermore, an additional cleaning step compared to the nozzle production in Uppsala is now applied: After the sinter filters are molten into the nozzles and the nozzles are constricted they are flushed with a cleaning agent. The finished nozzles are flushed again with nitrogen in order to check whether there is a blocking. The nozzles that are now produced are working extremely stable and have lifetimes in the range of at least several months.

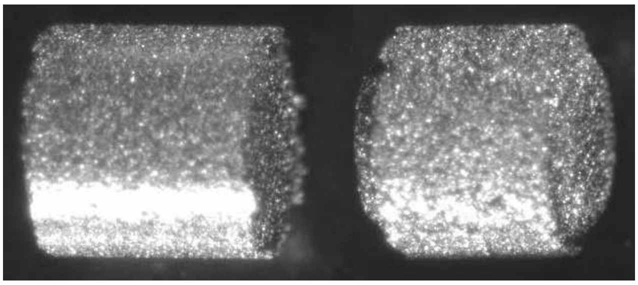

Fig. 2: Photography of the sinter filters for the nozzles. Left: old filter (GKN), right: new filter (MOTT).

A further improvement for the operation of the pellet target is the use of a gas generator that produces deuterium from heavy water by electrolysis. Thus, instead of conventional deuterium gas bottles, comparably cheap heavy water can be used now. The typical throughput during target operation is approx. 1 liter of heavy water per week.

In addition the gas lines in the cold head have been replaced and improved in order to prevent them from being twisted during a nozzle maintenance work.

While the comparability of the target performance with the one at CELSIUS/Uppsala has already been demonstrated for hydrogen pellets, now with the successful beam time in November and December 2007 this goal was also reached for deuterium pellets. Here with the improved nozzles life times of up to 60 hours followed by a regeneration of 6-8 hours have been achieved. With a stable pellet beam, a deuterium target thickness of approx. $4 \cdot 10^{15}$ atoms$\cdot$cm^{-2}, and pellet rates up to more than 10000 pellets/s, the target performance obtained at CELSIUS/Uppsala [3] could be fully reproduced.

References:

[1] B. Trostell, Nucl. Instr. and Meth. **A 362**, 41 (1995)
[2] C. Ekström et al., Nucl. Instr. and Meth. **A371**, 572 (1996)
[3] H.-H. Adam et al., *Proposal for WASA at COSY* COSY-PAC 29 (2004); nucl-ex/0411038

* Supported by FZ Jülich FFE
1 Institut für Kernphysik, Universität Münster, 48149 Münster, Germany
2 IKP, Forschungszentrum Jülich
3 ZAT, Forschungszentrum Jülich

A Pellet Tracking System for WASA at COSY

T. Tolba [1], J. Ritman [1] for the WASA-at-COSY collaboration

A Pellet Tracking System for WASA at COSY is being planned in order to determine the interaction point (the primary interaction vertex) between the COSY beam and the target pellets. The knowledge of the interaction vertex helps to reconstruct the paths of the different decay products and thus to improve the momentum resolution of the events. Furthermore, the system gives information about the position distribution of the pellets below their place of production and below the interaction point, allowing the geometrical alignment of the system to be improved.
The idea is to measure the x and z position of a pellet before and after the interaction point. That can be done by using a laser beam to illuminate the pellet and photographing it (using the scattered laser light from the pellet) by pairs of fast CCD line scan cameras, below and above the interaction point. The cameras are arranged at 90° relative to each other. The pellet trajectories can be tracked from the position information of each plane and the relative timing, for more details see [ref. 1].
First results of setting up this system are presented below.

Lens-target distance optimization

The FWHM was measured at different distances between the lens and a strand of hair and the relation between them was plotted (see Fig. 1).
The calculated distance D = (175 ± 7) mm.
The optimum measured distance for the sharpest picture is D = (173.0 ± 0.5) mm.

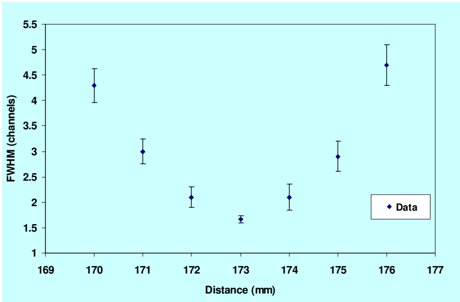

Fig.1: Measured width (FWHM) of the image of a hair as a function of the lens-target distance.

Pixel size calibration

With the following camera operating parameters (512 pixels of 14 µm x 14 µm, D = 173 mm and lens focal length l = 50 mm), an image of a grating with pitch (2.00 ± 0.03) mm was taken in order to verify the size of the sensor pixels and to measure the magnification factor of the lens(see Fig. 2).
The calculated magnification factor is M = (40 ± 3)%.
The measured magnification factor is M = (39.2 ± 1)% (i.e. 1 pixel = (35±1.8) µm).

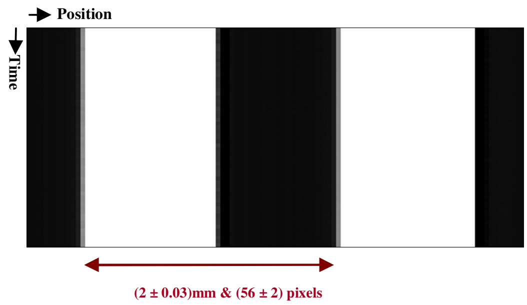

Fig.2: pixel image for two edges a grating.

Hair thickness measurement

With D = 173 mm and M = 39.2%, a strand of hair was photographed and the hair thickness was measured and compared with the thickness directly measured with a micrometer. This allowed the optimum lens-target distance, the pixel size and the magnification factor of the lens to be verified. The FWHM of the hair was found to be (63 ± 2) µm, (Fig. 3) in good agreement with the hair thickness directly measured with a micrometer (70.0 ± 0.5) µm.

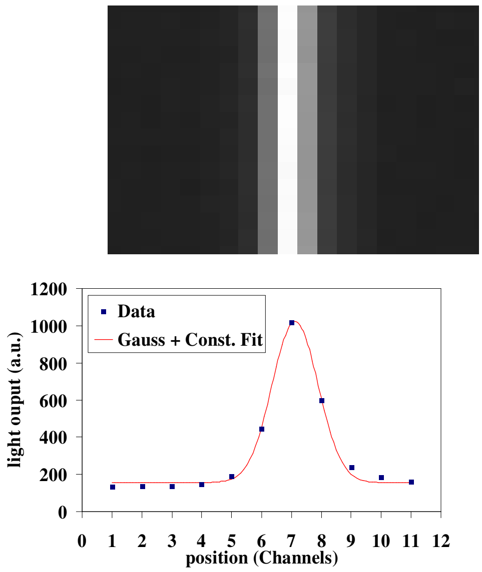

Fig.3: Gauss fit of the measured light intensity in the camera to the scattered light from a hair.

Time calibration

The pellet frequency at the interaction point is supposed to be 8 – 12 kHz, which means that we have to use a very fast (i.e. high repetition frequency) line scan camera to be sure that we will not miss any pellet. The camera chosen has a line rate frequency 100 kHz [2].
In order to verify that, a 70000 line picture of a rotating source with (138 ± 3) Hz was taken. The maximum line rate frequency is measured to be (97.8 ± 1.7) kHz, corresponding to a time resolution of 10.2 µs, (Fig. 4).

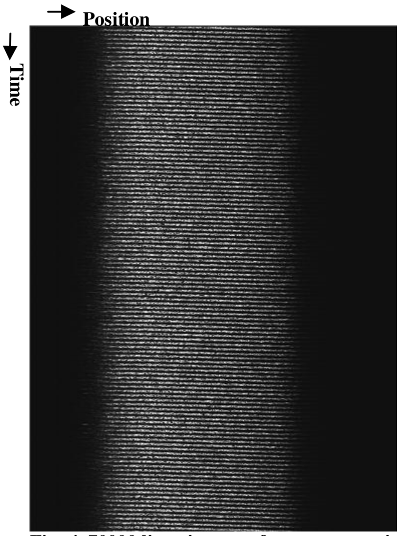

Fig: 4, 70000 line pictures of a source rotating at (138 ± 3) Hz.

Frame grabber and software

The frame grabber used is DALSA *CORECO* with the Sapera CamExpert program as the software for taking pictures with the line scan camera. In order to control the camera the CommCam program is used [3].
In order to perform an online analysis, a special program is under construction, with the help of the Sapera LT SDK (Software Development Kit) and ROOT software as the user graphical interface.

A vacuum chamber and holders for the laser and camera were built in the central workshop of the research center Jülich and in the workshop of IKP. The first prototype of the system with one camera and one laser is now ready (see Fig. 5).

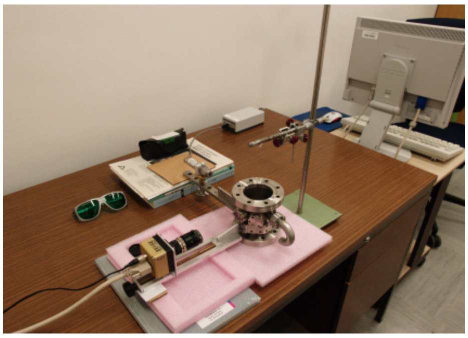

Fig. 5: Photograph of the first prototype of the PTS

Summary

- The optimum distance between the lens and the object is measured to be D = 173 mm.
- The magnification factor is M = (39.2 ± 1)%.
- Thickness of a hair was measured to be (63 ± 2) µm.
- The maximum line repetition frequency is (97.8 ± 1.7) kHz.

References:

[1] "A Pellet Tracking System for WASA at COSY", T.Tolba, J.Ritman. COSY/IKP Annual report, 2006.
[2] ATMEL. AVIIVA™ M2 Cl Cameralink™ Line Scan Camera, 2006, Data sheet.
[3]DALSA *CORECO*. X64-CL iPro Series User's Manual.

[1] IKP-1, Forschungszenturm - Jülich

Studies for a Cherenkov detector @ WASA-at-COSY

A. Teufel, C. Adolph, W. Eyrich, C.Pizzolotto, A. Schmidt, W. Schroeder,
Physikalisches Institut, Universität Erlangen, for the WASA-at-COSY collaboration

The WASA-at-COSY experiment allows the study of production and decay of η and η' mesons in proton proton reactions with an almost full 4π covering detector including a forward spectrometer section. Particle identification for the decay products and to separate the huge background, one has to cope with, is substantial for this kind of investigation. Actually the so called Forward Range Hodoscope (FRH) in the forward angle spectrometer region determines the identity of the particles by measuring the energy loss ΔE-E. Simulations concerning the estimated background have shown, that an additional ring imaging Cherenkov detector in front of the FRH would significantly improve the particle identification and the energy resolution as well. Due to the very limited space, available at the intended detector position, the development of a DIRC (Detection of Internally Reflected Cherenkov light) detection system is under discussion: Cherenkov light is produced in a radiator bar by particles with velocity larger than the speed of light in this medium and then guided by total internally reflection at the inner surface of the bar to photon sensors located at the far end. In order to reduce the optical detection surface, additional optical focusing elements are used (compare fig. 1).

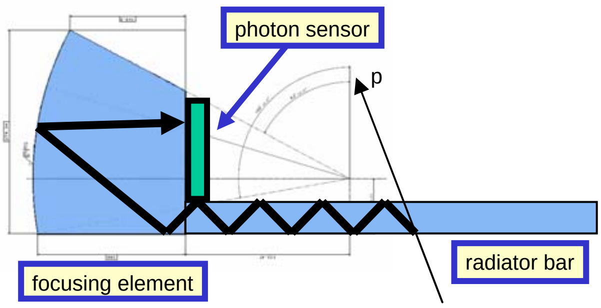

Fig. 1: Schematic view of the DIRC principle: radiator bar with focusing element and photon sensor.

Primary objectives of our research have been the investigation of suitable photon sensors and their key features, as well as the study of different radiator bars with respect to parameters like material and surface quality. Also a first prototype of a focusing element was tested.

Radiator Bars The surface quality of the radiator bar is the most critical parameter when using the DIRC principle. Light transmission and angular resolution are dominated by this quantitiy. Radiators made of fused silica are preferably used, but since they are very expensive, we have tested as an alternative bars made of PlexiGlas® (PMMA). In particular the surface constitution depends strongly on the manufacturing process. We have measured the light transmission coefficient as a function of the number of internal reflections from two different PMMA bars: one cut out of a block, surface machined and polished, the other with two casted surfaces. Both of them had a length of 700 mm and a cross section surface of about 50x50mm^2. The measured reflection coefficient was about 95% for the polished and about 98% for the casted material, respectively.

Photonsensors The measurement of the produced Cherenkov photons has to be done with photon sensors which are able to detect single photons. Multianode photomultiplier tubes are found to be very suited for that. Three possible devices where tested on parameters like gain, uniformity, dark current, time resolution etc.:

- Hamamatsu R7600-03-M16 : MAPMT with 16 channels
- Hamamatsu H8500C : MAPMT with 64 channels
- Burle 85011 : Microchannel PMT with 64 channels

Both Hamamatsu models showed excellent uniformity behaviour with less then 20% variation in signal height. Gain factors of about 5x10^6 to 5x10^7 have been measured. The time resolution of these devices was determined to be σ = 140 ps at single photon event level (compare fig. 2). An outstanding parameter is the dark current with less then 100 pA at 10 Hz count rate.

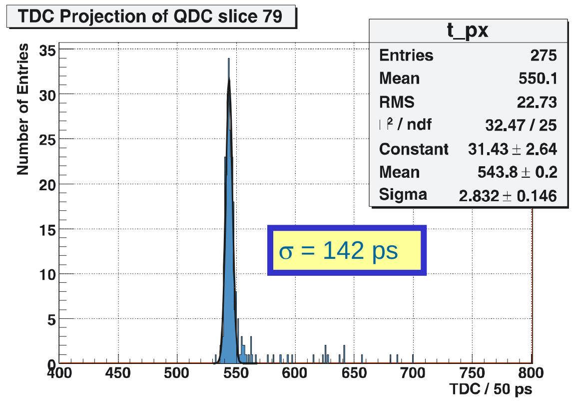

Fig. 2: Time resolution of H8500C for single photon events.

The Burle microchannel plate photomultiplier features excellent time resolution values of less then σ = 50 ps. The dark current frequency with 20 kHz is comparatively high and at photon rates above 10^5 per second, the signal amplitude drops down significantly.

Focusing elements In order to keep the photon read-out surface small, focusing elements are used. A first prototype was built and tested (compare fig. 3). It makes use of total internal reflection at the surface. Other solutions with e.g. aluminium coated surfaces are under investigation.

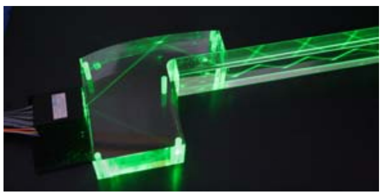

Fig. 3: Focusing element based on internal reflection

A complete DIRC prototype submodule with radiator, focusing element and photonsensor for WASA-at-COSY will be tested in autumn 2008.

A Statistical Method of Event Reconstruction for a Cerenkov Detector.

V. Kyryanchuk, H. Machner, R. Siudak, J. Ritman

It is planned to measure rare decays of η' mesons at WASA at COSY. The foreseen production reaction is

$$p + p \rightarrow \eta' + p + p \qquad (1)$$

where the two protons will be measured and the η' will be identified via missing mass technique. Since no nucleon resonance couples to the $\eta' p$ channel, in contrary to η production, the cross section is small. The η' peak will be on top of a huge multi-pion background. The only chance to identify the η' is to measure the four momentum vectors of the two protons with high accuracy. A possible option to do so seems to be a DIRC Cherenkov detector in the forward detection system of WASA.

Cherenkov detectors are widely used in high energy physics. They can have different applications: particle identification, energy measuring, threshold detector for detecting specific type of particles in a definite energy range.

Our aim is to measure the energy of protons in the energy range from 400 MeV to 1000 MeV.

Different materials were studied as radiator: LiF, CaF and quartz. All materials have different refractive indices (see Fig. 1) and transmittances (Fig. 2) (taken from Ref. [1]). The radiator should have large refractive index and high transmittance to measure particles with "low" energy. LiF has wider transmittance in the UV range in comparison with CaF and quartz. This gives the possibility to build a Cherenkov detector with LiF as radiator and a proper photocathode for detecting photons in UV range. The LiF radiator should be thin because of the low transmittance (large probability to absorb photon). The quartz radiator on the other hand has larger transmittance and could thus be much thicker.

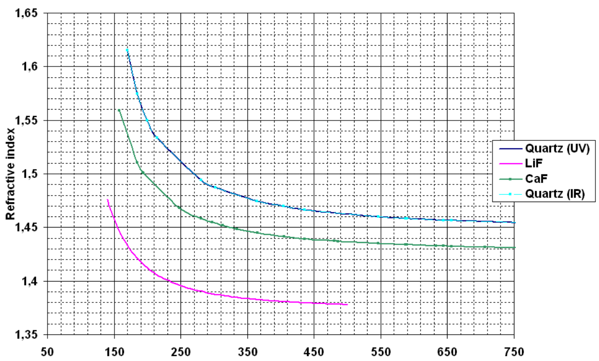

Fig. 1: Refractive index for quartz (UV-grade and IR-grade), CaF and LiF as function of the wave length in nm (from Ref. [1].

Quantum efficiencies for different photocathodes are shown in Fig. 2 (see Refs. [2, 3]). CsI and CsTe are used for photon detecting in UV range. Bi-alkali (KCsSb) and multi-alkali (GaAsP) photocathodes are used for upper UV and the visible light range. These types of photocathodes have larger and broader distributions of the corresponding quantum efficiency function. This could compensate a smaller amount of emitted photons in this wave range. In simulations for a DIRC-type detector fused silica was chosen as radiator because of its high refractive index and large transmittance, as photocathode bi-alkali material should be used.

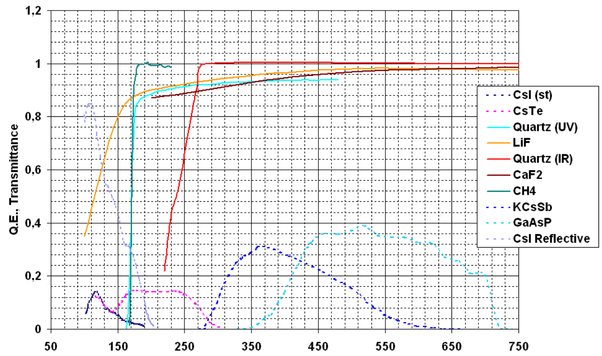

Fig. 2: Quantum efficiencies of photocathodes (dotted curves) and radiator transmittances (solid curves) as function of the wave length in nm (from Ref. [1].

We will now concentrate on the DIRC detector. It consists of radiator bars with dimensions 2x6x50 cm^3 and a focusing bar with reflective rear side (Figs. 3 and 4. Fused silica is used as detector material. The construction is tilted by 20 degree to the beam axis. Emitted Cherenkov photons create an image on a segmented screen. Each segment is a bi-alkali photocathode with dimension 5x5 mm^2.

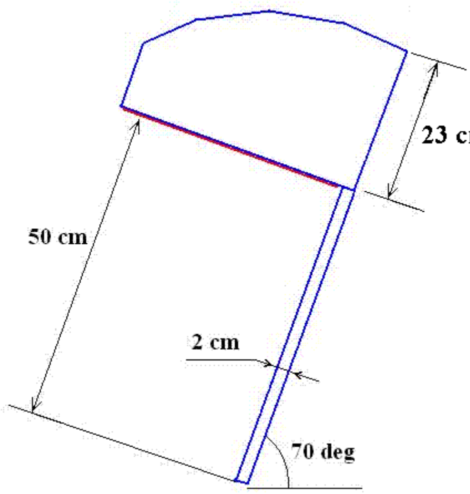

Fig. 3: Cross section of the detector. Radiator bars are inclined by 70 degree to the vertical axis. The focussing bar is ontop.

A single event image consists of two arcs, which are result of the internal reflection from the left and right side of the radiator bar. Shapes of the arcs depend on the energy and type of particle. Relative positions of the arcs depend on the horizontal (azimuthal) angle of the detected particle track: the larger the horizontal angle, the larger the distance between arc centers. An example is shown in Fig. 6 [3].

We have simulated Cherenkov images for protons with

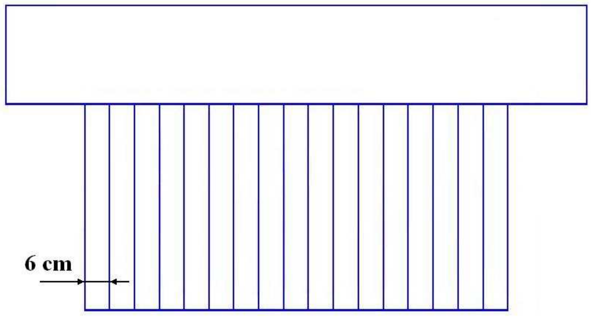

Fig. 4: Same as Fig. 3 but seen from the front side.

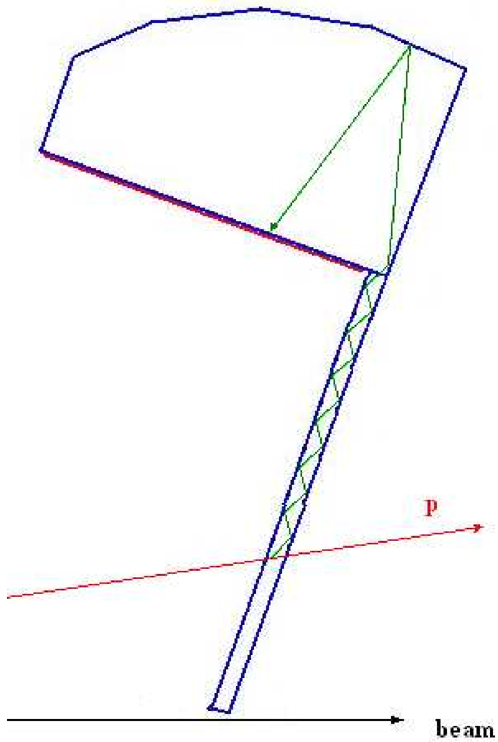

Fig. 5: Light propagation through the detector after interaction with a proton.

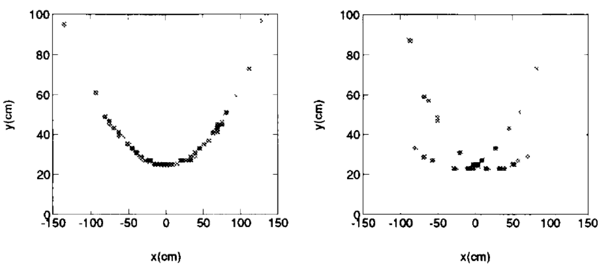

Fig. 6: Loci of Cherenkov images for different azimuthal angles. The left panel shows the case for 0 degree and the right panel for 10 degree.

600 MeV (Fig. 7 and 1000 MeV and track direction $\theta^{o}_{horiz,vert}$ $\sim 8.5^{o}$ relative to the beam are shown on Fig. 4. The average number of the emitted photons depends on the particle path in the radiator. Fig. and Fig 10 show the num-

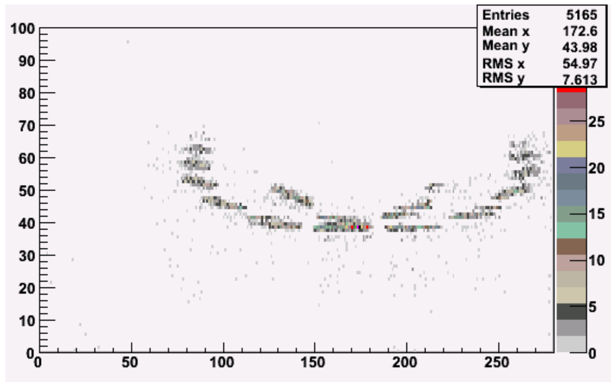

Fig. 7: Scatter plot of simulated events for protons with energy E = 600 MeV. The x- and y-axis are horizontal and vertical position number of the photocathode on the screen. "Entries" is the number of detected photons per 100 events.

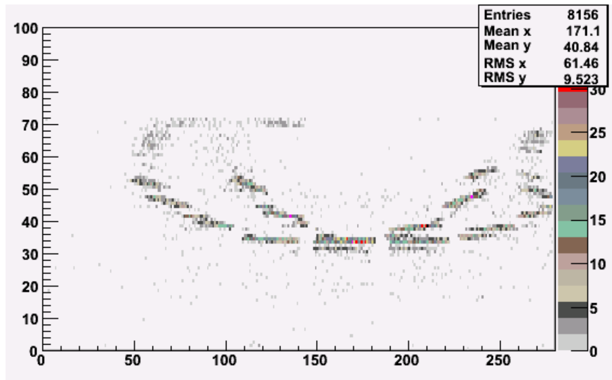

Fig. 8: Same as Fig. 7 but for protons with energy E = 1000 MeV.

ber of detected photons depending on the horizontal track direction for protons with E = 600 MeV. The amount of the detected photons drops sharply, when the particle passes through the edges of the radiator bars. This effect appears due to detector construction, and could be reduced by reducing the number of bars.

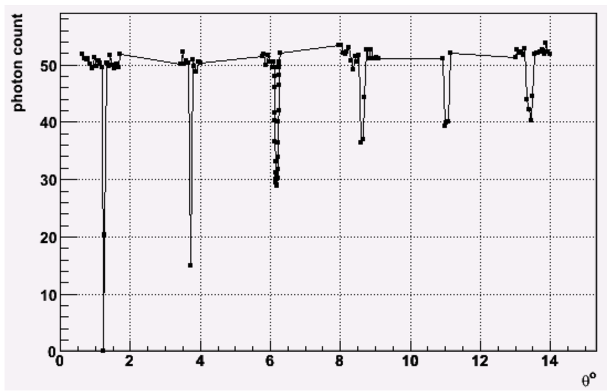

Fig. 9: The average number of the detected photons as function of the angle for protons with E = 600 MeV.

In addition to this effect image distortion is also observed. Smeared arcs or even four arcs could be observed when the particle goes through the edges of two neighboring bars (Fig.

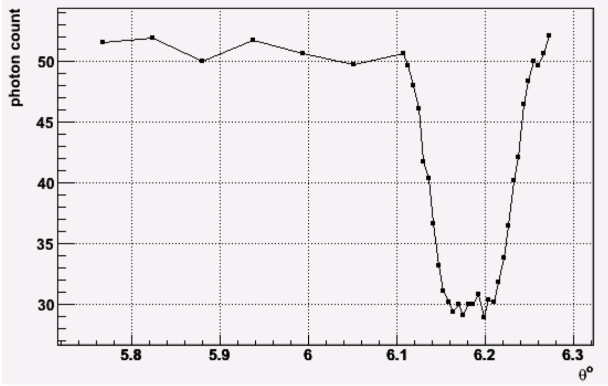

Fig. 10: Same as Fig. but for an expanded range.

11).

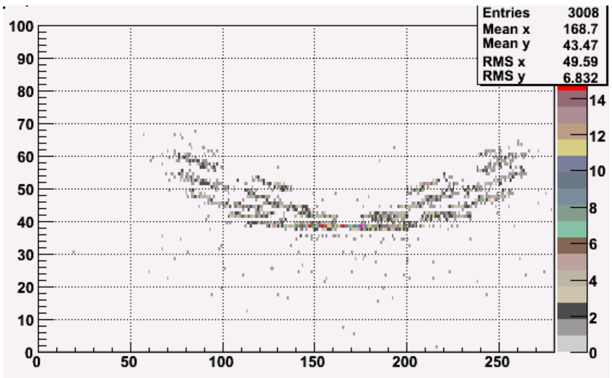

Fig. 11: Same as Fig. 7 but for “edge” deformation of the Cherenkov image.

For event reconstruction the following method is used. At first a set of events for different particle types with different energies and directions is simulated. Then the experimental data are “compared” with the simulated data. The comparison is realized by the function F [2]

$$F(k,(E,P)) = \sum_{i,j} exp(i,j) \cdot \overline{sim(i,j)}. \qquad (2)$$

Here k denotes the particle type, E,P the energy and momentum of the particle, $exp(i,j)$ is the number of detected photons in (i,j)-th photoelement in the experiment and $\overline{sim(i,j)}$ the simulated average number of detected photons in (i,j)-th photoelement. The expression gives a maximum when the experimental image on the screen is similar to the simulated one. Such method gives an opportunity to define β and the direction of a particle. With additional detectors it is possible to find either the energy (momentum) or the particle type.
Fig. 12 shows the β-resolution for protons. The method gives a resolution for protons better than 0.3%.
The possibility of track reconstruction is demonstrated in the Fig. **??**. The particle direction is extracted under the assumption that energy and particle type are known. Horizontal and vertical angles relative to the beam direction are reconstructed under the assumption that one of both is fixed. A precision of ∼0.3 degree and ∼0.5 degree was found, respectively for protons with 600 MeV. Similar results were obtained for protons with 1000 MeV.
The method presented here gives reliable information for event reconstruction: β-resolution for protons is better than 0.3%. The routine is capable to reconstruct tracks and identify particles when additional information is provided by complementary detectors. The necessary large data base of simulated events is a disadvantage of this method. However, optimization of the algorithm should increase the speed.

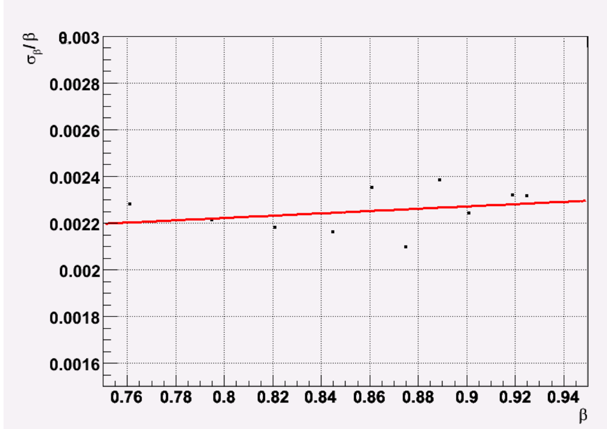

Fig. 12: β-resolution for protons.

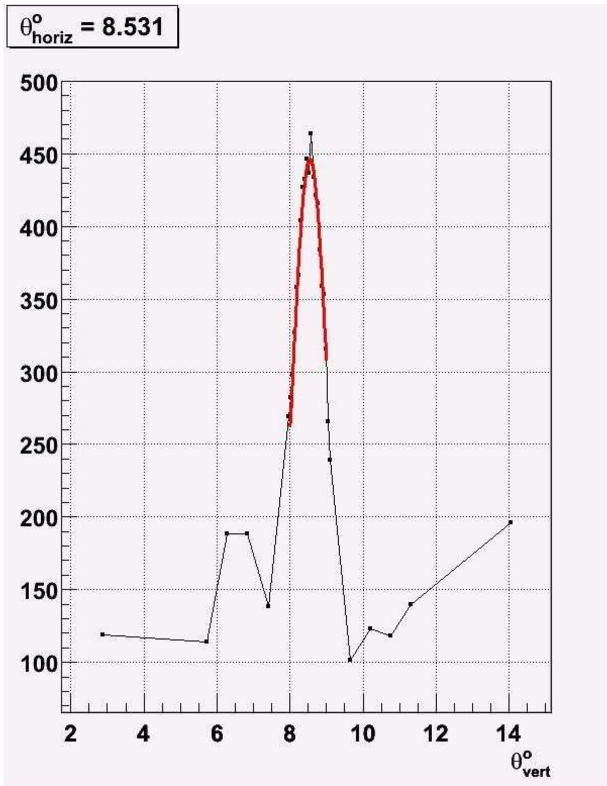

Fig. 13: Track reconstruction. The track’s vertical angle is reconstructed while the horizontal angle is fixed.

References:

[1] SCHOTT optical glass data sheets.
[2] A.Breskin, Nucl. Instr. and Methods in Phys. Research A 371, 116 (1996).
[3] P. Coyle et al. / Nucl Instr. and Meth. in Phys. Res A 343 (1994) 292-299.

Two proton correlation function determined for the $pp \to pp\eta'$ reaction

P. Klaja and P. Moskal[a] for the COSY-11 collaboration

The momentum correlations of particles at small relative velocities are widely used to study the spatio-temporal characteristics of the production processes in the relativistic heavy ion collisions [1]. This technique, called *correlation femtoscopy* [2], originated from intensity interferometry [3]. It is based on the correlation function [2]. The importance of correlation femtoscopy has been well established in heavy ion collisions with high multiplicity of produced particles. However, as pointed out by Chajecki [4], in the case of low-multiplicity collisions the interpretation of the correlation function measurements is still not fully satisfactory [5]. The understanding of contributions from the non-femtoscopic correlations which may be induced by the decays of resonances, global conservations laws [4], or by other unaccounted for interactions, is a major goal of present investigations. In particle physics the best place to study two-proton correlations is exclusive measurements of meson production in the collisions of hadrons conducted close to the kinematical threshold [6]. Here, we report on measurement of the two-proton correlation function for the η meson production in the collisions of protons at the beam momentum close to the kinematical threshold for the $pp \to pp\eta$ reaction [7]. The two-proton correlation function $R(q)$ [1] was calculated as the ratio of the reaction yield $Y(q)$ to the uncorrelated yield $Y^*(q)$ according to the formula (c.f. [9])

$$R(q)+1 = C^* \, \frac{Y(q)}{Y^*(q)}, \tag{1}$$

where C^* denotes an appropriate normalization constant. $Y^*(q)$ was derived from the uncorrelated reference sample obtained by using the event mixing technique [10]. In this experiment, only the four-momenta of two protons were measured and the unobserved meson was identified via the missing mass technique [7, 11]. Therefore, it is impossible to establish whether in a given event the η meson or several pions have been created. However, one can statistically separate these groups of events on the basis of the missing mass spectra for each chosen region of the phase-space. As a next step, we calculated the acceptance and efficiency of the COSY-11 system for the registration and reconstruction of the $pp \to pp\eta$ reaction as a function of the relative momentum of the outgoing protons. For details of the analysis the interested reader is referred to articles [12] and [13]. In order to estimate the influence of the shape induced by the kinematical bounds we have reconstructed the correlation functions for the simulated sample of $pp \to pp\eta'$ events assuming a point-like source. Next, the shape of the correlation function free from the influence of the energy and momentum conservation was extracted from the experimental data by constructing a double ratio:

$$R(q)+1 = C_{exp/MC} \, \left(\frac{Y_{exp}(q)}{Y^*_{exp}(q)} \Big/ \frac{Y_{MC}(q)}{Y^*_{MC}(q)} \right), \tag{2}$$

where $C_{exp/MC}$ denotes the normalization constant, and the indices 'exp' and 'MC' refer to the experimental and simulated samples, respectively. The determined double ratios are presented in figure 1. Such procedure is used e.g. by the

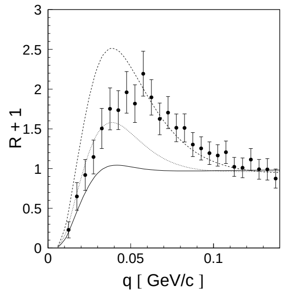

Fig. 1: The two-proton correlation function corrected for acceptance and normalized to the corresponding correlation function simulated for a point-like source. Full dots represent experimental points for the $pp \to pp\eta$ reaction. The superimposed lines show the result of calculations [8] for the reaction volume parametrized by a Gaussian with radius $r_0 = 2.0$ fm (dashed line), $r_0 = 3.0$ fm (dotted line) and $r_0 = 5.0$ fm (solid line), respectively.

ALEPH collaboration [14, 15]. In order to estimate the size of the emission source the results are compared with theoretical predictions, obtained by assuming a simultaneous emission of the two protons and derived under the assumption that the final-state interaction between the two detected particles dominates, while other interactions are negligible. The source density was taken to be a Gaussian specified by a radius parameter r_0 [8]. A rough comparison between the theoretical correlation function and the experimental points indicates that the effective size of the emission source amounts to about 2.4 fm for the $pp\eta$ system. Extended calculations including the production of the η meson [16] and a detailed comparison and interpretation of results are in progress.

References:

[1] M. A. Lisa et al., Ann. Rev. Nucl. Part. Sci. **55**, (2005) 357.
[2] R. Lednicky, Nukleonika 49 **(Sup. 2)**, S3 (2004)
[3] R. Hanbury-Brown, R. G. Twiss, Phil. Mag. **45**, (1954) 663.
[4] Z. Chajecki, Eur. Phys. J. C **49**, (2007) 81.
[5] Z. Chajecki, M. Lisa, e-Print Archive: nucl-th/0612080.
[6] P. Moskal, M. Wolke, A. Khoukaz, W. Oelert, Prog. Part. Nucl. Phys. **49**, (2002) 1
[7] P. Moskal et al., Phys. Rev. **C 69**, 025203 (2004)
[8] A. Deloff, AIP Conf. Proc. 950 (2007) 150.
[9] D. H. Boal et al., Rev. Mod. Phys. **62**, 553 (1990)
[10] G. I. Kopylov, M. I. Podgoretsky, Sov. J. Nucl. Phys. **15**, (1972) 219.
[11] P. Moskal, e-Print Archive: hep-ph/0408162
[12] P. Klaja et al., Acta Phys. Slovaca **56**, (2006) 251.
[13] P. Klaja, P. Moskal and A. Deloff, AIP Conf. Proc. 950 (2007) 156.
[14] R. Barate et al., Phys. Lett. B **475**, (2000) 395.
[15] R. Barate et al., Phys. Lett. B **478**, (2000) 50.
[16] A. Deloff, Private communication (2007).

[a] Institute of Physics, Jagellonian University, Cracow, Poland

[1] Here, $R(q)$ denotes a projection of the correlation function onto the relative momentum of the emitted particles $q = |\vec{p}_1 - \vec{p}_2|$. Note, that some authors instead of q take as the independent variable the proton-proton center-of-mass momentum $k = q/2$ (c.f. reference [8]).

Study of the interaction in the $pp\eta'$ system: analysis status

P. Klaja and P. Moskal[a] for the COSY-11 collaboration

The COSY-11 collaboration has taken data of the $pp \to pp\eta'$ reaction, during three weeks of measurement. That experiment has been performed at Q = 15.5 MeV, the same excess energy at which the differential distributions of the invariant masses had been determined for the $pp \to pp\eta$ reaction [1]. The determination of analogous distributions for the $pp\eta'$ system in the final state could illuminate the still completely unknown proton-η' interaction. Such observables, which in case of the $pp\eta$ were very sensitive to the proton-η interaction could deliver the first strong experimental evidence for that interaction of nucleons with the η' meson. We would like to perform a similar analysis aiming at the estimation of the low energy $pp\eta'$ interaction. Here we report on the progress in the extraction of the differential cross sections as well as in the determination of the luminosity.

The experiment performed using the COSY-11 detection setup, was based on the registration of two outgoing protons. Then, we selected only these events with registered two tracks, which could have corresponded to the $pp \to ppX$ reaction. The unobserved meson has been identified via the missing mass technique. In Figure 1 we present the preliminary missing mass spectrum, determined for the whole data set, for the $pp \to ppX$ reaction measured at the beam momentum 3.257 GeV/c. In the figure a clear signal is visible with around 17000 events corresponding to the $pp \to pp\eta'$ reaction. In order to search for the small effects of a possible proton-meson interaction on the population density of the phase-space, one must either include the experimental resolution in theoretical calculations, or perform kinematical fitting of the data. In the experiment we have measured 6 variables (2 times 3 components of the protons momentum vector). In the analysis we assumed that the event with the missing mass equal (within an experimental resolution) to the mass of the η' meson corresponds to the $pp \to pp\eta'$ reaction. Under this assumption only five of the kinematical variables are independent. Hence, we varied the protons momenta demanding that the missing mass of the unregistered meson is equal to the mass of the η' meson and we have chosen the momentum vectors which were the closest to the vectors determined from the experiment. The inverse of the covariance matrix was used as a metric for the distance calculation. The kinematical fit improves the resolution, as seen in Figure 2. For the further selection of events corresponding to the η' production, we checked the χ^2 distribution from the kinematical fit procedure, which is shown in Figure 3 as a function of the missing mass. For the determination of the differential distributions we have taken events with $\chi^2 < 1.5$. Ongoing analysis is being done to substract the background from the multi-meson production.

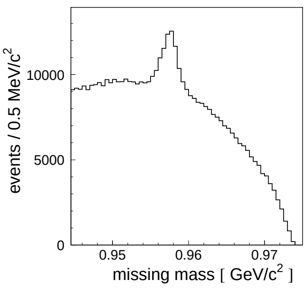

Fig. 1: Experimental missing mass spectrum for the $pp \to ppX$ reaction measured at the beam momentum 3.257 GeV/c.

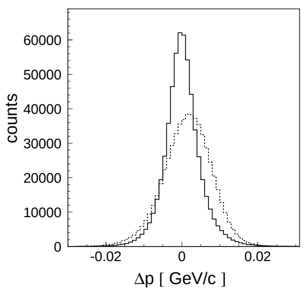

Fig. 2: Simulated spectrum of the difference between the generated and reconstructed proton momentum. Dashed line deonotes the spectrum before kinematical fit. Solid line corresponds to the situation after the fitting.

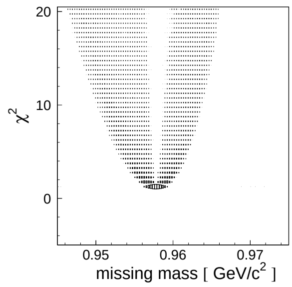

Fig. 3: The distribution of the χ^2 versus the missing mass.

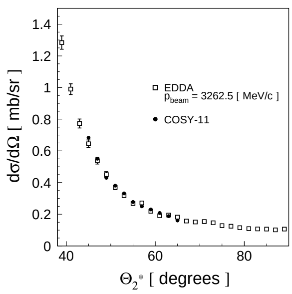

Fig. 4: Differntial cross section for the proton-proton elastic scattering measured at the beam momentum $p_B = 3.257$ GeV/c, depicted by full circles. Cross sections measured by the EDDA collaboration are shown by open squares [2].

In order to determine the absolute magnitude of the differential cross sections, the luminosity integrated during the measurement time was established by the comparison of the angular distributions of the elastically scattered protons with the results of the EDDA collaboration [2]. The achieved value of the integrated luminosity amounts to L = (5.842 ± 0.072) pb^{-1} [3].

References:

[1] P. Moskal et al., Phys. Rev. **C 69** (2004) 025203.
[2] D. Albers et al., Phys. Rev. Lett. **78** (1997) 1652.
[3] P. Klaja et al., AIP Conf. Proc. **950** (2007) 103.

[a] M. Smoluchowski Institute of Physics, Jagellonian University, 30-059 Cracow, Poland

Luminosity determination for the quasi-free $pn \to pn\eta'$ reaction

J. Przerwa and P. Moskal for the COSY-11 collaboration

In this report we give an account on the determination of the luminosity for the measurement of the $pn \to pn\eta'$ reaction conducted using the proton beam and a deuteron target. The determination of the luminosity is based on the registration of the quasi-free $pp \to pp$ reaction [1].

The quasi-free proton-proton scattering was measured simultaneously with the η' meson production in proton-neutron collisions. In this kind of scattering, a proton from the beam interacts with a proton bound inside the deuteron target. The recoil proton is measured by the scintillator and by the position sensitive silicon detector. The forward proton is bent in the magnetic field of the dipole towards the drift chambers and scintillator detectors. Details concerning the detection setup can be found in [2]. The momentum of the fast proton is determined by tracking back the trajectory reconstructed from signals in the drift chambers. Figure 1 shows parallel versus transversal component of the reconstucted momentum of the forward scattered proton. Events corresponding to the elastic scattered protons are seen near the kinematical ellipse, which is marked as a solid line.

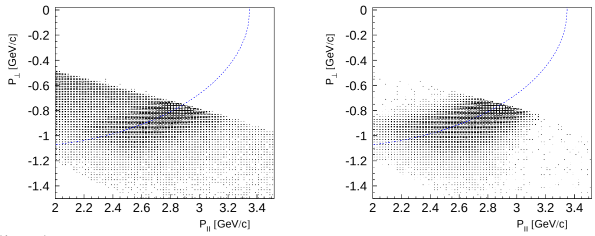

Fig. 1: Parallel versus transversal momentum component of the reconstructed forward proton momentum as obtained in the experiment **(left)** and in the simulation **(right)**.

To determine the luminosity, the known differential cross section for elastically scattered protons is compared to the number of scattered protons from the experimental data. However, in case of quasi–free ellasctic scattering we have to deal with Fermi motion of nucleons inside the deuteron. This motion implies that the value of the total energy in the center-of-mass system as well as the direction of the center-of-mass velocity varies from event to event. This means that

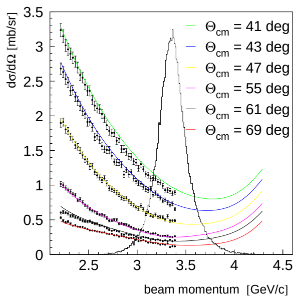

Fig. 2: Differential cross sections as a function of beam momentum for few values of a scattering angle in the center-of-mass system θ_{cm}. Black points stand for EDDA collaboration data [3], lines denote SAID calculations [4]. The solid histogram denotes the distribution of the effective beam momentum for quasi-free $pp \to pp$ reaction calculated at the beam momentum of 3.35 GeV/c.

in a single subrange of the scattering angle in the laboratory system there are events originating from scattering at different values of the total energy $\sqrt{s}$, as well as different scattering angles in the proton-proton center-of-mass system.

Therefore, in order to calculate the integral luminosity, we have to perform simulations taking into account these effects. Each simulated event we have associated with a weight corresponding to the differential cross section which is a function of the scattering angle and the total energy in the center-of-mass system $\sqrt{s}$. For this purpose we have used cross section values for the $pp \to pp$ reaction computed by means of the SAID programme [4] because an accessible data base of the EDDA collaboration was insufficient. In our case, the effective beam momentum which is seen from the nucleon inside the deuteron changes from 2.2 GeV/c up to 4.5 GeV/c whereas EDDA measurements were performed in the range of beam momentum from 0.712 GeV/c to 3.387 GeV/c. Figure 2 shows a comparison of the existing differential cross sections from EDDA measurement and SAID calculations. In the same figure the distribution of the effective beam momentum is also shown.

In order to calculate the integrated luminosity, we have divided the avaiable range of the S1 detector into four subranges. For each subrange, the projection of the distance of the points from the kinematical ellipse was extracted, the background was subtracted and the real number of scattered events $\Delta N_{exp}(\theta_{lab})$ was obtained. The result for one subrange is shown in Fig. 3 (left).

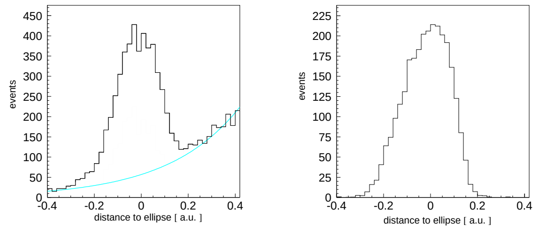

Fig. 3: Projection of the experimental event distribution from Fig. 1 (left) onto the expected kinematical ellipse **(left)**. Projection of the simulated event distribution from Fig. 1 (right) onto the expected kinematical ellipse **(right)**.

In order to determine the $\Delta N_{MC}(\theta_{lab})$ number, we have simulated $N_0 = 10^8$ quasi-free $pp \to pp$ events, which have been analysed using the same procedure as in the case of experimental data. The result for an analogous subrange as for the experimental distribution is shown in fig 3 (right). Assuming, that N_0 is the total number of simulated events, the equation for calculation of the integrated luminosity is as follows [1]:

$$L = \frac{N_0}{2\pi} \frac{\Delta N_{exp}(\theta_{lab})}{\Delta N_{MC}(\theta_{lab})}.$$

We have determined the integral luminosity for all subranges of the S1 detector individually and subsequently the average value. The average integrated luminosity is equal to $L = (4.77 \pm 0.06)x10^{36}cm^{-2}$. The value of the systematical error is still under evaluation.

References:

[1] P. Moskal, R. Czyżykiewicz, AIP Conf.Proc. **950**, 118 (2007).
[2] P. Klaja et al., AIP Conf.Proc. **796**, 160 (2005).
[3] D. Albers et al., Phys. Rev. Lett. **78**, 1652 (1997)
[4] The CNS Data Analysis Center, http://www.gwu.edu

Status of the analysis of the $pn \to pn\eta'$ reaction

J. Przerwa and P. Moskal for the COSY-11 collaboration

In August 2004 the COSY–11 group has conducted a measurement of the η' meson production in the proton-neutron collision [2]. The aim of the experiment is the determination of the total cross section of the $pn \to pn\eta'$ reaction near the kinematical threshold. The comparison of the $pp \to pp\eta'$ and $pn \to pn\eta'$ total cross sections will allow to learn about the production of the η' meson in different isospin channels and to investigate aspects of the gluonium component of this meson.

The experimental precision of the missing mass determination of the $pn \to pn\eta'$ reaction rely on the accuracy of the momentum reconstruction of protons and neutrons. In this report we give an account on our investigations of the time walk effect in the neutral particle detector, where neutrons are registered and on the calibration of the silicon-pad detector, where protons considered as spectators are measured.

The time walk effect is caused by variations in the amplitude and risetime of the incoming signals. Therefore, signals exactly coincident in time may trigger the discriminator at different times. An offline correction can be applied to minimize this effect. The function used for offline time-walk correction was

$$t_c = t_m - \alpha + \beta\left(\frac{1}{\sqrt{ADC^{up}}} + \frac{1}{\sqrt{ADC^{dw}}}\right),$$

where t_c and t_m are corrected and measured time, α and β are coefficient determined from the data, and ADC^{up} and ADC^{dw} denote the charge of the signal measured at upper and lower edge of the detection module.

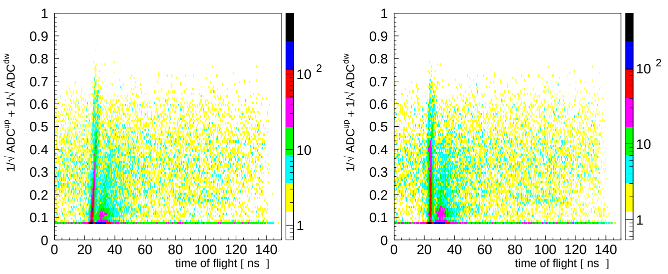

Fig. 1: Time walk effect. ADC signals in the neutral particle detector as a function of the time-of-flight (TOF) between the target and the neutron detector as obtained before (left) and after (right) time walk correction.

Figure 1 shows the dependence of the ADC signals in the neutral particle detector on the time-of-flight between the target and the neutron detector. The ADC signals are expressed as a combination of signals in the upper and lower photomultiplier by means of the formula: $\frac{1}{\sqrt{ADC^{up}}} + \frac{1}{\sqrt{ADC^{dw}}}$. The left panel of this figure shows the distribution, which was used to determine the α and β coefficients. The right panel presents the analogous distribution with the corrected time. After applying the time walk correction the time resolution improved from 1.2 ns to 0.6 ns (σ). It is worth to note that this is an overall figure, including the resolution of the neutron and S1 detectors and the accuracy of the momentum reconstruction of charged particles, needed for the determination of the time of the reaction in the target.

In order to identify the unobserved meson η' in the $pn \to pnX$ process by means of the missing mass technique, one has to measure not only momenta and hence energies of the outgoing proton and neutron, but also registration of the spectator proton is needed. The spectator detector consists of four double-layered modules. Each of the front layer, which is the plane closer to the beam, contains eighteen silicon pads, whereas back layers consist of only six silicon pads. During the experiment, we have measured the charge of the signal induced in the detector by the particles, which is proportional to the energy deposited in the detection unit. Denoting by ADC_1 and ADC_2 the measured charge in the first and second layer, respectively, the real energy loss can be expressed as: $dE_1 = \alpha_1 ADC_1$ and $dE_2 = \alpha_2 ADC_2$, where α_1 and α_2 are the calibration constants for two layers. Moreover, we are able to derive not only the spectator kinetic energy but also the emission angle. The aim of the spectator detector calibration was to find the exact position of the detector and than to establish the calibration constants for each of 96 detection units. The position of the spectator detector inside the beam pipe is described by only three parameters [3]. Assuming that the set of calibrations constants (α_1, α_2) are correct, we have fitted experimental distributions of the $dE_1(dE_2)$ to the calculated energy losses, and examine the value of χ^2 as a function of the parameters describing the position of the spectator detector. Having the new position of the detector the experimental data points on the $dE_1(dE_2)$ plot were fited to the expected $dE_1(dE_2)$ function, with calibration constans α_1 and α_2 as free parameters for each detection pair. The procedure was repeated until the changes become negligible.

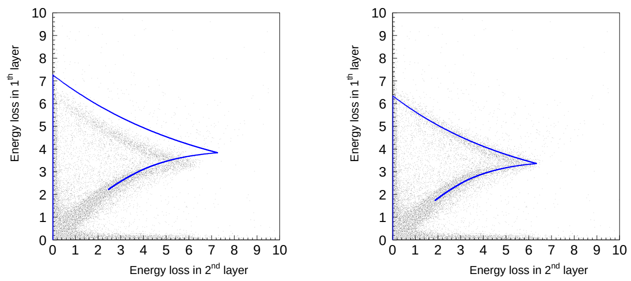

Fig. 2: Energy losses in the first layer versus the second layer as measured at COSY–11 with a deuteron target and a proton beam with momentum of 3.35 GeV/c before (left) and after (right) calibration. Points represent the experimental data, whereas the theoretical calculations are indicated by the solid curve.

Figure 2 (left) shows the energy losses in the first layer versus the second layer before the calibration constants α_1 and α_2 were determined. The calculated energy losses are indicated by the solid curve. Fig. 2 (right) shows the example of this plot after the calibration.

References:

[1] S. Brauksiepe et al., NIM **A 376** 396 (1996).
[2] P. Moskal et al., COSY Proposal **No. 133** (2003).
[3] R. Czyżykiewicz, Diploma Thesis, Jagiellonian Uni. (2002).

Status of the analysis of the $pn \to d\eta'$ reaction measured using the COSY–11 facility.

B. Rejdych[1], P. Moskal[1] for the COSY-11 collaboration

One of the research topics of the COSY–11 collaboration is the investigation of the η' meson production in nucleon-nucleon collisions. The aim is to explain the reaction mechanism and gain information on the unknown interaction between the η' meson and the proton.

In previous experiments the near threshold excitation function for the $pp \to pp\eta'$ reaction was determined [1, 2, 3, 4, 5]. However, it was not possible uniquely identify mechanism responsible for the η' meson production from this reaction channel only. Therefore, it is desirable to determine the dependence of the η' meson production on the isospin of the interacting nucleons [6, 7, 8].

For this purpose in August 2004 we investigated the $pn \to pn\eta'$ reaction [8, 9]. Subsequently, in February 2006 we extended the research to the production of the η' meson in nucleon-nucleon collisions in a pure isospin zero state of the interacting nucleons. The study was carried out via measuring of the quasi–free $pn \to d\eta'$ reaction, using the deuteron cluster-jet target and the proton beam with a momentum of 3.365 GeV/c.

The reaction may be symbolically presented as:

$$p\begin{pmatrix} n \\ p_{sp} \end{pmatrix} \to \begin{matrix} d\eta' \\ p_{sp} \end{matrix}$$

where p_{sp} denotes the proton from the deuteron regarded as a spectator which does not interact with other particles.

The identification of the $pn \to d\eta'$ reaction is based on the determination of four-momentum vectors of the outgoing deuteron and the spectator proton. The missing mass technique is used for identification of the η' meson. The momentum of the interacting neutron is deduced from the momentum of the spectator proton under the assumption that the spectator was on its mass shell at the moment of the collision. The main result of the analysis of the $pn \to d\eta'$ reaction will be the determination of the near threshold excitation function.

During the measurement of the $pn \to d\eta'$ reaction also other processes were simultaneously registered. The measurement of the $pn \to pn\eta'$ reaction was continued, as well as the $pp \to pp$ quasi-free proton-proton elastic scattering events, indispensable to estimate the luminosity, were registered.

The measurement of the $pn \to d\eta'$ process was possible at COSY-11 facility using the spectator detector and the deuteron chamber denoted in Fig. 1 as Si_{spec} and $D4$, respectively. These detectors were installed formerly to study the $pd \to pd\eta$ [10] and $pn \to pn\eta'$ [11] reactions. In the year 2007 the decoding of the data and examination of the functioning of all relevant detector components was performed. Next, the whole data sample was preselected and divided into three subsamples of those events, which probably were due to one of the reactions of interest. Events giving signals in the spectator detector Si_{spec}, the deuteron chamber $D4$ and in any of the five scintillation detectors $S1^{D4} \ldots S5^{D4}$ were assinged to the subsample with $pn \to d\eta'$ reactions. In parallel events were included into the subsample with $pn \to pn\eta'$ reactions if the signals in the spectator detector, the drift chambers $D1$ and $D2$, scintillation detectors $S1$ and $S3$, as well as the signals in the neutron detector N were registered. After preliminary examination of the whole data sample with 233 294 934 events, written on digital linear tape (DLT), the number of events decreased to 76 047 930, including 22 746 013 events which might correspond to the $pn \to d\eta'$ reaction, and 48 496 695 supposed to be $pn \to pn\eta'$ reaction. As as result, the first preselection of the data sample reduced significantly the number of events for the further analysis. In particular, the subsample including events from the main investigated reaction consitutes only 10% of the whole data set written on DLT during the experimental run. We conclude that this was time consuming but neccessary work which will accelerate the more advanced off-line analysis presently in progress.

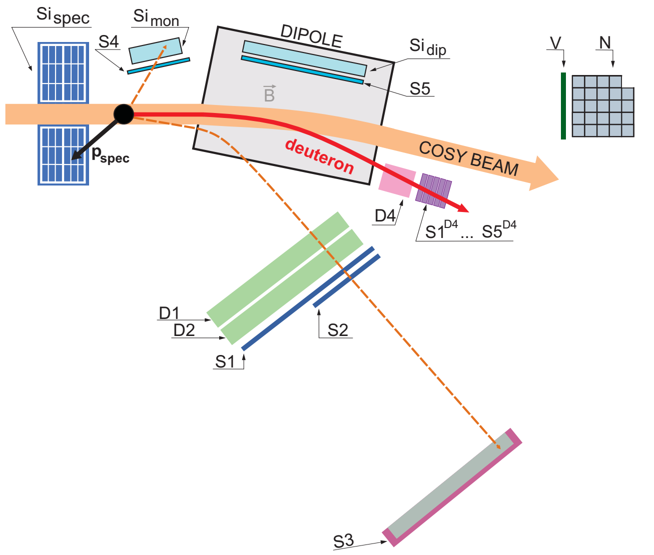

Fig. 1: Schematic view of the COSY-11 detection setup. D1, D2, and D4 denote the drift chambers; S1, S2, S3, S4, S5, $S1^{D4}$ ... $S5^{D4}$ and V stand for the scintillation detectors; N is the neutron detector and Si_{mon}, Si_{spec} and Si_{dip} are silicon strip detectors to detect elastically scattered protons, spectator protons and negatively charged particles, respectively. Superimposed solid lines indicates spectator proton and deutron from the quasi free $pd \to p_{sp}d\eta'$ reaction and the dashed lines show an example of the quasi-free elastically scatterd protons. The sizes of detectors and their relative distances are not to scale.

References:

[1] A. Khoukaz at al., Eur. Phys. J. **A 20**, 345 (2004).
[2] P. Moskal et al., Phys. Lett. **B 474**, 416 (2000).
[3] F. Balestra et al., Phys. Lett. **B 491**, 29 (2000).
[4] F. Hibou et al., Phys. Lett. **B 438**, 41 (1998).
[5] P. Moskal et al., Phys. Rev. Lett.**80**, 3202 (1998).
[6] S. D. Bass, Phys. Scripta **T 99**, 96 (2002).
[7] S. D. Bass, Phys. Lett. **B 463**, 286 (1999).
[8] P. Moskal et al., Int. J. Mod. Phys. **22**, 305 (2007).
[9] J. Przerwa, AIP Conf. Proc. **950**, (2007) 112.
[10] C. Piskor-Ignatowicz, IKP, FZ-Jülich, Ann. Rep. 2006.
[11] J. Przerwa, IKP, FZ-Jülich, Ann. Reps. 2006 and 2007.

[1] Institute of Physics, Jagellonian University, Poland

Status of the total width determination of the η' meson

E. Czerwiński, D. Grzonka and P. Moskal for the COSY–11 collaboration

Using the stochastically cooled proton beam of the cooler synchrotron COSY and the COSY–11 apparatus we have measured the mass distribution of the η' meson producing it via the $pp \to pp\eta'$ reaction. Studies of the η' meson production [1] and decays [2] are of interest on its own and provide inputs to the phenomenology of the Quantum Chromo-Dynamics in the non-perturbative regime [3]. The important input parameters are e.g. values of the partial decay widths. The experimental precision of the partial width for various decay channels – where only the branching ratio is known or will be measured – is governed by the precision of the knowledge of the total width. In the case of the η' meson the branching ratios are typically known with accuracies better than 1.5%, while the total width is established about 10 times less accurate [4]. In comparison to previous measurements of the η' meson production at the COSY–11 detection setup the supply voltage of the drift chambers was increased up to the maximum allowed value in order to improve the experimental resolution of the four-momentum determination. A charged particle passing through the drift cell ionizes gas molecules. Released electrons drift towards the sense wire with a drift time related to the distance between the sense wire and the particle trajectory. The drift time to distance relation was calibrated for each 20 - 24 hours of the data taking period in order to minimize fluctuations of the drift velocity caused by variations of the atmospheric pressure, air humidity and gas mixture changes. Figure 1 (left) illustrates that the obtained spatial resolution is about 100 μm. The measurement of the missing mass distributions at five different beam energies will allow for monitoring the systematic uncertainties in the determination of the experimental mass resolution. This is mainly because the smearing of the missing mass due to the natural width of the η' meson remains unaltered when the beam momentum changes, whereas the smearing caused by the experimental uncertainties will narrow with decreasing beam momentum and at threshold it will reach a constant value directly proportional to the spread of the beam momentum. The effect is shown on the right in Fig. 1, which also illustrates that the reduction of the target thickness from 9 mm to 1 mm results in an improvement of the mass resolution by about 0.3 MeV. Since we expect to control the target thickness with an accuracy better than 0.2 mm, the systematical error due to the determination of the target size will be smaller than 0.01 MeV. Closest to the threshold the width of the missing mass distribution is approximately 0.4 MeV (FWHM). Taking into account that the width of the η' meson is around 0.2 MeV the achieved experimental resolution is of the same order as the width of the signal. The presented spectra were obtained with a very preliminary calibration of the detection system. Hence, there is still room for an improvement of the experimental resolution in the ongoing off-line analysis.

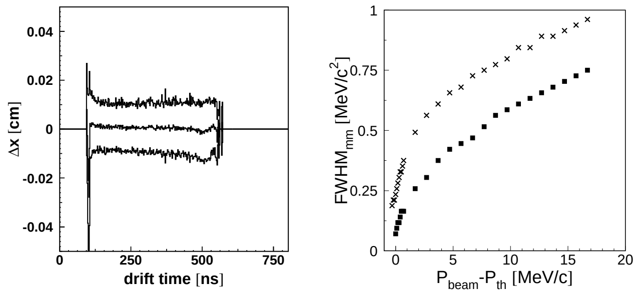

Fig. 1: (Left) Average deviation (ΔX) between the measured and the fitted distances of tracks from the sense wire as a function of the drift time. The line around 0 corresponds to the average value of the ΔX distribution and the upper and lower lines denotes the spatial resolution ($\pm 1\sigma$) of the drift chamber. (Right) FWHM of the missing mass spectrum as a function of beam momentum above the threshold for the η' meson creation in proton-proton collisions simulated for 9 mm (crosses) and 1 mm (squares) target width [5].

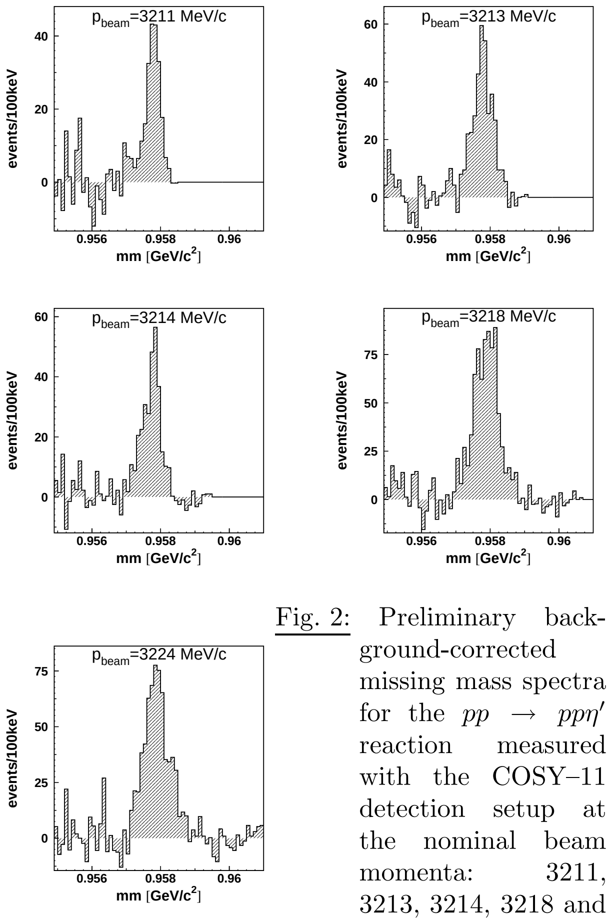

Fig. 2: Preliminary background-corrected missing mass spectra for the $pp \to pp\eta'$ reaction measured with the COSY–11 detection setup at the nominal beam momenta: 3211, 3213, 3214, 3218 and 3224 MeV/c.

References:

[1] P. Moskal, e-Print: hep-ph/0408162 (2004).
[2] A. Kupść, AIP Conf. Proc. **950**, 165 (2007).
[3] B. Borasoy and R. Nißler, AIP Conf. Proc. **950**, 180 (2007).
[4] W.-M. Yao *et al.*, J. Phys. G **33**, 1 (2006).
[5] E. Czerwiński, Diploma thesis, Jagiellonian University (2006).

Analysis of the differential cross-sections for the reaction $pp \to ppK^+K^-$ in view of the K^+K^- interaction

M. Silarski[a] and P. Moskal[a] for the COSY-11 collaboration

Measurements of the total cross section of the reaction $pp \to ppK^+K^-$ were performed at the cooler synchrotron COSY near the kinematical threshold by the COSY-11 collaboration [1, 2], and for higher energies by the ANKE collaboration [3]. This reaction channel was studied also by the DISTO collaboration [4] at Q = 114 MeV at the SATURN accelerator. The results indicate that near threshold data points lie significantly above theoretical expectations.

The enhancement may be due to the influence of K^+K^- or Kp interactions which were neglected in the calculations. This interaction should manifest itself also in the distributions of the differential cross-sections [5]. A significant effect observed for the excitation function for the $pp \to ppK^+K^-$ reaction encourages us to carry out the analysis of double differential cross sections in spite of the fact that the available statistics is quite low. In our investigation we use experimental data obtained from two COSY-11 measurements at excess energies of Q = 10 MeV (27 events) and 28 MeV (30 events) [2]. At present we are, however, at the early stage of the analysis.

For three particles in the final state the process of analysing data by plotting them in the space of two internal parameters is a very convenient way to study the interaction. It was originated by Dalitz in a nonrelativistic application. In the original paper [6] Dalitz let the distances to the sides of an equilateral triangle be the energies of the three particles in the center-of-mass system. Another convenient coordinate is the squared invariant masses of the two-body subsystems. Using such coordinates we obtain event distributions bounded by a well defined smooth closed curve [7]. The area of the Dalitz Plot is proportional to the phase space volume. Moreover, for no dynamics and the absence of any final state interaction, the occupation of the Dalitz plot would be fully homogeneous because the creation in any phase space interval would be equally probable. Thus, final state interactions should show up as a modification of the event density in the Dalitz plot.

For four particles in the final state the analysis is more complex, because one needs five variables to fully describe a relative movement of particles. Nevertheless, there are many different types of generalization of the Dalitz plot for four-particle final states, which make possible to study interaction between particles in the exit channel. For studying the K^+K^- or Kp interaction we use two convenient generalizations proposed by Chodrow [8] and Goldhaber [9, 10].

In his work [8] Chodrow assumed, that the invariant matrix element for the process depends only on the energies of the particles. For four particles with masses m_i and total energy E in the center-of-mass frame, the probability of a reaction yielding a state with the ith particle in the energy range dE_i (when two of the particles are identical) is:

$$d^3P = 32\pi^2 \left|M\right|^2 dF_1 dE_2 dE_3, \tag{1}$$

where $dF_1 = \sqrt{E_1^2 - m_1^2} dE_1$ and M denotes the invariant matrix element for the process. This implies that $F_1 = \frac{1}{2}\left[E_1\sqrt{E_1^2-m_1^2} - m_1^2 cosh^{-1}\left(\frac{E_1}{m_1}\right)\right]$. The distribution of events can then be plotted in the F_1E_2-plane, and resonances may be directly read off this part of the plot, where $E_1 < E_2$. Similarly as in the case of three particle final states the physically allowed region in a Chodrow plot is bounded by a well defined curve, but the event density is not homogeneous and the area of the plot is not proportional to the phase space volume.

According to Nyborg, several other extensions of the Dalitz plot can be obtained if one assumes, that the matrix element M depends only on invariant masses of two- and three particle subsystems [7]. Suppose that M depends at most on M_{12}^2, M_{34}^2, and M_{124}^2, which corresponds to the situation were only two two-particle or one three-particle resonances are present [7]. The distribution of events is then given by:

$$d^3P = \frac{\pi^3}{8E^2M_{12}^2}\left|M\right|^2 g\left(M_{12}^2, m_1^2, m_2^2\right) dM_{12}^2\, dM_{34}^2\, dM_{124}^2 \tag{2}$$

where:

$$g\left(M_{12}^2, m_1^2, m_2^2\right) = \sqrt{\left[M_{12}^2 - (m_1+m_2)^2\right]\left[M_{12}^2 - (m_1-m_2)^2\right]}.$$

The projection of the physical region on the (M_{12}, M_{34})-plane, referred to as a Goldhaber plot, gives a right isosceles triangle within which the area is not proportional to the phase space volume. It is worth mentioning that the event density in the Goldhaber plot is not homogeneous and goes to zero on the entire boundary of the plot given by following equations: $M_{12} + M_{34} = E$, $M_{12} = m_1 + m_2$, $M_{34} = m_3 + m_4$ [7]. So far we conducted Monte Carlo simulations of the $pp \to ppK^+K^-$ reaction [11] using a FORTRAN-based code, called GENBOD [12]. The simulations were first made assuming that there is no final state interaction, then the pp-FSI was included [13]. The pp-FSI was taken into account as weights proportional to the inverse of a squared Jost-function of the Bonn potential [14]. In order to compare these spectra with the experimental distributions we need to correct them for the acceptance and detection efficiency of the COSY-11 facility. This will be the next step of the ongoing investigations.

References:

[1] C. Quentmeier, et al., Phys. Lett. B **515**, 276-282 (2001).
[2] P. Winter, et al., Phys. Lett. B **635**, 23-29 (2006).
[3] Y. Maeda, et al., Phys. Rev. C **77**, 015204 (2008).
[4] F. Balestra, et al., Phys. Lett. B **468**, 7-12 (1999).
[5] P. Moskal, et. al., Prog. Part. Nucl. Phys. **49**, 1-90 (2002).
[6] R.H. Dalitz, Phil. Mag. **44**, 1068 (1953).
[7] P. Nyborg, et al., Phys. Rev. **140**, 914 (1965).
[8] D. Chodrow, Nuovo Cimento **50**, 674 (1967).
[9] G. Goldhaber, et al., Phys. Rev. Lett. **9**, 330 (1962).
[10] G. Goldhaber, et al., Phys. Rev. Lett. **6**, 62 (1963).
[11] M. Silarski, P.Moskal, AIP Conf. Proc. **950**, 77 (2007).
[12] F. James, Monte Carlo phase space, CERN 68-15 (1968).
[13] P. Moskal, et. al., Phys. Lett. B **482**, 356-362 (2000).
[14] B. L. Druzhinin, et al., Phys. A **359**, 205 (1997).

[a] M. Smoluchowski Institute of Physics, Jagellonian University, 30-059 Cracow, Poland

A method for the luminosity determination in the quasi-free meson production reactions

R. Czyżykiewicz and P. Moskal for the COSY-11 collaboration

A method for luminosity determination in the quasi-free meson production was developed for the COSY-11 experiment on the production of the η meson in the quasi-free proton-neutron collisions, close to the kinematical threshold [1]. However, this method is of universal nature and may be applied to determine the luminosity in any quasi-free production reaction.

The reference reaction chosen for the purpose of calculation of the luminosity was the quasi-free $pp \to pp$ scattering. For the free proton-proton scattering the luminosity could be determined as a normalization constant between the measured angular distribution of the cross section and the corresponding spectrum extracted from the previous experiments. For the quasi-free reaction the evaluation becomes more complicated due to the Fermi motion of nucleons inside the nucleus. Since the direction and momentum of the bound nucleon varies from event to event this implies that the direction of the center-of-mass velocity of the colliding nucleons as well as the total available energy for the reaction also varies from event to event. Therefore, protons registered in the laboratory under a given scattering angle or at a given part of the detection system correspond to the finite range of scattering angles in the proton-proton center-of-mass frame. This implies that the experimental angular distributions cannot be directly compared to literature values. Instead an evaluation of the luminosity requires simulations taking into account the Fermi motion of the nucleons, and the variations of differential cross sections for the elastic scattering as a function of the scattering angle and energy.

For each simulated event we know the generated Fermi momentum of the nucleon, as well as the scattering angle of protons in their center-of-mass system. This permits us to assign to each event a weight corresponding to the differential cross section, which is uniquely determined by the scattering angle and the total collision energy $\sqrt{s}$.

For free proton-proton scattering we could measure the number of events - $\Delta N(\theta,\phi)$ scattered into the solid angle $\Delta\Omega(\theta,\phi)$ around the polar and azimuthal angles θ and ϕ, respectively. In this case the angles in laboratory and in the center-of-mass systems are univocally related to each other. With the known differential cross section for proton-proton scattering into that particular solid angle, and having known the value of the solid angle $\Delta\Omega(\theta,\phi)$ from the Monte-Carlo simulations the luminosity can be calculated according to the formula:

$$L = \frac{\Delta N(\theta,\phi)}{\Delta\Omega(\theta,\phi)\frac{d\sigma}{d\Omega}(\theta,\phi)}. \tag{1}$$

In the case of quasi-free proton-proton scattering the number of elastically scattered protons ΔN into a solid angle $\Delta\Omega(\theta_{lab},\phi_{lab})$ is proportional to L – the integrated luminosity and also to the inner product of the differential cross section for scattering into the solid angle around θ^* and ϕ^* angles – $\frac{d\sigma}{d\Omega}(\theta^*,\phi^*,p_F,\theta_F,\phi_F)$ – and the probability density of the distribution of the Fermi momentum $f(p_F,\theta_F,\phi_F)$:

$$\Delta N_{exp}(\Delta\Omega(\theta_{lab},\phi_{lab})) = L\int_{\Delta\Omega(\theta_{lab},\phi_{lab})}\frac{d\sigma}{d\Omega}(\theta^*,\phi^*,p_F,\theta_F,\phi_F)\,f(p_F,\theta_F,\phi_F)\,dp_F\,d\cos\theta_F\,d\phi_F\,d\phi^*\,d\cos\theta^*. \tag{2}$$

The angles θ^* and ϕ^* are expressed in the proton-proton center-of-mass system, while the angles θ_{lab} and ϕ_{lab} describe the directions in the laboratory. In the case of the complex detection geometry, with a magnetic field a solid angle corresponding to a given part of the detector cannot, in general, be expressed in a closed analytical form. Therefore, the integral in Equation 2 must be computed using the Monte-Carlo method. For the evaluation of a given event by the Monte Carlo program, first we choose randomly the momentum of a nucleon inside a deuteron according to the Fermi distribution. Next, the total energy $\sqrt{s}$ for the proton-proton scattering and the vector of the center-of-mass velocity are determined. Then, assuming an isotropic distribution we generate the momentum of protons in the proton-proton center-of-mass frame. Further on, according to the generated angle and the total energy $\sqrt{s}$ we assign to the event a probability equal to the differential cross section, utilizing the bilinear interpolation in the $\sqrt{s}$–θ^* space. Next, the momenta of protons are transformed to the laboratory frame and are used as an input in the simulation of the detector signals with the use of the GEANT package.

In order to calculate the integral on the right hand side of this equation we simulated N_0 events according to the procedure described above. Due to the weights assigned to the events the integral is not dimensionless and its units correspond to the units of the cross section used for the calculations. The number obtained from the Monte-Carlo simulations must be then normalized such that the integral over the full solid angle equals the cross section for the elastic scattering averaged over the distribution of the total reaction energy $\sqrt{s}$ resulting from the Fermi distribution of the target nucleon. This means that we need to divide the resultant Monte-Carlo integral by the number of generated events N_0 and multiply it by the factor of 2π. A factor of 2π comes from the normalization of the differential cross section, regarding the fact that protons taking part in the scattering are indistinguishable. Hence, the formula for the calculation of the integrated luminosity for the quasi-free reaction reads:

$$L = \frac{N_0\Delta N_{exp}}{2\pi I}, \tag{3}$$

where the normalization constant $N_0/2\pi$ is subject to the Monte-Carlo method used for the integral computation, and I in the denominator denotes the integral obtained from simulation of N_0 events.

ΔN_{exp} from Equation 2 can be determined as a number of elastically scattered protons registered in a given part of the detection system.

A more detailed description of the method described above and its application to the calculation of the luminosity for the measurement of the quasi-free $pn \to pn\eta$ reaction can be found in [2].

References:

[1] P. Moskal et al., J. Phys. **G 32** (2006) 629.

[2] P. Moskal, R. Czyżykiewicz, AIP Conf. Proc. **950** (2007) 118.

Study of the $\vec{d}+d \to \eta+\alpha$ reaction 16 MeV above threshold.

GEM Collaboration

The quest of the existence of bound states of eta mesons on nuclei is a long standing question. The large η nucleon scattering length makes this rather likely. While some theorists find binding in their calculations only for nuclei heavier than carbon others predict even the α particle to be sufficient heavy to bind the η. One possibility to observe binding is to study the η nucleon interaction in *fsi*. According to the Watson-Migdal theory [1, 2] for a weak transition and a strong *fsi*, one can approximate the total reaction amplitude, f_s, at low energies by

$$f_s = \frac{f_B}{1-iap_\eta} \tag{1}$$

with $a \equiv a_r + ia_i$ the complex s-wave η nucleus scattering length. f_B is the production amplitude usually taken as a constant. In the case of binding the following relations have to be fulfilled [3]:

$$a_r < 0, \tag{2}$$

$$a_i > 0 \tag{3}$$

from unitarity and

$$R = \frac{|a_i|}{|a_r|} < 1 \tag{4}$$

to have a pole in the complex p_η plane. In order to test data against these criteria we have measured the reaction $\vec{d}+d \to \eta+\alpha$ close to threshold. A vector and tensor polarized deuteron beam allows to measure in addition to cross sections analyzing powers and thus to deduce partial wave amplitudes.

We have measured α particles from the reaction of interest with the magnetic spectrograph BIG KARL at an excess energy of 16 MeV above threshold. The observables measured were the differential cross section $d\sigma/d\Omega$ for an unpolarized beam as well as for a polarized beam with analyzing powers given in Table 1 and the polarization tensor $A_{xx}(\theta)$.

p_z nominal	p_z measured	p_{zz} nominal	p_{zz} measured
-1/3	-0.33 $\pm$ 0.02	-1	-0.87 $\pm$ 0.11 $\pm$ 0.01
-1/3	-0.32 $\pm$ 0.02	+1	+0.91 $\pm$ 0.14 $\pm$ 0.01

Table 1: Results of the vector and tensor polarizations measurement.

The differential cross sections are shown in Fig. 1 for the unpolarized beam. The data were fitted by a Legendre polynomial

$$\frac{d\sigma(\theta)}{d\Omega} = \sum_{l=0,\Delta l=2}^{l_{max}} a_l P_l(cos\theta). \tag{5}$$

The smallest number for l_{max} was found to be four indicating that no only s- and p-waves contribute but also d-waves. This is in contrast to data from ANKE [4] where $l_{max} = 2$ suffices to describe the data (see Fig. 1). In order to study a possible

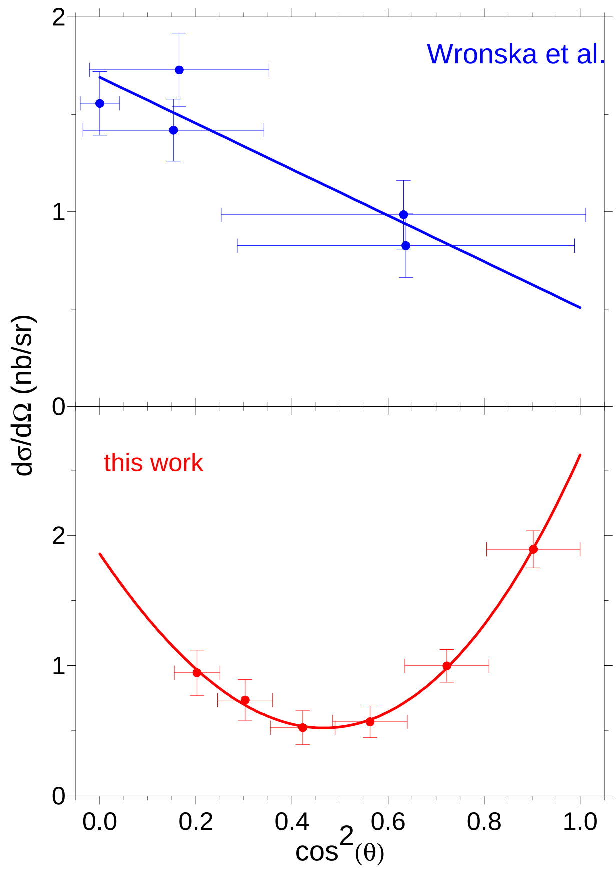

Fig. 1: Upper panel: differential cross sections from Ref. [4] at 7.7 MeV above threshold. The solid line is a second order Legendre polynomial fit. Lower panel: same as above but for the present data at $Q = 16$ MeV and also an unpolarized beam. The solid curve is a fourth order Legendre polynomial fit.

binding the s-wave has to be extracted. We have fitted s-, p- and two d-waves to the data. Since there is always one free parameter we have made the s-wave amplitude a_s real. Unfortunately there is a strong correlation among the different parameters. Only the s-wave could be extracted with a reasonable small error thus yielding the s-wave fraction of the differential cross section. From this we obtain a spin averaged amplitude

$$\frac{d\sigma_s}{d\Omega} = \frac{p_\eta}{p_d}|f_s|^2 \propto \frac{p_\eta}{p_d}|a_s|^2. \tag{6}$$

This amplitude is for the present measurement compared with previous measurements in Fig. 2. In Ref. [4] the origin of the term $\propto \cos^2\theta$ in the ANKE data shown in Fig. 1 remained unclear. It could be attributed either to a p-wave or due to a $s-d$-wave interference. Because the present result is quite small it rules out the $s-d$-wave interference scenario. Thus one can extract the s-wave amplitude from the angular distribution also shown in Fig. 2.

The authors of Ref. [5] did a combined optical-model fit to all the near-threshold $pd \to {}^3He\eta$ and $dd \to {}^4He\eta$ data, assuming that only s-wave production occurs, and this resulted

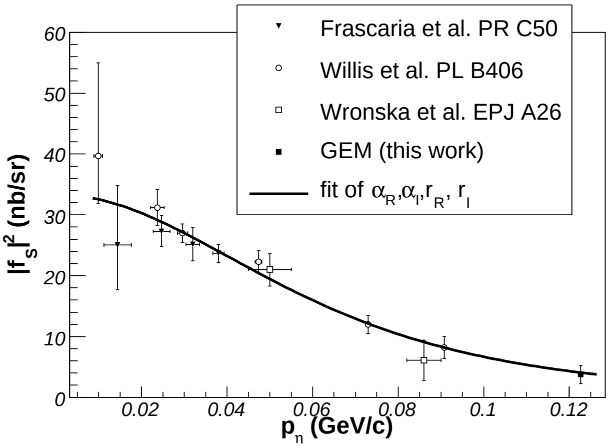

Fig. 2: The spin averaged s-wave amplitude as a function of the excess energy. The data are shown by the symbols, the fit described in the text as solid curve.

in a value $a = (-2.2 + i1.1)$ fm. In this analysis the real part of a was fixed mainly by the $^3He\eta$ data and so the scattering length has been carried out by varying just a_i. This resulted in $a = (-2.2 + i2.3)$ fm for the $s + p$ assumption. When we repeat this exercise -keeping $a_r = -2.2$- we get a fit with a large χ^2. This becomes much better if we introduce the effective range $r \equiv r_r + ir_i$. Then the spin averaged amplitude is

$$f_s = \frac{f_B}{1 - p_\eta a + \frac{1}{2} a r p_\eta^2}. \tag{7}$$

A fit of all four effective range parameters to the data is shown in Fig. 2 which shows a remarkable quality. The ratio Eq. [4] was found to be $R = 0.19 \pm 0.66$ which fulfills the requirement for a bound eta. However, the sign of the real part of the scattering amplitude needs to be extracted in order to be decisive.

References:

[1] K. Watson: Phys. Rev., **88** (1952) 1163.
[2] A. B. Migdal: Soviet Phys. JETP, **1** (1955) 2.
[3] Q. Haider, L. C. Liu: Phys. Rev., **C 66** (2002) 045208.
[4] A. Wrońska et al.: The European Physical Journal, **A 26** (2005) 421.
[5] N. Willis et al.: Phys. Lett., **B 406** (1997) 14.

Search for η bound nuclei in a transfer reaction.

GEM Collaboration

The large η nucleon scattering length makes the existence of bound states of eta mesons on nuclei rather likely. While some theorists find binding in their calculations only for nu clei heavier than carbon others predict even the α particle to be sufficient heavy to bind the η. Similar to the production of hyper nuclei or pionic atoms we make use of a transfer reaction at recoil free kinematic. The reaction chosen here is the

$$p + {}^{27}Al \to {}^{3}He + {}^{25}Mg \otimes \eta. \quad (1)$$

Because the $N^*(1535)$ resonance extends down to the η-nucleon threshold a second step

$$\eta + N \to N^* \quad (2)$$

has high probability. When an η is bound, the associated N*(1535) has its mass below the ηN threshold and, therefore, cannot decay into an observable *eta* plus an observable nucleon because of energy conservation; that is what is call binding of η. The only probable decay is into an πN. Such a scenario is shown in Fig. 1.

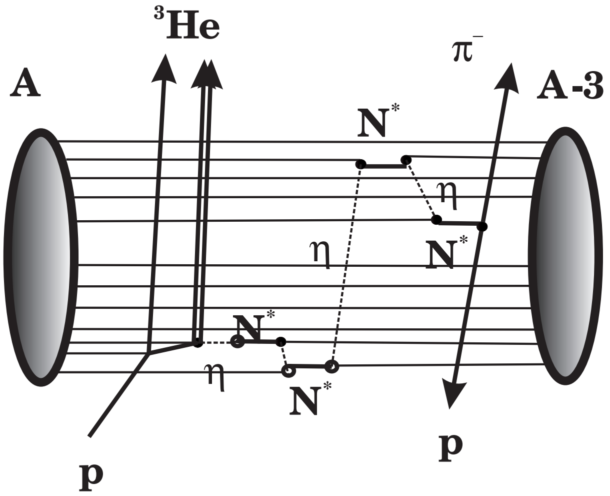

Fig. 1: Production and evolution of a η bound nucleus and and decay into a pion and a proton of an N^*.

The ^3He ion carries away almost al beam momentum. Then the residual system is at rest and the η wave function has large overlap with the nuclear wave function in phase space, thus the probability of having a bound system is large. Because of this the pion and the nucleon from the second step 2 have to be emitted almost back to back. The underlying kinematics is shown in Fig. 2. The transferred momentum as function of the bean energy is shown for different bindings. The solid line shows the actual chosen beam momentum. For binding energies up to $0 > B > -30$ MeV is the transferred momentum less than 30 MeV/c. It is this range where bound systems are expected to occur. Predictions for the binding energy and the widths from different references [1–5] are shown in Fig. 3. There is a general trend: binding becomes stronger with increasing nuclear mass number as does the width. Since one can expect the state to be superimposed on some background heavy nuclei will be not the

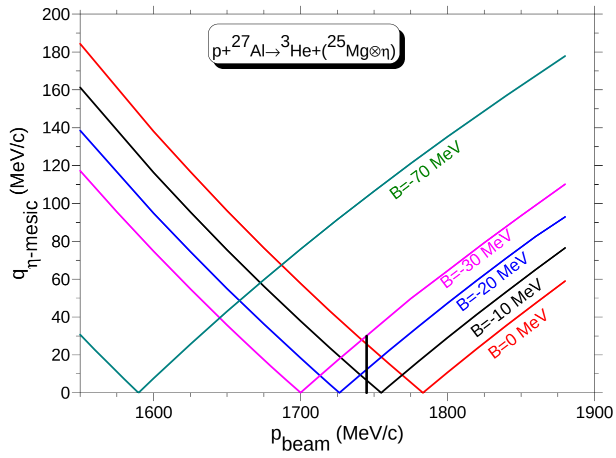

Fig. 2: Momentum transfer as function of the beam momentum for different binding energies B in the mesic nucleus. The vertical line indicates the beam momentum.

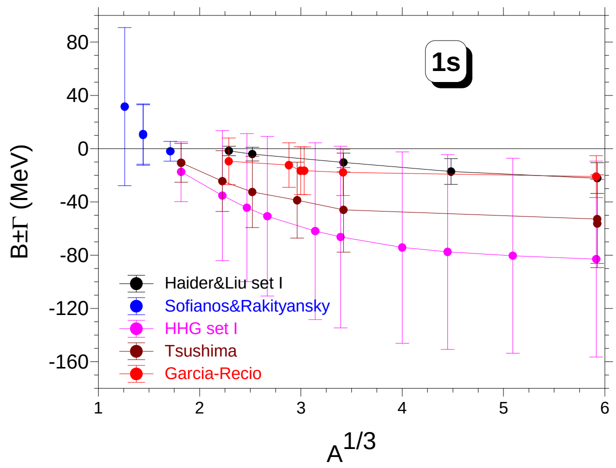

Fig. 3: Theoretical predictions (Refs. [1–5]) of binding energies and widths of η mesic nuclei with the η and the nucleus in their ground state as function of the nuclear mass number.

favorite choice. For light nuclei the effect may be to small. Therefore a medium to light nucleus was chosen. In order to avoid a lot of nuclear excitations the ideal target nucleus would be an odd-odd nucleus yielding after quasi deuteron transfer finally an even-even nucleus. However, there is no solid target available and as a compromise an odd-even nucleus ^{27}Al was chosen leading to ^{25}Mg and even-odd nucleus. A two nucleon transfer was chosen, in spite of the smaller cross section compared to a one nucleon transfer, because in a $d + {}^{27}Al \to {}^{3}He + p + \pi^- + X$ reaction the ^3He spectrum will be dominated by protons from deuteron break up, having the same magnetic rigidity as the ^3He ions of interest have. Where as Hayano et al. [3] predict always very strong binding the other calculations predict for the present mass number values around $B \approx -10$ MeV [1,5].

We have performed the experiment by detecting the ^3He with the magnetic spectrograph BIG KARL [6]. The decay from a neutral N^* was detected with a dedicated detector named ENSTAR [7]. In two settings of the spectrograph an enhancement was found close to threshold. The data were added weighted by the acquired luminosity. The resulting missing mass spectrum is shown in Fig. 4 The upper abscissa shows

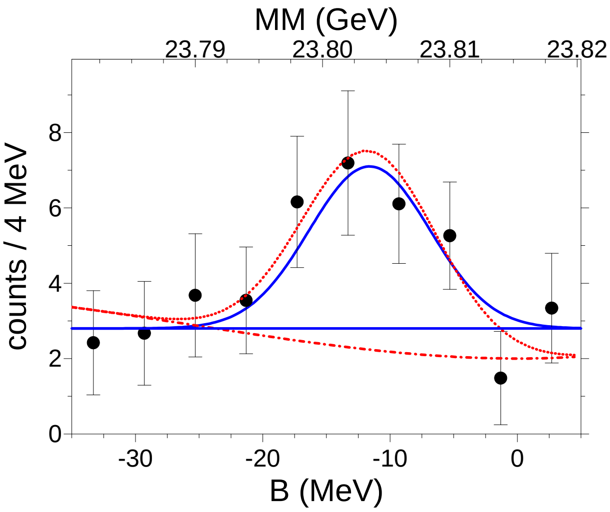

Fig. 4: Missing mass spectrum from two different settings of the spectrograph requiring a coincidence between ^3He in the spectrograph and a π^- and a proton in the ENSTAR detector being emitted almost back to back. Curves see text.

the missing mass MM, while the lower abscissa the binding energy assuming $B = [m(\eta) + m(^{25}Mg) - MM]$. The enhancement close to threshold is accounted for by a background plus a peak, assumed for simplicity ba a Gaussian. We analyzed the data under two different assumptions. The background is assumed either as a constant (solid line in the figure) or fitted by a polynomial (dashed-dotted curve). The total fit is shown as solid curve and dashed curve for the two cases, respectively. A statistical analysis yields a significance larger than 4σ.

References:

[1] Q. Haider, L. C. Liu: Phys. Rev., **C 66** (2002) 045208.

[2] S. A. Sofianos, S. A. Rakityansky: arXive, **nucl-th** (1997) 070044.

[3] R.S. Hayano, S. Hirenzaki, A. Gillitzer: Eur. Phys. J., **A 6** (1999) 99.

[4] K. Tsushima: Nucl. Phys., **A 670** (2000) 198c.

[5] C. Garcia-Recio, T. Inoue, J. Nieves, E. Oset: Phys. Lett., **B 550** (2002) 47.

[6] H. Bojowald et al.: Nucl. Instruments and Meth. in Phys. Res., **A 487** (2002) 314.

[7] M.G.Betigeri et al. (GEM Collaboration): Nucl. Instruments and Meth. in Phys. Res., **A 578** (2007) 198.

Nonequilibrium emission of light charged particles from p+Ag collisions

PISA - **P**roton **I**nduced **S**p**A**llation collaboration

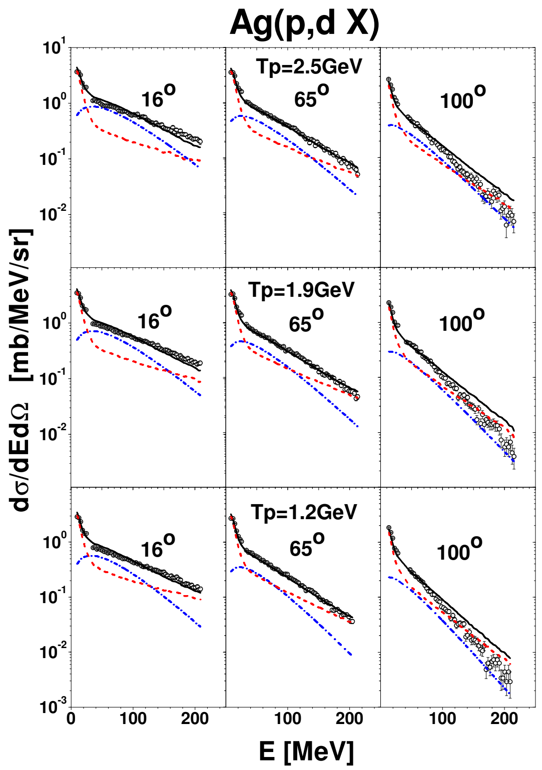

Fig. 1: Open circles represent experimental energy spectra of deuterons measured at 16°, 65°, and 100° for three beam energies. Dot-dashed lines present the contribution of deuteron emission from the "fireball", the dashed lines show results of INCL4.3+GEM2 calculations. and the solid lines - sum of both contributions.

Double differential cross sections $d\sigma/d\Omega dE$ were measured at several angles (16, 20, 35, 50, 65, 80, and 100 deg.) for proton induced reactions on the silver target for three proton beam energies: 1.2, 1.9 and 2.5 GeV. The light charged particles ($p,d,t,^{3,4,6}$He) and intermediate mass fragments (^{6,7,8,9}Li, ^{7,9,10}Be, and ^{10,11,12}B) were detected. A striking similarity of energy behavior of the present data to those obtained for the gold target was observed (see the highlights of the present Annual Report). The spectra almost do not change their shape when the beam energy varies, however, the absolute values of the cross sections increase with the increasing beam energy. The obtained data set was analyzed using the same reaction models as those applied for previously studied data for proton induced reactions on the Au target. The microscopic model of intranuclear cascade with possibility to form clusters implemented via coalescence mechanism was used to describe emission of high energy light charged particles ($p,d,t,^{3}$He, and ^{4}He). The calculations were performed by means of the INCL4.3 computer program using default values of the parameters proposed by the authors [1]. It was also taken into account that the excited remnant of the target nucleus can evaporate low energy particles. The contribution of this mechanism was evaluated by means of the GEM2 program of Furihata [2]. The theoretical cross sections are presented as red dashed lines in Fig. 1, where the deuteron spectra measured at 16, 65, and 100 deg. are depicted (points) for three beam energies: 1.2, 1.9, and 2.5 GeV - lower, middle and upper part of the Figure, respectively.

It is evident that some other reaction mechanism should be additionally taken into consideration to reproduce quantitatively the experimental data. The contribution of this mechanism should be the largest at small emission angles. The phenomenological model of the hot source ("fireball"), moving fast in the forward direction, and emitting particles isotropically (in its c.m. system) can account for the observed difference between the experimental data and the microscopic model calculations. The parameters of such phenomenological model [3] were fitted to reproduce the experimental data. The blue, dot - dashed lines present in the Fig. 1 the contribution from this phenomenological model, whereas the black, solid lines show the sum of all contributions. Very good description of all spectra for light charged particles was obtained with values of the parameters smoothly varying with the beam energy.

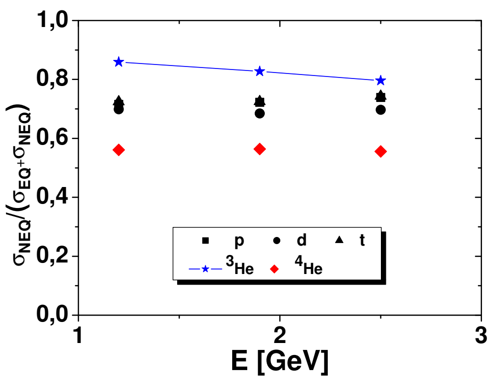

Fig. 2: Ratio of the cross sections for nonequilibrium processes (coalescence & "fireball") to the total one (nonequilibrium & evaporation) as a function of the beam energy. For α-particles the nonequilibrium cross section includes emission from an additional (slower) moving source.

The ratio of the cross sections of nonequilibrium mechanism (coalescence and "fireball" emission) to the sum of all processes is shown in Fig. 2 for all light charged particles as a function of the beam energy. It seems that this ratio does not change significantly with the beam energy in spite of the fact that the absolute cross sections for all processes increase with the energy. This fact, together with the necessity to introduce presence of the "fireball" agrees very well with the results found for the Au target. Investigations, planned by PISA collaboration, of the proton induced reactions on targets lighter than Ag should answer the question whether the observed effects are common for all targets or they are specific only for heavy target nuclei.

References:

[1] A. Boudard *et al*., Nucl. Phys. A **740**, 195 (2004)
[2] S. Furihata, NIM B **71**, 251 (2000)
[3] A. Bubak *et al*., Phys. Rev. C**76**,014618 (2007)

Energy dependence of the Au+p reaction cross sections

PISA collaboration

It is well known that the total cross section for fragment emission in proton induced reactions on heavy targets increases rapidly at GeV proton energies and it levels at almost constant value for energies higher than $\sim$ 10 GeV (see fig. 1).

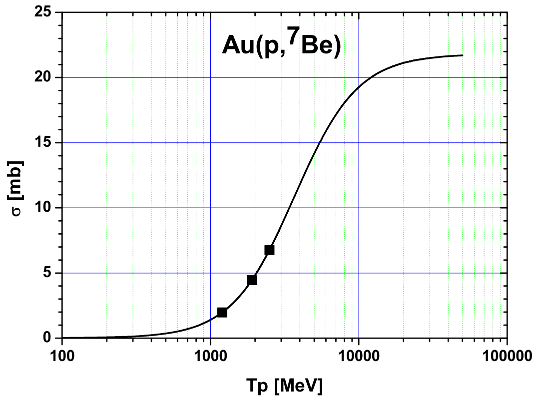

Fig. 1: Energy dependence of the total production cross section for ^{7}Be emission from proton induced reactions on the gold target. The line and the dots show prediction of the phenomenological parameterization (ref. [1]). The squares correspond to proton energies of the PISA experiment.

Moreover, experimental observations lead to the, so called, *hypothesis of limiting fragmentation*, which claims that not only total but also differential cross sections for fragment emission become energy independent in the limit of very high energies. In the present contribution results are reported of the measurements performed by PISA (Proton Induced SpAllation) collaboration for Au+p system at three energies (1.2, 1.9, and 2.5 GeV). This is the energy region where strong increase of the total production cross sections is expected. The aim of the present study was to check, whether the distributions of the differential cross sections also vary strongly in this energy interval. The apparatus of PISA project (described in details in ref. [2]) has been applied for detection and identification of the reaction products. Typical spectra of ^{4}He, ^{7}Li, and ^{11}B ejectiles are presented in figs 2, 3, and 4, respectively.

It is clearly visible that the shape of the spectra practically does not change in spite of the fact that the proton beam energy increases by more than factor two from the lowest to the highest energy. The absolute value of the cross sections increases for all observed reaction products in almost the same fashion as the cross section for ^{7}Be production predicted by the phenomenological parameterization [1] based on a large body of experimental data.

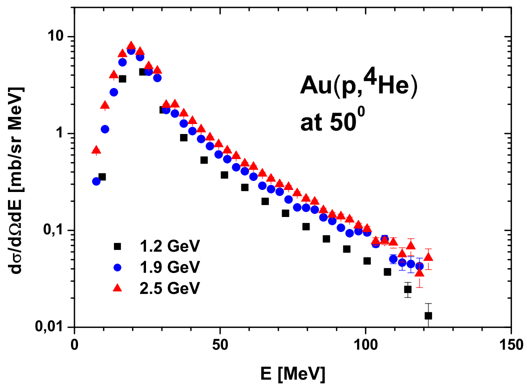

Fig. 2: Typical experimental cross section distributions obtained for Au(p,^{4}He)X reaction at T_p=1.2 (squares), 1.9 (dots), and 2.5 GeV (triangles) from telescopes of silicon detectors placed at 50 degree (in the LAB system).

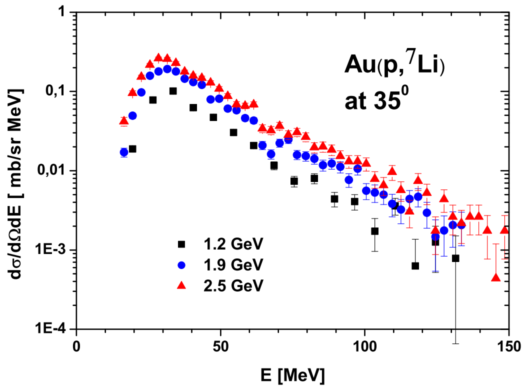

Fig. 3: Typical experimental cross section distributions obtained for Au(p,^{7}Li)X reaction at T_p=1.2 (squares), 1.9 (dots), and 2.5 GeV (triangles) from telescopes of silicon detectors placed at 35 degree (in the LAB system).

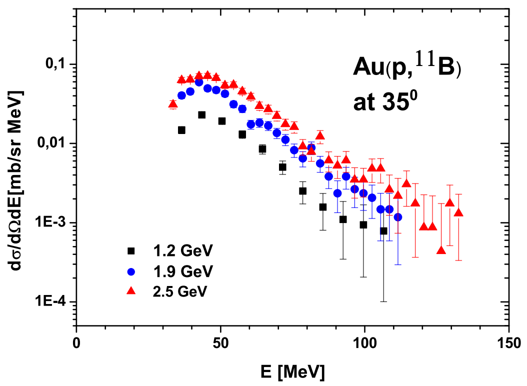

Fig. 4: Typical experimental cross section distributions obtained for Au(p,^{11}B)X reaction at T_p=1.2 (squares), 1.9 (dots), and 2.5 GeV (triangles) from telescopes of silicon detectors placed at 35 degree (in the LAB system).

References:

[1] A. Bubak, B. Kamys, M. Kistryn, and B. Piskor-Ignatowicz, Nucl. Instr. and Methods in Phys. Research B **226**, 507 (2004)

[2] R.Barna, V. Bollini, A. Bubak et al., Nucl. Instr. and Methods in Phys. Research A **519**, 610 (2004)

Stopping time criterion for QMD model calculations on proton induced reactions

PISA collaboration

The microscopic models of proton nucleus reactions at GeV energies usually assume that the reaction proceeds via two stages. A cascade of nucleon-nucleon collisions takes place in the first step of reaction leading to equilibration of excited heavy residual nuclei. Then statistical evaporation of particles or fission process appears from the equilibrated system. An important question arises - how to determine the duration of the preequilibrium stage of the reaction, i.e. what should be taken as stopping criterion for microscopic intranuclear cascade (INC) , Boltzmann-Uehling-Uhlenback (BUU) model, or quantum molecular dynamics (QMD) calculations. This question is especiallly difficult to be answered for QMD model, because the preequilibrium emission of composite particles present in this model makes transition from the preequilibrium to equilibrium stage quite diffuse.

In the present report it is shown that product mass distributions from spallation and especially from fission is very sensitive to the duration time of the preequilibrium stage of the reaction calculated in QMD model. Due to this fact the agreement of theoretical and experimental mass distribution may be used as criterion of terminating of QMD calculations and switching to statistical model evaluation.

In fig.1 the experimental mass distribution of products of Au+p interaction at E_p=1 GeV [1] is compared with model calculations performed for four different times of the fast stage of the reaction: for 50, 80, 100, and 130 fm/c. The calculations were done by means of PHITS v. 2.13 (Particle and Heavy Ion Transport code System) [2] with standard values of parameters, recommended by authors. This program package contains JQMD [3] and statistical model GEM [4] routines. The result of combined QMD and statistical model calculations are shown as solid line histograms. It is well visible in the figure that mass distribution of spallation residua broadens in direction of lower masses when the time of the first step of reaction increases. This is, of course, connected with preequilibrium emission of particles modeled by QMD. On the contrary, the final mass distribution of spallation residua - after the second stage of calculations - becomes narrower when the calculations of first step of reaction are terminated after longer time. This may indicate that the preequilibrium emission, as modeled by QMD, favors nucleon emission which does not change strongly a mass but significantly lowers excitation energy of equilibrated system available for statistical emission of composite particles.

The maximum of fission products distribution decreases significantly with the time of the first stage of reaction. It is thus evident that only rather well defined range of the time of the first stage of reaction is acceptable - between approx. 80 fm/c and 100 fm/c. The shorter and longer times give significantly poorer reproduction of the experimental data.

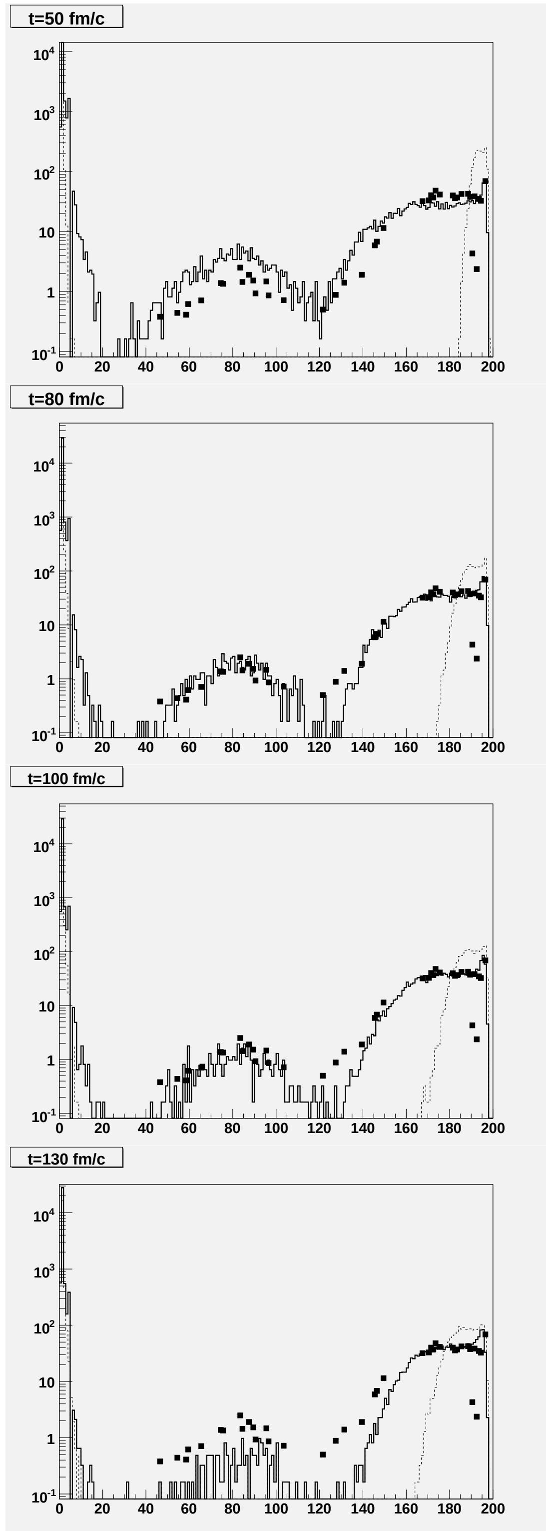

Fig. 1: Experimental fragment mass distribution in (mb/mass unit) from Au+p reactions at E_p=1.GeV [1] (squares) and predictions of QMD and GEM calculations (histograms). Dashed line histogram presents results of QMD alone, solid line histogram shows results of QMD calculations plus evaporation and fission evaluated by GEM with the time of nucleon-nucleon cascade varying from 50 fm/c (the highest part of the figure) to 130 fm/c (the lowest part of the figure)

References:

[1] S.B. Kaufmann, E.P. Steinberg , Phys. Rev. C **22**, 167 (1980)

[2] K. Niita, private information

[3] K. Niita, S. Chiba, Toshiki Maruyama, Tomoyuki Maruyama, et al., Phys. Rev. C **52**, 2620 (1995)

[4] S. Furihata, Nucl. Instr. Methods in Phys. Research B **171**, 251 (2000)

Energy spectra of isotopes produced in 175 MeV p+Ni reaction.

PISA Collaboration

One of the goals of PISA experiment [1] is to measure double differential cross sections of proton induced reactions in a broad range of energies. This report is devoted to description of experiment performed for Ni target at the lowest energy of internal proton beam of COSY used in PISA measurements, i.e. 175 MeV. This energy was selected because the production cross sections of various ejectiles appearing in this reaction are important for many applications, e.g. for *accelerator driven energy amplification* (ADEA) and *transmutation of nuclear waste* (ADTW) [2]. Telescopes consisted of silicon semiconductor detectors measuring ΔE and 7 cm thick CsI scintillator detectors applied for measuring of the total deposited energy were positioned at 7 angles (from 15^0 to 100^0). They allowed to identify charge and mass of light ejectiles (up to ^{4}He). Heavier particles were identified by telescopes built of semiconductor silicon detectors. Absolute normalization of the cross sections was achieved by comparison of proton spectra measured in the present experiment with the data of Ni(p,p X) reaction studied in National Accelerator Center in South Africa by Förtsch et al. [3] at exactly the same energy. The present data are shown in fig. 1 as symbols whereas the data of Förtsch et al. are depicted as solid lines.

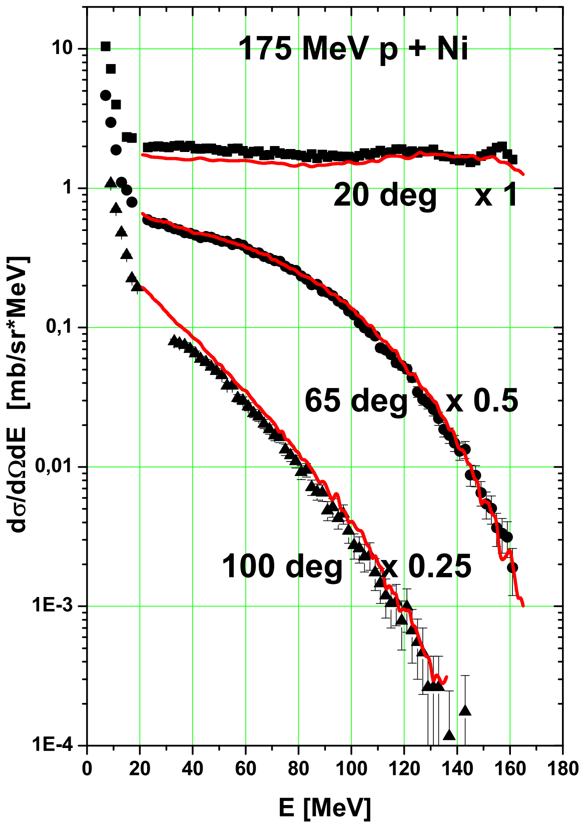

Fig. 1: Proton energy spectra measured at 20^0, 65^0 and 100^0. Lines represent data of Förtsch et al. [3], symbols correspond to data from PISA experiment. To avoid overlapping of spectra they were multiplied by arbitrary factors written in the figure.

Agreement between proton energy spectra from both experiments is better than 15% for all angles. It is worthy to point out that current PISA energy spectra are extended to lower energies for protons than Förtsch et al. data and, moreover, the experiment allowed for determination of other light charged particles (H, He) and intermediate mass fragments (Li,Be, and B) isotopically resolved.

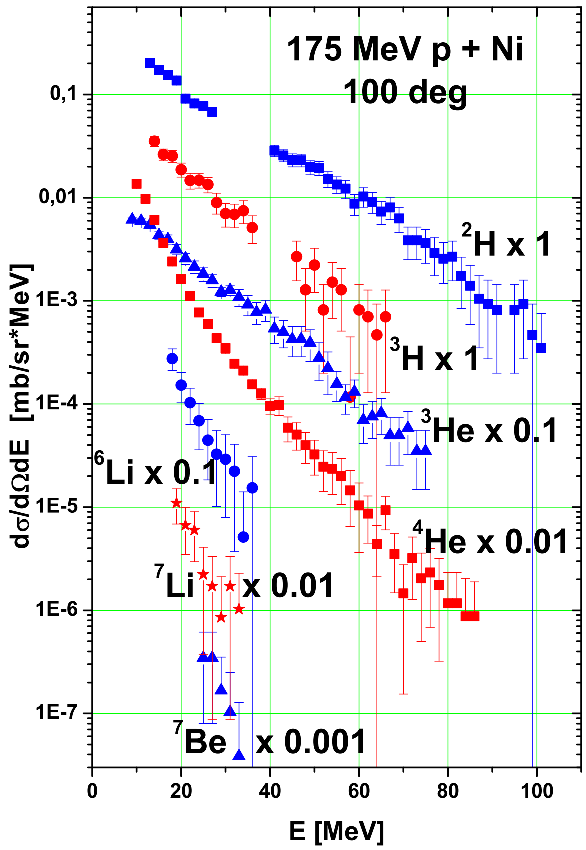

Fig. 2: Energy spectra measured in the present experiment at 100^0 for ^{2}H, ^{3}H, ^{3}He, ^{4}He, ^{6}Li, and ^{7}Be ejectiles. To avoid overlapping of spectra they were multiplied by arbitrary factors written in the figure.

Examples of the 100^0 spectra from the present experiment are shown in fig. 2. As can be seen the cross sections decrease strongly with increasing mass of the products. At this scattering angle only products presented in the fig. 2 are abundant enough to be presented in a form of spectra. It is worthy to note that slopes of ^{2}H, ^{3}H, and ^{3}He spectra are almost the same, similarly as slopes of ^{4}He, ^{6,7}Li, and ^{7}Be spectra, whereas they differ significantly between these two groups of products. This may indicate another reaction mechanism of emission for lighter than that for heavier products.

We acknowledge gratefully the financial support of present PISA investigations by the EU FP6 program EUROTRANS (contr. no. FI6 W-CT-2004-516520) and EU-programme LIFE (Light Ion Facility Europe).

References:

[1] R. Barna et al, Nucl. Instr. Meth. **A519**, 610 (2004)

[2] Proc. of the Fifth Workshop On Simulating Accelerator Radiation Environments (SARE-5), July 17-18 (2000), ISSN 1433-559X, editors D. Filges, F. Goldenbaum, and Y. Yariv

[3] S. V. Förtsch et al., Phys.Rev. **C43**, 691 (1991)

A Polarized Internal Gas Target for Spin-Filtering Studies at COSY and AD

A. Nass[a], G. Ciullo[b], K. Grigoriev[c], H. Kleines[c], P. Lenisa[b], F.Rathmann[c], J. Sarkadi[c], M. Statera[b], E. Steffens[a], H.Ströher[c] and G. Tagliente[d]

The high physics potential of experiments with stored high-energy polarized antiprotons led to the PAX proposal [1] for the High Energy Storage Ring (HESR) of the FAIR facility (Facility for Antiproton and Ion Research) at GSI (Darmstadt/Germany). It is proposed to polarize a stored antiproton beam by spin filtering with a polarized hydrogen (deuterium) gas target. The feasibility of spin filtering has been demonstrated in the FILTEX experiment [2] but the theoretical understanding is controversial [3] [4]. In order to clarify this situation several experimental studies with protons (at COSY) as well as with antiprotons (at AD/CERN) have to be carried out. These investigations require an experimental set-up of a polarized internal gas target (PIT) with a system of Silicon detectors implemented into a large acceptance section of the storage ring.

Fig. 1: The reassembled polarized atomic beam source on a new support with the analysis chamber (mounted on the lower end) in the laboratory.

The former HERMES polarized atomic beam source was set up in Jülich with a modified vacuum system, mounted on a new support (Fig. 1). It was completely recabled to allow a fast assembly and disassembly at COSY and AD. Making use of the earlier experience in the development of the control system for the polarized internal gas target for ANKE/COSY, the control system was renewed to allow for a full remote control via computer. The vacuum system with the microwave dissociator is operating well and intensities up to $6 \cdot 10^{16}$ atoms/s were reached. The former HERMES Breit-Rabi polarimeter was rebuilt on a new support stucture (Fig. 2). The sextupole magnet configuration was modified and a new strong field transition "Dual Cavity" was designed and built in order to measure the polarization of hydrogen and deuterium. The slow control is supposed to be running in spring 2008.

Fig. 2: The reassembled Breit-Rabi polarimeter on the new support.

To reach the necessary areal densities for spin filtering, the use of a storage cell is mandatory. The present cell design consists of 5 μm Teflon walls supported by an aluminum frame. Thin walls allow low energy recoil particles to pass and to be detected by the Silicon Tracking Telescopes. Furthermore, Teflon suppresses depolarization and recombination of the target gas inside the cell. The first prototype of the target cell is expected for spring 2008.
The vacuum system of the target section comprises two turbo molecular pumps, backed with smaller turbo molecular pumps and a dry forevacuum pump. This will ensure that most of the target gas exiting the storage cell is pumped within the target chamber. The adjacent chambers containing the quadrupole magnets of the large acceptance section will be pumped by ion getter pumps. In addition, the cold surfaces of the superconducting magnets are covered with charcoal to use them as cryogenic pumps.

References:

[1] *Antiproton-Proton Scattering Experiments with Polarization*, Technical Proposal for the HESR at FAIR, Jülich (2006), Spokespersons: P. Lenisa and F. Rathmann, and references therein. Available from *www.fz-juelich.de/ikp/pax.*

[2] F. Rathmann et al., Phys. Rev. Lett. 72, 1379 (1993).

[3] C.J. Horowitz and H.O. Meyer, Phys. Rev. Lett. 72, 3981 (1994).

[4] A.I. Milstein and V.M. Strakhovenko, Phys. Rev. E 72, 066503 (2005).

[a] Phys. Institut der Univerität Erlangen Nürnberg, Germany
[b] Istituto Nationale di Fisica Nucleare, Ferrara, Italy
[c] Forschungszentrum Jülich, IKP, Jülich, Germany
[d] Istituto Nationale di Fisica Nucleare, Bari, Italy

Simulation Results for Depolarization Experiment at 45 MeV.

S. Barsov[a], S. Bertelli[b], P. Lenisa[b], N. Lomidze[c], G. Macharashvili[a,c], M. Nikipelov[d], D. Oellers[d], F. Rathman[d], M. Tabidze[c], P. Thörgren Engblom[e], R. Schleichert[d] *for the PAX Collaboration*

In order to optimize the detector setup and to estimate the pd elastic count rate for the beam depolarization study at COSY (Exp. 169 and 181), a GEANT simulation has been done using the current setup of the ANKE Silicon Tracking Telescope (STT) system [1] with two detector layers. The proton beam energy was 46.3 MeV and the size of the deuterium cluster target was 0.5 cm × 1 cm. For the asymmetry measurement a left-right detector system was used.

In Fig. 1 the available experimental data are shown for the differential cross section at T_p=46.3 MeV [2], the analyzing power (A_y) data for pd elastic at T_p=49.3 MeV [3] and corresponding (in some approximation) Figure of Merit $FoM(\vartheta) = A_y^2(\vartheta) \cdot \frac{d\sigma}{d\Omega}$.

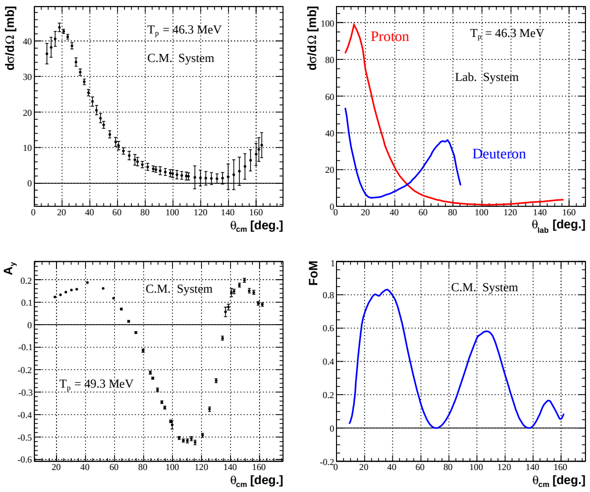

Fig. 1: (*Top panel*) Differential cross section for pd elastic in cm and lab system. (*Bottom panel*) Analyzing power and Figure of Merit (FoM) for pd elastic. The estimated elastic cross section $\sigma_{el} = 113.2\ mb$ in the angular range $\vartheta_{CM} = (9-169)^o$.

The silicon layers were separated by a distance of 2 cm and they were placed parallel to the beam line. The distance between the first layer and the beam axis is 3 cm. The whole telescope was shifted by 1.75 cm in the downstream direction. The dimensions of the sensitive area are 6.62x5.11 cm^2 and the thickness is 300 μm for all detectors.

The number of events $N_{gen} = 2 \cdot 10^6$ was generated according to the $d\sigma/d\Omega$ differential cross section form (see fig. 1) for the cm angular range $\vartheta_{CM} = (9-169)^o$. The azimuthal angle ϕ was distributed uniformly (no polarization). The numbers of detected particles in each layer (STT Left and Right) is shown in Table 1. Most of the deuterons were stopped in the telescope, about 70 % were stopped in the first layer and all entering the second one were stopped. For the protons about 2 % were stopped in each layer. Roughly 50 % (30 %) of outgoing deuteron's (protons) from first layer enters the second one.

	detected particles		count rate (ev/s)	
layer	p	d	p	d
I	0.363 10^6	0.825 10^6	205	467
II	0.122 10^6	0.131 10^6	69	74
L+R	0.642 10^5		36	

Table 1.

In Fig. 2 we show energy deposit in the layer I *vs* energy deposit in second one, and the energy deposit in the same layer *vs* particle kinetic energy.

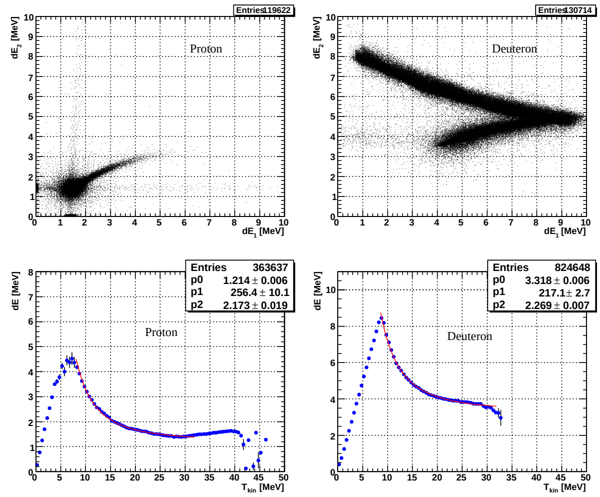

Fig. 2: (*Top panel*) Energy deposit in layer I *vs* energy deposit in layer II. (*Bottom panel*) Profile distributions for deposited energy in layer I *vs* the kinetic energy of the particles. Red lines corresponds to a fit using the function $p_0 \cdot (1 + p_1/x^{p_2})$

See Fig. 3 for the deviation of θ and ϕ angles due to multiple scattering in layer I for protons and deuterons.

With a known luminosity L, dead–time factor f_{dt} and detected cross–section σ_{det}, we can calculate count rate R in the following way:

$$R = L \cdot \sigma_{det}/f_{dt}. \tag{1}$$

We use the following form for the detected cross section σ_{det} calculation:

$$\sigma_{det} = 2\pi \cdot \sum_i (\frac{d\sigma}{d\Omega})_i \cdot sin\theta_i \cdot \Delta\theta_i \cdot \frac{N^{det}(\theta_i)}{N^0(\theta_i)}, \tag{2}$$

where $2\pi \cdot \frac{N^{det}(\theta_i)}{N^0(\theta_i)} \cdot sin\theta_i \cdot \Delta\theta_i$ denotes the geometrical angular acceptance.

To estimate proton–deuteron elastic rates a luminosity of L $\approx 1 \cdot 10^{28}$cm^{-2}s^{-1} was used: $L = N_p \cdot f \cdot d_t = 1{\cdot}10^8{\cdot}4.9{\cdot}10^5\,\mathrm{s}^{-1}{\cdot}2{\cdot}10^{14}\,\mathrm{atoms/cm^2} = 9.8{\cdot}10^{27}\,\mathrm{cm^{-2}s^{-1}}$. In our calculations the detection efficiency was assumed 100 % and dead–time factor f_{dt}=1. Table 1 contains the count rates for protons and deuterons in each layer.

In Fig. 4 the calculated asymmetry is shown for deuterons assuming a proton beam polarization of

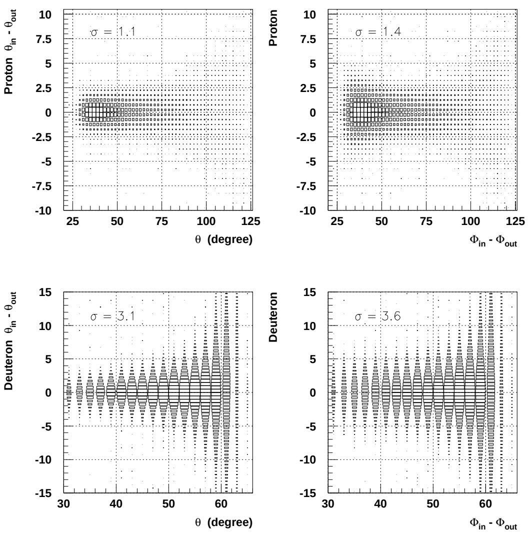

Fig. 3: The effect of multiple scattering in layer I for protons (*Top panel*) and deuterons (*Bottom panel*). The rms is denoted by σ.

P=0.6. Even at angles where multiple scattering effects for deuterons are sizable (see Fig. 3), the smearing of the analyzing power is negligible.

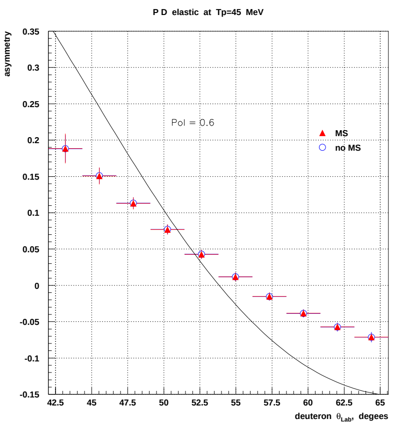

Fig. 4: Estimated asymmetry for deuterons detected in the STT. The Black line is the extrapolated analyzing power for deuterons at 45 MeV ([2],[3]), used in the asymmetry calculations. The proton beam polarization was assumed P=0.6.

To estimate the background from deuteron break-up reactions the event generator Pluto [4] was used. $N_{gen} = 1 \cdot 10^6$ number of events were generated covering the full phase space. In Fig. 5 we show the polar angle and kinetic energy distributions of the outgoing nucleons.

In Fig. 6 we show the energy deposit in layer I *vs* energy deposit in layer II for pd elastic and for deuteron break-up processes weighted according cross sections. The preliminary raw data spectra with no cuts looks very similar.

In summary, we have simulated the response of the STT for pd elastic and breakup reactions at a proton beam energy of 46.3 MeV and consistency with preliminary raw data spectra was found.

References:

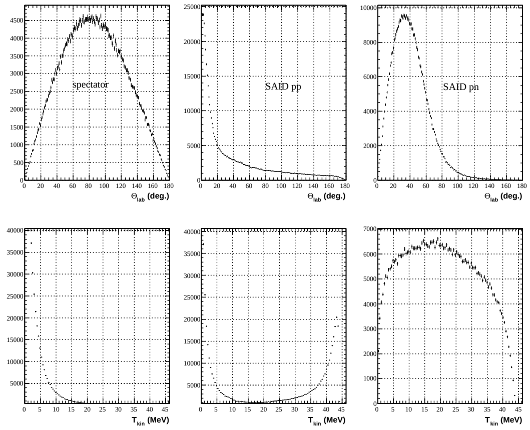

Fig. 5: Kinematics for the deuteron break-up reaction, generated by Pluto. In half of events neutron was suggested as spectator particle and in half of events proton was

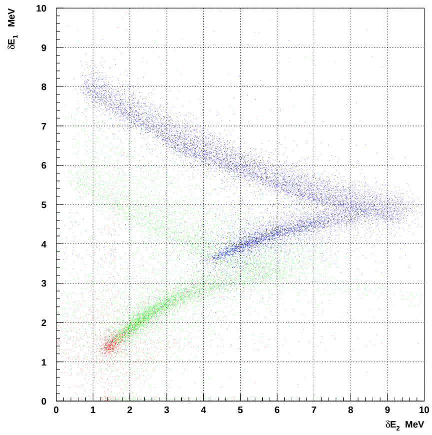

Fig. 6: Energy deposit in layer I *vs* energy deposit in layer II for elastic and break-up events.

[1] A. Mussgiller, Ph.D. thesis, University of Cologne (2005).
[2] S.N. Bunker at al., Nucl. Phys. A113 (1968), p.461.
[3] N.S. King et al., Phys. Lett. 69B (1977), p.151.
[4] I.Frölich et al., arXiv:0708.2382v2, (Nov 2007)

[a] JINR, Dubna, Russia
[b] INFN, Ferrara, Italy
[c] Tbilisi State University, Tbilisi, Georgia
[d] IKP, Jülich, Germany
[e] Uppsala University, Uppsala, Sweden

Lattice Studies for Low Beta Sections at COSY and AD Rings

A. Garishvili [b,c], A. Lehrach [a], P. Lenisa [d], B. Lorentz [a], R. Maier [a], S. Martin [e], A. Nass [c], F. Rathmann [a], M. Statera [d], R. Schleichert [a], E. Steffens [c] and H. Ströher[a].

In the framework of the FAIR [1] project, the PAX collaboration has suggested new experiments using polarized antiprotons [2]. The central physics issue is now to study the polarization build-up by spin filtering of antiprotons via multiple passages through an internal polarized gas target. The goals for spin-filtering experiments with protons at COSY are to test our understanding of the spin-filtering processes and to commission the setup for the experiments with antiprotons at the Antiproton Decelerator AD at CERN. Spin-filtering experiments with antiprotons at the AD will allow us to determine the total spin-dependent transversal and longitudinal cross sections.

The low-beta section at COSY

The maximum momentum at COSY is 3.77 GeV/c, therefore magnetic rigidity is 12.34 Tm. The acceptance of the machine is around 27.8 π mm mrad, in both planes, after cooling the emittance in both planes goes down to around 3 π mm mrad. At COSY, the lowest beta function for regular lattice settings is around 2 m. The polarization buildup experiments use an internal polarized storage cell. For most efficient use of such a storage cell target lower values for the beta functions are required. This is the reason why we want to have low beta section at COSY. The available space at COSY for the low-beta section foreseen at TP1 is 3610 mm.

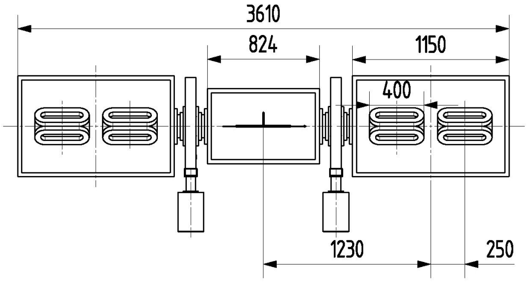

Fig. 1: The low beta section at COSY.

The low-beta section at COSY (figure 1) is composed of two 400 mm long superconducting quadrupole magnets on each side of the target. The drift space between the magnets is 100 mm. For the target chamber a length of 824 mm is reserved.

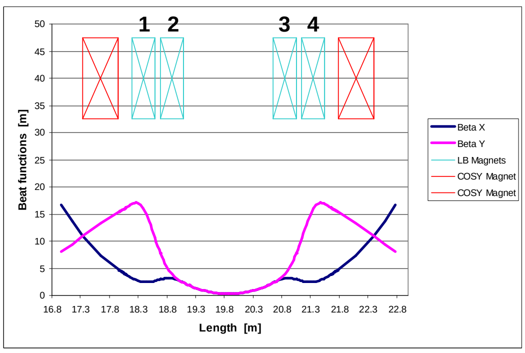

Fig. 2: Distribution of the beta functions along the low beta section. Red magnets are existing COSY quads, green new low beta quads.

To calculate the betatron amplitude function (beta function) in the low-beta section, we fixed the original input lattice parameters (α_x, α_y, β_x and β_y) at the beginning of the available space and matched to the original input parameters at the end of the available space. The highest focusing strength for corresponding quadrupole magnets is 4.49 m^{-2}. The minimum beta functions at the center of the target are $\beta_x = 0.3$ m and $\beta_y = 0.3$ m as displayed in figure 2. The maximum of the beta functions in the low-beta section is around 17m. For the corresponding beta functions, even uncooled beam can be injected through the target cell (figure 3).

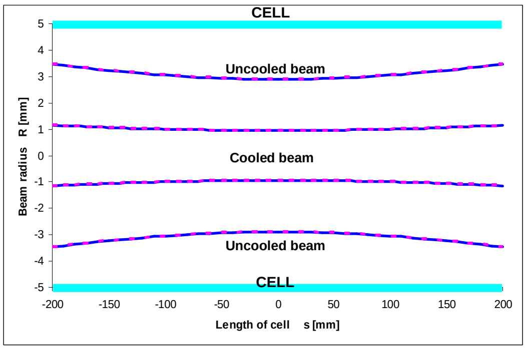

Fig. 3: Beam envelope at the cell. Dark blue lines are R_x, dashed red lines denote R_y. Blue lines show the size of the cell (10 mm).

At COSY, we have the possibility to turn on and off the low beta section, because of the ring telescopic mode; phase advance can be compensated with the regular COSY quadrupoles.

The low-beta section at the AD

The maximum momentum at the Antiproton Decelerator ring is 3.57 GeV/c, corresponding to a magnetic rigidity $B\rho = 11.9$ Tm. The horizontal acceptance is 220 π mm mrad and the vertical 190 π mm mrad, after electron cooling at the lowest energies, the emittance in both planes goes down to around 5 π mm mrad. The available space for low beta section is 5410 mm. One regular AD quadrupole in the center of the foreseen straight section has to be removed. For this case, one can use the presented low beta section at COSY as a part of low beta section at the AD.

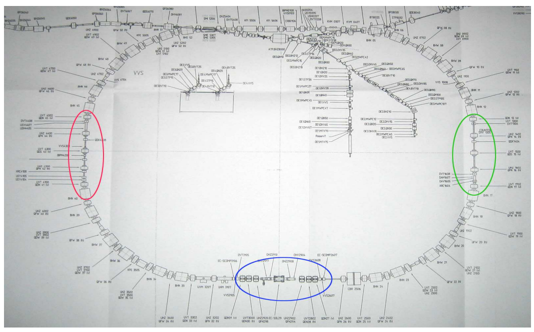

Fig. 4: Antiproton Decelerator (AD). With a green circle the place for the low-beta section is marked, with blue the electron cooling section and with red the possible place for the snake section.

The position of the low beta section at the AD is shown in figure 4 and the layout is displayed in figure 5.

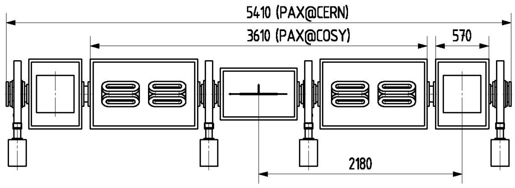

Fig. 5: Low beta section at AD.

At the AD, we need one more quadrupole on each side of the target. The foreseen gap between the additional and the quadrupoles used at COSY is 300 mm.

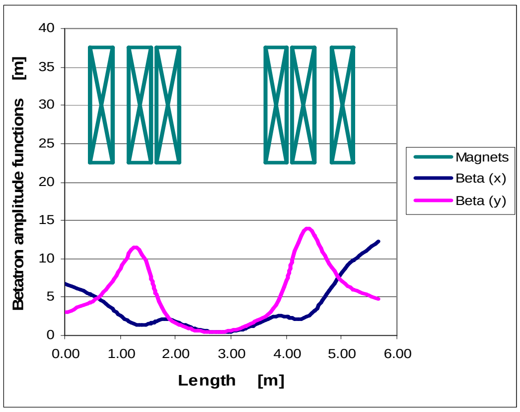

Fig. 6: Distribution of the beta functions along the low beta section.

We calculated the distribution of the beta function in the same way as at COSY. The highest focusing strength for corresponding quadrupoles is 5.1 m^{-2}. The minimum beta functions at the center of the target are β_x = 0.42 m and β_y = 0.44 m. The maximum beta function in the low-beta section is around 13.9 m.

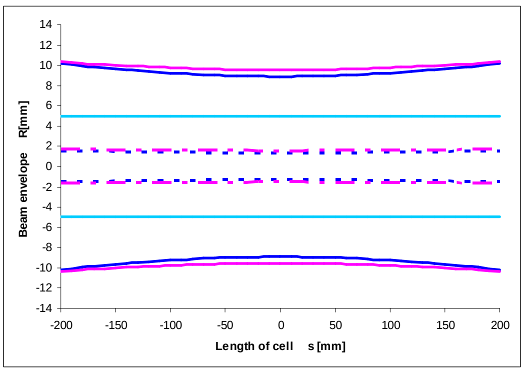

Fig. 7: Beam envelope at the cell. Dark blue lines are R_x, red lines Ry. Solid lines are uncooled beam, and dashed lines cooled beam. Blue lines show the size of the cell (10 mm).

For these beta functions, the uncooled beam cannot be injected through the target cell (figure 7). For this reason at the AD, we have to open the cell to about 2 cm, before the beam will be cooled. At the AD the low beta section has to be on during the whole deceleration cycle.

Conceptual design of the superconducting quadrupoles

The magnets used at COSY will be installed also at AD so they have to be designed for the most demanding conditions. The main constraints are the longitudinal space, the focusing force and the inner bore. It has to be noticed that the longitudinal space is a major constraint since the thermal insulation of the cryostat and valves on the beam line to insulate the magnets are of primary importance and reducing the magnets' length force the designer to increase the field, so that reducing the length of the magnets implies an increase of the required gradient and maximum field.

Given a gradient, increasing the inner bore, increases the maximum field of the magnet. A higher maximum field in the conductor reduces the maximum allowed current in the wire. The focusing force is proportional to the integrated radial gradient (or radial field at a fixed radius) along the longitudinal direction (z). These constraints make the magnetic design challenging, their impact on the magnetic design is reported below together with the final design.

The beam envelope radius is 52 mm; considering 5 mm for the uncertainties and some more safety we chose the reference radius for the field region to be R_b = 57 mm. The minimum radius for the windings of the quadrupoles is 75 mm.

The main constraint for the quadrupole is the available longitudinal space: the magnets must be superconducting to fulfill the field requirements so that both the thermal insulation and the vacuum connections (and valves) have been taken in account in the scheme used to calculate the maximum longitudinal dimension of the magnets.

The latter is about 400 mm and thus the designed coils have that total length. The coils are simple racetrack to maximize the integrated field in such short magnets. The goal of the design is to reach an integrated field corresponding to a 59 T/m (radial gradient) box (ideal) quadrupole 400 mm long. The integrated field at the reference radius along the z axis is 1.60 T·m.

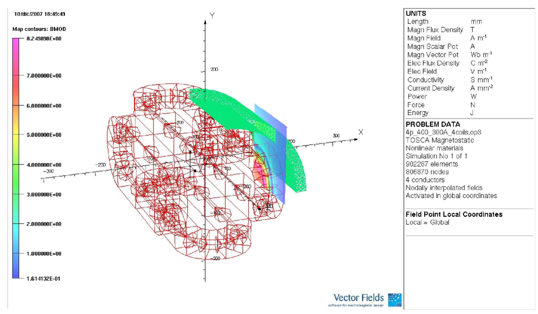

Fig. 8: The coils of the designed racetrack coils quadrupole. Part of the iron shielding is also plotted; the shielding cylinder is attained using four fold and longitudinal symmetry. A field calculation into the coil is shown, the magnetic flux density is plotted (the maximum is 8.25 Tesla).

The presented coils are 75 mm far from the z axis, have a 45 x 40 mm^2 cross section and the minimum bending radius is 30 mm (half of the 'pole' transverse dimension). An iron shielding 20 mm thick and with a minimum radius of 140 mm is used.

The geometry of the coils and a part of the iron shield is plotted in figure 8. It can be noticed that the geometry allows winding the coils using ribbon wires and thus reducing the inductance of the winding at a lower cost with respect to Rutherford cables.

The engineering current density in the coil is 300 A/mm^2 and the maximum field in the superconductor is 8.25 T. The safety margin is about 28% for a square cross section NbTi wire. The integrated radial magnetic flux density at 68 mm is 1.6 Tm along the magnet (evaluating the contribution of the fringing field); the plot of the calculated field is reported in figure 9. The energy stored is about 195 kJ.

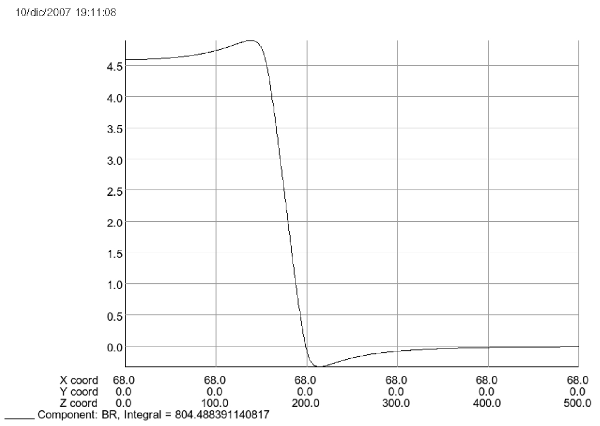

Fig. 9: Radial magnetic flux density at the reference radius from the centre of the quadrupole to 500 mm. The coils limit is 200 mm, the integrated field is also shown.

The ratio of each Fourier component (B_i) of the field with respect to the quadrupolar one (B_2) at the reference radius have to be below 10^{-3}. The simulated ratio B_i/B_2 (up to i = 6) is below 10^{-4} at the beam envelope limit even in the fringing field. These values must be directly measured in each magnet.

References:

[1] Conceptual Design Report for an International Facility for Antiproton and Ion Research, *www.gsi.de/GSI-future/cdr.*

[2] PAX Technical Proposal, *www.fz-juelich.de/ikp/pax*.

[a] Institut für Kernphysik, Forschungszentrum Jülich, Jülich, Germany
[b] Institute of High Energy Physics, Tbilisi State University, Tbilisi, Georgia
[c] Physikalisches Institut, Universität Erlangen-Nürnberg, Erlangen, Germany
[d] Istituto Nazionale di Fisica Nucleare, Ferrara, Italy
[e] UGS Gerlinde Schulteis & Partner, Langenbernsdorf, Germany

Preparation of an Atomic Spectroscopy Experiment with a Modified Lamb-shift Polarimeter

M. Westig[a,b], R. Engels[a], K. Grigoryev[a,c], M. Mikirtychyants[a,c], H. Paetz gen. Schieck[b], F. Rathmann[a], G. Schug[a], V. Trofimov[c], A. Vasilyev[c] and H. Ströher[a]

It is planned to perform atomic spectroscopy experiments with metastable hydrogen or deuterium atoms during periods when the Lamb-shift Polarimeter (LSP) is not in use at ANKE. Starting from June 2007, the LSP was modified to prepare these experiments which can be explained in a brief way as follows.

A Glavish-type ionizer as part of the LSP ionizes inflowing hydrogen (deuterium) gas and accelerates the protons (deuterons) to about 1 keV beam energy. After passing a 90 degree electrostatic deflector and further selection of the required velocity component with a Wien filter, the beam enters a cesium vapour cell. Here, metallic cesium is heated to a temperature of about 160 $^{\circ}C$, vaporizes and diffuses in the cell. With this method a cesium vapour target density of about 10^{14} atoms/cm^2 can be build up. The incoming protons (deuterons) hit cesium atoms in the cell and catch an electron. In this process, a metastable hydrogen (deuterium) beam can be produced with up to 15 % atoms in the metastable state with principal quantum number $n = 2$. The metastable atoms then enter the centrepiece of the polarimeter, the spinfilter, where single Zeeman components of the hyperfine structure can be selected to finally pass the spinfilter while other components are extracted from the metastable beam.

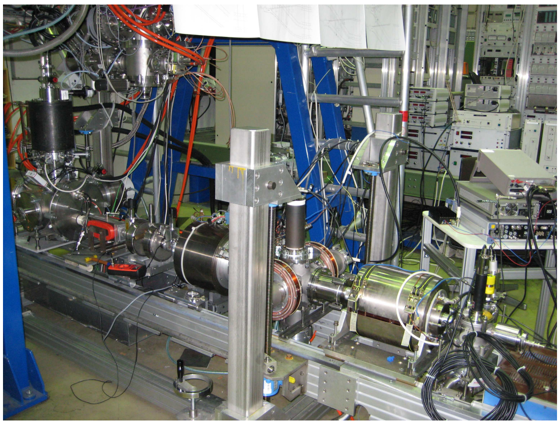

Fig. 1: Setup of the spectroscopy experiment

The modification of the LSP consists of the devices behind the spinfilter, composed of a spectroscopy chamber, briefly described below, and a second spinfilter.

The spectroscopy chamber is constructed out of a vacuum chamber with six ISO-K-100 openings, surrounded by a pair of magnetic field coils. Inside, a so called TEM[1] waveguide is installed closed with a 50 Ohm resistance, which works in a frequency range of 800 to 1400 MHz behind an amplifier and allows to keep the power of the electromagnetic wave constant. With the TEM waveguide electric dipole transitions can be induced from single Zeeman components of the $2S_{1/2}$ hyperfine structure into the $2P_{1/2}$ state. The occurence of a transition can be measured by detecting Lyman-α-photons with a photomultiplier on the top of the chamber. Dependent on the magnetic field geometry, i.e. parallel or perpendicular to the electric field vector of the TEM waveguide, specific transitions according to the selection rules of quantum mechanics can be selected.

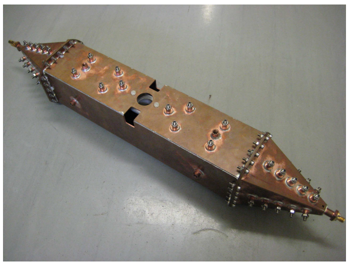

Fig. 2: TEM waveguide (total length $\approx$ 50 cm), consisting of an outer copper conductor and an inner aluminum conductor. The complex shape and the tuning screws distributed over the outer surface allow to produce a homogenous electromagnetic wave and match the wave resistance to 50 Ohm.

A high-frequency magnetic field coil is currently designed to induce magnetic dipole transitions in the $2S_{1/2}$ state. The occurence of magnetic dipole transitions can be measured with the second spinfilter and a quenching chamber also used in the usual LSP.

With this setup in the very next future the measurement of the "classical" Lamb-shift ($2S_{1/2} - 2P_{1/2}$), the $2S_{1/2}$, $2P_{1/2}$ hyperfine splitting and the Breit-Rabi-diagram of the $2S_{1/2}$ and $2P_{1/2}$ states, i.e. the energy dependence of the single Zeeman components of the hyperfine structure in an external magnetic field, is planned. For the last one, the aspiration is a comparision with state-of-the-art QED calculations [1, 2]. Furthermore, the measurement of the Lamb-shift and the hyperfine splitting gives access to nuclear structure dependent quantities like charge radii, nuclear charge and nuclear magnetization distributions. First tests show that the experiment, in principle, works properly. To perform a first measurement, the power dependency on the frequency in the TEM waveguide has to be minimized to eliminate shifting and deformation of the resonance peak. First measurements are expected in 2008.

References:

[1] D.L. Moskovkin and V.M. Shabaev, Phys. Rev. A 73, 1 (2006).

[2] D.L. Moskovkin and D.A. Glazov, Private communication (2007).

[a] Forschungszentrum Jülich, IKP, Jülich, Germany
[b] Universität zu Köln, IKP, Köln, Germany
[c] PNPI Gatchina, Gatchina, Russia

[1] Transversal Electro Magnetic

Proof of principle of SAPIS (Stored Atoms Polarized Ion Source), a new type of polarized negative-ion source

R. Emmerich, M.P Westig, H. Paetz gen. Schieck

Institut für Kernphysik, Universität zu Köln, Zülpicher Str. 77, 50937 Köln

In 1968 the basic idea of the colliding-beams source (CBS), consisting of an intense neutral Cs beam colliding with polarized H or D atoms from a ground-state atomic-beam source, was proposed [1] and first demonstrated in 1978 [2]. The successful development of this idea culminated in recent achievements of this type of source at COSY [3].

In Refs. [4]-[6] proposals were made to combine the atomic-beam source (ABS) and the neutral Cs source (CS) with a collision region of increased atomic-beam density inside a storage cell. At the University of Köln this idea has been realized for the first time. Fig. 1 shows the complete setup.

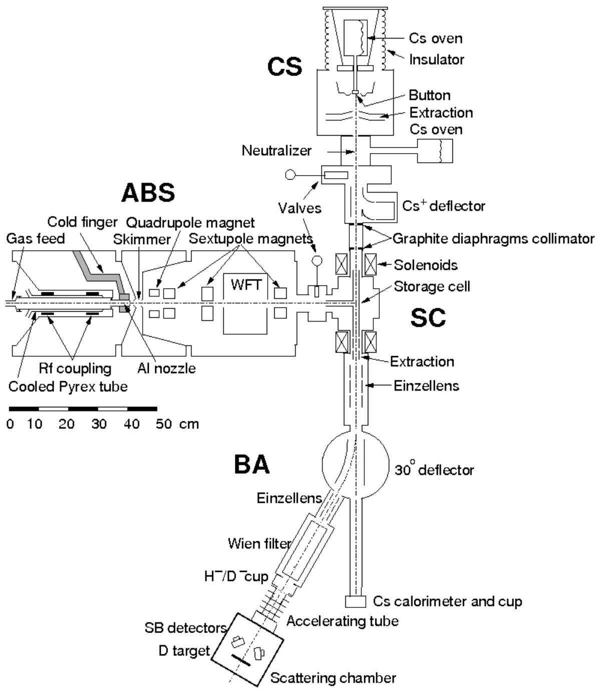

Fig. 1: Setup of SAPIS with one option of beam analysis.

Using the Cs source originally developed at Köln for the first version of the COSY CBS, an atomic-beam source partly built from existing parts, and a storage cell with a segmented design and internally coated with "Drifilm", it was possible to

- pass a 45 keV neutral Cs beam equivalent to 300 µA through the cell without serious losses,
- get an atomic-beam intensity at the cell location of 1.2 x10^{15} s^{-1} with polarizations, as measured with the Cologne Lambshift polarimeter, of about 86% of the theoretical values,
- extract and analyze negative H or D ions with currents of up to 7 nA. A comparison with currents expected from the present design yielded a relative efficiency of up to 47% showing low recombination and no detrimental effects of the Cs. The current was, however, too low to measure the negative-ion polarizations, neither with the Lambshift polarimeter (which required a conversion to positive ions by double charge-exchange on He) nor with a nuclear reaction (the D(d,p)^{3}H reaction has high vector and tensor analyzing powers even at very low energies). The known polarization-conserving properties of coated storage cells and small recombination make us believe that the negative ions are probably highly polarized.

Fig. 2 shows the design of the storage cell. The polarized atomic beam enters from the side tube, the Cs^0 beam passes through the long segmented section over which an electric extraction field and a magnetic guiding field are maintained.

Fig.2: Design of the storage cell.

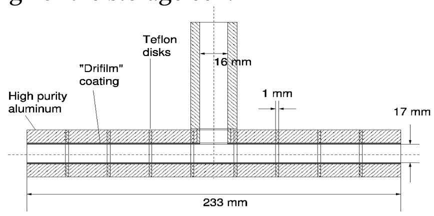

Although the absolute performance of SAPIS is low, it has an appreciable development potential. Applying reasonable extrapolations to today's best sources (such as the Brookhaven ABS), an improved CS as well as an optimized design of the storage cell including cooling, negative-ion DC currents of up to 70 µA (H) or 150 µA (D) seem possible. Details of SAPIS are described in Ref. [7].

References:

[1] W. Haeberli, Nucl. Instr. and Meth. A 62 (1968) 355
[2] D. Hennies et al., Phys. Rev. Lett. 40 (1978) 1234
[3] R. Gebel et al., Proc. 10th EPAC, Edinburgh, 2006, p. 1705
[4] S. Lemaître et al., in: H. Paetz gen. Schieck, L. Sydow (Eds.), Proc. Int. Workshop on Pol. Beams and Pol. Gas Targets, Köln, 1995, World Scientific, Singapore , 1996, p. 231
[5] T. Clegg, ibid., p. 155
[6] A.S. Belov, ibid., p. 208
[7] R. Emmerich, H. Paetz gen. Schieck, Nucl. Instr. and Meth. in Phys. Res. A 586 (2008) 387

Acknowlegments: This work was supported by BMBF grants 06 OK 958 and 06 K 167 and by COSY FFE.

Measurement of the nuclear polarization in H_2 and D_2 molecules after recombination of polarized hydrogen or deuterium atoms

R. Engels, K. Grigoryev[a,b], L. Kotchenda[b], P. Kravtsov[b], M. Mikirtychyants[a,b], F. Rathmann, H. Paetz gen. Schieck[c], H. Seyfarth, H. Ströher, V. Trofimov[b], N. Chernov [b], and A. Vasilyev[b]

In collaboration with Petersburg Nuclear Physics Institute and Institut für Kernphysik of Universität zu Köln measurements of the nuclear polarization of H_2 molecules maintained after the recombination of polarized hydrogen atoms will be performed. In an additional way of application, the polarized atomic beam source (ABS) [1], developed for the internal polarized gas target at the ANKE spectrometer in COSY, could be used when it was not installed at that target place. The $\vec{\mathrm{H}}$ beam from the ABS was utilized to feed a special T-shape storage-cell setup (feeding tube and storage tube) made from quartz. The inner surface of the storage tube is covered by a 5 μm gold layer. An electric current through this layer results in a potential distribution along the tube, by which ions are extracted. Appropriate materials like Teflon can be deposited on the gold layer to measure the preservation or destruction of the nuclear polarization in wall collisions, during recombination of the atoms into molecules at the surface of the inner material, and by inner-molecular interaction between the collsions. The storage tube is placed on the common axis of two superconducting coils, which can produce magnetic field strenghts up to 1.5 T. The mechanical contact to the liquid-helium vessel and counter-heating allows to vary the temperature of the storage cell between 10 and 150 K or even higher.

A well-focused electron beam is used to ionize atoms or molecules inside the cell by electron impact. By the magnetic field, produced by the solenoid, the nuclear polarization is maintained in the ionization process. Protons from ionization of $\vec{\mathrm{H}}$ and $\vec{\mathrm{H}}_2^+$ ions are extracted from the storage tube by the potential drop along the tube axis. Then they are accelerated to an energy up to 10 keV towards a thin carbon foil of thickness ≤ 100 nm. There, by stripping of the residual electron, the $\vec{\mathrm{H}}_2^+$ ions get dissociated. Each of the resulting two protons takes half of the kinetic energy achieved during acceleration, whereas the protons from the ionization of atoms carry the full energy. The difference in the energy behind the foil allows to discriminate protons, stemming from atoms, from those, originating from ions, and to measure the nuclear polarization of the recombined molecules with the subsequent Lamb-shift polarimeter (LSP) [2].

In 2007, in a number of test periods the solenoids were cooled down to the liquid-helium temperature. In a first attempt to measure the polarization of extracted ions, a tremendous flux of secondary electrons from the carbon target into the LSP foiled this aim. To deflect these electrons from the ion beam, an electrostatic deflector (Fig. 1) was constructed, succesfully installed, and tested. After this improvement, a first polarization measurement with the LSP could be performed. The storage cell with inner surface covering by Teflon was kept at 90 K in a longitudinal magnetic field of 0.19 T. For protons from atoms, populating either the pure $\mid 1 >$ or

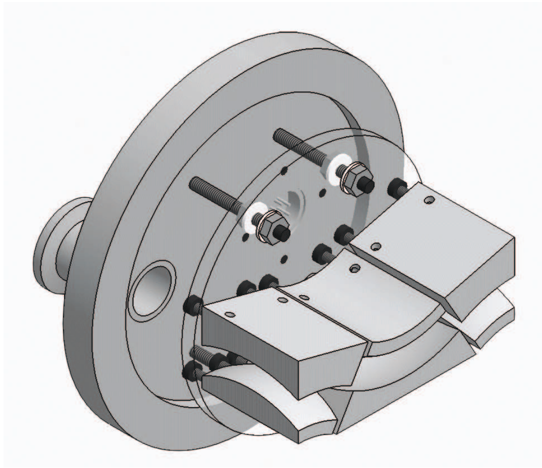

Fig. 1: 3D CAD drawing of the electrostatic deflector (flange diameter 130 mm).

the pure $\mid 3 >$ state in the ABS beam, the asymmetry of the peaks in the Lyman α spectrum was measured as 0.55 to 0.65 (Fig. 2). The necessary correction factors,

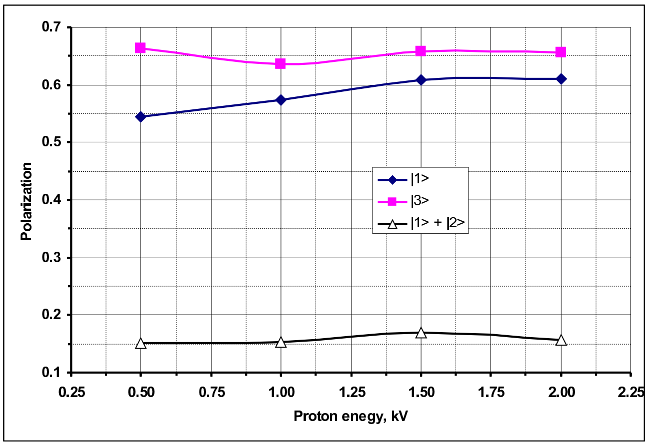

Fig. 2: Measured asymmetry of the peaks in the Lyman α spectrum, measured with the Lamb-shift polarimeter for polarized protons extracted from the storage cell with the atoms in the ABS beam in the hyperfine states $\mid 1 >$, $\mid 3 >$, and in $\mid 1 > + \mid 2 >$ (magnetic solenoid field strength 0.19 T).

to be applied to the measured ratio, increase this value to 0.70 to 0.80. It is still lower than ~0.9 which would result in complete polarization of the atoms in the storage tube. Both deviations from the expected values may be explained by a rotation of the polarization vector in the deflector, where the direction of the ion trajectory deviates from the magnetic field direction. In 2008 this effect will be studied. It can be compensated by the installation of a Wien filter. When the atoms in the ABS beam equally populate the hyperfine states $\mid 1 >$ and $\mid 2 >$, the nuclear polarization of the beam is depending on the magnetic field and the peak asymmetry in the Lyman α spectrum should be about 0.05. A finite value of $\sim$0.15, however, is measured. One possible explanation is the magnetic stray field of the superconducting magnet in the spinfilter of the LSP, which may influence the asymmetry.

The measurements, leading to the results of Fig. 2 for a magnetic field strength of 0.19 T at the cell, were based on earlier investigations of the dependence on the field strength. The results, obtained at a cell temperature of 90 K, are shown in Fig. 4. In agreement with earlier

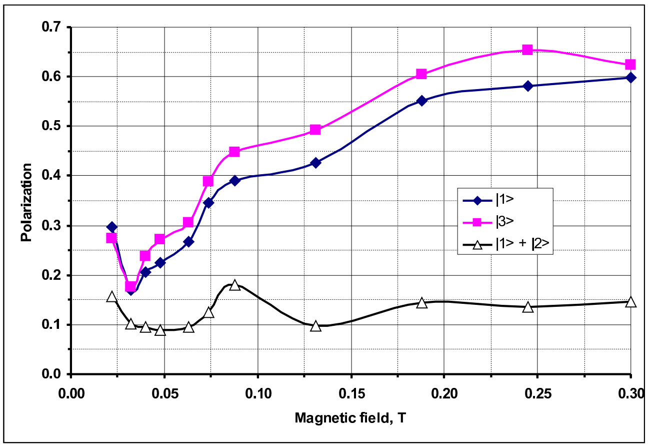

Fig. 3: Measured asymmetry of the peaks in the Lyman α spectrum as function of the magnetic field strength imposed on the storage cell (cell temperature 90 K, inner cell surface covered by Teflon.

measurements, at low field strengths the polarization of the atoms gets reduced by the interaction in collisions with the inner surface of the storage-cell walls. With field strength above $\sim$0.2 T, the coupling of the electron and nuclear magnetic moments to the field is sufficiently strong to protect against depolarization by interaction at the wall surface.

Furthermore, measurements were carried out to study the dependence of the asymmetry, i.e., the nuclear polarization, on the gas density in the storage cell by variation of the intensity of the $\vec{\mathrm{H}}$ beam from the ABS (see Fig. 4). The decrease of the measured asymmetry was less then 3%, when the intensity was twice that used in the measurements leading to the results of Fig. 2. By variation of the ABS beam intensity it could be derived that the density of residual, molecular gas within the cell-tube volume is less than 5% of that which is produced by the incoming beam from the ABS.

Finally, measurements with three different populations of the hyperfine states in the ABS beam were performed. In these experiments the use of an extremely thin carbon foil of 25 nm only was sucessfully tested.

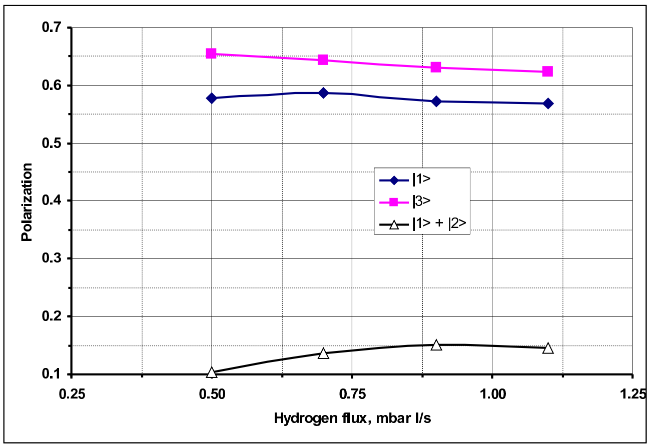

Fig. 4: Measured asymmetry of the peaks in the Lyman α spectrum as function of the hydrogen flux into the dissoziator of the ABS.

References:

[1] F. Rathmann et al., Proc. 15^{th} Int. Spin Physics Symposium, 2002, Upton, NY, USA. Y.I. Makdisi, A.U. Luccio, W.W. MacKay (Eds.) (AIP Conf. Proc. **675**, 2003) P. 924.

[2] R. Engels et al., Rev. Sci. Instr. **74** (2003) 4607.

[a] Institut für Kernphysik, Forschungszentrum Jülich, Germany

[b] Petersburg Nuclear Physics Institute, Gatchina, Russia

[c] Institut für Kernphysik, Universität zu Köln, Germany

Chemical Shift of K transitions in Manganese

D. Gotta, T. Strauch, C. Weidemann

Precision measurements of X-ray energies in the few keV range must take into account chemical shifts of the Kα fluorescence radiation. In a recent measurement MnO_2 was used as calibration standard, which itself had to be calibrated against the precisely measured values of metallic Mn. Due to its electron configuration ($[Ar]3d^5 4s^2$) the manganese atom could appear in many possible oxidation states. For that, a systematic study of the shift in manganese compounds was performed. Measured compounds are $Mn(II)F_3$, $Mn(II)(CH_3COO)_2$, $Mn(IV)O_2$ and $KMn(VII)O_4$ (valences in brackets).
The experimental set-up consists of the target with different manganese compounds, a reflection-type crystal spectrometer equipped with a spherically bent crystal and a large-area CCD for position sensitive X-ray detection. The rotatable target allows a reference measurement with metallic Mn without vacuum distortion.
The energies of the $K\alpha_{1,2}$ transitions from Mn metal and Mn compounds were measured with a relative accuracy of 10 - 20 meV. According to the line shape model of [1] the Mn metal spectrum was fitted and the tabulated peak energy has been used for absolute calibration for the $K\alpha_1$ lines.

$K\alpha_1$	$1s^{-1} \rightarrow 2p_{3/2}^{-1}$	5898.801 eV
$K\alpha_2$	$1s^{-1} \rightarrow 2p_{1/2}^{-1}$	5887.686 eV
$K\beta_{13}$	$1s^{-1} \rightarrow 3p_{1/2,3/2}^{-1}$	6490.585 eV

The transition energies of the various Mn compounds, representing different valences of manganese, show significant chemical effects (Fig 1 and 2).

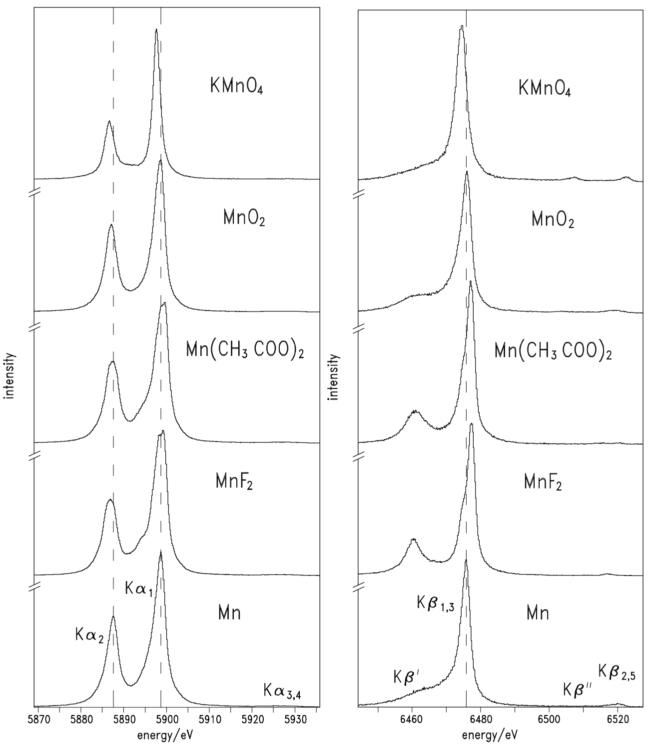

Fig. 1: *Kα and Kβ spectra of manganese compounds*

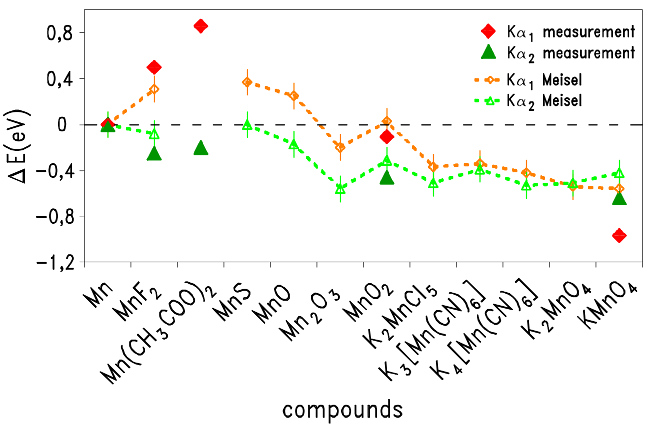

Fig. 2: *Chemical shift compared to metallic Mn*

The observed energy shifts are mainly caused by the spin-orbit coupling of the electrons. For the $K\alpha_{1,2}$ doublet the jj coupling between the $3d^n$ electrons and the incomplete 2p shell leads to a splitting of the $2p_{3/2}$ and the $2p_{1/2}$ term increasing with the number of unpaired 3d electrons. Therefore the maximal splitting is achieved for MnF_2 and $Mn(CH_3COO)_2$ because of five unpaired 3d electrons. This splitting of the $K\alpha_1$ and $K\alpha_2$ line (Fig 1) is influenced and overlayed by additional effects like multiple ionisation, exchange interaction or hybridization of the atomic orbitals. Therefore multiconfiguration Dirac-Fock (MCDF) calculations could not reproduce the measured values within the quoted errors. Furthermore the mentioned effects cause a hugh number of satellites, which also give information about the electron configuration of different Mn compounds. The weak $K\alpha_{3,4}$ satellites for example are caused by an additional hole in the L shell.
Compared to previous measurements [2] the accuracy could be improved by factors 6 to 10. To check the spectrometer system for consistency the well known Kβ spectra were measured for the same compounds. In agreement with previously obtained data, chemical shifts up to 1.6 eV were found for the $K\beta_{1,3}$ transition. The chemical shifts and the structure of the Kβ spectra show larger changes due to interactions and couplings because of the smaller binding energy of the 3p electrons.
For a larger overlap with existing data, $Mn(III)F_3$, $Mn_2(III)O_3$ and $Mn(II)O$ have been measured. The expected minimum for the K energies of Mn_2O_3 according to [2] (Fig 2) could not be reproduced from preliminary results.

References:

[1] Förster, E. et al., *Phys. Rev.* A 56 No. 6 (1997).
[2] Meisel, A.; Döring, E., *Über den Einfluss chemischer Bindung auf das Kα-Dublett von Mangan, Leipzig (1962).*

Trapping of Positrons at ATRAP-II

M.C. George, for the ATRAP–Collaboration

The forming of anti-hydrogen ($\bar{H}$) requires populations of the two constituent particles, namely anti-protons ($\bar{p}$) and positrons (e^+). The $\bar{p}$ are supplied from the CERN anti-proton decelerator, moderated through a Be degrader, and trapped in the ATRAP-II penning-trap electrodes. Concurrently, the e^+ are accumulated in the ATRAP positron accumulator, then are loaded in pulses into different electrodes of the same ATRAP-II penning trap.
The buffer-gas-cooled positron accumulator (see Fig. 1), commissioned last year, benefited from further development and optimization. A new feature implemented is that during the accumulation of the positrons, a rotating electric field is applied to the positron cloud which spins up the particles and reduces the radius of the cloud. The presence of the cooling gas SF6 serves to counteract possible heating from this rotating electric field. Actively forcing the e^+ to central magnetic field lines of the accumulator minimizes a main loss mechanism during accumulation- so called radial walk off, and 25 million e^+ are now accumulated twice during each 100-second AD cycle. In addition to improved accumulation

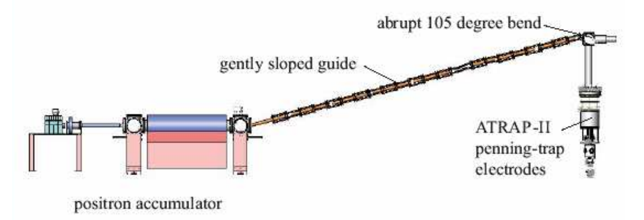

Fig. 1: ATRAP positron accumulator and transfer guide.

efficiency, the smaller radius e^+ cloud allows for easier transferring of the particles from the 0.15 T of the accumulator, through the 0.02 T of the transfer line, into the 1–T region of the penning-trap electrodes.
The ATRAP collaboration successfully implemented and optimized the delicate process of transferring e^+ from the horizontally-aligned positron accumulator, through a 6-meter-long gently-sloped positron guide, around an abrupt 105 degree change in direction, down a 2-meter-long vertical transfer guide, through a 1-mm-diameter aperture, into the vertically-aligned Penning-trap electrodes of ATRAP-II. An illustration of the apparatus is shown in Fig. 1. This required the precise setting of some 95 electromagnets which were used to produce and trim the magnetic field along the positron guide. This steering was made challenging by the presence of the fringing field from the large-bore 1–T ATRAP super-conducting solenoid in which the ATRAP-II Penning trap is housed. Nearly 10 million out of the 25 million e^+ accumulated each 50 seconds were steered successfully into the Penning-trap electrodes of ATRAP-II.
The IKP contributed to developing a technique to catch and cool the incoming pulse of positrons efficiently. Electrons (typically 150 million) are loaded (using excimer-laser-induced photo-emission) into an electric potential nested-well structure as shown in Fig.2. An incoming pulse of e^+ enters when the front door is lowered momentarily to trap the e^+ in the long potential well. As is shown in Fig.3, the presence of the electrons drastically reduces the time required for

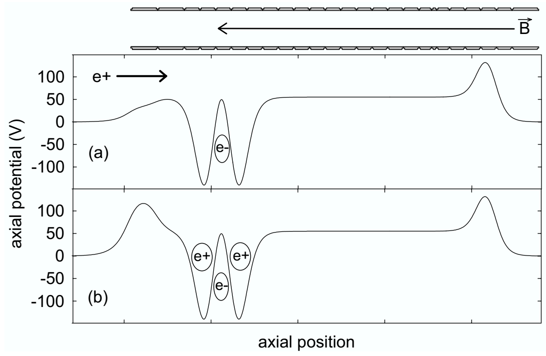

Fig. 2: Trap electrode outlines shown at top, and the positions of the electrons and positrons with the potentials and particle positions as positrons are pulsed into the trap (a) and after electron cooling of positrons (b).

the positrons to cool into the short, deep nested well, such that when the next pulse of e^+ arrives 50 seconds later, all e^+ have cooled into these deeper side wells of the nested well structure and are not released again when the front door is lowered to admit the next e^+ pulse. These techniques al-

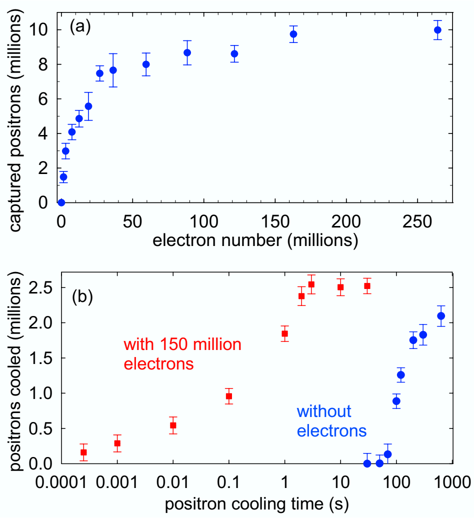

Fig. 3: Accumulated positron number depends upon the number of electrons used (a), and upon the duration of the cooling (b).

lowed for 10 million e^+ to be trapped and available for anti-hydrogen production experiments at ATRAP every 100 second AD cycle.
Summarizing, to facilitate the production of large numbers of $\bar{H}$ during short experiments, positrons from a distant accumulator are transferred successfully into the ATRAP-II apparatus, in which the $\bar{H}$ is formed. The success of accumulation and transferring of e^+ drastically reduces the time for ATRAP to accumulate positrons, allowing for a much faster repetition rate of $\bar{H}$ production experiments using more positrons. These major advances are expected to provide ATRAP with e^+ for exciting physics experiments for years to come.

2 Theoretical Physics

$\bar{D}N$ interaction from meson-exchange and quark-gluon dynamics

J. Haidenbauer, G. Krein (São Paulo), Ulf-G. Meißner (Bonn & FZJ), A. Sibirtsev (Bonn)

We investigate the $\bar{D}N$ interaction at low energies using a meson-exchange model supplemented with a short-distance contribution from one-gluon-exchange. The model is developed in close analogy to the meson-exchange KN interaction of the Jülich group utilizing SU(4) symmetry constraints. The main ingredients of the interaction are provided by vector meson (ρ, ω) exchange and higher-order box diagrams involving $\bar{D}^*N$, $\bar{D}\Delta$, and $\bar{D}^*\Delta$ intermediate states. The short range part is assumed to receive additional contributions from genuine quark-gluon processes. The predicted cross sections for $\bar{D}N$ for excess energies up to 150 MeV are of the same order of magnitude as those for KN but with average values of around 20 mb, roughly a factor two larger than for the latter system. It is found that the ω-exchange plays a very important role. Its interference pattern with the ρ-exchange, which is basically fixed by the assumed SU(4) symmetry, clearly determines the qualitative features of the $\bar{D}N$ interaction – very similiar to what happens also for the KN system. The results are published in Ref. [1].

References:

[1] J. Haidenbauer, G. Krein, U.-G. Meißner and A. Sibirtsev, Eur. Phys. J. A **33**, 107 (2007) [arXiv:0704.3668 [nucl-th]].

Regge approach to charged-pion photoproduction at invariant energies above 2 GeV

A. Sibirtsev (Bonn), J. Haidenbauer, S. Krewald, T.-S.H. Lee (Jlab), U.-G. Meißner (Bonn & FZJ), A.W. Thomas (Jlab)

A Regge model with absorptive corrections is employed in a global analysis of the world data on positive and negative pion photoproduction for photon energies from 3 to 8 GeV. In this region resonance contributions are expected to be negligible so that the available experimental information on differential cross sections and single polarization observables at $-t \leq 2$ GeV^2 allows us to determine the non-resonant part of the reaction amplitude reliably. The model amplitude is then used to predict observables for photon energies below 3 GeV. Differences between our predictions and data in this energy region are systematically examined as possible signals for the presence of excited baryons. We find that the data available for the polarized photon asymmetry show promising resonance signatures at invariant energies around 2 GeV. With regard to differential cross sections the analysis of negative pion photoproduction data, obtained recently at JLab, indicates likewise the presence of resonance structures around 2 GeV. The results are published in Ref. [1].

References:

[1] A. Sibirtsev, J. Haidenbauer, S. Krewald, T. S. H. Lee, U.-G. Meißner and A. W. Thomas, Eur. Phys. J. A **34**, 49 (2007) [arXiv:0706.0183 [nucl-th]].

Comment on 'Mass and $K\Lambda$ coupling of the $N^*(1535)$'

A. Sibirtsev (Bonn), J. Haidenbauer, U.-G. Meißner (Bonn & FZJ)

We comment on a recent paper by B.C. Liu and B.S. Zou [Phys. Rev. Lett. 96, 042002 (2006)] where it was argued that the coupling of the $N^*(1535)$ to $K\Lambda$ is even larger than its coupling to the ηN channel. Specifically, we point out that recently measured Dalitz plot distributions for the reaction $pp \to pK^+\Lambda$ provide clear evidence for the importance of $p\Lambda$ final-state interactions in this reaction and, at the same time, exclude a decisive role of the $N^*(1535)$ resonance, in contradiction to claims made by Liu and Zou. The results are published in Ref. [1].

References:

[1] A. Sibirtsev, J. Haidenbauer and U.-G. Meißner, Phys. Rev. Lett. **98**, 039101 (2007) [arXiv:hep-ph/0607212].

$K\bar{K}$ photoproduction from protons

A. Sibirtsev (Bonn), J. Haidenbauer, S. Krewald, Ulf-G. Meißner (Bonn & FZJ), A.W. Thomas (Jlab)

We study the contribution of the Drell mechanism driven by K^+ and K^- exchange to the reaction $\gamma N \to K\bar{K}N$. Our calculation implements the full KN and $\bar{K}N$ reaction amplitudes in the form of partial wave amplitudes taken from a meson-exchange model (KN) and a partial wave analysis ($\bar{K}N$), respectively. Comparing our results to data of the LAMP2 collaboration we observe that the Drell mechanism alone cannot describe the large $\Lambda(1520)$ photoproduction rate observed experimentally. We argue that the discrepancy could be due to significant contributions from K^*-meson exchange with subsequent excitation of the $\Lambda(1520)$ resonance. After adding such contributions to our model a good agreement of the LAMP2 experiment is achieved. When applying the same model to the recent SAPHIR data we find an excellent description of the K^+p spectrum and can determine the parameters of the $\Lambda(1600)$ P_{01} resonance, $M_R = 1617 \pm 2\,\mathrm{MeV}$ and $\Gamma_R = 117 \pm 4\,\mathrm{MeV}$, from the K^-p mass distribution. The results are published in Ref. [1].

References:

[1] A. Sibirtsev, J. Haidenbauer, S. Krewald, U.-G. Meißner and A. W. Thomas, Eur. Phys. J. A **31**, 221 (2007) [arXiv:hep-ph/0509145].

The pp→$K^+\Sigma^+$n cross section from missing mass spectra

A. Sibirtsev (Bonn), J. Haidenbauer, H.-W. Hammer (Bonn), Ulf-G. Meißner (Bonn & FZJ)

We utilize existing inclusive data on K^+-meson momentum spectra of the reaction $pp{\to}K^+X$ at T_p = 2.3 - 2.85 GeV to deduce total cross sections for $pp{\to}K^+\Sigma^+n$. The method used to extract those cross sections is explained and discussed in detail. Our result for T_p = 2.85 GeV is consistent with the data point from a direct measurement at the same beam energy. The cross section obtained for T_p = 2.3 GeV is with 13.7 ± 2.3 μb considerably smaller than the value found in a recent experiment by the COSY-11 Collaboration at a somewhat lower beam energy, indicating that the $pp{\to}K^+\Sigma^+n$ reaction cross section could exhibit a rather unusual energy dependence. The results are published in Ref. [1].

References:

[1] A. Sibirtsev, J. Haidenbauer, H.-W. Hammer and U.-G. Meißner, Eur. Phys. J. A **32**, 229 (2007) [arXiv:hep-ph/0701269].

Spin observables of the reactions $NN \to \Delta N$ and $pd \to \Delta(pp)(^1S_0)$ in collinear kinematics

Yu.N. Uzikov (JINR) and J. Haidenbauer

A general formalism for double and triple spin-correlations of the reaction $\vec{N}\vec{N} \to \vec{\Delta}N$ is developed for the case of collinear kinematics. A complete polarization experiment allowing to reconstruct all of the four amplitudes describing this process is suggested. Furthermore, the spin observables of the inelastic charge-exchange reaction $\vec{p}\vec{d} \to \vec{\Delta}^0(pp)(^1S_0)$ are analyzed in collinear kinematics within the single pN scattering mechanism involving the subprocess $pn \to \Delta^0 p$. The full set of spin observables related to the polarization of one or two initial particles and one final particle is obtained in terms of three invariant amplitudes of the reaction $pd \to \Delta(pp)(^1S_0)$ and the transition form factor $d \to (pp)(^1S_0)$. A complete polarization experiment for the reaction $\vec{p}\vec{d} \to \vec{\Delta}^0(pp)(^1S_0)$ is suggested which allows one to determine three independent combinations of the four amplitudes of the elementary subprocess $\vec{N}\vec{N} \to \vec{\Delta}N$. The results are published in Ref. [1].

References:

[1] Y. N. Uzikov and J. Haidenbauer, Phys. At. Nucl. **70**, 2138 (2007) [arXiv:nucl-th/0509023].

Dynamics of $^1S_0$ diproton formation in the $pd \to \{pp\}_s n$ and $pN \to \{pp\}_s \pi$ reactions in the GeV region

Yu.N. Uzikov (JINR), J. Haidenbauer, C. Wilkin (UCL)

Mechanisms for the production of $^1S_0$ diproton pairs, $\{pp\}_s$, in the $pd \to \{pp\}_s n$ reaction are studied at proton beam energies $0.5 - 2$ GeV in kinematics similar to those of backward elastic pd scattering. This reaction provides valuable information on the short-range NN and pd interactions that is complementary to that investigated in the well known $pd \to dp$ and $dp \to p(0^\circ)X$ processes. The $pd \to \{pp\}_s n$ reaction is related to the subprocesses $\pi^0 d \to pn$ and $pN \to \{pp\}_s \pi$ using two different one–pion–exchange (OPE) diagrams. Within both these models a reasonable agreement could be obtained with the data below 1 GeV. The similar energy dependence of the $pd \to \{pp\}_s n$ and $pd \to dp$ cross sections and the small ratio of about 1.5% in the production of $\{pp\}_s$ to deuteron final states follow naturally within the OPE models. The results are published in Ref. [1].

References:

[1] Yu. N. Uzikov, J. Haidenbauer and C. Wilkin, Phys. Rev. C **75**, 014008 (2007) [arXiv:nucl-th/0611006].

Strangeness $S = -2$ baryon-baryon interactions using chiral effective field theory

H. Polinder, J. Haidenbauer, Ulf-G. Meißner (Bonn & FZJ)

We derive the leading order strangeness $S = -2$ baryon-baryon interactions in chiral ef fective field theory. The potential consists of contact terms without derivatives and of one-pseudoscalar-meson exchanges. The contact terms and the couplings of the pseudo scalar mesons to the baryons are related via $\mathrm{SU}(3)_\mathrm{f}$ symmetry to the $S = -1$ hyperon-nucleon channels. We show that the chiral effective field theory predictio ns with natural values for the low-energy constants agree with the experimental inform ation in the $S = -2$ sector. The results are published in Ref. [1].

References:

[1] H. Polinder, J. Haidenbauer and U.-G. Meißner, Phys. Lett. B **653**, 29 (2007) [arXiv:0705.3753 [nucl-th]].

On the sign of the $\pi - \rho - \omega$ coupling constant

K. Nakayama (Athens), Yongseok Oh (Athens), J. Haidenbauer, T.-S. H. Lee (Jlab)

It is shown that the relative sign between the $NN\omega$ and $\pi\rho\omega$ coupling constants can be determined most sensitively from ω production processes in NN collisions. Recent data on these reactions clearly favor the sign of the $\pi\rho\omega$ coupling constant which is opposite to that inferred from studies of the photoproduction reaction in combination with the vector meson dominance assumption and used by many authors. Implication of this finding in the description of other reactions is discussed. The results are published in Ref. [1].

References:

[1] K. Nakayama, Y. Oh, J. Haidenbauer and T. S. Lee, Phys. Lett. B **648**, 351 (2007) [arXiv:nucl-th/0611101].

Comment on "Once more about the $K\bar{K}$ molecule approach to the light scalars"

Yu. S. Kalashnikova (ITEP), A. E. Kudryavtsev (ITEP), A. V. Nefediev (ITEP), J. Haidenbauer, C. Hanhart

In this work we comment on the criticism raised recently by Achasov and Kiselev [Phys. Rev. D 76, 077501 (2007)] on our work on the radiative decays $\phi \to \gamma a_0/f_0$ [Eur. Phys. J. A 24, 437 (2005)]. Specifically, we demonstrate that their criticism relies on results that violate gauge–invariance and is therefore invalid. The results are are avalable at [1].

References:

[1] Yu. S. Kalashnikova, A. E. Kudryavtsev, A. V. Nefediev, J. Haidenbauer and C. Hanhart, arXiv:0711.2902 [hep-ph].

ΛN scattering length from the reaction $\gamma d \to K^+\Lambda n$

A. Gasparyan (Darmstadt), J. Haidenbauer, C. Hanhart, K. Miyagawa (Okayama)

The prospects of utilizing the strangeness-production reaction $\gamma d \to K^+\Lambda n$ for the determination of the Λn low-energy scattering parameters are investigated. The spin observables that need to be measured in order to isolate the Λn singlet ($^1S_0$) and triplet ($^3S_1$) states are identified. Possible kinematical regions where the extraction of the Λn scattering lengths might be feasible are discussed. The results are published in Ref. [1].

References:

[1] A. Gasparyan, J. Haidenbauer, C. Hanhart and K. Miyagawa, Eur. Phys. J. A **32**, 61 (2007) [arXiv:nucl-th/0701090].

Role of the delta isobar in pion-deuteron scattering at threshold within chiral effective field theory

V. Baru (ITEP), J. Haidenbauer, C. Hanhart, A. Kudryavtsev (ITEP), V. Lensky, Ulf-G. Meißner (Bonn & FZJ)

We investigate the role of the delta isobar in the reaction $\pi d \to \pi d$ at threshold in chiral effective field theory. We discuss the corresponding power counting and argue that this calculation completes the evaluation of diagrams up to the order $\chi^{3/2}$, where $\chi = m_\pi/M_N$. The net effect of all delta contributions at this order to the πd scattering length is $\delta a_{\pi d}^{\Delta} = (2.4 \pm 0.4) \times 10^{-3}\ m_\pi^{-1}$. The results are published in Ref. [1].

References:

[1] V. Baru, J. Haidenbauer, C. Hanhart, A. Kudryavtsev, V. Lensky and U.-G. Meißner, Phys. Lett. B **659**, 184 (2008) [arXiv:0706.4023 [nucl-th]].

Neutron–neutron scattering length from the reaction $\gamma \mathbf{d} \to \pi^+ \mathbf{nn}$ employing chiral perturbation theory

V. Lensky, V. Baru (ITEP), E. Epelbaum (Bonn & FZJ), C. Hanhart, J. Haidenbauer, A. Kudryavtsev (ITEP), Ulf-G. Meißner (Bonn & FZJ)

We discuss the possibility to extract the neutron-neutron scattering length a_{nn} from experimental spectra on the reaction $\gamma d \to \pi^+ nn$. The transition operator is calculated to high accuracy from chiral perturbation theory. We argue that for properly chosen kinematics, the theoretical uncertainty of the method can be as low as 0.1 fm. The results are published in Ref. [1].

References:

[1] V. Lensky, V. Baru, E. Epelbaum, C. Hanhart, J. Haidenbauer, A. E. Kudryavtsev and U.-G. Meißner, Eur. Phys. J. A **33**, 339 (2007) [arXiv:0704.0443 [nucl-th]].

Dispersive and absorptive corrections to the pion-deuteron scattering length

V. Lensky, V. Baru (ITEP), J. Haidenbauer, C. Hanhart, A. Kudryavtsev (ITEP), Ulf-G. Meißner (Bonn & FZJ)

We present a parameter–free calculation of the dispersive and absorptive contributions to the pion–deuteron scattering length based on chiral perturbation theory. We show that once all diagrams contributing to leading order to this process are included, their net effect provides a small correction to the real part of the pion–deuteron scattering length. At the same time the sizable imaginary part of the pion–deuteron scattering length is reproduced accurately. The results are published in Ref. [1].

References:

[1] V. Lensky, V. Baru, J. Haidenbauer, C. Hanhart, A. E. Kudryavtsev and U.-G. Meißner, Phys. Lett. B **648**, 46 (2007) [arXiv:nucl-th/0608042].

E0 emission in $\alpha + ^{12}C$ fusion at astrophysical energies [1]

G. Baur, K.A. Snover*, and S. Typel**

We show that E0 emission in $\alpha + ^{12}C$ fusion at astrophysically interesting energies is negligible compared to E1 and E2 emission

References:

[1] G.Baur, K.A. Snover, and S. Typel, Phys. Rev C75(2007)058801, nucl-th/0701027

*Center for Experimental Physics and Astrophysics, University of Washington, Seattle, Washington 98195, USA
** GANIL, Bd. Henri Becquerel, F-14076 Caen, France

Electron-positron pair production in ultrarelativistic heavy ion collisions [1]

G. Baur, K. Hencken*,** and D. Trautmann*

In recent years, a large number of papers have appeared that dealt with e^+e^- pair production in heavy ion collisions at high energies. To a large extent these studies were motivated by the existence of relativistic heavy ion accelerators all over the world. There pair production can be studied in so called "ultra-peripheral collisions", where the ions do not come close enough to interact strongly with each other. Various different methods have been used and it is the purpose of this review to present a unified picture of the present status of the field. The lowest order Born result has been known for more than seven decades. The interest and focus is now on higher order effects for values of $Z\alpha \leq 1$, where Z is the charge number of the ion. A similar problem appears for the Bethe-Heitler process, the production of e^+e^- pairs in photon-nucleus collisions. It was solved essentially some five decades ago by Bethe and Maximon. The result of Bethe and Maximon can also be recovered by summing over a class of Feynman diagrams to infinite order. These results can be used for a study of Coulomb corrections in nucleus-nucleus collisions. Indeed, the major part of these corrections have a structure closely related to the Bethe-Maximon solution. There are additional terms which give a small contribution to the total cross section at high energies. Their importance can be enhanced by concentrating on small impact parameters. An interesting exact solution of the one-particle Dirac equation in the high-energy limit was found independently by several authors. This led to some discussion about the interpretation of these results within QED and the correct regularization necessary to get the correct result. The dust of previous debates has settled and, indeed, a consistent picture has emerged. Another interesting higher order effect is multiple pair production, which we also discuss. We compare experimental results obtained recently at RHIC for free and bound-free pair production with theoretical results. We also make some more remarks on the physics of strong electric fields of longer duration. A new field is opened up by ultra-intense laser pulses. We argue that due to the short interaction time in ultraperipheral heavy ion collisions pair production can be well understood in the frame of QED perturbation theory.

References:

[1] Gerhard Baur, Kai Hencken, and Dirk Trautmann, Physics Reports 453(2007)1 arXiv:0706.0654

* Universität Basel, CH4056 Basel, Switzerland
**ABB Corporate Research, Baden Dättwil, Switzerland

Photoproduction at collider energies: from RHIC and HERA to the LHC

G. Baur

A workshop on “Photoproduction at collider energies: from RHIC and HERA to the LHC” was organized at the European Centre for Theoretical Studies in Nuclear Physics and Related Areas (ECT*, Trento) from January 15 to 19, 2007, see [1]. The miniproceedings can be found in [2]. The workshop gathered both theorists and experimentalists to discuss the current status of investigations of high-energy photon-induced processes at different colliders (HERA, RHIC, and Tevatron) as well as preparations for extension of these studies at the LHC. The main physics topics covered were:

(i) small-x QCD in photoproduction studies with protons and in electromagnetic (aka. ultraperipheral) nucleus-nucleus collisions,

(ii) hard diffraction physics at hadron colliders, and

(iii) photon-photon collisions at very high energies: electroweak and beyond the Standard Model processes. These mini-proceedings consist of an introduction and short summaries of the talks presented at the meeting.

A brief introduction to the physics of ultraperipheral collisions at collider energies is given in [3]. Photon-hadron (proton/ nucleus) and photon-photon interactions can be studied in a hitherto unexplored energy regime.

References:

[1] http://indico.cern.ch/conferenceDisplay.py?confId=9422
[2] A.J. Baltz, et al. (29 authors), hep-ph/0702212
[3] G.Baur, invited talk on ’Introductory remarks on Ultraperipheral Heavy Ion Collisions(UPC)’ as a co-convener of the session on Photon and Electroweak boson physics from HERA, RHIC and Tevatron to LHC at PHOTON2007, Paris, 9-13 July 2007 Proceedings to be published in Nucl. Phys. B, arXiv:0711.2882

* Physics Department, Brookhaven National Laboratory, Upton, NY, USA

Coulomb dissociation, a tool for nuclear astrophysics [1]

G. Baur, S. Typel*

A short status report on Coulomb dissociation, an indirect method for nuclear astrophysics is given. An analytically solvable approach to study electromagnetic excitation in ^{11}Be, the archetype of a halo nucleus, is proposed.

References:

[1] G.Baur and S. Typel, J.Phys. G (Proceedings of Nuclear Physics in Astrophysics III, 26-31 March 2007, Dresden, Germany) 35 (2008)014028, arXiv:0705.3307

* GANIL, Bd. Henri Becquerel, F-14076 Caen, France

The Physics of Ultraperipheral Collisions at the LHC [1]

A. J. Baltz *, G. Baur, et al. (23 authors)

We discuss the physics of large impact parameter interactions at the LHC: ultraperipheral collisions (UPCs). The dominant processes in UPCs are photon-nucleon (nucleus) interactions. The current LHC detector configurations can explore small x hard phenomena with nuclei and nucleons at photon-nucleon center-of-mass energies above 1 TeV, extending the x range of HERA by a factor of ten. In particular, it will be possible to probe diffractive and inclusive parton densities in nuclei using several processes. The interaction of small dipoles with protons and nuclei can be investigated in elastic and quasi-elastic J/ψ and Υ production as well as in high t ρ^0 production accompanied by a rapidity gap. Several of these phenomena provide clean signatures of the onset of the new high gluon density QCD regime. The LHC is in the kinematic range where nonlinear effects are several times larger than at HERA. Two-photon processes in UPCs are also studied. In addition, while UPCs play a role in limiting the maximum beam luminosity, they can also be used a luminosity monitor by measuring mutual electromagnetic dissociation of the beam nuclei. We also review similar studies at HERA and RHIC as well as describe the potential use of the LHC detectors for UPC measurements.

References:

[1] A.J. Baltz et al. Physics Reports, in print, arXiv:0706.3356

* Physics Department, Brookhaven National Laboratory, Upton, NY, USA

Two-photon decays of hadronic molecules

C.Hanhart, Yu.S.Kalashnikova*, A.E.Kudryavtsev*, A.V.Nefediev*

In many calculations of the two–photon decay of hadronic molecules, the decay matrix element is estimated using the wave function at the origin prescription, in analogy to the two-photon decay of parapositronium. We question the applicability of this procedure to the two-photon decay of hadronic molecules for it introduces an uncontrolled model dependence into the calculation. As an alternative approach, we propose an explicit evaluation of the hadron loop. For shallow bound states, this can be done as an expansion in powers of the range of the molecule binding force. In the leading order one gets the well-known point-like limit answer. We estimate, in a self-consistent and gauge invariant way, the leading range corrections for the two-photon decay width of weakly bound hadronic molecules emerging from kaon loops. We find them to be small. The role of possible short-ranged operators and of the width of the scalars remains to be investigated. The results are published in Ref. [1].

References:

[1] C. Hanhart, Yu. S. Kalashnikova, A. E. Kudryavtsev and A. V. Nefediev, Phys. Rev. D **75** (2007) 074015 [arXiv:hep-ph/0701214].

* ITEP, Moscow

Reconciling the $X(3872)$ with the near-threshold enhancement in the $D^0\bar{D}^{*0}$ final state

C.Hanhart, Yu.S.Kalashnikova*, A.E.Kudryavtsev*, A.V.Nefediev*

We investigate the enhancement in the $D^0\bar{D}^0\pi^0$ final state with the mass M=$3875.2\pm0.7^{+0.3}_{-1.6}\pm0.8$ MeV found recently by the Belle Collaboration in the $B\to KD^0\bar{D}^0\pi^0$ decay and test the possibility that this is yet another manifestation of the well-established resonance X(3872). We perform a combined Flatte analysis of the data for the $D^0\bar{D}^0\pi^0$ mode, and for the $\pi^+\pi^-J/\psi$ mode of the X(3872). Only if the X(3872) is a virtual state in the $D^0\bar{D}^{*0}$ channel, the data on the new enhancement comply with those on the X(3872). In our fits, the mass distribution in the $D^0\bar{D}^{*0}$ mode exhibits a peak at 2-3 MeV above the $D^0\bar{D}^{*0}$ threshold, with a distinctive non-Breit-Wigner shape. The results are published in Ref. [1].

References:

[1] C. Hanhart, Yu. S. Kalashnikova, A. E. Kudryavtsev and A. V. Nefediev, Phys. Rev. D **76** (2007) 034007 [arXiv:0704.0605 [hep-ph]].

* ITEP, Moscow

Investigation of $a_0 - f_0$ mixing

Christoph Hanhart, Bastian Kubis*, Jose R. Pelaez**

We investigate the isospin-violating mixing of the light scalar mesons a0(980) and f0(980) within the unitarized chiral approach. Isospin-violating effects are considered to leading order in the quark mass differences and electromagnetism. In this approach both mesons are generated through meson-meson dynamics. Our results provide a description of the mixing phenomenon within a framework consistent with chiral symmetry and unitarity, where these resonances are not predominantly q q-bar states. Amongst the possible experimental signals, we discuss observable consequences for the reaction J/Psi -¿ phi pi0 eta in detail. In particular we demonstrate that the effect of a0-f0 mixing is by far the most important isospin-breaking effect in the resonance region and can indeed be extracted from experiment. The results are published in Ref. [1].

References:

[1] C. Hanhart, B. Kubis and J. R. Pelaez, Phys. Rev. D **76** (2007) 074028 [arXiv:0707.0262 [hep-ph]].

* HISKP, Bonn University
**Facultad de Ciencias Fisicas, Univ. Complutense de Madrid

Dispersion analysis of the nucleon form factors including meson continua

M. Belushkin (Bonn), H.-W. Hammer (Bonn), and Ulf-G. Meißner (Bonn & FZJ)

Dispersion relations provide a powerful tool to analyse the electromagnetic form factors of the nucleon for all momentum transfers. Constraints from meson-nucleon scattering data, unitarity, and perturbative QCD can be included in a straightforward way. In particular, we include the 2pi, rho-pi, and KKbar continua as independent input in our analysis and provide an error band for our results [1]. Moreover, we discuss two different methods to include the asymptotic constraints from perturbative QCD. We simultaneously analyze the world data for all four form factors in both the space-like and time-like regions and generally find good agreement with the data. We also extract the nucleon radii and the omega-NN coupling constants. For the radii, we generally find good agreement with other determinations with the exception of the electric charge radius of the proton which comes out smaller. The omega-NN vector coupling constant is determined relatively well by the fits, but for the tensor coupling constant even the sign can not be determined.

References:

[1] M. A. Belushkin, H. W. Hammer and U.-G. Meißner, Phys. Rev. C **75** (2007) 035202 [arXiv:hep-ph/0608337].

Hyperon decay form factors in chiral perturbation theory

A. Lacour (Bonn), B. Kubis (Bonn) and Ulf-G. Meißner (Bonn & FZJ)

We present a complete calculation of the SU(3)-breaking corrections to the hyperon vector form factors up to $O(p^4)$ in covariant baryon chiral perturbation theory [1]. Partial higher-order contributions are obtained, and we discuss chiral extrapolations of the vector form factor at zero momentum transfer. In addition we derive low-energy theorems for the subleading moments in hyperon decays, the weak Dirac radii and the weak anomalous magnetic moments, up to $O(p^4)$.

References:

[1] A. Lacour, B. Kubis and U.-G. Meißner, JHEP **0710** (2007) 083 [arXiv:0708.3957 [hep-ph]].

Chiral perturbation theory

V. Bernard (Strasbourg) and Ulf-G. Meißner (Bonn & FZJ)

We give a brief introduction to chiral perturbation theory in its various settings. We discuss some applications of recent interest including chiral extrapolations for lattice gauge theory [1].

References:

[1] V. Bernard and U.-G. Meißner, Ann. Rev. Nucl. Part. Sci. **57** (2007) 33 [arXiv:hep-ph/0611231].

A gauge invariant chiral unitary framework for kaon photo- and electroproduction on the proton

B. Borasoy (Bonn), P. C. Bruns (Bonn), Ulf-G. Meißner (Bonn & FZJ) and R. Nißler (Bonn)

We present a gauge invariant approach to photoproduction of mesons on nucleons within a chiral unitary framework [1]. The interaction kernel for meson-baryon scattering is derived from the chiral effective Lagrangian and iterated in a Bethe-Salpeter equation. Within the leading order approximation to the interaction kernel, data on kaon photoproduction from SAPHIR, CLAS and CBELSA/TAPS are analyzed in the threshold region. The importance of gauge invariance and the precision of various approximations in the interaction kernel utilized in earlier works are discussed.

References:

[1] B. Borasoy, P. C. Bruns, U.-G. Meißner and R. Nißler, Eur. Phys. J. A **34** (2007) 161 [arXiv:0709.3181 [nucl-th]].

Lattice simulations for light nuclei: Chiral effective field theory at leading order

B. Borasoy (Bonn), E. Epelbaum (FZJ & Bonn), H. Krebs (Bonn), D. Lee (North Carolina),
U.-G. Meißner (Bonn & FZJ)

We discuss lattice simulations of light nuclei at leading order in chiral effective field theory. Using lattice pion fields and auxiliary fields, we include the physics of instantaneous one-pion exchange and the leading-order S-wave contact interactions. We also consider higher-derivative contact interactions which adjust the S-wave scattering amplitude at higher momenta. By construction our lattice path integral is positive definite in the limit of exact Wigner SU(4) symmetry for any even number of nucleons. This SU(4) positivity and the approximate SU(4) symmetry of the low-energy interactions play an important role in suppressing sign and phase oscillations in Monte Carlo simulations. We assess the computational scaling of the lattice algorithm for light nuclei with up to eight nucleons and analyze in detail calculations of the deuteron, triton, and ^{4}He.

References:

[1] B. Borasoy, E. Epelbaum, H. Krebs, D. Lee and U. G. Meissner, Eur. Phys. J. A **31** (2007) 105 [arXiv:nucl-th/0611087].

The Three-nucleon system as a laboratory for nuclear physics: The Need for 3N forces

N. Kalantar-Nayestanaki (KVI), E. Epelbaum (FZJ & Bonn)

Recent experimental results in three-body systems have unambiguously shown that calculations based on nucleon-nucleon forces fail to accurately describe many experimental observables and one needs to include effects which are beyond the realm of the two-body potentials. This conclusion owes its significance to the fact that experiments and calculations can both be performed with a high accuracy. In this short review, a sample of recent experimental results along with the results of the state-of-the-art calculations are presented and discussed.

References:

[1] N. Kalantar-Nayestanaki, E. Epelbaum, Nucl. Phys. News **17** (2007) 22 [arXiv:nucl-th/0703089].

Nuclear forces with Delta-excitations up to next-to-next-to-leading order I: Peripheral nucleon-nucleon waves

H. Krebs (Bonn), E. Epelbaum (FZJ & Bonn), U.-G. Meißner (Bonn & FZJ)

We study the two-nucleon force at next-to-next-to-leading order in a chiral effective field theory with explicit Delta degrees of freedom. Fixing the appearing low-energy constants from a next-to-leading order calculation of pion-nucleon threshold parameters, we find an improved convergence of most peripheral nucleon-nucleon phases compared to the theory with pions and nucleons only. In the delta-full theory, the next-to-leading order corrections are dominant in most partial waves considered.

References:

[1] H. Krebs, E. Epelbaum and U. G. Meissner, Eur. Phys. J. A **32** (2007) 127 [arXiv:nucl-th/0703087].

Vector and tensor analyzing powers of elastic deuteron-proton scattering at 130 MeV deuteron beam energy

E. Stephan (Katowice), St. Kistryn, R. Sworst, A. Biegun, K. Bodek, I. Ciepa (Krakow), A. Deltuva (Lisboa), E. Epelbaum (FZJ & Bonn), A. Fonseca (Lisboa), W. Glöckle (Bochum), J. Golak (Krakow), N. Kalantar-Nayestanaki (KVI), H. Kamada (Kyushu), M. Kis (KVI), A. Kozela (Krakow), M. Mahjour-Shafiei (KVI), A. Micherdzinska (Katowice), A. Nogga (FZJ), P. U. Sauer (Hannover), R. Skibinski, H. Witala, J. Zejma (Krakow) and W. Zipper (Katowice),

High precision vector and tensor analyzing power data of the deuteron-proton elastic scattering at 130 MeV deuteron beam energy have been measured in a large range of angles. They are compared with theoretical predictions obtained in various approaches: with realistic potentials for pure NN interactions, with the inclusion of a three-nucleon force, and in the framework of chiral perturbation theory. All the theoretical calculations describe roughly the main features of the measured distributions, but none of them can reproduce all their details. This indicates the need for further development of the three-nucleon force models.

References:

[1] E. Stephan et al., Phys. Rev. C **76** (2007) 057001.

Four-nucleon force using the method of unitary transformation

E. Epelbaum (FZJ & Bonn)

We discuss in detail the derivation of the leading four-nucleon force in chiral effective field theory using the method of unitary transformation. The resulting four-nucleon force is given in both momentum and configuration space. It does not contain any unknown parameters and can be used in few- and many-nucleon studies.

References:

[1] E. Epelbaum, Eur. Phys. J. A **34** (2007) 197 [arXiv:0710.4250 [nucl-th]].

Two-particle scattering on the lattice: Phase shifts, spin-orbit coupling, and mixing angles

B. Borasoy (Bonn), E. Epelbaum (FZJ & Bonn), H. Krebs (Bonn), D. Lee (North Carolina),
U.-G. Meißner (Bonn & FZJ)

We determine two-particle scattering phase shifts and mixing angles for quantum theories defined with lattice regularization. The method is suitable for any nonrelativistic effective theory of point particles on the lattice. In the center-of-mass frame of the two-particle system we impose a hard spherical wall at some fixed large radius. For channels without partial-wave mixing the partial-wave phase shifts are determined from the energies of the nearly-spherical standing waves. For channels with partial-wave mixing further information is extracted by decomposing the standing wave at the wall boundary into spherical harmonics, and we solve coupled-channels equations to extract the phase shifts and mixing angles. The method is illustrated and tested by computing phase shifts and mixing angles on the lattice for spin-1/2 particles with an attractive Gaussian potential containing both central and tensor force parts.

References:

[1] B. Borasoy, E. Epelbaum, H. Krebs, D. Lee and U. G. Meissner, Eur. Phys. J. A **34** (2007) 185 [arXiv:0708.1780 [nucl-th].

Extended Theory of Finite Fermi Systems: Application to the collective and non-collective E1 strength in ^{208} Pb

V.Tselyaev (St. Petersburg State U.), J. Speth, F.Grümmer,
S.Krewald, A.Avdeenkov (Obninsk), E.Litvinova, G.Tertychny (Obninsk)

The Extended Theory of Finite Fermi Systems is based on the conventional Landau-Migdal theory and includes the coupling to the low-lying phonons in a consistent way. The phonons give rise to a fragmentation of the single-particle strength and to a compression of the single-particle spectrum. Both effects are crucial for a quantitative understanding of nuclear structure properties. We demonstrate the effects on the electric dipole states in ^{208}Pb (which possesses 50 percent more neutrons then protons) where we calculated the low-lying non-collective spectrum as well as the high-lying collective resonances. Below 8 MeV, where one expects the so called isovector pygmy resonances, we also find a strong admixture of isoscalar strength that comes from the coupling to the high-lying isoscalar electric dipole resonance, which we obtain at about 22 MeV. The transition density of this resonance is very similar to the breathing mode, which we also calculated. We shall show that the extended theory is the correct approach for self-consistent calculations, where one starts with effective Lagrangians and effective Hamiltonians, respectively, if one wishes to describe simultaneously collective and non-collective properties of the nuclear spectrum. In all cases for which experimental data exist the agreement with the present theory results is good.

References:

[1] V. Tselyaev, J. Speth, F. Grummer, S. Krewald, A. Avdeeenko, E. Litviniva and G. Tertychny, Phys. Rev. C **75**, 014315 (2007) [arXiv:nucl-th/0612064].

Microscopic description of the pygmy and giant electric dipole resonances in stable Ca isotopes

G. Tertychny (Obninsk), V. Tselyaev (St. Petersburg State U.), S. Kamerdzhiev (Obninsk),
F. Grümmer, S. Krewald, J. Speth, A. Avdeenkov (Obninsk), E. Litvinova(Obninsk)

The properties of the low lying and high lying electric dipole strength in the stable 40Ca, 44Ca and 48Ca isotopes have been calculated within the Extended Theory of Finite Fermi Systems (ETFFS). This approach is based on the random phase approximation (RPA) and includes the single particle continuum as well as the coupling to low lying collective states which are considered in a consistent microscopic way. For 44Ca we also include pairing correlations. We obtain good agreement with the existing experimental data for the gross properties of the low lying and high lying strength. It is demonstrated that the recently measured A-dependence of the electric dipole strength below 10 MeV is well understood in our model: due to the phonon coupling some of the strength in 48Ca is simply shifted beyond 10 MeV. The predicted fragmentation of the strength can be investigated in (e, e') and (γ, γ') experiments. The isovector dipole strength below 10 MeV is small in all Ca isotopes. Surprisingly, the proton and neutron transition densities of these low lying electric dipole states are in phase, which indicate isoscalar structure. We conclude that for the detailed understanding of the structure of excited nuclei e.g. the low lying and high lying electric dipole strength an approach like the present one is absolutely necessary.

References:

[1] G. Tertychny *et al.*, Phys. Lett. B **647**, 104 (2007), arXiv:nucl-th/0603051.

Selfconsistent calculations within the extended theory of finite Fermi systems

N. Avdeenkov (Obninsk), F. Grümmer, S. Kamerdzhiev (Obninsk),
S. Krewald, A. Lyutorovich (St. Petersburg) and J. Speth

The Extended Theory of Finite Fermi Systems (ETFFS) describes nuclear excitations considering phonons and pairing degrees of freedom, using the effective Landau-Migdal interaction and nuclear mean fields obtained from experimental data. Here we employ the nuclear mean field derived from Skyrme interactions and the corresponding particle-hole interaction. This allows to extend the range of applicability of the ETFFS to experimentally not yet investigated short-lived isotopes. We find that Skyrme interactions which reproduce at the mean field level both ground state properties and nuclear excitations are able to describe the spreading widths of the giant resonances in the new approach, but produce shifts of the centroid energies. A renormalization of the Skyrme interactions is required for approaches going beyond the mean field level.

References:

[1] N. Avdeenkov, F. Grummer, S. Kamerdzhiev, S. Krewald, A. Lyutorovich and J. Speth, Phys. Lett. B **653**, 196 (2007), arXiv:0706.2764 [nucl-th]

Compton Scattering on ^{3}He

D. Choudhury (Ohio U.), D.R. Phillips (Ohio U.), A. Nogga (Jülich, Forschungszentrum)

We examine manifestations of neutron electromagnetic polarizabilities in coherent Compton scattering from the Helium-3 nucleus. We calculate γ^3He elastic scattering observables using chiral perturbation theory to next-to-leading order ($\mathcal{O}(e^2Q)$). We find that the unpolarized differential cross section can be used to measure neutron electric and magnetic polarizabilities, while two double-polarization observables are sensitive to different linear combinations of the four neutron spin polarizabilities. The results are published in [1].

References:

[1] D. Choudhury, A. Nogga and D. R. Phillips, Phys. Rev. Lett. **98**, 232303 (2007) [arXiv:nucl-th/0701078].

Coupled-cluster theory for three-body Hamiltonians

G. Hagen (Oak Ridge & Tennessee U. & Oslo U.), T. Papenbrock (Oak Ridge & Tennessee U.), D.J. Dean (Oak Ridge), A. Schwenk (TRIUMF & Washington U., Seattle), A. Nogga (Jülich, Forschungszentrum), M. Wloch, P. Piecuch (Michigan State U.)

We derive coupled-cluster equations for three-body Hamiltonians. The equations for the one- and two-body cluster amplitudes are presented in a factorized form that leads to an efficient numerical implementation. We employ low-momentum two- and three-nucleon interactions and calculate the binding energy of He-4. The results show that the main contribution of the three-nucleon interaction stems from its density-dependent zero-, one-, and two-body terms that result from the normal ordering of the Hamiltonian in coupled-cluster theory. The residual three-body terms that remain after normal ordering can be neglected. The results are published in [1].

References:

[1] G. Hagen, T. Papenbrock, D. J. Dean, A. Schwenk, A. Nogga, M. Wloch and P. Piecuch, Phys. Rev. C **76**, 034302 (2007) [arXiv:0704.2854 [nucl-th]].

The Hyperon-nucleon interaction: Conventional versus effective field theory approach

J. Haidenbauer (Jülich, Forschungszentrum), Ulf-G. Meißner (Jülich, Forschungszentrum & Bonn U.),
A. Nogga, H. Polinder (Jülich, Forschungszentrum)

Hyperon-nucleon interactions are presented that are derived either in the conventional meson-exchange picture or within leading order chiral effective field theory. The chiral potential consists of one-pseudoscalar-meson exchanges and non-derivative four-baryon contact terms. With regard to meson-exchange hyperon-nucleon models we focus on the new potential of the Juelich group, whose most salient feature is that the contributions in the scalar–isoscalar (σ) and vector–isovector (ρ) exchange channels are constrained by a microscopic model of correlated $\pi\pi$ and $K\bar{K}$ exchange. The results are published in [1].

References:

[1] J. Haidenbauer, U.-G. Meißner, A. Nogga and H. Polinder, Lect. Notes Phys. **724**, 113 (2007) [arXiv:nucl-th/0702015].

Differential cross section and analyzing power measurements for $\vec{n}d$ elastic scattering at 248 MeV

Y. Maeda (Tokyo U.), H. Sakai (Tokyo U. & RIKEN), K. Fujita(RCNP), M. B. Greenfield (Christian U. Tokyo), K. Hatanaka(RCNP), M. Hatano(Tokyo U.), J. Kamiya (Tokai), T. Kawabata, H. Kuboki (Tokyo U.), H. Okamura(RCNP), J. Rapaport (Ohio U.) , T. Saito (Tokyo U.), Y. Sakemi(RCNP), M. Sasano (Tokyo U.), K. Sekiguchi(RIKEN), Y. Shimizu(RCNP), K. Suda (Tokyo U.), Y. Tameshige, A. Tamii(RCNP), T. Wakasa (Kyushu U.), K. Yako (Tokyo U.), J. Blomgren (Uppsala U.), P. Mermod, A. Öhrn, M. Österlund (Uppsala U.), H. Witala (Crakow), A. Deltuva, A. C. Fonseca (Lisbon), P. U. Sauer (Hanover U.), W. Glöckle (Bochum U.) , J. Golak (Crakow), H. Kamada (Kyushu U.), A. Nogga (Jülich, Forschungszentrum), R. Skibinski (Crakow)

The differential cross sections and vector analyzing powers for nd elastic scattering at E_n =248 MeV were measured for 10 deg-180 deg in the center-of-mass (c.m.) system. To cover the wide angular range, the experiments were performed separately by using two different setups for forward and backward angles. The data are compared with theoretical results based on Faddeev calculations with realistic nucleon-nucleon (NN) forces such as AV18, CD Bonn, and Nijmegen I and II, and their combinations with the three-nucleon forces (3NFs), such as Tucson-Melbourne 99 (TM99), Urbana IX, and the coupled-channel potential with -isobar excitation. Large discrepancies are found between the experimental cross sections and theory with only 2N forces for $\theta_{\mathrm{c.m.}} > 90$deg. The inclusion of 3NFs brings the theoretical cross sections closer to the data but only partially explains this discrepancy. For the analyzing power, no significant improvement is found when 3NFs are included. Relativistic corrections are shown to be small for both the cross sections and the analyzing powers at this energy. For the cross sections, these effects are mostly seen in the very backward angles. Compared with the pd cross section data, quite significant differences are observed at all scattering angles that cannot be explained only by the Coulomb interaction, which is usually significant at small angles. The results are published in [1].

References:

[1] Y. Maeda *et al.*, Phys. Rev. C **76**, 014004 (2007).

Structure of $A = 10 - 13$ nuclei with two plus three-nucleon interactions from chiral effective field theory

P. Navratil, V.G. Gueorguiev (LLNL, Livermore), J.P. Vary (LLNL, Livermore & Iowa State U.), W.E. Ormand (LLNL, Livermore), A. Nogga (Jülich, Forschungszentrum)

Properties of finite nuclei are evaluated with two-nucleon (NN) and three-nucleon (NNN) interactions derived within chiral effective field theory (EFT). The nuclear Hamiltonian is fixed by properties of the $A = 2$ system, except for two low-energy constants (LECs) that parameterize the short range NNN interaction. We constrain those two LECs by a fit to the $A = 3$ system binding energy and investigate sensitivity of ^{4}He, ^{6}Li, ^{10,11}B and ^{12,13}C properties to the variation of the constrained LECs. We identify a preferred choice that gives globally the best description. We demonstrate that the NNN interaction terms significantly improve the binding energies and spectra of mid-p-shell nuclei not just with the preferred choice of the LECs but even within a wide range of the constrained LECs. At the same time, we find that a very high quality description of these nuclei requires further improvements to the chiral Hamiltonian. The results are published in [1].

References:

[1] P. Navratil, V. G. Gueorguiev, J. P. Vary, W. E. Ormand and A. Nogga, Phys. Rev. Lett. **99**, 042501 (2007) [arXiv:nucl-th/0701038].

S=-1,-2 baryon-baryon interactions in chiral effective field theory

H. Polinder

We have constructed the leading order strangeness S=-1,-2 baryon-baryon potential in a chiral effective field theory approach. The chiral potential consists of one-pseudoscalar-meson exchanges and non-derivative four-baryon contact terms. The potential, derived using SU(3) symmetry constraints, contains six independent low-energy coefficients. We have solved a regularized Lippmann-Schwinger equation and achieved a good description of the available scattering data. Furthermore a correctly bound hypertriton has been obtained.
This work has been published in Ref. [1].

References:

[1] H. Polinder, arXiv:0708.0773v1 [nucl-th].

Strange two-baryon interactions using chiral effective field theory

H. Polinder

We have constructed the leading order strangeness S=-1,-2 baryon-baryon potential in a chiral effective field theory approach. The chiral potential consists of one-pseudoscalar-meson exchanges and non-derivative four-baryon contact terms. The potential, derived using $SU(3)_f$ symmetry constraints, contains six independent low-energy coefficients. We have solved a regularized Lippmann-Schwinger equation and achieved a good description of the available scattering data. Furthermore a correctly bound hypertriton has been obtained.
This work has been published in Ref. [1].

References:

[1] H. Polinder, arXiv:0711.5024v1 [nucl-th].

Neutron-proton mass difference in nuclear matter

U.-G. Meißner, A.M. Rakhimov (Tashkent), A. Wirzba, U.T. Yakhshiev (Bonn & FZJ)

Isospin-breaking effects in nuclear matter are studied in the framework of a medium-modified Skyrme model. The proposed effective Lagrangian incorporates both the medium influence of the surrounding nuclear environment on the single nucleon properties and an explicit isospin-breaking effect in the mesonic sector. The approach predicts that the neutron-proton mass difference decreases in isospin-symmetric nuclear matter but by a very small amount only. The results can be found in Ref. [1].

References:

[1] U.-G. Meißner, A.M. Rakhimov, A. Wirzba, U.T. Yakhshiev, Eur. Phys. J. A **31**, 357-364 (2007).

Neutron-proton mass difference in isospin asymmetric nuclear matter

Ulf-G. Meißner, A.M. Rakhimov (Tashkent), A. Wirzba, U.T. Yakhshiev (Bonn & FZJ)

Isospin-breaking effects in the baryonic sector are studied in the framework of a medium-modified Skyrme model in Ref. [1]. The neutron-proton mass difference in infinite, asymmetric nuclear matter is discussed. In order to describe the influence of the nuclear environment on the skyrmions, energy-dependent charged and neutral pion optical potentials in the s - and p -wave channels are included. The present approach predicts that the neutron-proton mass difference is mainly dictated by its strong part and that it strongly decreases in neutron matter. More results can be found in Ref. [1].

References:

[1] U.-G. Meißner, A.M. Rakhimov, A. Wirzba, U.T. Yakhshiev, Eur. Phys. J. A **32**, 299-309 (2007) [arXiv:0705.1603].

The Casimir effect as scattering problem

A. Wirzba

In Ref. [1] we show that Casimir-force calculations for a finite number of non-overlapping obstacles can be mapped onto quantum mechanical billiard-type problems which are characterized by the scattering of a fictitious point particle off the very same obstacles. With the help of a modified Krein trace formula the genuine/finite part of the Casimir energy is determined as the energy-weighted integral over the log-determinant of the multi-scattering matrix of the analog billiard problem. The formalism is self-regulating and inherently shows that the Casimir energy is governed by the infrared end of the multi-scattering phase shifts or spectrum of the fluctuating field. The calculation is exact and in principle applicable for any separation(s) between the obstacles. In practice, it is more suited for large- to medium-range separations. We report especially about the Casimir energy of a fluctuating massless scalar field between two spheres or a sphere and a plate under Dirichlet and Neumann boundary conditions. But the formalism can easily be extended to any number of spheres and/or planes in three or arbitrary dimensions, with a variety of boundary conditions or non-overlapping potentials/non-ideal reflectors.

References:

[1] A. Wirzba, J. Phys. A: Math. Gen. in print [arXiv:0711.2395].

Remarks on $NN \to NN\pi$ beyond leading order

C. Hanhart, A. Wirzba

In recent years a two-scale expansion was established to study reactions of the type $NN \to NN\pi$ within chiral perturbation theory. Then the diagrams of some subclasses that are invariant under the choice of the pion field no longer appear at the same chiral order. In Ref. [1] we show that the proposed expansion still leads to well defined results. Also the appropriate choice of the heavy baryon propagator is discussed.

References:

[1] C. Hanhart, A. Wirzba, Phys. Lett. B **650**, 354-361 (2007) [arXiv:nucl-th/0703012].

Unitarity constraints for DIS off nuclei: predictions for electron-ion colliders

N.N. Nikolaev, W. Schäfer, B.G. Zakharov (Landau Inst., Moscow), V.R. Zoller (ITEP, Moscow)

Future electron-ion colliders (eIC) will focus on the unitarity properties of deep inelastic scattering (DIS) in the limit of strong nuclear absorption. Strong nuclear shadowing and a large abundance of coherent diffraction are the most striking consequences of unitarity, and here we report quantitative predictions for these effects in the kinematical range of the planned eIC.

The results are published in Ref. [1].

References:

[1] N. N. Nikolaev, W. Schafer, B. G. Zakharov and V. R. Zoller, JETP Lett. **84** (2007) 537

3 Accelerator Division

Prototype of the High Voltage Section for the 2 MeV Electron Cooler at COSY

J. Dietrich, V. V. Parkhomchuk[1]

A 2 MeV electron cooling system for COSY-Juelich is proposed to further boost the luminosity even with strong heating effects of high-density internal targets [1]. In addition the 2 MeV electron cooler for COSY is intended to test some new features of the high energy electron cooler for HESR at FAIR/GSI. The design of the 2 MeV electron cooler will be accomplished in cooperation with the Budker Institute of Nuclear Physics in Novosibirsk, Russia.
The basic parameters and requirements are listed in Table1.

Table 1: Basic Parameters and Requirements.

COSY 2 MeV Electron Cooler	Parameter
Energy Range	0.025 ... 2 MeV
High Voltage Stability	$< 10^{-4}$
Electron Current	0.1 ... 3 A
Electron Beam Diameter	10 ... 30 mm
Cooling Length	3 m
Toroid Radius	1.5 m
Variable Magnetic Field (cooling section solenoid)	0.5 ... 2 kG
Vacuum at Cooler	10^{-8} ... 10^{-9} mbar
Available Overall Length	7 m
Maximum Height	7 m
COSY Beam Axis above Ground	1.8 m

The proposed electron cooler consists of a high voltage vessel with electrostatic acceleration and deceleration columns, two bending toroids and cooling drift section. The basic features of the design are i) the longitudinal magnet field from the electron gun to the collector, in which the electron beam is embedded, ii) the collector and electron gun placed at the common high voltage terminal and iii) the power for magnet field coils at accelerating and decelerating column is generated by turbines. The gas flux which drives the turbines is also used for cooling the magnetic coils and for keeping the temperature inside the vessel constant. A prototyp of the high voltage section, consisting of a gas turbine, magnetic coils and high voltage generator with electronics is completed and first tests are performed.

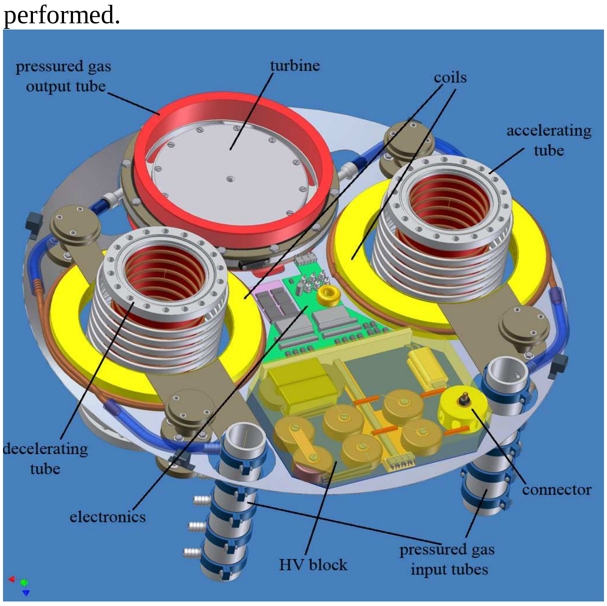

Fig. 1: Layout of the high voltage section with tubes.

The high voltage sections for the 2 MeV electron cooler (Fig. 1) contains: high voltage power supply, coils for the magnet field along acceleration and deceleration columns, power source and control units for measurement and control of section parameters. Each section has two high voltage power units on 30 kV. Using of two power units allow to decrease the voltage for insulation from 60 kV to 30 kV. The whole 2 MV column consists of 34 sections. The electric field between the sections will be 30 kV/cm. Pressured SF_6 gas will be used for protection from sparking.

Fig. 2: Gas turbine of the high voltage section.

The maximal power produced by the generator amounts 685 W. The electricity production efficiency of the turbine is estimated to 17%. The temperarture of the exhaust pressurized gas (air) is 4-5 degrees less the initial temperature and will be used for cooling the electronic elements inside the sections.

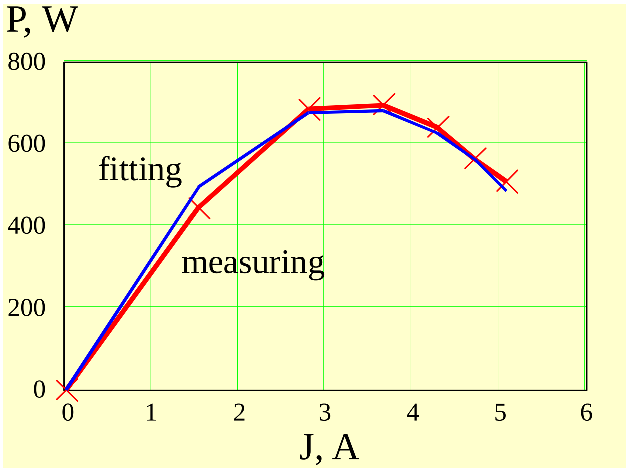

Fig. 3: Generator power versus loading current.

References:

[1] V. V. Parkhomchuk, Electron Cooling for COSY, Internal Report (2005).
[2] V. V. Parkhomchuk et al., Electron Cooling for COSY, Prototyp of the High Voltage Section, Internal Report (2007).

[1] BINP, Novosibirsk

Beam Profile Measurements with a Beam Induced Fluorescence Monitor

C. Boehme[1], A.H. Botha[2], J.L. Conradie[2], J. Dietrich[3], T.Weis[1]

Several kinds of diagnostic devices based on the registration of products produced by the interaction between the beam particles and the residual gas atoms are under development or already in practical use [1]. Usually these devices are used as beam profile monitors, which register electrons and / or ions as secondary particles. Some attempts have been already accomplished which utilize the light emitted by beam excited residual gas atoms. In our case the light emitted by the residual gas atoms is focused using a glass lens onto a position sensitive photomultiplier (PMT) array (see Fig. 1). In the presented setup a Hamamatsu PMT array has been used (32 pixels, 7 x 0.8 mm^2 size each, 1 mm pitch, sensitive between 200 nm and 600 nm with the maximum between 300 nm and 450 nm) perpendicular to the beam axis. From the signals the beam position as well as the profile can be evaluated in one dimension.

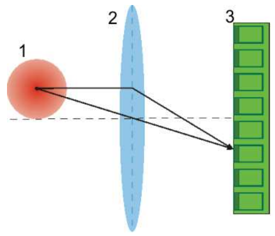

Fig. 1: Measurement principle (not to scale): The light from the beam (1) is focused with a glass lens (2) onto the multichannel photomultiplier (3).

The latest experiments were performed at iThemba LABS, Somerset West, South Africa. The fluorescence beam monitor was installed at the SPC1 injector cyclotron beam transfer line. Here a 3.14 MeV proton beam with typical beam currents of several 100 μA has been available at residual gas pressures of approximately 10^{-5} mbar. The 32 individual PMT pixels were divided into groups of respectively 2 neighboring pixels combined. Seven of these groups, located at the center of the array, were used for readout. One additional group located at the side was shielded from visible light by a thin black paper in order to measure the background. A standard capacitive beam position monitor (BPM) has been available a couple of cm downstream the PMT device. In a first series of experiments the beam position at the location of the PMT-monitor was varied using an upstream steering magnet. The displacement of the beam center was simultaneously measured with our optical beam profile monitor and the BPM. The displacement as a function of the steering magnet strength is shown in Fig. 2. The location of the BPM further downstream gives a steeper slope of the curve. Taking the longitudinal BPM monitor offset into account, the results of both monitors are in good agreement. In a second series of experiments a quadrupole magnet located in front of the monitor was used to vary the beam width. The σ-beam widths determined from the beam profile versus quadrupole strength is shown in Fig. 3 for two slightly different beam transfer line settings. For small variations in the neighborhood of the horizontal focus the beam widths show the expected behavior. Deviations seen for larger beam diameters are expected to be caused by partial beam loss or beam optics nonlinearities. In addition the beam profile and the light production has been measured at different pressures between 10^{-5} and $5 \cdot 10^{-4}$ mbar. The cross section for optical emission within the sensitivity of the PMT has been calculated. From the experiments we deduced cross sections which are apparently almost one (1.35 GeV / COSY) or even two orders of magnitude (3.1 MeV / iThemba) larger than expected from [2], the reason for the discrepancy is subject to further investigations.

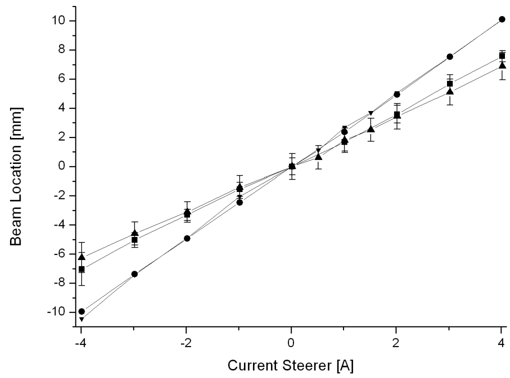

Fig. 2: Beam position versus steerer strength measured with our optical beam profile monitor (▲ and ■) and a BPM (●) located downstream.

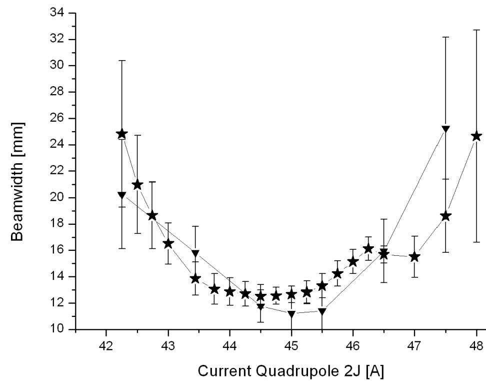

Fig. 3: Horizontal σ-beam widths versus quadrupole strength for a 3.14 MeV proton beam.

References:

[1] J. Dietrich et al., Proceedings of the 8th Int. Topical Meeting on Nuclear Applications and Utilization of Accelerators, ACCAPP'07, Pocatello, USA, July 29 – August 2, 2007.

[2] M.A. Plum et al., Nucl. Instr. Meth. A492 (2002), p.74

[1] Universität Dortmund, [2] iThemba LABS South Africa, [3] Forschungszentrum Jülich

*Work supported by BMBF and NRF, Project-code SUA 06/003 and by the European Community-Research Infrastructure Activity under the FP6 "Structuring the European Research Area" programme (CARE, contract number RII3-CT-2003-506395).

R. Gebel, A.S. Belov, R. Brings, W. Derissen, R. Engels, O. Felden, H. Hadamek, A. Kieven, N. Rotert

Injector operation

In 2007 the injector cyclotron did provide beams for 6590 hours for the accelerator facility COSY. In December 2007 the injector passed 115,171 hours of operation since it started delivering beams as COSY injector in 1989. The time distribution over the years is shown in fig. 1.

The operation of the cyclotron was interrupted for around 300 hours in 2007 due to several failures. The distribution of the failures exceeding 2 hours is depicted in fig. 2. The most common reasons for unavailability of the injector for times were power failures. The winter storm Kyrill caused one black-out. A localized power failure was introduced by flooding of the lowest level of the cyclotron building after a leak of a large water supply tube. Intermediate unavailability, exceeding the start-up time of the main rf system, had been its originate in the rf system with varying reasons. Vacuum leaks at the NMR feeding tube and the septum needed additional attention. The operation of the ion sources showed no major failures in 2007.

Besides serving COSY as injector the cyclotron was successful in providing three irradiations with protons and a first one with deuterons at the internal target station for the Institute for Nuclear Chemistry (INB-4).

Replacement of cyclotron components

The cyclotron is in use since the mid 60s of the last century. Most of the systems were refurbished between 1980 and 1989. Since 2004 several magnet power supplies have been replaced. The main magnet, the compensated channel as well as the correcting coils are operated with new power converters. In summer 2007 the transfer beam line between the sources and the injection into the cyclotron has been equipped with new power supplies.

During the summer shutdown 2006 the damages at the linear tuning element of the central tuner became obvious. Severe burn-out, scratches and broken contact springs made it necessary to overhaul the linear tuner completely. After refurbishment of the parts the operation has been continued delayed and with reduced working range for the frequency.

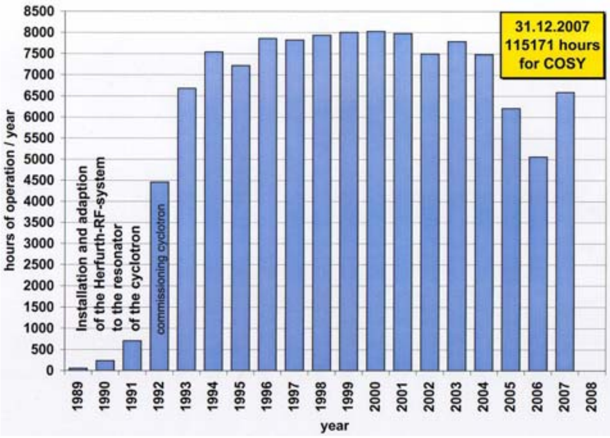

Fig. 1: Operation of the Cyclotron as the injector for COSY. At the end of 2007 the total operating time of the cyclotron rf reached 223,800 hours.

The needed operational modes for COSY have been realized without problems. In summer 2007 the complete functionality has been recovered by an exchange of the support structure of the tuning element. The water cooled condensators with the motor driven positioning unit has been replaced successfully already by a new construction in 2006. The new construction is depicted in fig. 3.

New installations at the ion sources

Until now it is only possible to determine the polarization by using the in-beam polarimeter in the transfer beam line from the cyclotron to the synchrotron based on the elastic scattering of H^- or D^- beams on a carbon target. For optimizing and tuning of the polarized beams the cyclotron had to be used and COSY operation is delayed. The Lambshift polarimeter (LSP) is connected to the low energy beam line. It consists of a stripping target, an electrostatic deflector, a Cesium charge exchange cell, a spin filter and a photon detector. In order to match the beam to the acceptance of the set-up einzel-lenses and steering devices have been integrated in the set-up. The LSP part is a copy of the routinely used ANKE polarimeter.

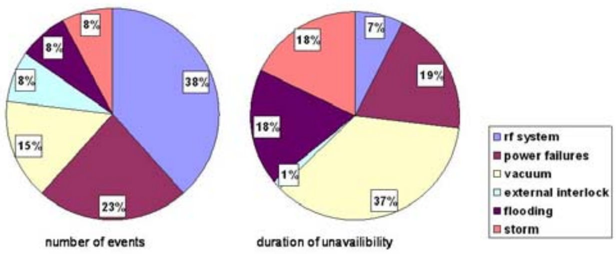

Fig. 2: The failure distribution of 13 events in 2007

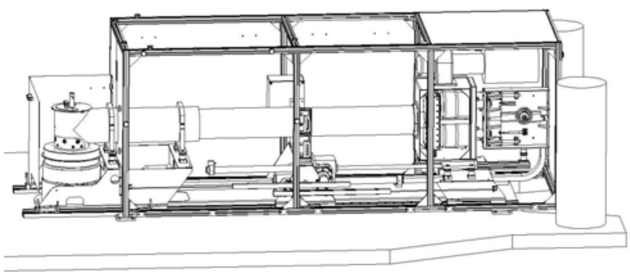

Fig. 3: The new construction for the matching hardware on the top of the cyclotron magnet's yoke. The air line has been improved in summer 2006.

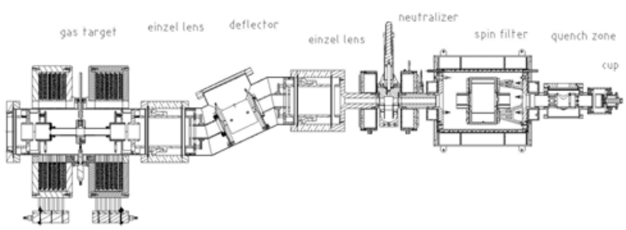

Fig. 4: The new Lambshift polarimeter for the polarized ion source with its main components.

Modernizing the User Software of QBL Vacuum System

F. Jordan[1], B. Dahmen[2], O. Felden[2], J.-D. Witt[2], H. Zens[2], N Bongers[2]

After nearly 15 years of operation the handling of the ion source beam line vacuum system needed an upgrade. The discontinued control panel (Fig.1 COROS System, Siemens™) was no longer sufficient in operation.

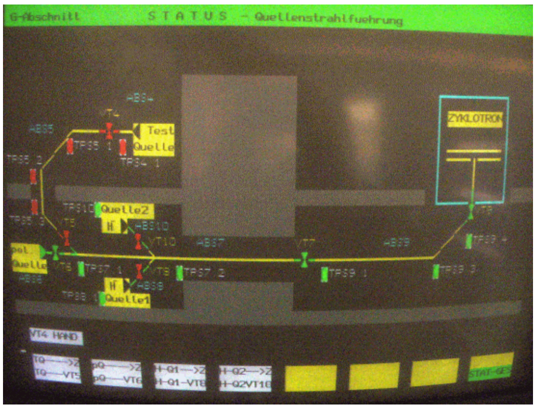

Fig. 1: Old Control Panel

Certainly a very short shutdown time is mandatory. The replacement shall be as little as possible. The wiring will not be changed to avoid errors and to save time.

The design goals are: A modern development system will be used (STEP 7, Siemens™) [1]. The handling of the components is changed to WinCC (Siemens™) [2]. A new hardware version based on S5-hardware is needed and a STEP7 software compatibility is required. A made-to-measure product is the X5/X7 CPU-board of INAT™. The X5/X7 [3] is a high performance CPU for S5 with a TCP/IP interface. The board is compatible to the CPU 948 (S5) and to the CPU 416 (S7). In synchronous mode the S7 and S5 Program run concurrently. And, easy migration from STEP5 to STEP7 is possible.

The system was upgraded in four steps. In step one the old CPU 928 was changed to the X5/X7 CPU. The old STEP5 software runs on the new hardware after telephone support from INAT™. Operating the vacuum system is still possible. Then one vacuum pumping station was deactivated in STEP5. A new code was generated in STEP7 and tested. The connection from the development system to the target by TCP/IP is fast and reliable. In the third step the tested STEP7 code is applied for every other pumping station after deactivating the corresponding STEP5 code.
Finally, in the fourth step all other components have been deactivated on the STEP5 side and integrated in the STEP7 software.
In parallel the new graphical user interface (GUI) was developed in WinCC (Fig.2). Every new integrated component was immediately tested.
Two different operating modes are implemented: (HAND) assembly mode and (AUTO) operating mode. Different paths of the beam can be selected and displayed. More than one path may be chosen at the same time for testing purposes.
The new GUI is integrated in the existing main WinCC-HMI of the beam sources.

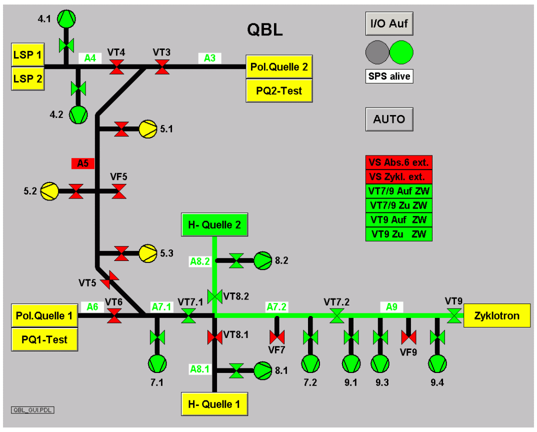

Fig. 2: The new graphical user interface (GUI

References:

[1] Programmieren mit STEP 7 V5.3
Handbuch Ausgabe 01/2004

[2] WinCC V6.0 Basis-Dokumentation
Handbuch Ausgabe 04/03

[3] Benutzerhandbuch INAT-CPU Systeme (03/2006)

[1] Zentralabteilung Technologie

[2] Institut für Kernphysik

Radiation Protection

H. Borsch, O. Felden, J. Göbbels

Driving an accelerator causes activation of materials while loosing high energetic particles. What kind of activation takes place and what strength will be reached depends on the used particles as well as the energy the particles will have. Beside the activation of insertions like magnets or beam pipes made e.g. from steel activation also occurs in the air inside the tunnel. The main radioactive components produced from air are N13, O15 and N16 [1]. The production processes as well as the threshold energies and half-lifetimes are summarized in table 1.

N14 (n,2n) N13	11,4 MeV	9,96 min
N14 (γ,n) N13	10,6 MeV	9,96 min
O16 (n,p) N16	10,2 MeV	7,13 sec
O16 (n,2n) O15	16,7 MeV	2,03 min
O16 (γ,n) O15	15,7 MeV	2,03 min

Tab. 1: The reaction processes as well as the production thresholds and half-lifetimes of the produced radioactive isotopes are listed. (More radioactive isotopes are produced but because of the small concentration they are paid less interest here.)

One of the tasks of the radiation protection group is to ensure that prescriptive limits demanded by the authorities will not be exceeded during the operation of COSY. Therefore the group operates a LB101 / LB5310 Data acquisition system from Berthold, measuring the activation inside the air coming from the air conditioning system of the accelerator.

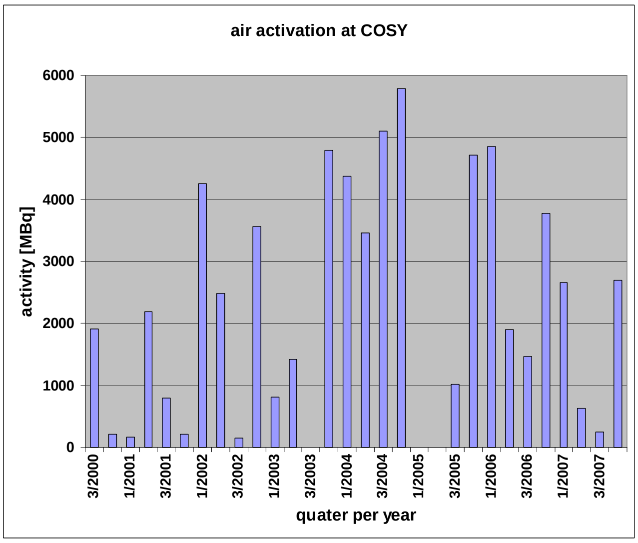

Fig. 1: The activity per quarter of the year since 2/2000 is given.

The recorded data are printed on a daily basis and are reported to the authorities each quarter of the year. Figure 1 gives the reported activation per trimester starting with the second half of 2000. It shows that the numbers are far beyond the limits of 15GBq/trimester which are the maximum numbers given by the authorities.

In 2003 the number of accelerated particles in COSY was improved which on the other hand directly led to an increased air activation as can be seen in figure 1. In 2005 the installation of the WASA Detector system inside the COSY tunnel was started.

Therefore the maintenance scheme was changed from 1 week 5 to 6 times a year to long lasting periods of several weeks during the summer. By that, the reduced activation during this maintenance times is not spread to all data but now to a single trimester per year where it can be found in 2005 as well as in 2006 and 2007. Figure 2 gives the run plan of 2003 while figure 3 presents the run plan for the year 2005 in order to display the different maintenance schemes as described before.

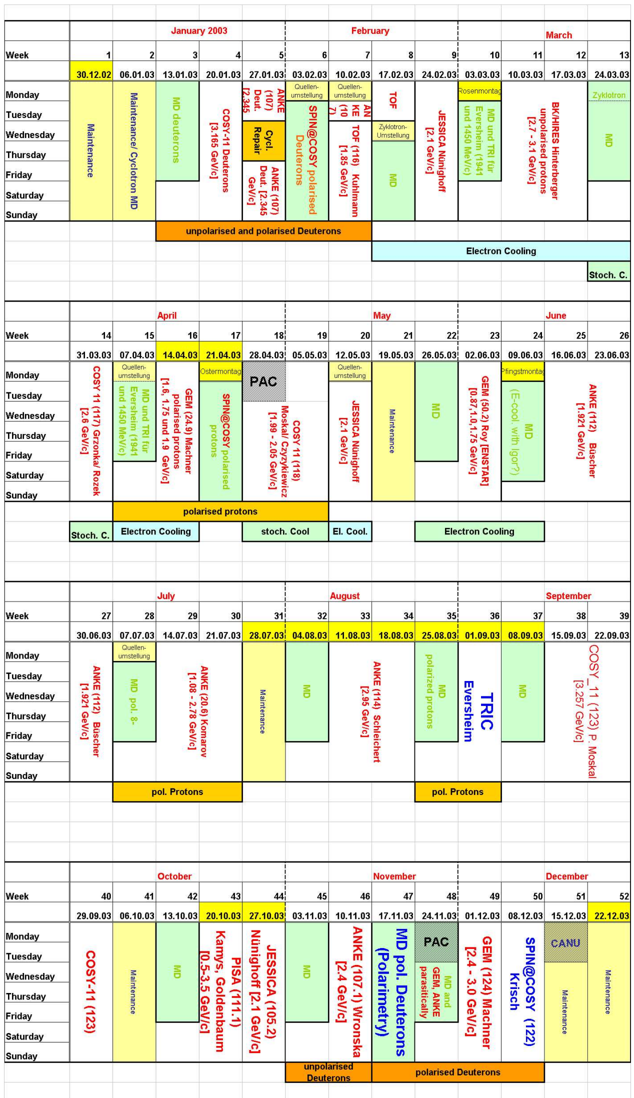

Fig. 2: Run plan of 2003. Maintaining periods are marked in yellow.

The maintenance periods are coloured in yellow. The WASA group started their experimental programs immediately after the new detector was fully installed in the year 2006.

In comparison to the measured particle numbers in 2004 the overall number of particles which were accelerated in COSY was smaller as usual and led to a decreasing air activation in 2006 and 2007. The reduced number of accelerated particles was due to instabilities caused by various experiments or the COSY machine itself, beam requests for smaller energies, polarized particles or due to a lack of the data acquisition capabilities.

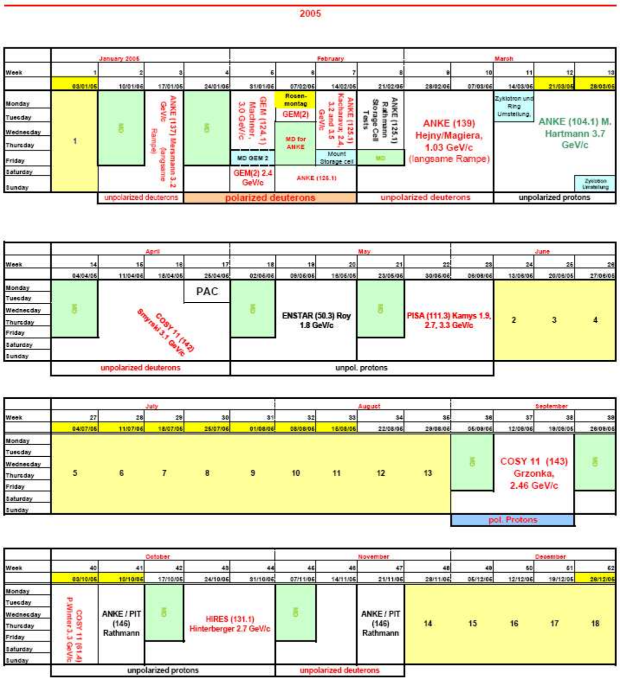

Fig. 3: Run plan 2005, the maintaining scheme is quite different to 2003 (figure 2).

In order to get a better understanding whether air activation is only related to the number of accelerated particles as described before, we also cabled the data acquisition system to the Control and Personal Safety System (PSA) [2]. As a result we now have online data access to monitor that air activation does not spread in unexpected directions. Additionally, the system offers the possibility to examine other reasons for an activation process such as those caused by the particles' energy or the ramp-rate of the machine. Furthermore, the new PSA facilitates a redundancy check with the reporting system that is still running from the beginning of operation of COSY.

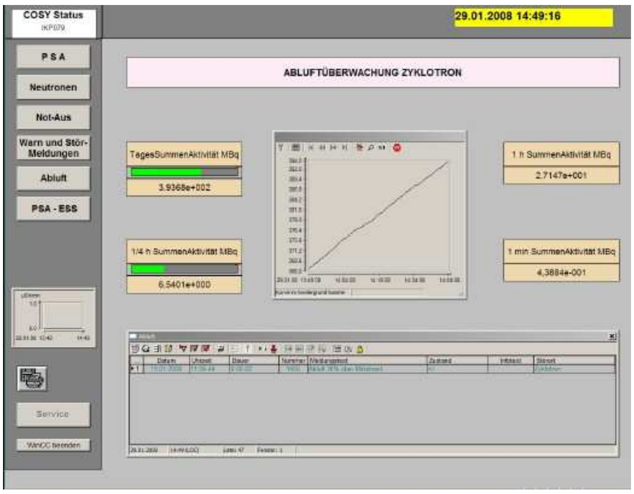

Fig. 4: On a clearly arranged window of the Control and safety system of COSY all necessary data of the air activation survey system are displayed. The picture shows the data from the cyclotron JULIC.

Figure 4 shows the information window on the Control and safety system in the COSY control room. All necessary data like alarm messages, measured activity since midnight or activation measures of the last hour are displayed on one clearly arranged window.

In case of any failure the control system will immediately inform the operator as well as the radiation protection group and displays what kind of failure happened. This is common to all alarm messages in the control system [3].

References:

[1] Strahlenschutz an Beschleunigern, K.Ewen, B.G.Teubner Verlag Stuttgart 1985
[2] Radiation Protection, Annual report 2005
[3] Status Survey System at COSY, Annual Report 2002

4 Preparations for FAIR

Emittance-dominated Long Bunches in Dual Harmonic RF System

S. An[1], K. Bongardt, R. Maier, J.Y. Tang[2], T.J. Zhang

The storage of long bunches for long time intervals needs flattened stationary buckets with a large bucket height. The motion of the initially mismatched beam has been studied for single & dual harmonic RF systems. The RF amplitude is determined to be r.m.s wise matched. The bucket height of the single harmonic system is too small even for shorter bunch with only 20 % increased energy spread. Halo formation and debunching are seen after a few synchrotron periods for single particles with large amplitude [1].

The single particle motion within a stationary bucket formed by the dual harmonic RF system is given in the smooth approximation by

$$\frac{d^2\phi}{dt^2} + \omega_{s0}^2 E(\phi) = 0 \qquad (1)$$

with $\omega_{s0}^2 = \dfrac{qV_0\eta}{2\pi\beta^2\gamma m_0 c^2}\omega_0^2$. The waveform $E(\phi)$ is defined by

$$E(\phi) = \sin(\phi) - d\sin(2\phi) \qquad (2)$$

where ω_0 is the angular revolution frequency and V_0 is the amplitude of the RF voltage per turn. $\phi = z/R$ is the phase value relative to the position of the bunch center.

1D tracking results by ORBIT are shown in figure 1 for a 1 GeV bunch in the 574 m long HESR with an imaginary γ_t value of 6.5i. Either the single or dual harmonic RF system with d = 0 or d = 0.31 is used. The Gaussian bunch has the length of 400 m or the bunching factor B = 0.7. The r.m.s phase width is 0.78 rad and the r.m.s energy spread amounts to 0.6 MeV.

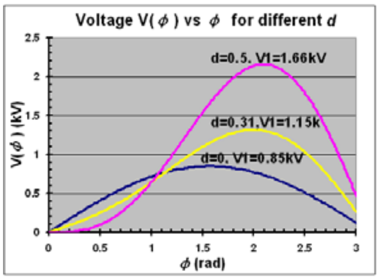

Fig. 1a: RF voltages for different d values.

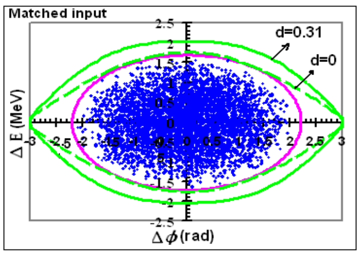

Fig 1b: Matched Gaussian input & RF acceptances

Resulting RF voltages are shown in figure 1a for different d values, determined from the r.m.s wise matching. The single harmonic RF system means d = 0. For small phase values all particles oscillate with same frequency. The dual harmonic RF system reduces the linear voltage by a factor of 1-2d and leads to flattened buckets with increased bucket height, see figure 1b.

Figure 2 shows the r.m.s phase oscillation for the single and dual harmonic systems demonstrating the r.m.s matching in both cases. Injecting a shorter bunch with 20 % increased energy spread but with unchanged r.m.s emittance excites the coherent quadrupole oscillations.

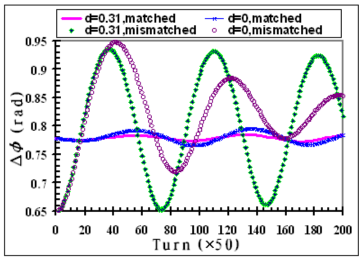

Fig 2: R.m.s phase oscillations, single & dual harmonics

The single particle motion for any kind of an external voltage $V_{rf}(z/R)$ and arbitrary line density $\lambda(z)$ is given by

$$z'' + \alpha\left[V_{rf}\left(\frac{z}{R}\right) + V_{SC}(z)\right] = 0 \qquad (3)$$

$$\alpha = \frac{q\omega_0^2\eta R}{2\pi\gamma m_0 c^2\beta^4 c^2} \qquad (4)$$

$$V_{SC}(z) = Nq\beta cR\left(\frac{gZ_0}{2\beta\gamma^2}\right)\frac{\partial\lambda(z)}{\partial z} \qquad (5)$$

N is the particle number, $Z_0 = 377\Omega$ is the free space impedance, the geometry factor is g = 1+2ln(b/a). a is 2*average r.m.s beam radius, b is the average pipe radius.

Below transition, the matched r.m.s bunch length for a given particle number N is kept unchanged by increasing the external RF voltage by a factor R(N). R(N) < 2 describes emittance-dominated bunches whereas R(N) > 2 describes space charge dominated bunches [1].

Figure 3 show an 1D ORBIT result for a mismatched bunch in a single harmonic RF system. The matched voltage is twice the 0.85kV value of figure 1a enlarged to compensate the SC induced voltage. Coherent quadrupole oscillations will be excited if the RF voltage is not increased for short bunches. However, debunching occurs after 10^4 turns, see figure 3. Results for adding resistive impedances are shown in [2]

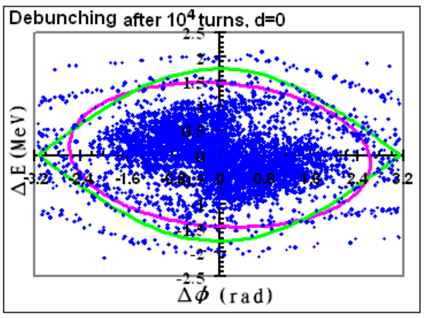

Fig. 3: Phase space distribution &full RF acceptance

References:

[1] S. An et al., Chinese Physics C , 2008, 32(1)p. 60 :
[2] S. An et al., Collective Effects for Long Bunches in Dual Harmonic RF systems, this publication

[1]CIAE Beijing
[2]IHEP Beijing

Collective Effects for Long Bunches in Dual Harmonic RF Systems

S. An[1], K. Bongardt, R. Maier, J.Y. Tang[2], T.J. Zhang

The storage of long bunches for large time intervals needs flattened stationary buckets with a large bucket height. Collective effects from the space charge and resistive impedance are studied by looking at the incoherent particle motion for matched and mismatched bunches. Increasing the RF amplitude with particle number provides r.m.s wise matching for modest intensities. The incoherent motion of large amplitude particles depends on the details of the RF system, resulting in different bucket heights. For modest intensities an irregular single particle motion is not associated with a coherent dipole instability.

For the stationary phase space distribution of the Hofmann-Pedersen approach and for the dual harmonic RF system the obtained stability limits are too low for realistic input distributions. Small resistive impedances lead to coherent oscillations around the equilibrium phase value as energy loss due to a resistive impedance is compensated by the energy gain of the RF system.

The energy change of a test particle within a vacuum chamber traveling behind a bunch is described either by time dependent wake fields or by frequency dependent longitudinal impedances linked via Fourier transformation. For a single bunch the retarding voltage $V_r(\phi)$ in time domain is given by a continuous Fourier transformation

$$V_r(\phi) = -\frac{1}{2\pi}\int_{-\infty}^{\infty} \operatorname{Im} Z_{\|}(\omega)\cdot\sin(\omega\phi) + \operatorname{Re} Z_{\|}(\omega)\cdot\cos(\omega\phi))\cdot I(\omega)d\omega \qquad (1)$$

where $Z_{\|}(\omega)$ is the complex longitudinal impedance and $I(\omega)$ is the Fourier component of the current distribution.

A single bunch with a symmetric line density $\lambda(\phi)$ in a circular ring of circumference $C = 2\pi R$ leads to the retarding voltage $V_r(\phi)$ given by the discrete Fourier transformation

$$V_r(\phi) = -(Nq\beta c)/R\cdot\sum \lambda_n[\sin(n\phi)\cdot\operatorname{Im} Z(n) + \cos(n\phi)\cdot\operatorname{Re} Z(n)] \qquad n\geq 1. \qquad (2)$$

The voltage $V_r(\phi)$ replaces $V_{SC}(\phi)$ in the single particle equation (3) of [2]. A symmetric line density and imaginary impedances mean asymmetric retarding voltages and no net energy loss of the bunch. Resistive impedances however lead to symmetric retarding voltages and therefore to net energy loss of the bunch.

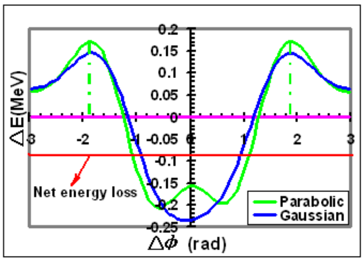

Fig. 1: Energy change of individual particles

Figure 1 shows the energy change of test particles for either a parabolic or a Gaussian line density obtained from 1D tracking with ORBIT with $Z_{\|}/n$ = 50 Ω for n = 1,4. A 1 GeV bunch is assumed in the 574 m long HESR with an imaginary γ_t value of 6.5i. The bunches have an identical r.m.s phase value of 0.78 rad but the parabolic line density is limited in phase to $\sqrt{5}$ × r.m.s value [2].

For N = 10^{11} a resistive impedance $Z_{\|}$ = 5 Ω causes an energy change -13meV*cos(ϕ)/turn of the particles only at n = 1. The greatest loss for particles occurs at the bunch center. Energy gain occurs for the outermost particles with phase values ϕ > π/2. The parasitic loss is 7 meV/turn increasing to 30 meV/turn by $Z_{\|}/n$ = 5 Ω, n = 1,4. Much larger resistive impedances are quoted for the SNS [3].

Coherent dipole oscillations are shown in figure 2 for a matched elliptical input but with a resistive impedance of $Z_{\|}/n$ = 50 Ω for n =1,4. Small resistive impedances in addition to a large SC impedance of 500 Ω, high harmonics, lead to coherent dipole oscillation around equilibrium values, i.e. about 50 % of the first maximal value. Intensity limits are dependent on the RF system. Blue curve shows undamped dipole oscillation as $Z_{\|}/n$ = 0.

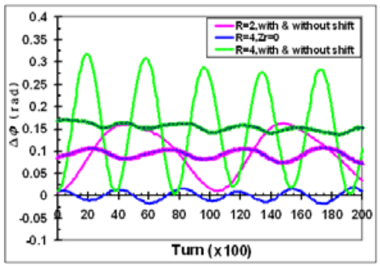

Fig. 2: Dipole oscillations, single & dual harmonics

Pink curves are for the dual harmonic system, d = 0.31 [2]. The matched voltage due to SC is twice the value of fig. 1a in ref. [2]. The intensity is a factor of 2 above the stability limit for a self-consistent Hofmann-Pedersen distribution [1] but a factor of 4 above the Keil-Schnell limit for short bunches [4]. Phase space distributions are shown in figure 3 for shorter elliptical bunches injected with 20 % increased energy spread in either a dual or single harmonic system. The bunch is initially shifted by –0.4 MeV. The matched voltage due to SC is twice the value of fig. 1a in ref. [2] with $Z_{\|}/n$ = 50 Ω for n = 1,4. For d = 0.31 no debunching & filamentation occur due to the large acceptance.

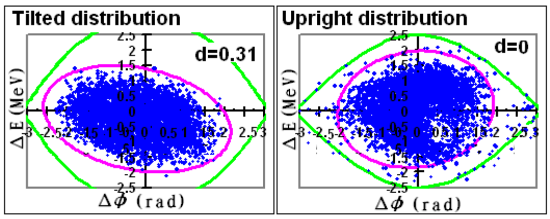

Fig. 3: Distributions after 2×10^4 turns & full acceptances

References:

[1] S. An et al., Chinese Physics C ,2008, 32(2) p. 139
[2] S. An et al., Collective Effects for Long Bunches in Dual Harmonic RF systems, this publication
[3] H. Hahn et al, Longitudinal Coupling Impedances of SNS cavity, BNL/SNS technical note 117, Oct. 2002
[4] HESR Technical Report, Feb. 2005

[1]CIAE Beijing
[2]IHEP Beijing

Ionisation Beam Profile Monitor for FAIR-Tests at COSY

C.Boehme[1], J. Dietrich[2], T. Giacomini[3], P. Forck[3], D. Liakin[4]

Versatile information of the beam parameters can be achieved by monitoring the beam profile of the circulating beam during injection, acceleration and cooling. A non-destructive Ionisation Beam Profile Monitor IPM is under construction in collaboration between IKP, GSI and ITEP Moscow for this purpose [1]. It aims for a 0.1 mm spatial resolution as well as a fast turn-by-turn readout with reduced spatial resolution. The device is based on the detection of the ionization products fro the beam interaction with the residual gas. The actual IPM acts as a prototype for the installation at all FAIR storage rings. COSY offers the best testing possibilities.

In December 2006 the vacuum components of the IPM were assembled and installed at COSY, see Fig. 1 to 3. It comprises of the electric field generation box, the MCP phosphor support, the calibration unit and all required electrical feed-through and supports. It is a quite complex system, but major improvements compared to precursor arrangement at GSI have been achieved resulting in a very compact installation. This compactness is required because of limited insertion space at the FAIR storage rings. But some problems occurred and delayed the installation: A vacuum feed-through delivered by a company did not satisfy the specified (and guaranteed) vacuum conditions and calls for long lasting vacuum tests to determine this unexpected source. After passing the vacuum test successfully, the general functionality of the IPM was demonstrated with a beam based measurement, as shown in Fig. 4. But due to some expected sparking between the MCP and the Phosphor screen it was removed for detailed offline tests to enable a save operation. All equipment is now installed in a dedicated dual use vacuum chamber, designed and built by FZJ, allowing installation in ESR as well as in COSY(Fig.3) and is available for beam based performance investigations at COSY.

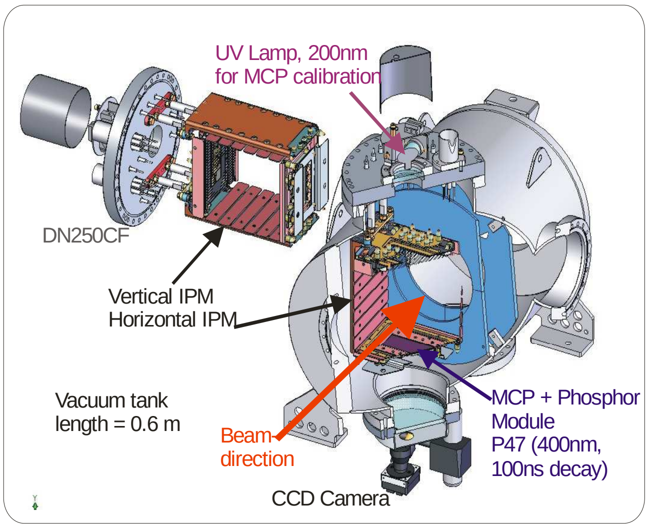

Fig. 1: Layout of the new IPM

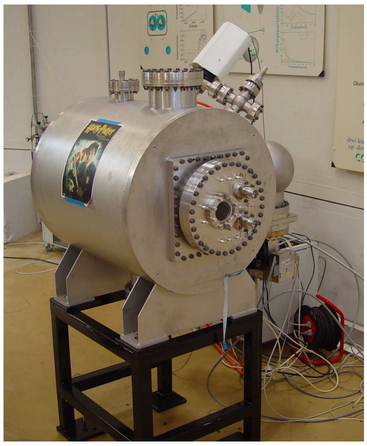

Fig. 2: IPM-Test chamber with installed one IPM

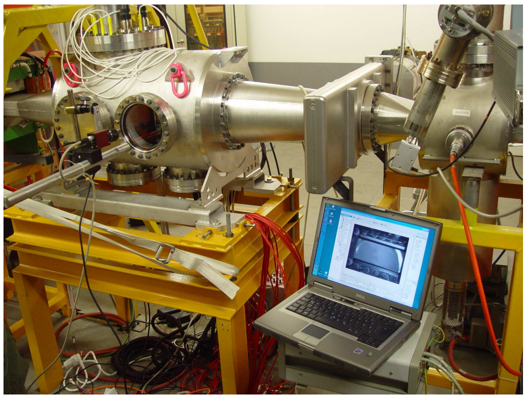

Fig. 3: IPM-chamber installed at COSY with two IPM

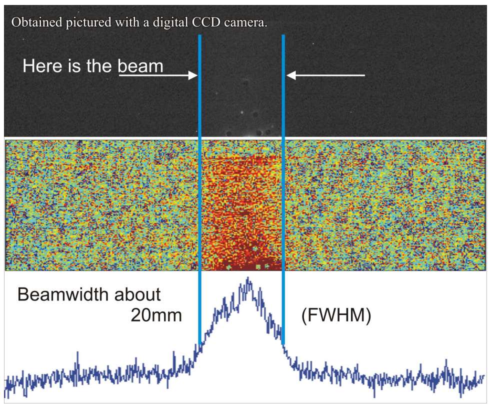

Fig. 4: Beam test at COSY with a proton beam. The original image is shown on top. To achieve a higher contrast, the image is processed (middle) and the projection, which reflects the beam size, is calculated (bottom)

References:

[1] T. Giacomini, P. Forck, J. Dietrich, D. Liakin, C. Böhme: *The Improved IPM Design for GSI Under Test Conditions*, Conference Proceeding DIPAC2007, Venice 2007.

[1] Universität Dortmund, [2] Forschungszentrum Jülich
[3] GSI Darmstadt, [4] ITEP, Moscow

Supported by the EU's FP6 under DIRAC-Phase1, contract number 515876

Stochastic Momentum Cooling for the HESR with Normal-Conducting Magnets

H. Stockhorst

Numerical and analytical simulations of stochastic filter cooling to provide the beam quality requirements in the HESR at FAIR [1] with a normal-conducting (NC) ring lattice [2] have been carried out. Using a target thickness of $4 \cdot 10^{15}$ *atoms* cm^{-2} the high luminosity mode (HL) is attained with 10^{11} antiprotons yielding a luminosity of $2 \cdot 10^{32}\ cm^{-2}\ s^{-1}$. The HL-mode has to be prepared in the whole energy range and beam cooling is needed to particularly prevent beam heating by the beam target interaction. Much higher requirements are necessary in the high resolution mode (HR) with 10^{10} antiprotons. Here, the same target thickness yields a luminosity of $2 \cdot 10^{31}\ cm^{-2}\ s^{-1}$. This mode is requested up to *8.9 GeV/c* with a rms-relative momentum spread smaller than $4 \cdot 10^{-5}$. The new NC-ring lattice offers the possibility to vary the value of transition gamma between $6 \le \gamma_{tr} \le 30$ at all energies while the horizontal and vertical tune can be kept at *7.6*. Additionally the dispersion and its derivative with arc length can be adjusted to zero [2]. A simple formula provides a first overview on possible beam momentum equilibrium values for *N* stored anti-protons with revolution frequency f_0

$$\delta_{eq,rms} = \frac{4}{5}\left(\frac{3}{16}\cdot\frac{N\,f_0^2}{|\eta| W f_C}\delta_{loss}^2\right)^{1/3} . \qquad (1)$$

The bandwidth *W* of the stochastic cooling system is centered at frequency f_C. The mean square relative momentum deviation per target traversal, δ_{loss}^2, describing the beam-target interaction is directly proportional to the target area density [3]. The formula assumes that the mean energy loss in the target is compensated e.g. with a barrier bucket cavity [4] and that there is no mixing from pickup to kicker [5]. The frequency slip factor $\eta = 1/\gamma^2 - 1/\gamma_{tr}^2$ in the NC-lattice is smaller as compared to the super-conducting lattice version with $\gamma_{tr} = 6i$ [1]. The advantage is less mixing from pickup to kicker that increases the cooling time as well as equilibrium values. Pickup and kicker devices can now be located in the long straight sections. On the other hand the beam momentum spread is increased if the cooling bandwidth is kept fixed, eq. (1). To circumvent larger equilibrium values in the NC lattice the cooling band *(2 – 4) GHz* [5] should be increased to *(2 – 6) GHz*. Figure 1 shows the range of values for the frequency slip factor if transition gamma is varied between $6 \le \gamma_{tr} \le 30$.

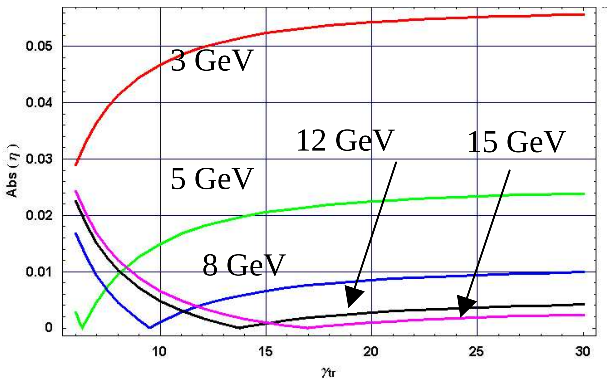

Fig. 1: Absolute value of the frequency slip factor as a function of possible transition gamma values.

Equation 1 can then be used to deduce the necessary frequency slip factor for a given equilibrium relative momentum spread. Figure 2 shows that an equilibrium relative momentum spread $\delta_{rms} = 5.4 \cdot 10^{-5}$ can be achieved in the HR-mode for a *(2-6) GHz* cooling system if the lattice is tuned to $\gamma_{tr} = 6$. The equilibrium value increases to $\delta_{rms} = 7.5 \cdot 10^{-5}$ if the upper frequency limit of the cooling system is restricted to *4 GHz*.

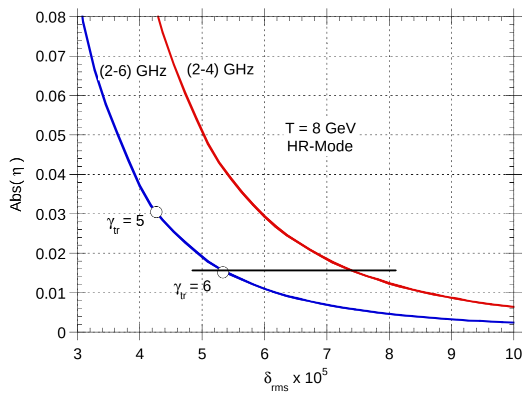

Fig. 2: Necessary $|\eta|$ for a given rel. momentum spread in the HR-mode at *T = 8 GeV* for *(2-4) GHz* and *(2-6) GHz*. The smallest value of γ_{tr} is 6. Larger values lead to smaller values of $|\eta|$ which increases the equilibrium value.

In table 1 and 2 the momentum cooling performance resulting from numerical solutions of the Fokker-Planck equation for momentum cooling is summarized [5]. The table include also the cooling down time t_{eq} to equilibrium and the required electronic gain G_A. The Schottky particle power and thermal noise power after filtering at the kicker entrance amounts up to *10 W* each.

Table 1: *High Resolution Mode*

T [GeV]	γ_{tr}	$\delta_{rms} \cdot 10^5$	t_{eq} *[s]*	G_A *[dB]*
3	13	5.4	60	109
8	6	5.4	150	116
15	6	3.9	150	119

Table 2: *High Luminosity Mode*

T [GeV]	γ_{tr}	$\delta_{rms} \cdot 10^5$	t_{eq} *[s]*	G_A *[dB]*
3	6	13.6	600	95
8	6	11.7	600	103
15	6	8.8	600	105

References:

[1] HESR, "Baseline Technical Report", http://www.fz-juelich.de/ikp/hesr/2-11-HESR.pdf

[2] B. Lorentz et al., to be published

[3] F. Hinterberger, "Beam-Target Interaction and Intrabeam Scattering in the HESR Ring", 2006, Jül-4206, ISSN 0944-2952

[4] R. Stassen et al., this contribution

[5] H. Stockhorst et al., "Stochastic Cooling for the HESR at FAIR", COOL 07, Bad Kreuznach, Germany, 10-14 Sept. 2007

A Micro Vertex Detector for the $\overline{\mathrm{P}}$ANDA experiment at FAIR

F. Hügging*, M.C. Mertens, J. Ritman and T. Stockmanns

One major component of the approved **F**acility for **A**ntiproton and **I**on **R**esearch (FAIR) at the GSI in Darmstadt is the **H**igh **E**nergy **S**torage **R**ing (HESR) with the "Anti**P**roton **AN**nihilations at **DA**rmstadt" - experiment ($\overline{\mathrm{P}}$ANDA). The HESR will provide a phase space cooled antiproton beam of unsurpassed quality, precision and intensity. A momentum range up to 15 GeV/c together with an average interaction rate of 10 MHz will allow the detailed study of a wide variety of topics, like the structure of hadrons in the charmonium mass range, the spectroscopy of double hyper nuclei and electromagnetic processes. To serve this wide physics program the general purpose experiment PANDA is currently planned.

An ongoing activity of the IKP for the $\overline{\mathrm{P}}$ANDA detector is focused on the design of the Micro Vertex Detector (MVD). The MVD plays a key role in the PANDA experiment to identify open charm and strangeness by detecting secondary decays of particles displaced from the primary interaction point. These decay lengths range from a few 100 μm for charmed mesons and baryons up to several cm for strange hadrons.

One of the most important issues for the design of the pixel part of the MVD is the data handling and transfer. In order to allow an open charm trigger based on secondary vertex tagging a quasi online data processing in the DAQ chain is envisaged. This requires a complete data transfer from the MVD to a certain DAQ stage and therefore the MVD itself must be readout without any trigger. Based on extensive hit rate simulations a VHDL model of the readout scheme of the pixel front-end electronics have been developed and tested.

The total data rate in the MVD for $\bar{p}p$ reactions at 15 GeV/c is 550 MHits/s which are strongly peeked in the forward direction. The maximum data rate of one module in the forward disk part is 8 MHits/s and 3 MHits/s in the barrel part. The average hit rate per module is 1 MHit/s. In contrast, the data rate with a nuclear target is more homogeneously distributed, but with 1.7 GHits/s three times higher. The maximum rate for one pixel module in the forward region is 25 MHits/s while the maximum rate in the barrel layers is 15 MHits/s. With approximately 40 bits of data to transmit for each hit this leads to a maximum data rate of about 1 Gbit/s for a module. This corresponds to the number of hits per front-end chip for the two different target and beam momentum options. The maximum hit rate for a gold target is 4 MHits/s or a data rate of 160 MBit/s. For the hydrogen target the rates are significantly lower with 1.2 MHits/s or 48 MBit/s [1].

The tested readout scheme can be seen in fig. 1. Basic concept of the pixel readout is a time-stamp architecture. In each pixel the leading and the trailing edge of the discriminator signal will be stored using a 10-bit Grey counter. A fast asynchronous scan will transfer the hit data together with the pixel-ID column wise to the end-of-column buffer. These buffers work like a FiFo storing the hit data until the readout control decides to transfer the data from the EoC buffers depending on their filling state to the serialiser and the LVDS output lines of the front-end chip. The shown scheme was successfully tested with the simulated hit rates; basic parameters to be adjusted for different data rate requirements are

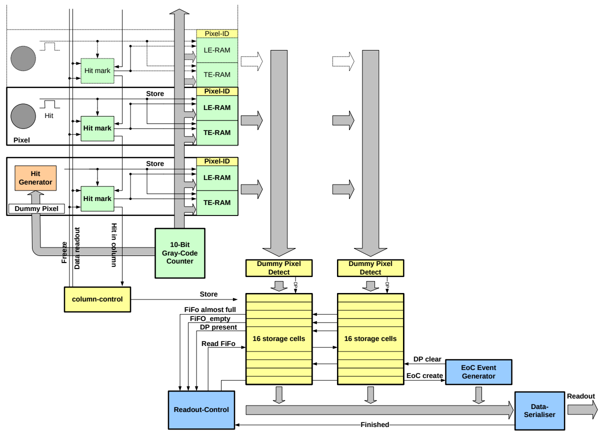

Fig. 1: Readout scheme for the front-end electronics of the pixel part of the MVD.

the numbers of storage cells per EoC buffer and the number of LVDS output line pairs.

For the data flow model of the MVD (see fig. 2) three different data flows have to be taken into account; in particular the distribution of the master clock, the control and configuration data and the hit data. The distribution of the master clock is a general problem with an own task force dealing with this problem.

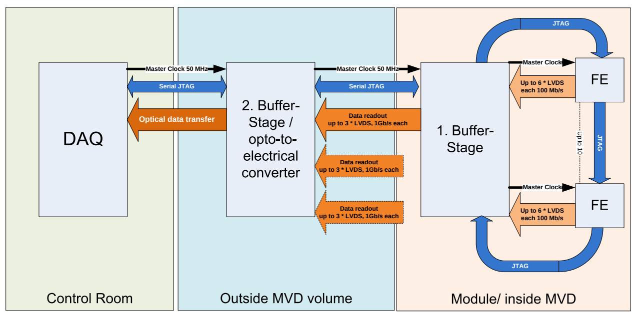

Fig. 2: Data flow model for the readout of the MVD.

The transmission rate of the control- and configuration data is not very high compared to the hit data of the MVD. Here the emphasis lies more in the reliability and the implementation. Therefore a modified version of the JTAG standard was chosen as a transmission protocol. In the so called serial JTAG protocol the amount of data lines is reduced from 5 to 2 to minimize the material budget.

The most challenging task of the data transmission is the readout of the hit data from the front-end electronics. After digitization and zero suppression the data to transmit from one front-end chip can still be up to 200 MBit/s. Including a safety margin up to six LVDS line pairs with 100 MBit/s data rate each are foreseen to connect the front-end chips with the first buffer stage on a module. Here large buffers are planned to average the data load between the connected front-ends and to do a first event building. From the first buffer stage the data is transmitted via up to three 1 GBit/s lines to the second buffer stage were a couple of modules are combined together and the electrical data flow is converted into an optical one. The second buffer stage is connected via long fiber-wires with MVD compute nodes sitting in the control room of the experiment.

References:

[1] T. Stockmanns, F. Hügging, M.C. Mertens and J. Ritman, to be published in the Proceedings of the 11th International Conference on Meson-Nucleon Physics and the Structure of the Nucleon (MENU 2007), Jülich 2007.

Versatile digital readout system for the PANDA MVD

M.C. Mertens, F. Hügging, J. Ritman and T. Stockmanns

1 Introduction

During the development of the **M**icro **V**ertex **D**etector (MVD) for the Anti**p**roton **An**nihilation at **Da**rmstadt (PANDA) experiment at the **F**acility for **A**ntiproton and **I**on **R**esearch (FAIR), a powerful test system is needed for examination of different pixel and strip detector prototypes. A main requirement is that the system is versatile enough to support a wide variety of frontend electronics. Thus, we deployed a flexible test environment with state-of-the-art hardware, which can be easily reconfigured to achieve the needed flexibility. This is accomplished by following a modular design concept of both hardware and software. Key features of the hardware platform are the modern FPGA (Virtex 4), 32 freely configurable LVDS I/O lines and consequent separation of analog and digital parts of the readout. This is accompanied by a modular software framework written in C++ which declares different communication layers for easy hardware access. These levels of abstraction (compare Figure 1a) make it easy to add support for changed or completely new devices.

2 System Overview

The readout system features a modular design of hardware, firmware and the corresponding software framework.

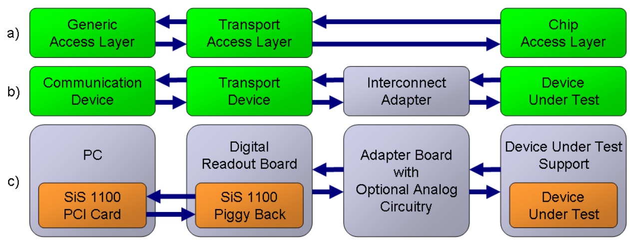

Fig. 1: Readout chain. a) shows the abstract model of the software modules, b) the abstract model of the hardware devices and c) shows the actual setup.

The software framework, in the following referred to as MRF[1], follows a modular design approach by implementing an abstract communication model which defines a hierarchy of communication layers, each layer corresponding to a single module in the software framework (compare Figure 1a) respectively a single hardware device within the readout chain (Figure 1b). Another module of the MRF is a special data storage class which provides a common interface for transfer, storage and display of both configuration data and data returned by the device.

The readout hardware strictly separates analog and digital parts of the readout. The classification of the hardware components closely follows the communication layer concept of the software, as shown in Figure 1b. While the digital readout board itself contains purely digital components, any (optional) analog circuitry is implemented on an additional adapter board which connects the frontend support with the digital readout board. Its embedded FPGA can be reconfigured to support arbitrary communication protocols and I/O pinouts. The connection to the PC is realized via two SiS 1100 optical gigabit links, one is installed as PCI card in the PC, the other integrated as piggy back on the readout board. The central component of the readout system is the *digital readout board*, developed by IKP in close cooperation with ZEL. It features a Xilinx XC4VLX60 Virtex 4 FPGA, DMA enabled data transfer at a rate of one gigabit per second to the PC via a SiS 1100 optical link, 32 LVDS I/O lines, four separately adjustable voltage lines and three differential clock lines. Its flexibility, resulting from the powerful FPGA, the freely configurable output lines, clock sources and supply voltages, allows to easily adapt this board for a wide variety of readout tasks. Next part within the chain is the *pinout adapter board*. Its main purpose is to interface between the connectors of the digital readout board and those on the DUT support, but it can also be used for placing possibly needed analog circuitry (e.g. in order to connect to frontend chips with analog output lines). This board has to be designed specific to the actual application. The *device under test* (typically a frontend chip) is then mounted on a corresponding support board (*DUT support*) which connects it to the pinout adapter board. Compare Figure 1c for an overview on the setup of the readout chain. Figure 2 shows how the system is set up in the laboratory.

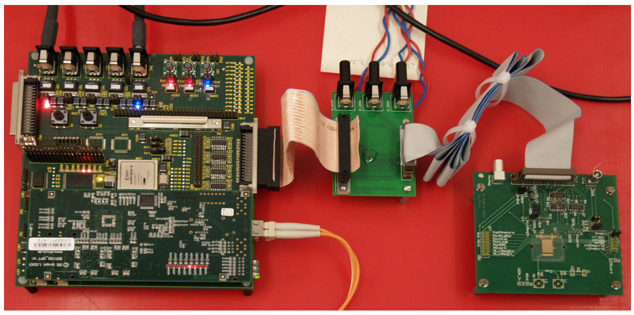

Fig. 2: Experimental Setup. From left to right, the digital readout board, the pin adapter board and the device under test support with the Atlas FE-I3 are shown.

The performance tests of the readout system are very promising. The current FPGA design runs stably at the desired internal clock rate of 40 MHz. Furthermore, even without any optimizations of signal timings, the system could handle more than twice this speed. Clock generation for the connected Atlas FE-I3 frontend chip yields stable frequencies of 5 MHz and 40 MHz on two independent external clock lines with signal rise and fall times well below 2 ns. The same results were obtained for the data lines. Data transmission is performed using access functions of the MRF. It also features a full digital representation of all of the frontend's configuration registers which is used for chip setup. Future plans include deploying the digital readout system as a test stand for prototypes of the Topix frontend chip for silicon pixel sensors which is currently under development at INFN Torino.

[1] MVD Readout Framework. This name originates from the initial motivation of building a generic readout system which is primarily intended to be used during development of the PANDA MVD.

Aging Tests of Straw Tubes for the PANDA Experiment

P. Wintz, J. Ritman and A. Sokolov

High rate tests of straws for the proposed central straw tube tracker (STT) of the future PANDA detector [1] were carried out at COSY. The goal was to check the influence of the beam exposure and charge deposition on the straw efficiency and to verify that all assembled materials including the gas system do not create harmful pollution, e.g. by outgassing. Within the short time of about 10 days beam irradiation, it was possible to collect a charge deposition in single tubes comparable to several years of operation of the PANDA detector at the desired luminosity.

1 Straw Setup

The straw design and all materials were the same used for the COSY-TOF straw tracker assembly, i.e. 30 μm thick mylar film tubes with 10 mm diameter and a length of 105 cm. For the PANDA detector the same straw tube design had been proposed, only the exact length is still open and may vary between about 120 cm to 150 cm. The straw setup consisted of a double-layer of 32 tubes, installed behind the COSY-TOF apparatus and exposed to the residual proton beam with a momentum of about 3 GeV/c. Due to the horizontal layout and a beam spot of about 2×2 cm^2 the particle rate through all tubes was almost the same. The surrounding alignment frame consisted of sandwich bars with a Rohacell core reinforced by Carbon fiber skins [2]. Therefore, interaction of the beam with this low-density foam material (ρ=0.05 g/cm^3) was negligible.

The gas supply of the 32 straws was divided into four individual gas circuits with one circuit for every eight straws. Thus, it was possible to test at the same time four different gas mixtures and gas gains with the same particle rates. The chosen gas mixtures were Argon based, with different fractions of CO_2 (10 % and 30 %) and one mixture with 10 % Ethane. The gas pressure for all mixtures was 1650 mbar. The typical gas flow was one volume exchange per hour. In total, 16 high voltage supply channels (one channel per two straws) allowed to operate the straws at different voltage levels and gas gains. The current of every voltage channel was monitored with a resolution of 2 nA. All straws were equipped with preamplifiers and 30 m long signal cables ending in the counting room. Therefore, it was possible to check analog signal shapes and signal rates during beam irradiation for every straw. Tab. 1 lists all settings during the beam test.

2 Particle Rates at PANDA

The expected particle rates for the individual tubes in the PANDA central tracker volume [3] were derived from a simulation of $\bar{p}p$ interactions and assuming an event rate of 10^7 s^{-1} (see Fig. 1). The mean particle flux for straws in the innermost layer was $\simeq$400 kHz per 1500 mm long tube and about $\simeq$3.5 kHz/cm in the forward region (z>0 cm). The maximum flux of $\simeq$7 kHz/cm in the tube was concentrated within z=2$\pm$2 cm (target position at z=0 cm) coming from $\bar{p}p$ elastic interactions with a laboratory scattering angle $\theta \simeq 90^o$ and relatively low momentum. These particles crossing the tubes around z=2$\pm$ 2 cm were highly ionising and produced a high charge load of $\simeq$0.4 C/cm, if one assumed a typical gas gain inside the tubes of 5×10^4. At other positions the mean charge load was about 0.05 C/cm, only. All quoted charge loads were equivalent to an expected typical beam time for PANDA of one year with 50 % live-time.

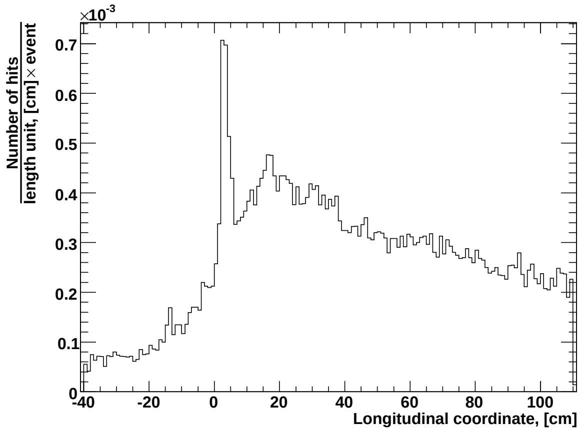

Fig. 1: Simulation of $\bar{p}p$ reactions and number of hits per event and per cm along the tubes in the innermost layer of the PANDA straw tube tracker. The target position is at z=0 cm.

3 Measurements and Results

The total live-time with beam on the straws was 199 hours after correcting the COSY spill time structure and beam breaks. All straws were exposed to the proton beam at the same longitudinal position, in the middle of each tube. The beam rate and cross section profile was measured by a scintillating fiber hodoscope placed behind the COSY-TOF apparatus and in front of the straw setup. The derived proton intensity per straw diameter during extraction was about 2.3×10^6 s^{-1}. The slightly lower pulse frequency of $\simeq1.8\times10^6$ s^{-1} measured for the single straws could be explained by losses of low amplitude signals due to the damping inside the 30 m long cables.

During the beam time no high voltage failures, dark currents or broken wires due to the high charge load were observed. A high maximum current of a single straw wire of about 2 μA was observed (see Tab.1). Fig. 2 shows the time structure of the monitored current flow per straw wire. The nice agreement with the (independently measured) event readout rate of the COSY-TOF data-acquisition confirmed that the current flow through all straw wires was directly and strictly caused by the beam particle ionisations of the gas mixtures inside the straws. The measured clean time structures with currents dropping to zero between the spills with no beam extraction indicated the non-existence of dark or self-sustaining currents.

Possible efficiency losses were checked after the beam time by exposing all tubes to a ^{55}Fe radioactive source with 5.9 keV γ-emission. In the Argon-based gas mixtures the photo-absorption produced a localised ionisation spot with

Table 1: List of straw settings, measured currents and calculated charge load per straw wire during the beam test. The gas gain difference at same voltage setting between beam and ^{55}Fe-source exposure was due to space charge effects at high beam particle rates, reducing the E-field and gas gain.

Straw no.	Gas mixture	Pressure (mbar)	Voltage (V)	Gas gain (beam)	Gas gain (^{55}Fe)	Current (μA) (max.)	Current (μA) (mean)	$\sum(Q)$ (C)
1–8	Ar/CO_2 (10 %)	1650	1750	4×10^4	10×10^4	1.4	1.0	0.72
9–16	Ar/CO_2 (10 %)	1650	1700	3×10^4	5×10^4	1.1	0.8	0.58
17–20	Ar/CO_2 (30 %)	1650	2200	7×10^4	$(25)\times10^4$	2.3	1.7	1.23
21–24	Ar/CO_2 (30 %)	1650	2100	4×10^4	$(14)\times10^4$	1.5	1.1	0.79
25–32	Ar/C_2H_6 (10 %)	1650	1550	5×10^4	15×10^4	1.7	1.2	0.87

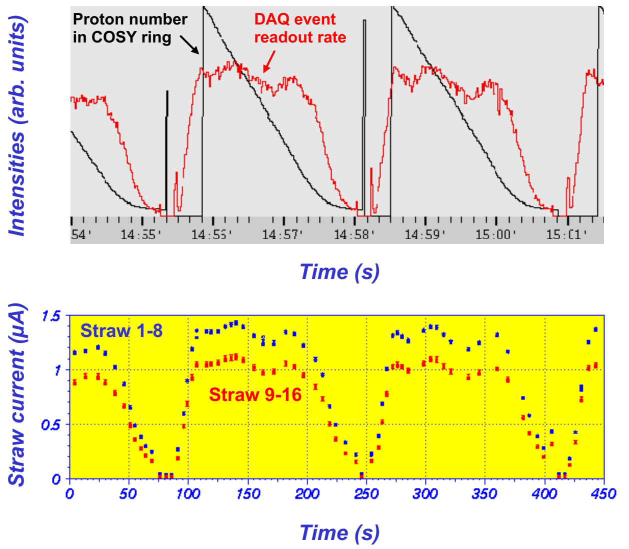

Fig. 2: Time structure of the monitored straw wire currents (straws no. 1–8 and 9–16 on different voltage). On top the proton intensity (black line) in the COSY ring and event readout rate (red line) of the COSY-TOF data acquisition are shown as an independent measure of the beam intensity.

a characteristic number of ionisation charges (220 e$^-$) [4]. Therefore, the recorded signal amplitude height was a direct measure of the gas gain, which could be affected by straw material or gas reactions during the high particle irradiation. Usually the reduction of the gas gain during the operation time of a detector is described as an aging property. The amplitude heights were checked for each straw at different longitudinal positions around the beam irradiation spot (see Fig. 3)

It can be seen that some straws (no. 9–16) showed an efficiency[1] drop of about 3–7 % where the beam hit the tubes. For other straws no change in amplitude height was measured. The sensitivity of the measurement was about 2 % of amplitude height, so that the observed effect for most of the straws was only slightly above resolution. To increase the sensitivity we changed the CO_2 fraction in the argon gas mixture from 10 % to 30 %. Due to the lower mean free path and better quenching capabilities in the 30 % CO_2 gas mixture the high voltage of the wire could be raised from about 1700 V to 2000 V and a stable operation at higher nominal gas gain was possible. Then, the observed amplitude drops at the beam exposure spots were larger and reached up to about 13 % for the straw no. 9–16. (see Fig.4).

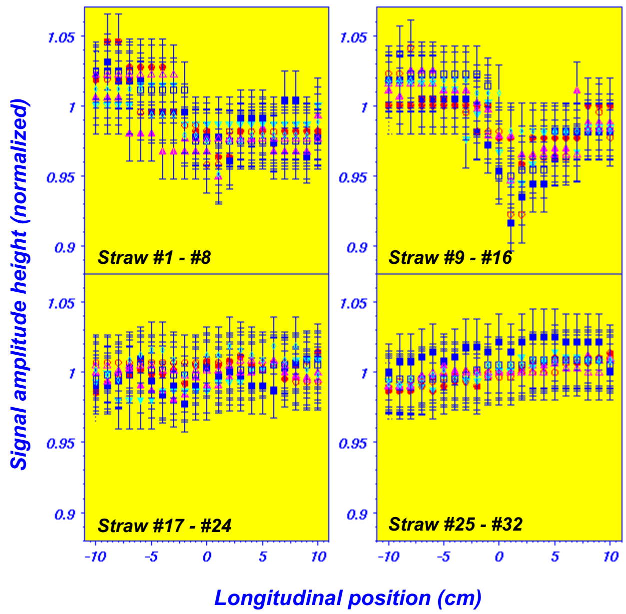

Fig. 3: Measured efficiency along the tube for all 32 straws. The beam hit all tubes around 0 cm.

A clean spatial correlation between efficiency loss and beam intensity in the irradiation spot was observed. On the other hand, the lower or absence of any amplitude change for other straws (see straw no. 1–8 and no. 17–32), even operated at higher gas gains, indicated that also a material quality difference had an influence on the absolute aging strength. A careful testing and optimisation of the materials (wire, cathode film, ...) might reduce the aging strength, but needs further investigation. A possible explanation of the lowered amplitudes could be a wire swelling induced by the high irradiation and leading to a lower electric field and lower gas gain at the wire surface. The different gas mixtures had no influence on the observed aging.

The gas gain in the different straw groups listed in Tab. 1 was calculated by the product of measured beam particle flux, mean track path and primary ionisation charge in the gas mixture, divided by the monitored current. The gas gain measured during exposure to the ^{55}Fe source was added for comparison. The difference between the two gain numbers of about a factor of 2–3 could be explained by space charge effects induced by the slow motion of positive ions. At high

[1] The efficiency is defined as the nominal amplitude height of the ^{55}Fe source signal.

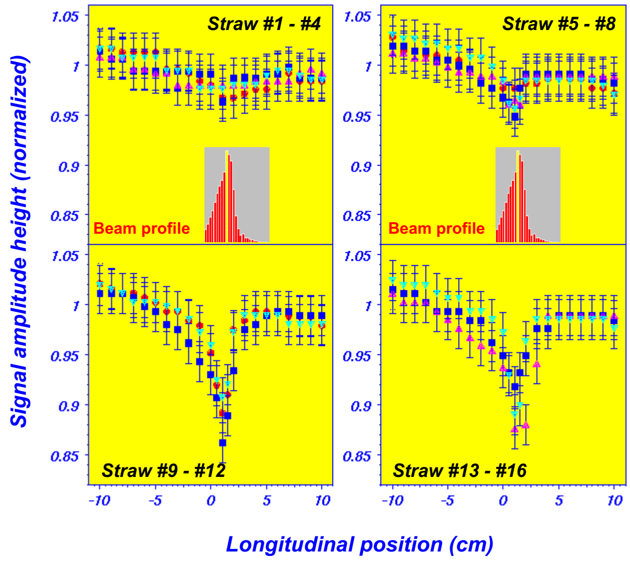

Fig. 4: Inefficiency profile of straws no. #1-#16 and comparison with the horizontal beam intensity profile measured by the fiber hodoscope. A clear agreement between efficiency drop and beam intensity could be seen.

particle ionisation rates the ion current to the cathode reduces the electric field at the wire and limits the gas gain.

4 Conclusion

High rate tests of straw tubes proposed for the PANDA central straw tracker were carried out with a total time of 199 hours of beam exposure. The charge load during this time corresponds to a minimum of about 3 years of PANDA operation at the final luminosity with an expected 50 % live-time or data-taking time per year. We observed for some straws a localized, small efficiency loss of up to about 7 % after this charge load. The quoted numbers are the worst-case and are limited to the hot spot area at the target pipe (z=2$\pm$2 cm) in the PANDA-STT setup. For all other regions the charge load is equivalent to about 10 years of PANDA operation. The absence of any efficiency changes for more than half of all straws could be explained by better material quality and properties, but needs further investigations.

The results confirmed that the straw design and used materials are suited and will not limit the life time of the STT detector to a remarkable extent. For a robust STT operation a gas mixture and pressure which allows lower high voltage operation should be preferred, e.g. an Argon-based gas mixture with a CO_2 fraction of about 10 % and gas gain of about 5×10^4 at a pressure of about 1600 mbar.

References:

[1] M. Kotulla et al., PANDA Technical Progress Report, http://www-panda.gsi.de/archive/public/panda_tpr.pdf, 2005

[2] P.Wintz, AIP Conf. Proc. 698:789-792, 2004.

[3] IKP Annual Report 2006, Highlights section, p31.

[4] IKP Annual Report 2001, Jül-3978, p40.

Optimization of the Moscow-Jülich Pellet Target*

A.Boukharov[a], M.Büscher[b], V.Chernetsky[c], P.Fedorets[b,c], A.Gerasimov[c], A.Semenov[a]

During 2007 the development of the Pellet Target focused at droplet generation from new gases and studies for the stabilization of operating parameters.

For the generation of a regular pellet beam with diameters well below one millimeter, it is mandatory to first produce an undistorted (without turbulences and intrinsic vibrations) liquid jet of the particular target material. This jet then undergoes forced break-up inside a triple-point chamber by inducing surface vibrations of well defined wavelengths at the ejection nozzle. Only for a certain choice of the excitation frequency, the disintegration into mono-disperse droplets (*i.e.* without any intermediate droplets of smaller radii) can be achieved. In earlier tests our pellet generator has been succeessfully used for the worldwide first generation of mono-disperse Hydrogen and Nitrogen droplets while additional target materials are desirable for *e.g.* carrying out experiments at PANDA.

Liquefaction of the different target substances in our cryostat is realized by the use of cooling liquids with suitable boiling temperatures. Argon liquefaction can be achieved with liquid Argon and Nitrogen as coolants, see Fig. 1.

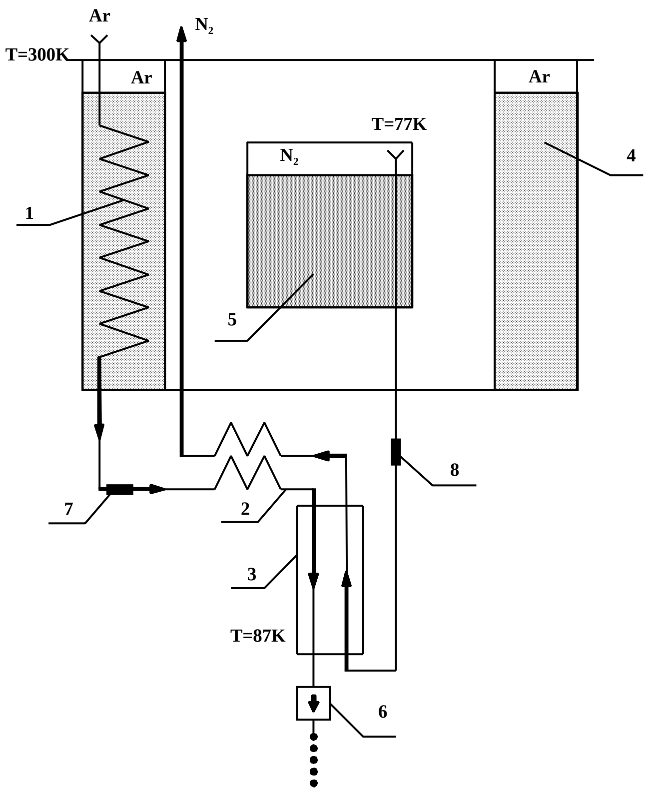

Fig. 1: Cooling scheme for Ar droplets: 1-primary heat-exchanger; 2- main heat-exchanger; 3- condenser; 4- first cooling bath; 5- second bath; 6- droplet generator; 7,8- heaters

Inexpensive technical liquid Argon of low purity has been used in the primary heat exchanger (1 in Fig. 1) for pre-cooling of the high-purity target Argon gas. The heater (7) is needed for fine tuning of the Argon temperature before it reaches the condenser (3) where it is liquefied. Such fine tuning is important to avoid boiling of the Argon in the condenser which would lead to unwanted vibrations on the ejection nozzle. Cold evaporated Nitrogen steam from the second bath (5) has been used for final Argon cooling and liquefaction in the condenser. A second heater (8) permits fine tuning of the Helium steam temperature. For Hydrogen and Nitrogen pellet production liquid Nitrogen had been used for pre-cooling and evaporated Helium for final liquefaction.

We have demonstrated that it is possible to obtain mono-disperse droplets from various cryogenic gases with the same experimental facility. The tests with Argon have been made with jet diameters from 10μm up to 20μm, some results are shown in Fig. 2.

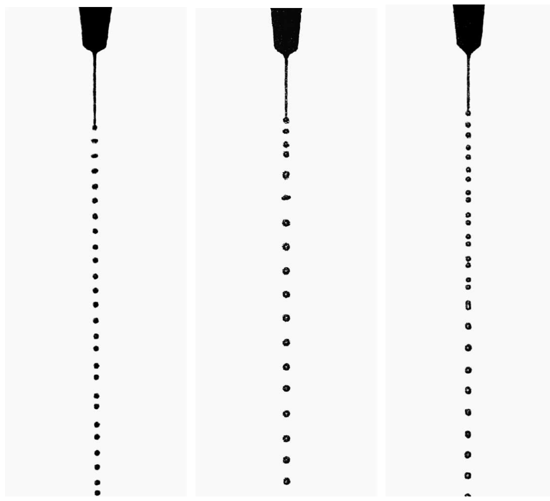

Fig. 2: First observation Argon jet production in the triple point chamber with subsequent brek-up into mono-disperse drops for a jet velocity of v=1-3m/s and a nozzle diameter of D_{nozzle}=17μm

We are also developing new algorithms and software for pressure stabilization in the hydrogen supply system as well as for temperature control inside the cryostat. For the latter the level of the liquid Helium bath (5) should be constant. In order to fulfill this requirement, drawings of a Helium filling siphon and elements of an automated cryosystem have been prepared and a special Helium valve has been prepared.

During our test runs deviations of the sluice and nozzle positions from the nominal axis due to the cryogenic temperatures have been measured. The adjustment system has been upgraded according to these data, which allows for a more reliable nozzle-sluice adjustment now.

[a]MPEI, Moscow, [b]IKP FZJ, [c]ITEP, Moscow

*Supported by grants INTAS 06-1000012-8787, DFG 436 RUS 113/948/0-1, COSY-FFE-095, EU-FP6

5 Technical Developments

Development of universal set of test electronic for tracking detectors at WASA and ANKE

J. Majewski[1], P. Kulessa[1,2], H.Ohm[1], K. Pysz[1,2]; V. Serdyuk[1,3]

Tracking detectors at WASA (MDC and FPC) as well as at ANKE (forward straw and drift chambers) are read out with CMP16 amplifier/discriminator boards which are mounted either immediately on the chambers or very close to them in order to minimize cross talk and signal pick up through cables between the chamber and the amplifier input. In addition, this concept keeps the space occupied by front-end electronics low which is mandatory in view of the big number of electronics channels in these detectors. On the drift chambers which have been developed for the ANKE forward detector CMP16-boards can be directly coupled with anodes since these are on ground potential. For the WASA trackers compromises had to be made in order to account for the electrical and geometrical constraints inherent in the system when it was taken over from TSL Uppsala.

For the central tracker MDC front-end electronics could only placed at a minimum distance of 4.5 meters over which primary signals are sent via coaxial cables. Dedicated boards for 64 channels deliver high voltage to the straws, decouples weak straw signals from HV and send logical signals to the TDCs. In addition, these boards receive threshold information via a serial input and deliver analog threshold voltages to the CMP16 chips. For the forward tracker FPC boards with two different form factors have been developed which permit placing the whole front end on the chamber in spite of the extremely narrow space available there. Logical LVDS signals are directly delivered by CMP16 via twisted pair cables to the F1-TDCs.

Analog signals from the chambers are not available. In order to monitor the chamber output directly for trouble shooting, optimization of operating conditions and detector development a universal set of electronics tools has been prepared. The first stage is a fast transresistance amplifier with a gain of 10 mV / µA and a signal risetime of < 8 ns. In view of high-voltage coupling into the anodes for all straw detectors various adapter boards had to be developed which fulfill the requirements for very fast signals and which can withstand voltages up to 3 kV.

The amplifier is followed by the "F1/GPX-CMP16-adapter" which serves two purposes, see fig. 1 and 2. It can deliver supply voltages to both the amplifier and the CMP16 board and it creates analog threshold voltages for the ANKE-type CMP16 board. Threshold setting is done either via a serial input, by an external analog reference voltage or with the help of an on-board trimmer. Furthermore, this board acts as a signal adapter from CMP16 to F1 or GPX TDCs and it comprises 8 x 16 channels.

For application for the chambers and the window straw detector in ANKE experiment the test-signal input is included. Device might be used also as a 34 pole – 40 pole flat cable connector adapter.

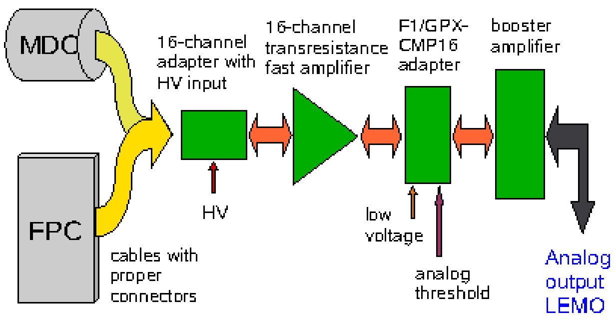

Fig. 1: Diagnostics electronics for analog signals of ANKE and WASA trackers

The F1/GPX-CMP16 adapter delivers bipolar signals from CMP16 or the fast amplifier into the booster amplifier which creates unipolar signals capable of driving long cables. It posses a standard flat connector differential output allowing a connection of sixteen 50 Ω cables with LEMO plugs. The baselines for analog outputs are adjustable. The polarity of the signals can be selected by a proper cables arrangement on the F1/GPX – CMP16 adapter.

Diagnostics electronics allows also to test a readout electronics for MDC and FPC. In this case the CMP-16 readout boards are connected to the F1/GPX – CMP16 adapter (fig. 2). They are supplied with +6V and have their own test inputs. The output signals can be then observed on the analog output of a booster amplifier or fed to the data acquisition through a TDC.

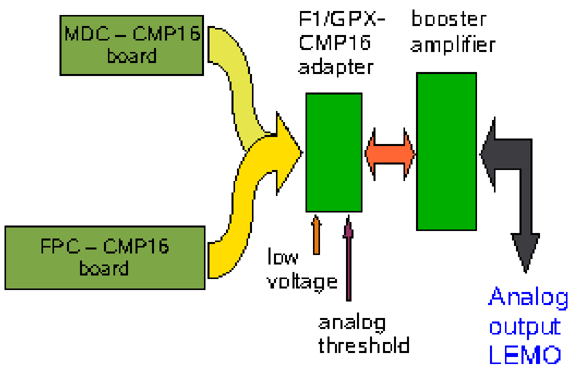

Fig. 2: Diagnostics for monitoring of LVDS signals

[1] FZJ-IKP
[2] IFJ PAN Kraków
[3] JINR Dubna

Electronics Laboratory

C.Berchem, N.Dolfus, W.Ernst, H.Metz–Nellen, M.Nau, R.Nellen, J.Sarkadi, H.Schiffer, T.Sefzick

The activities of the IKP Electronics Laboratory can be assigned to mainly the following three topics:

Electronics and Data Acquisition for experiments

For the straw chamber project at TOF pre–amplifiers and signal conversion circuitry for 3200 channels were produced. Adapter boards and system crates for the ASD8 bases readout system were finally developed and produced. Connection units consisting of 0,5mm thick coaxial cables, connecting the pre–amplifiers and the ASD8 circuitry were produced for appr. 2500 channels. The production of vacuum and light tight printed circuit boards carrying 3000 high density feedthrough contacts was finished.

For the spectator detector at ANKE extensive support was given to the ADC development at ZEL. A facility for automatic testing of silicon microstrip detectors was designed. Development and production of test units for the wire chambers was supported as well.

The atomic beam source (ABS) setup for the polarized internal target (PIT) was checked under beam time conditions at the ANKE experiment, the process visualisation was modified. The positioning system was calibrated. At the Lamb shift polarimeter a remote control of the Heinzinger power supplies was set up using the analog I/O modules of the S7–300 PLC system. For the interlock system needed to protect detectors at ANKE and in laboratory setups against damage in case of vacuum leakage the WinCC user interface and the S7 PLC development system were upgraded. Feasibility studies for automatic configuration of the various setups (FT, CT, ABS, LSP, UGSS) at the ANKE site were carried out.

For the PAX experiment the algorithm for the vacuum slow control interlock system of the ABS setup was improved, the PLC program code was adapted. The slow control system was tested using WinCC's process control user interface. For the Breit–Rabi polarimeter at PAX the electrical specifications of the system were defined, the patch fields (one for the vacuum slow control the other for polarised beam diagnostic purposes) and signal distributor boxes were designed, and the process visualisation was set up. The cabling of the system is ongoing.

The LabView program for the crystal spectrometer of the pionic hydrogen experiment (formerly at PSI) was extended for continuous data acquisition.

Within a collaboration with the Atomic Energy Authority Nuclear Research Center in Cairo/Egypt the cyclotron there will get a new Simatic S7 based beam line control system. For this purpose various signal distributors for the S7 control units were designed and built here and installed and taken into operation on–site.

Support was given to the development of amplifiers and discriminators for the MCD and FPC at WASA. A prototype for a new PMT base for the central detector was developed and is currently under testing. Moreover, the electronic lab assisted in purchasing materials and the setup of file servers and network infrastructure.

For the ATRAP–II experiment pre–amplifiers were repaired and 16–fold PMT were tested.

COSY diagnostics

Maintenance was provided for the multi–wire chambers for beam diagnostics in the extraction beamlines und for the viewer cameras. This also included repair of broken components, e.g. power supplies.

Computer network

After planning and measurements the installation of wireless LAN access points in the institute and cyclotron buildings still awaits completion. In the COSY building the installation has been completed. For the installation in building 09.6 (COSY office building with accommodation facility) new WLAN components were installed. Frequent support was granted to ensure continuous operation of the existing networks.

Miscellaneous

Like every year substantial support was given with regard to short term maintenance and repair or replacement of electronics. In some cases the urgent demand didn't allow a time consuming outside repair procedure, in other cases the manufacturer doesn't even exists anymore, but the electronics can not be replaced easily, or the manufacturer was unable to perform the repair.

Prototypes and small series of cables or electronics, for which an outside production would not have been reasonable, were delegated to infrastructure facilities or done here, mainly by trainees and student auxiliary workers.

The standard data acquisition systems at several COSY experiments were taken care of to assure stable operation during several beamtimes.

Regarding S5 and S7 systems continuous support was given to the experiments TOF and WASA, the radiation safety division, and to the cyclotron group.

Part time supervision of BSc and MSc students of the FH Aachen was provided in the field of process automation.

A relaunch of the IKP webpages is completed, future modifications of the pages await further specifications from the public relations office.

A Councils

A.1 HGF Midterm Review Council

Prof. J. Bisplinghoff	Universität Bonn	
Prof. C. Guaraldo	INFN Frascati, I	
Prof. M. Harakeh	KVI Groningen, NL	
Prof. A. Merschenz-Quack	FH Aachen	
Prof. V. Metag	Universität Gießen	
Prof. E. Moulinari	Universita de Modena, I	
Dr. D. Müller	BMBF/GSI Darmstadt	
Dr. R. Opitz	Helmholtz Gemeinschaft	
Prof. St. Paul	TU München	Chairperson
Prof. K. Peters	GSI Darmstadt	
Prof. D.O. Riska	Helsinki Institute of Physics, FI	
Prof. A. Schäfer	Universität Regensburg	
Dr. S. Schmidt	Helmholtz Gemeinschaft	
Prof. J. Stachel	Universität Heidelberg	
Prof. W.T.H. van Oers	University of Manitoba, CA	
Dr. M. Wappelhorst	Ministerium IWFT/NRW, Düsseldorf	

A.2 COSY Program Advisory Committee

Prof. D. Barber	DESY, DE	
Prof. J. Bijnens	Lund University, SE	
Prof. H. Freiesleben	TU Dresden, DE	
Prof. B. Friman	GSI Darmstadt, DE	
Prof. N. Herrmann	Universität Heidelberg, DE	
Prof. T. Johansson	Uppsala Universitet, SE	
Prof. H. Löhner	KVI Groningen, NL	
Prof. A. Magiera	Jagellonian University Cracow, PL	
Prof. W. Meyer	Universität Bochum, DE	
Prof. W.T.H. van Oers	University of Manitoba, CA	Chairperson
Prof. E. Oset	Universitat de Valencia, ES	
Prof. C. Schaerf	INFN Roma II, IT	

B Publications 2007

1. Experiment

1. Abdel-Bary, M.; Abdel-Samad, S.; Brinkmann, K. T.; Castelijns, R.; Clement, H.; Dietrich, J.; Doroshkevich, E.; Dshemuchadse, S.; Ehrhardt, K.; Erhardt, A; Eyrich, W.; Freiesleben, H.; Gast, W.; Georgi, J.; Gillitzer, A.; Karsch, L.; Kilian, K.; Krapp, M.; Kuhlmann, E.; Lehmann, A.; Morsch, H.-P.; Paul, N.; Pinna, L.; Pizzolotto, C.; Ritman, J.; Roderburg, E.; Schadmand, S.; Schönmeier, P.; Schröder, W.; Schulte-Wissermann, M.; Sefzick, T.; Teufel, A.; Ucar, A.; Wüstner, P.; Zupranski, P.
   Improved study of a possible Θ^+ production in the $pp \to pK^0\Sigma^+$ reaction with the COSY-TOF spectrometer
   Physics Letters B **649** (2007) 252.

2. Abdel-Bary, M.; Abdel-Samad, S.; Brinkmann, K.-T.; Clement, H.; Dietrich, J.; Doroshkevich, E.; Dshemuchadse, S.; Ehrhart, K.; Erhardt, A.; Eyrich, W.; Filippi, A.; Freiesleben, H.; Fritsch, M.; Gillitzer, A.; Hesselbarth, D.; Jä, R.; Karsch, L.; Kilian, K.; Kuhlmann, E.; Marcello, S.; Michel, P.; Mö, K.; Morsch, H. P.; Pizzolotto, C.; Plettner, C.; Ritman, J.; Roderburg, E.; Schö, P.; Schroeder, W.; Schulte-Wissermann, M.; Steinke, M.; Sun, G. J.; Ullrich, W.; Wenzel, R.; Wintz, P.; Wagner, M.; Wilms, A.; Wirth, S.; Zupranski, P.;
   Comparison of isoscalar vector meson production cross sections in proton-proton collisions
   Physics Letters B **647** (2007) 351.

3. Abdel-Bary, M.; Abdel-Samad, S.; Kilian, K.; Ritman, J.
   Performance measurements of a 7 mm-diameter hydrogen heat pipe
   Cryogenics **47** (2007) 158.

4. Adam, H.-H.; Geck, I.; Khoukaz, A.; Lister, T.; Santo, R.; Steltenkamp, S.; Täschner, A.; Czerwinski, E.; Czyzykiewicz, R.; Janusz, M.; Jarczyk, L.; Kamys, B.; Klaja, P.; Moskal, P.; Piskor-Ignatowicz, B.; Przerwa, J.; Smyrski, J.; Grzonka, D.; Kilian, K.; Oelert, W.; Sefzick, T.; Winter, P.; Wolke, M.; Wüstner, P.; Budzanowski, A.; Rozek, T.; Siemaszko, M.; Zipper, W.
   Hadronic ^{3}He eta production near threshold
   Physical Review C **75** (2007) 14004.

5. Agakichiev, B.; Agodi, C.; Alvarez-Pol, H.; Balanda, A.; Bertini, D.; Bielcik, J.; Bellia, G.; Bohmer, M.; Bokemeyer, H.; Boyard, J. L.; Braun-Munzinger, P.; Cabanelas, P.; Chernenko, S.; Christ, T.; Coniglione, R.; Cosentino, L.; Diaz, J.; Dohrmann, F.; Duran, I.; Eberl, T.; Enghardt, W.; Fabbietti, L.; Fateev, O.; Fernandez, C.; Finocchiaro, P.; Friese, J.; Frohlich, I.; Fuentes, B.; Garabatos, C.; Garzon, J. A.; Gernhauser, R.; Golubeva, M.; Gonzalez-Diaz, D.; Grosse, E.; Guber, F.; Hennino, T.; Hlavac, S.; Holzmann, R.; Homolka, J.; Ierusalimov, A.; Iori, I.; Ivashkin, A.; Jaskula, M.; Jurkovic, M.; Kagarlis, M.; Kajetanowicz, M.; Kampfer, B.; Kanaki, K.; Karavicheva, T.; Kastenmuller, A.; Kidon, L.; Kienle, P.; Koenig, I.; Koenig, W.; Korner, H. J.; Kolb, B. W.; Kotte, R.; Krucken, R.; Kugler, A.; Kuhn, W.; Kulessa, R.; Kurepin, A.; Lang, S.; Lange, S.; Lehnert, J.; Lins, E.; Magestro, D.; Maiolino, C.; Malarz, A.; Markert, J.; Metag, V.; Mousa, J.; Munch, M.; Muntz, C.; Naumann, L.; Nekhaev, A.; Novotny, J.; Otwinowski, J.; Pachmayer, Y.C.; Pechenov, V.; Perez, T.; Piattelli, P.; Pietraszko, J.; Pleskac, R.; Ploskon, M.; Pospisil, V.; Prokopowicz, W.; Przygoda, W.; Ramstein, B.; Reshetin, A.; Ritman, J.; Roy-Stephan, M.; Rustamov, A.; Sadovsky, A.; Sailer, B.; Salabura, P.; Sanchez, M.; Sapienza, P.; Schmah, A.; Schon, H.; Schon, W.; Schroder, C.; Schwab, E.; Simon, R. S.; Smolyankin, V.; Smykov, L.; Spataro, S.; Spruck, B.; Strobele, H.; Stroth, J.; Sturm, C.; Sudol, M.; Suk, M.; Taranenko, A.; Tlusty, P.; Toia, A.; Traxler, M.; Tsertos, H.; Vassiliev, D.; Vazquez, A.; Wagner, V.; Walus, W.; Wisniowski, W.; Wojcik, T.; Wustenfeld, J.; Zanevsky, Y.; Zeitelhack, K.; Zovinec, D.; Zumbruch, P.
   Dielectron production in ^{12}C+^{12}C collisions at 2-AGeV with HADES
   Physical Review Letters **98** (2007) 052302.

6. Bargholtz, C.; Bashkanov, M.; Bogoslawsky, D.; Calen, H.; Cappellaro, F.; Clement, H.; Demirörs, L.; Ekström, C.; Fransson, K.; Geren, L.; Gustafsson, L.; Höistad, B.; Ivanov, G.; Jacewicz, M.; Jiganov, E.; Johansson, T.; Keleta, S.; Koch, I.; Kullander, S.; Kupsc, A.; Kuznetsov, A.; Laukhin, I. V.; Lindberg, K.; Marciniewski, P.; Meier, R.; Morosov, B.; Oelert, W.; Pauly, C.; Pettersson, H.; Petukhov, Y.; Povtorejko, A.; Ruber, R.J.M.Y.; Schönning, K.; Scobel, W.; Shafigullin, R.; Shwartz, B.; Skorodko, T.; Sopov, V.; Stepaniak, J.; Tchernyshev, V.; Tegner, P. E.; Thörngren-Engblom, P.; Tikhomirov, V.; Turowiecki, A.; Wagner, G. J.; Wolke, M.; Yamamoto, A.; Zabierowski, J.; Zartova, I.; Zlomanczuk, J.
   Measurement of the $\eta \to \pi^+\pi^-e^+e^-$ decay branching ratio
   Physics Letters B **644** (2007) 299.

7. Barsov, S.; Büscher, M.; Hartmann, M.; Hejny, V.; Kacharava, A.; Keshelashvili, I.; Khoukaz, A.; Koptev, V.; Kulessa, P.; Kulikov, A.; Lehmann, I.; Leontyev, V.; Macharashvili, G.; Maeda, Y.; Mersmann, T.; Merzliakov, S.;

Mikirtichyants, S.; Mussgiller, A.; Oellers, D.; Ohm, H.; Rathmann, F.; Schleichert, R.; Seyfarth, H.; Ströher, H.; Trusov, S.; Valdau, Yu.; Wüstner, P.; Yaschenko, S.; Wilkin, C.
Study of omega-meson production in *pp* collisions at ANKE
European Physical Journal A **31** (2007) 95.

8. Bashkanov, M.; Bogoslawsky, D.; Calen, H.; Capellaro, F.; Clement, H.; Demirörs, L.; Ekström, C.; Fransson, K.; Gustafsson, L.; Höistad, B.; Ivanov, G.; Jacewicz, M.; Jiganov, E.; Johansson, T.; Keleta, S.; Koch, I.; Kullander, S.; Kupsc, A.; Kuznetsov, A.; Marciniewski, P.; Meier, R.; Morosov, B.; Oelert, W.; Pauly, C.; Petukhov, Y.; Pettersson, H.; Povtorejko, A.; Ruber, R.J.M.Y.; Schönning, K.; Scobel, W.; Skorodko, T.; Shwartz, B.; Sopov, V.; Stepaniak, J.; Tchernyshev, V.; Thörngren Engblom, P.; Tikhomirov, V.; Turowiecki, A.; Wagner, G. J.; Wiedner, U.; Wolke, M.; Yamamoto, A.; Zabierowski, J.; Zlomanczuk, J.
Measurement of the slope parameter for the $\eta \to 3\pi^0$ decay in the $pp \to pp\eta$ reaction
Physical Review C **76** (2007) 048201.

9. Bellemann, F.; Berg, A.; Bisplinghoff, J.; Bohlscheid, G.; Ernst, J.; Henrich, C.; Hinterberger, F.; Ibald, R.; Jahn, R.; Joosten, R.; Kilian, K.; Kozela, A.; Machner, H.; Magiera, A.; Munkel, J.; von Neumann-Cosel, P.; von Rossen, P.; Schnitker, H.; Scho, K.; Smyrski, J.; Tölle, R.; Wilkin, C.
Experimental study of the $pd \to {}^3\mathrm{He}K^+K^-$ and $pd \to {}^3\mathrm{He}\phi$ reactions close to threshold
Physical Review C **75** (2007) 015204.

10. Betigeri, M. G.; Biswas, P. K.; Budzanowski, A.; Chatterjee, A.; Jahn, R.; Guha, S.; Hawranek, P.; Jain, B. K.; Jha, V.; Kilian, K.; Kliczewski, S.; Kirillov, Da.; Kirillov, Di.; Kolev, D.; Kravcikova, M.; Kutsarova, T.; Lesiak, M.; Lieb, J.; Machner, H.; Magiera, A.; Maier, R.; Martinska, G.; Nedev, S.; Piskunov, N.; Prasuhn, D.; Protic, D.; Ritman, J.; von Rossen, P.; Roy, B. J.; Shukla, P.; Sitnik, I.; Siudak, R.; Tsenov, R.; Ulicny, M.; Urban, J.; Vankova, G.
A large acceptance scintillator detector with wavelength shifting fibre readout for search of η-nucleus bound states
Nuclear Instruments and Methods in Physics Research Section A **578** (2007) 198.

11. Bubak, A.; Budzanowski, A.; Filges, D.; Goldenbaum, F.; Heczko, A.; Hodde, H.; Jarczyk, L.; Kamys, B.; Kistryn, M.; Kistryn, St.; Kliczewski, St.; Kowalczyk, A.; Kozik, E.; Kulessa, P.; Machner, H.; Magiera, A.; Migdal, W.; Paul, N.; Piskor-Ignatowicz, B.; Puchala, M.; Pysz, K.; Rudy, Z.; Siudak, R.; Wojciechowski, M.; Wüstner, P.
Non-equilibrium emission of complex fragments from *p*+Au collisions at 2.5 GeV proton beam energy
Physical Review C **76** (2007) 014618.

12. Czyzcykiewicz, R.; Moskal, P.; Adam, H.-H.; Budzanowski, A.; Czerwinski, E.; Gil, D.; Grzonka, D.; Hodana, M.; Janusz, M.; Jarczyk, L.; Kamys, B.; Khoukaz, A.; Kilian, K.; Klaja, P.; Lorentz, B.; Oelert, W.; Piskor-Ignatowicz, B.; Przerwa, J.; Rejdych, B.; Ritman, J.; Sefzick, T.; Siemaszko, M.; Smyrski, J.; Täschner, A.; Ulbrich, K.; Winter, P.; Wolke, M.; Wüstner, P.; Zipper, W.
Mechanism of Near-Threshold Production of the η Meson
Physical Review Letters **98** (2007) 122003.

13. Czyzykiewicz, R.; Moskal, P.; Adam, H.-H.; Budzanowski, A.; Czerwinski, E.; Gil, D.; Grzonka, D.; Janusz, M.; Jarczyk, L.; Kamys, B.; Khoukaz, A.; Klaja, P.; Majewski, J.; Oelert, W.; Piskor-Ignatowicz, C.; Przerwa, J.; Ritman, J.; Rohdjess, H.; Rozek, T.; Sefzick, T.; Siemasko, M.; Smyrski, J.; Täschner, A.; Ulbrich, K.; Winter, P.; Wolke, M.; Wüstner, P.; Zipper, W.
Study of the production mechanism of the η meson by means of analysing power measurements International
Journal of Modern Physics A **22** (2007) 518.

14. Gabrielse, G.; Larochelle, P.; Le Sage, D.; Levitt, B.; Kolthammer, W. S.; Kultjanishvili, I.; McConnell, R.; Wrubel, J.; Esser, F. M.; Glückler, H.; Grzonka, D.; Hansen, G.; Martin, S.; Oelert, W.; Schillings, J.; Schmitt, M.; Sefzick, T.; Soltner, H.; Zhang, Z.; Comeau, D.; George, M. C.; Hessels, E. A.; Storry, C. H.; Weel, M.; Speck, A.; Nillius, F.; Walz, J.; Hänsch, T. W.
Antiproton Confinement in a Penning-Ioffe Trap for Antihydrogen
Physical Review Letters **98** (2007) 113002.

15. Herskind, B.; Hagemann, G. B.; Dossing, Th.; Ronn Hansen, C.; Schunk, N.; Sletten, G.; Oedegard, S.; Hübel, H.; Bringel, P.; Bürger, A.; Neusser, A.; Singh, A. K.; Al-Khatib, A.; Patel, S. B.; Nyako, B. M.; Algora, A.; Dombradi, Z.; Gal, J.; Kalinka, G.; Sohler, D.; Molnar, J.; Timar, J.; Zolnai, L.; Juhasz, K.; Bracco, A.; Leoni, S.; Camera, F.; Benzoni, G.; Mason, P.; Paleni, A.; Million, B.; Wieland, O.; Bednarczyk, P.; Azaiez, F.; Byrski, Th.; Curien, D.; Dakov, O.; Duchene, G.; Khalfallah, F.; Gall, B.; Piqeras, L.; Robin, J.; Dudek, J.; Rowley, N.;

Redon, N.; Hannachi, F.; Scheurer, J. N.; Wilson, J. N.; Lopez-Martens, A.; Korichi, A.; Hauschild, K.; Roccaz, J.; Siem, S.; Fallon, P.; Lee, I. Y.; Görgen, A.; Maj, A.; Kmiecik, M.; Brekiesz, M.; Styczen, J.; Zuber, K.; Lisle, J. C.; Cederwall, B.; Lagergren, K.; Evans, A. O.; Rainovski, G.; De Angelis, G.; La Rana, G.; Moro, R.; Lieder, R. M.; Lieder, E. O.; Gast, W.; Jäger, H.; Pasternak, A. A.; Petrache, C. M.; Petrache, D.
Light Charged Particles as Gateway to Hyperdeformation
Acta Physica Polonica B **38** (2007) 1421.

16. Indelicato, P.; Boucard, S.; Covita, D. S.; Gotta, D.; Gruber, A.; Hirtl, A.; Fuhrmann, H.; Le Bigot, E.-O.; Schlesser, S.; dos Santos, J. M. F.; Simons, L. M.; Stingelin, L.; Trassinelli, M.; Veloso, J.; Wasser, A.; Zmeskal, J.
Highly charged ion X-rays from Electron-Cyclotron Resonance Ion Sources
Nuclear Instruments and Methods in Physics Research Section A **580** (2007) 8.

17. Indelicato, P.; Trassinelli, M.; Anagnostopoulos, D. F.; Boucard, S.; Covita, D. S.; Borchert, G.; Dax, A.; Egger, J. P.; Gotta, D.; Gruber, A.; Hirtl, A.; Hennebach, M.; Fuhrmann, H.; Le Bigot, E.-O.; Liu, Y.-W.; Manil, B.; Nelms, N.; Schlesser, S.; dos Santos, J. M. F.; Simons, L. M.; Stingelin, L.; Veloso, J.; Wasser, A.; Wells, A.; Zmeskal, J.
Experiments on Highly Charged Heavy Ions in Conjunction with Exotic Atoms
Advances in Quantum Chemistry **53** (2007) 217.

18. Levitt, B.; Gabrielse, G.; Larochelle, P.; Le Sage, D.; Kolthammer, W. S.; McConnell, R.; Wrubel, J.; Speck, A.; Grzonka, D.; Oelert, W.; Sefzick, T.; Zhang, Z.; Comeau, D.; George, M. C.; Hessels, E. A.; Storry, C. H.; Weel, M.; Walz, J.
Single-Component Plasma of Photoelectons
Physics Letters B **656** (2007) 25.

19. Maeda, Y.; Sakai, H.; Fujita, K.; Greenfield, M. B.; Hatanaka, K.; Hatano, M.; Kamiya, J.; Kawabata, T.; Kuboki, H.; Okamura, H.; Rapaport, J.; Saito, T.; Sakemi, Y.; Sasano, M.; Sekiguchi, K.; Shimizu, Y.; Suda, K.; Tameshige, Y.; Tamii, A.; Wakasa, T.; Yako, K.; Blomgren, J.; Mermod, P.; Öhrn, A.; Österlund, M.; Witala, H.; Deltuva, A.; Fonseca, A. C.; Sauer, P. U.; Glöckle, W.; Golak, J.; Kamada, H.; Nogga, A.; Skibinski, R.
Differential cross section and analyzing power measurements for $\vec{n}$ elastic scattering at 248 MeV
Physical Review C **76** (2007) 014004.

20. Mersmann, T.; Khoukaz, A.; Büscher, M.; D. Chiladze, D.; Dymov, S.; Hartmann, M.; Hejny, V.; Kacharava, A.; Keshelashvili, I.; Kulessa, P.; Maeda, Y.; Mielke, M.; Mikirtychiants, S.; Ohm, H.; Papenbrock, M.; Prasuhn, D.; Rathmann, F.; Rausmann, T.; Schleichert, R.; Serdyuk, V.; Stein, H.-J.; Ströher, H.; Täschner, A.; Valdau, Yu.; Wilkin, C.; Wronska, A.
Precision Study of the η^3He System Using the $dp \to {}^3$Heη Reaction
Physical Review Letters **98** (2007) 242301.

21. Moskal, P.; Adam, H.-H.; Budzanowski, A.; Czerwinski, E.; Czyzykiewicz, R.; Gil, D.; Grzonka, D.; Janusz, M.; Jarczyk, L.; Kamys, B.; Khoukaz, A.; Klaja, P.; Majewski, J.; Oelert, W.; Piskor-Ignatowicz, C.; Przerwa, J.; Ritman, J.; Rejdych, B.; Rozek, T.; Sefzick, T.; Siemasko, M.; Smyrski, J.; Täschner, A.; Winter, P.; Wolke, M.; Wüstner, P.; Zipper, W.
η and η' meson production at COSY-11
International Journal of Modern Physics A **22** (2007) 305.

22. Nekipelov, M.; Büscher, M.; Hartmann, M.; Keshelashvili, I.; Kleber, V.; Koptev, V.; Maeda, Y.; Mikirtychiants, S.; Schleichert, R.; Sibirtsev, A.; Ströher, H.; Valdau, Yu.
Investigation of the reaction $pp \to pK^0\pi^+\Lambda$ in search of the pentaquark
Journal of Physics G **34** (2007) 627.

23. Oelert, W.; Adam, H.-H.; Budzanowski, A.; Czerwinski, E.; Czyzykiewicz, R.; Gil, D.; Grzonka, D.; Janusz, M.; Jarczyk, L.; Kamys, B.; Khoukaz, A.; Klaja, P.; Moskal, P.; Piskor-Ignatowicz, B.; Przerwa, J.; Rozek, T.; Santo, R.; Sefzick, T.; Siemaszko, M.; Smyrski, J.; Täschner, A.; Winter, P.; Wolke, M.; Wüstner, P.; Zipper, W.
General thoughts to the Kaon pair production in the threshold region
International Journal of Modern Physics A **22** (2007) 502.

24. Piskor-Ignatowicz, C.; Smyrski, J.; Moskal, P.; Adam, H.-H.; Budzanowski, A.; Czerwinski, E.; Czyzykiewicz, R.; Gil, D.; Grzonka, D.; Janusz, M.; Jarczyk, L.; Kamys, B.; Khoukaz, A.; Klaja, P.; Majewski, J.; Oelert, W.; Przerwa, J.; Ritman, J.; Rozek, T.; Sefzick, T.; Siemasko, M.; Täschner, A.; Winter, P.; Wolke, M.; Wüstner, P.; Zipper, W.
Near threshold η meson production in dp collisions
International Journal of Modern Physics A **22** (2007) 528.

25. Smyrski, J.; Adam, H.-H.; Budzanowski, A.; Czerwinski, E.; Czyzykiewicz, R.; Gil, D.; Grzonka, D.; Janusz, M.; Jarczyk, L.; Kamys, B.; Khoukaz, A.; Klaja, P.; Moskal, P.; Oelert, W.; Piskor-Ignatowicz, C.; Przerwa, J.; Ritman, J.; Rozek, T.; Sefzick, T.; Siemasko, M.; Täschner, A.; Winter, P.; Wolke, M.; Wüstner, P.; Zipper, W.
Study of the ^{3}He-η system in *dp* collisions
Nuclear Physics A **790** (2007) 438.

26. Smyrski, J.; Adam, H.-H.; Budzanowski, A.; Czerwinski, E.; Czyzykiewicz, R.; Gil, D.; Grzonka, D.; Janusz, M.; Jarczyk, L.; Kamys, B.; Khoukaz, A.; Klaja, P.; Moskal, P.; Oelert, W.; Piskor-Ignatowicz, C.; Przerwa, J.; Ritman, J.; Rozek, T.; Sefzick, T.; Siemaszko, M.; Täschner, A.; Winter, P.; Wolke, M.; Wüstner, P.; Zipper, W.
Measurement of the $dp \to {}^3\mathrm{He}\eta$ reaction near threshold
Physics Letters B **649** (2007) 258.

27. Sokolov, A.; Ritman, J.; Wintz, P.
Application of the time-dependent charge asymmetry method for longitudinal position determination in prototype proportional chambers for the PANDA experiment
Nuclear Instruments and Methods in Physics Research Section A **574** (2007) 50.

28. Speck, A.; Gabrielse, G.; Larochelle, P.; Le Sage, D.; Levitt, B.; Kolthammer, W. S.; McConnell, R.; Wrubel, J.; Grzonka, D.; Oelert, W.; Sefzick, T.; Zhang, Z.; Comeau, D.; George, M. C.; Hessels, E. A.; Storry, C. H.; Weel, M.; Walz, J.
Density and geometry of single component plasmas
Physics Letters B **650** (2007) 119.

29. Stephan, E.; Kistryn, St.; Sworst, R.; Biegun, A.; Bodek, K.; Ciepal, I.; Deltuva, A.; Epelbaum, E.; Fonseca, A.; Glöckle, W.; Golak, J.; Kalantar-Nayestanaki, N.; Kamada, H.; Kis, M.; Kozela, A.; Mahjour-Shafiei, M.; Micherdzinska, A.; Nogga, A.; Sauer, P.; Skibinski, R.; Witala, H.; Zejma, J.; Zipper, W.
Vector and tensor analyzing powers of elastic deuteron-proton scattering at 130 MeV deuteron beam energy
Physical Review C **76** (2007) 057001.

30. Thorngren Engblom, P.; Negasi Keleta, S.; Cappellaro, F.; Hoistad, B.; Jacewicz, M.; Johansson, T.; Koch, I.; Kullander, S.; Pettersson, H.; Schonning, K.; Zlomanczuk, J.; Calen, H.; Fransson, K.; Kupsc, A.; Marciniewski, P.; Wolke, M.; Pauly, C.; Demirors, L.; Scobel, W.; Stepaniak, J.; Zabierowski, J.; Bashkanov, M.; Clement, H.; Khakimova, O.; Kren, F.; Skorodko, T.
Anisotropy in the pion angular distribution of the reaction $pp \to pp\pi^0$ at 400 MeV
Physical Review C **76** (2007) 011602.

31. Trassinelli, M.; Boucard, S.; Covita, D. S.; Gotta, D.; Hirtl, A.; Indelicato, P.; Le Bigot, E.-O.; dos Santos, J. M. F.; Simons, L. M.; Stingelin, L.; Veloso, J.F.C.A.; Wasser, A.; Zmeskal, J.
He-like argon, chlorine and sulfur spectra measurement from an Electron Cyclotron Resonance Ion Trap
Journal of Physics, Conference Series **58** (2007) 129.

32. Ullrich, W.; Abdel-Bary, M.; Brinkmann, K. T.; Clement, H.; Dietrich, J.; Doroshkevich, E.; Dshemuchadse, S.; Ehrhardt, K.; Erhardt, A; Eyrich, W.; Freiesleben, H.; Gillitzer, A.; Jäkel, R.; Karsch, L.; Kilian, K.; Kuhlmann, E.; Marcello, S.; Morsch, H.-P.; Pizzolotto, C.; Ritman, J.; Roderburg, E.; Schröder, W.; Schulter-Wissermann, M.; Teufel, A.; Ucar, A.; Wenzel, R.; Wintz, P.; Wüstner, P.; Zupranski, P.
Omega meson production in proton proton collisions
International Journal of Modern Physics A **22** (2007) 621.

33. Valdau, Y.; Koptev, V.; Barsov, S.; Büscher, M.; Dymov, S.; Hartmann, M.; Kacharava, A.; Merzliakov, S.; Mikirtychyants, S.; Mussgiller, A.; Nekipelov, M.; Schleichert, R.; Ströher, H.; Wilkin, C.
The $pp \to K^+ n \Sigma^+$ reaction near threshold
Physics Letters B **652** (2007) 245.

34. Vlasov, P.; Hinterberger, F.; Povtoreiko, A.; Ritman, J.; Siudak, R.
A Cherenkov detector for WASA at COSY
International Journal of Modern Physics A **22** (2007) 612.

35. Wilkin, C.; Büscher, M.; Chiladze, D.; Dymov, S.; Hanhart, C.; Hartmann, M.; Hejny, V.; Kacharava, A.; Keshelashvili, I.; Khoukaz, A.; Maeda, Y.; Mersmann, T.; Mielke, M.; Mikirtychiants, S.; Papenbrock, M.; Rathmann, F.; Rausmann, T.; Schleichert, R.; Ströher, H.; Täschner, A.; Valdau, Yu.; Wronska, A.
Is there an η^3He quasi-bound state?
Physics Letters B **654** (2007) 92.

2. Theory

36. Avdeenkov, A.; Grümmer, F.; Kamerdzhiev, S.; Krewald, S.; Lyutorovich, N.; Speth, J.
Self-consistent calculations within the extended theory of finite Fermi systems
Physics Letters B **653** (2007) 196.

37. Baur, G.; Hencken, K.; Trautmann, D.
Electron-positron pair production in ultrarelativistic heavy ion collisions
Physics Reports **453** (2007) 1.

38. Baur, G.; Snover, K. A.; Typel, S.
E0 emission in $\alpha +^{12}$ C fusion at astrophysical energies
Physical Review C **75** (2007) 058801.

39. Baur, G.; Typel, S.
Direct reactions with exotic nuclei, nuclear structure and astrophysics
Progress in Particle and Nuclear Physics **59** (2007) 122.

40. Belushkin, M. A.; Hammer, H.-W.; Meißner, U.-G.
Dispersion analysis of the nucleon form factors including meson continua
Physical Review C **75** (2007) 035202.

41. Bernard, V.; Meißner, Ulf-G.
Chiral perturbation theory
Annual Review of Nuclear and Particle Science **57** (2007) 33.

42. Borasoy, B.; Epelbaum, E.; Krebs, H.; Lee, D.; Meißner, U.-G.
Lattice simulations for light nuclei: Chiral effective field theory at leading order
European Physical Journal A **31** (2007) 105.

43. Borasoy, B.; Epelbaum, E.; Krebs, H.; Lee, D.; Meißner, U.-G.
Two-particle scattering on the lattice: Phase shifts, spin-orbit coupling, and mixing angles
European Physical Journal A **34** (2007) 185.

44. Borasoy, B.; Bruns, P. C.; Meißner, U.-G.; Nißler, R.
A gauge invariant chiral unitary framework for kaon photo- and electroproduction on the proton
European Physical Journal A **34** (2007) 161.

45. Borasoy, B.; Epelbaum, E.; Krebs, H.; Lee, D.; Meißner, U.-G.
Two-particle scattering on the lattice: Phase shifts, spin-orbit coupling and mixing angles
European Physical Journal A **34** (2007) 185.

46. Choudhury, D.; Nogga, A.; Phillips, D. R.
Investigating neutron polarizabilities through Compton scattering on ^{3}He
Physical Review Letters **98** (2007) 232303.

47. Döring, M.
Radiative decay of the Δ(1700)
Nuclear Physics A **786** (2007) 164.

48. Döring, M.; Geng, L.S.; Oset, E.
The Radiative decay of the Λ(1405) and its two-pole structure
European Physical Journal A **32** (2007) 201.

49. Döring, M.; Koch, V.
Charge Fluctuations and electric mass in a hot meson gas
Physical Review C **76** (2007) 054906.

50. Döring, M.; Oset, E.; Strottmann, D.
Chiral dynamics in the $\pi^0\eta$ photoproduction on the proton
International Journal of Modern Physics A **22** (2007) 537.

51. Gasparyan, A.; Haidenbauer, J.; Hanhart, C.; Miyagawa, K.
ΛN scattering length from the reaction $\gamma d \to K^+\Lambda n$
European Physical Journal A **32** (2007) 61.

52. Golak, J.; Skinbinski, R.; Witala, H.; Glöckle, W.; Nogga, A.; Kamada, H.
Lorentz boosted nucleon-nucleon potential applied to the $^3\vec{\mathrm{He}}(\vec{e},e'p)pn$ and $^3\vec{\mathrm{He}}(\vec{e},e'n)pp$
Acta Physica Polonica B **38** (2007) 2143.

53. Grishina, V. Yu.; Büscher, M.; Kondratyuk, L. A.
$K^-\,^3$He and K^+K^- interactions in the $pd \to {}^3\mathrm{He}K^+K^-$ reaction
Physical Review C **75** (2007) 015208.

54. Hagen, G.; Papenbrock, T.; Dean, D. J.; Schwenk, A.; Nogga, A.; Wloch, M.; Piecuch, P.
Coupled-cluster theory for three-body Hamiltonians
Physical Review C **76** (2007) 034302.

55. Haidenbauer, J.
Meson exchange hyperon-nucleon interaction based on correlated $\pi\pi/K\bar{K}$ exchange
European Physical Journal A **33** (2007) 287.

56. Haidenbauer, J.
Meson-exchange description of hadronic systems: Recent developments
Nuclear Physics A 790 (2007) 457.

57. Haidenbauer, J.; Krein, G.; Meißner, U. G.; Sibirtsev, A.
Meson-exchange description of $\bar{D}-N$ interaction from meson-exchange and quark-gluon dynamics hadronic systems: Recent developments
European Physical Journal A **33** (2007) 107.

58. Hanhart, C.
Towards an understanding of the light scalar mesons
European Physical Journal A **31** (2007) 543.

59. Hanhart, C.; Kalashnikova, Yu. S.; Kudryavtsev, A. E.; Nefediev, A.
Two-photon decays of hadronic molecules
Physical Review D **75** (2007) 074015.

60. Hanhart, C.; Kalashnikova, Yu. S.; Kudryavtsev, A. E.; Nefediev, A. V.
Reconciling the $X(3872)$ with the near-threshold enhancement in the $D^0\bar{D}^0$ final state
Physical Review D **76** (2007) 034007.

61. Hanhart, C.; Kubis, B.; Pelaez, J. R.
Towards an understanding of a_0-f_0 mixing
Physical Review D **76** (2007) 074028.

62. Hanhart, C.; Wirzba, A.
Remarks on $NN \to NN\pi$ beyond leading order
Physics Letters B **650** (2007) 354.

63. Kalantar-Nayestanaki, N.; Epelbaum, E.
The Three-nucleon system as a laboratory for nuclear physics: The need for 3N forces
Nuclear Physics News **17** (2007) 22.

64. Krebs, H.; Epelbaum, E.; Meißner, U.-G.
Nuclear forces with Δ excitations up to next-to-next-to-leading order, part I: Peripheral nucleon-nucleon waves
European Physical Journal A **32** (2007) 127.

65. Lacour, A.; Kubis, B.; Meißner, U.-G.
Hyperon decay form factors in chiral perturbation theory
Journal of High Energy Physics **10** (2007) 083.

66. Lensky, V.; Baru, V.; Epelbaum, E.; Hanhart, C.; Haidenbauer, J.; Kudryavtsev, A.; Meißner, U. G.
Neutron-neutron scattering length from the reaction $\gamma d \to \pi^+ nn$ employing chiral perturbation theory
European Physical Journal A **33** (2007) 339.

67. Lensky, V.; Baru, V.; Haidenbauer, J.; Hanhart, C.; Kudryavtsev, A.; Meißner, U.-G.
Dispersive and absorptive corrections to the pion-deuteron scattering length
Physics Letters B **648** (2007) 46.

68. Meißner, U.-G.
Modern theory of nuclear forces A.D. 2006
European Physical Journal A **31** (2007) 397.

69. Meißner, U.-G.; Rakhimov, A. M.; Wirzba, A.; Yakhshiev, U. T.
Neutron-proton mass difference in isospin-asymmetric nuclear matter
European Physical Journal A **32** (2007) 299.

70. Meißner, U.-G.; Rakhimov, A. M.; Wirzba, A.; Yakhshiev, U. T.
Neutron-proton mass difference in nuclear matter
European Physical Journal A **31** (2007) 357.

71. Nakayama, K.; Oh, Y.; Haidenbauer, J.; Lee, T.-S. H.
On the sign of the $\pi\rho\omega$ coupling constant
Physics Letters B **648** (2007) 351.

72. Navratil, P.; Gueorguiev, V. G.; Vary, J. P.; Ormand, W. E.; Nogga, A.
Structure of $A = 10 - 13$ nuclei with two plus three-nucleon interactions from chiral effective field theory
Physical Review Letters **99** (2007) 042501.

73. Nikolaev, N. N.; Schäfer, W.; Zakharov, B. G.; Zoller, V. R.
Unitarity constraints for deep-inelastic scattering on nuclei: Predictions for electron-ion colliders
JETP Letters **84** (2007) 537.

74. Polinder, H.; Haidenbauer, J.; Meißner, U.-G.
Strangeness $S = -2$ baryon-baryon interactions using chiral effective field theory
Physics Letters B **653** (2007) 29.

75. Sibirtsev, A.; Haidenbauer, J.; Hammer, H.-W.; Meißner, U.-G.
The $pp \to K^+\Sigma^+ n$ cross-section from missing-mass spectra
European Physical Journal A **32** (2007) 229.

76. Sibirtsev, A.; Haidenbauer, J.; Krewald, S.; Meißner, U.-G.; Thomas, A. W.
$K\bar{K}$ photoproduction from protons
European Physical Journal A **31** (2007) 221.

77. Sibirtsev, A.; Haidenbauer, J.; Krewald, S.; Lee, T. S.; Meißner, U.-G.; Thomas, A. W.
Regge approach to charged-pion photoproduction at invariant energies above 2 GeV
European Physical Journal A **34** (2007) 49.

78. Sibirtsev, A.; Haidenbauer, J.; Meißner, U. G.
Comment on "Mass and $K\Lambda$ Coupling of the $N(1535)$"
Physical Review Letters **98** (2007) 039101.

79. Tertychny, G.; Tselyaev, V.; Kamerdzhiev, S.; Grümmer, F.; Krewald, S.; Speth, J.; Avdeenkov, A.; Litvinova, E.
Microscopic description of the low lying and high lying electric dipole strength in stable Ca isotopes
Physics Letters B **647** (2007) 104.

80. Tertychny, G.; Tselyaev, V.; Kamerdzhiev, S.; Grümmer, F.; Krewald, S.; Speth, J.; Litvinova, E.; Avdeenkov, A.
Pygmy dipole resonance in stable Ca isotopes
Nuclear Physics A **788** (2007) 159.

81. Tselyaev, V.; Speth, J.; Grümmer, F.; Krewald, S.; Avdeenkov, A.; Litvinova, E.; Tertychny, G.
Extended theory of finite Fermi systems: Application to the collective and noncollective E1 strength in ^{208}Pb
Physical Review C **75** (2007) 014315.

82. Uzikov, Yu. N.; Haidenbauer, J.
Spin observables of the reactions $NN \to \Delta N$ and $pd \to \Delta pp(^1S_0)$ in collinear kinematics
Physics of Atomic Nuclei **70** (2007) 2138.

83. Uzikov, Yu. N.; Haidenbauer, J.; Wilkin, C.
Dynamics of $^1S_0$ diproton formation in the $pd \to (pp)_s n$ and $pN \to (pp)_s \pi$ reactions in the GeV region
Physical Review C **75** (2007) 014008.

3. Accelerator (including conference proceedings)

84. Chechenin, A.; Senichev, Y.; Vasyukhin, N.
The Optimum Chromacity Scheme Correction for Monochromatic and Non-Monochromatic Beam in HESR
Proceedings of the 22nd Particle Accelerator Conference 2007 (PAC 2007), p. 3286.

85. Chechenin, A.; Senichev, Y.; Vasyukhin, N.
The Regular and Random Multi-pole Errors Influence on the HESR Dynamic Aperture
Proceedings of the 22nd Particle Accelerator Conference 2007 (PAC 2007), p. 3949.

86. Conradie, J.L.; Celliers, P.J.; Villiers, J.G.; Delsink, J.L.G.; du Plessis, H.; du Toit, J.H.; Fenemore, R.E.F.; Fourie, D.T.; Kohler, I.H.; Lussi, C.; Mansfield, P.T.; Mostert, H.; Muller, G.S.; Price, G.S.; Rohwer, P.F.; Sakildien, M.; Thomae, R.W.; Â van Niekerk, M.J.; van Schalkwyk, P.A.; Kormany, Z.; Dietrich, J.; Weis, T.; Adam, S.; Goetz, D.; Schmelzbach, P.A.
Improvements to the iThemba LABS Cyclotron Facilities
Proceedings of the 18th Int. Conference on Cyclotrons and their Applications.

87. Dietrich, J.; Boehme, C.; Weis, T.; Botha, A. H.; Conradie, J. L.; Rohwer, P. F.
Beam Profile Measurements Based on Light Radiation of Atoms Excited by the Particle Beam
Proceedings of the 22nd Particle Accelerator Conference 2007 (PAC 2007), p. 3955.

88. Dietrich, J.; Boehme, C.; Kamerdzhiev, V.
Beam Profile Measurements Based onBeam Interaction with Residual Gas
Proceedings of the 8th Int. Topical Meeting on Nuclear Applications and Utilization of Accelerators (ACCAPP'07), p. 138.

89. Dietrich, J.; Boehme, C.; Weis, T.; Botha, A.H.; Conradie, J.L.; Rohwer, P.F.
Beam Profile Measurements Based on Light Radiation of Atoms Excited by the Particle Beam
CARE-Report-2007-029-HIPPI.

90. Esser, F.; Eichhorn, R.; Laatsch, B.; Singer, H.; Stassen, R.
Results of the first cool down of the Juelich accelerator module
Proceedings of the International Cryogenic Engineering Conference (ICEC21), p. 51.

91. Gebel, R.; Felden, O.; Maier, R.; von Rossen, P.
Tripling the total charge perpulse of the polarized light ion source at COSY/Jülich
Proceedings of the 11th International Symposium on the Production and Neutralization of Negative Ion Beams (PNNIB 2006); AIP Conference Proceedings **925** p. 105.

92. Krisch, A. D.; Leonova, M. A.; Morozov, V. S.; Raymond, R. S.; Sivers, D. W.; Wong, V. K.; Gebel, R.; Lehrach, A.; Lorentz, B.; Maier, R.; Prasuhn, D.; Schnase, A.; Stockhorst, H.; Hinterberger, F.; Ulrich, K.
Unexpected reduction of rf spin resonance strength for stored deuteron beams
Physical Review Special Topics, Accelerators and Beams **10** (2007) 071001.

93. Krisch, A. D.; Leonova, M. A.; Morozov, V. S.; Raymond, R. S.; Sivers, D. W.; Wong, V. K.; Gebel, R.; Lehrach, A.; Lorentz, B.; Maier, R.; Prasuhn, D.; Schnase, A.; Stockhorst, H.; Hinterberger, F.; Ulrich, K.
Experimental test of the new analytic matrix formalism for spin dynamics
Physical Review Special Topics, Accelerators and Beams **10** (2007) 041001.

94. Senichev, Y.
HESR Lattice with Non-Similar Arcs for Stochastic Cooling
Proceedings of the 22nd Particle Accelerator Conference 2007 (PAC 2007), p. 3289.

95. Smirnov, A.V.; Meshkov, I.N.; Sidorin, A.O.; Dietrich, J.; Noda, A.; Shirai, T.; Souda, H.; Tongu, H.; Noda, K.
Necessary Condition for Beam Ordering
Proceedings of the Workshop on Beam Cooling and Related Topics (COOL07), p. 87.

96. Stockhorst, H.; Stassen, R.; Katayama, T.; Thorndahl, L.
Experimental Test of Momentum Cooling Model Predictions at COSY and Conclusions for WASA and HESR
Proceedings of the Symposium on Meson Physics at COSY-11 and WASA at COSY. (AIP Conference Proceedings **950**) p. 239.

97. Stockhorst, H.; Stassen, R.; Maier, R.; Prasuhn, D.; Katayama, T.; Thorndahl, L.
Stochastic Cooling for the HESR at FAIR
Proceedings of COOL 2007, p. 30.

98. Toelle, R.; Bongardt, K.; Dietrich, J.; Esser, F.; Felden, O.; Greven, R.; Hansen, G.; Klehr, F.; Lehrach, A.; Lorentz, B.; Maier, R.; Prasuhn, D.; Raccanelli, A.; Schmitt, M.; Senichev, Y.; Senicheva, E.; Stassen, R.; Stockhorst, H.; Steck, M.; Bergmark, T.; Galnander, B.; Johnson, S.; Johnson, T.; Lofnes, T.; Norman, G.; Peterson, T.; Rathsman, K.; Reistad, D.; Hinterberger, F.
HESR at FAIR: Status of Technical Planning
Proceedings of the 22nd Particle Accelerator Conference (PAC 2007), p. 1442.

4. Miscellaneous

99. Schult, O. W. B.
Die Tatsachen und der Glaube
Die Neue Ordnung **61** (2007) 275.

100. Schult, O. W. B., Feinendegen, L.E.; Shreeve, W.W.; Pierson, R.N.
Optimal use of weight and height for evaluation of obesity and other disorders
International Journal of Body Composition Research **5** (2007) 153.

C Diploma and Ph.D. Theses

1. Diploma

1. F. Ballout,
   Pion-Nucleus Scattering in Chiral Perturbation Theory,
   Universität Bonn

2. M. Freunek,
   Nucleon-Nucleon Interaction in Chiral Effective Field Theory in Configuration Space,
   Universität Bonn

3. M. Mittag,
   Messung zur Ortsabhängigkeit der Energiedeposition geladener Teilchen in Szintillationszählern am Beispiel des WASA-Zentraldetektors,
   Hochschule Merseburg (FH)

4. S. Reimann,
   Untersuchungen zum Energieverlust im Startdetektor des Flugzeitspektrometers TOF und Analyse der Reaktion $pp \rightarrow d\pi^+$ *bei 3059 MeV/c*,
   Technische Universität Dresden

5. E. Schlauch,
   Derivation of a chiral effective operator for the electromagnetic current coupling to a two-nucleon system,
   Universität Bonn

6. C. Weidemann,
   Messung der chemischen Verschiebung von $K\alpha$*- und* $K\beta$*-Übergängen in Mangan*,
   Universität zu Köln

2. Ph.D.

7. S. Dymov,
   Investigation of the deuteron breakup by protons of 0.6 – 0.9 GeV with emission of a forward proton pair,
   JINR Dubna, Russia

8. K. Grigoryev,
   A storage cell production for experiments with polarized internal gas target (PIT) at ANKE spectrometer at the COSY storage ring,
   Petersburg, Nuclear Physics Institute, Russia

9. A. Kowalczyk,
   Proton induced spallation reactions in the energy range 0.1 – 10 GeV,
   Jagellionian University Cracow, Poland

10. V. Lensky,
    Elastic and inelastic pion reactions an few nucleon systems,
    Universität Bonn

11. T.Mersmann,
    Untersuchung der η*-*^{3}*He Endzustandswechselwirkung am Experimentaufbau ANKE*,
    Universität Münster

12. V.S. Morozov,
    Using Spin Resonances to Manipulate the Polarization of Spin-1/2 and Spin-1 Particle Beams,
    University of Michigan, U.S.A.

13. C. Pizzolotto,
    Measurement of polarisation observables at the COSY-TOF spectrometer,
    Universität Erlangen

14. Z. Zhang,
    The Detection of Cold Antihydrogen Atoms,
    Universität Bochum

D Invited Talks and Colloquia

1. Baur, G.
   Strong electromagnetic fields in ultraperipheral heavy ion collisions: multiphoton processes
   ECT* Workshop on Photoproduction at Collider Energies: from RHIC and HERA to LHC
   Trento, Italy: 15.01.2007 – 19.01.2007

2. Baur, G.
   Direct reactions with exotic nuclei and nuclear astrophysics
   Nuclear Physics in Astrophysics III
   Dresden, Germany: 26.03.2007 – 31.03.2007

3. Baur, G.
   Introductory remarks on Ultraperipheral Heavy Ion Collisions (UPC)
   Session on Photon and Electroweak Boson Physics from HERA, RHIC and Tevatron to LHC, PHOTON 2007
   Paris, France: 09.07.2007 – 13.07.2007

4. Baur, G.
   Very strong electromagnetic fields for a very short time: pair production and ionization in relativistic heavy ion collisions
   Theory Group Meeting of the SPARC Collaboration Atomic Physics in Strong Fields
   Darmstadt, Germany: 17.07.2007 – 18.07.2007

5. Büscher, M.
   The Moscow-Jülich Pellet Target
   PANDA Collaboration Meeting, plenary talk
   Dubna, Russia: 02.07.2007 – 06.07.2007

6. Dietrich, J.
   HESR- Beam Diagnostics — Changes since 7/8 September 2005
   Review Meeting on Beam Diagnostics for the FAIR Project
   Darmstadt, Germany: 14.05.2007

7. Dietrich, J.
   Beam Profile Measurements Based on Light Radiation of Atoms Excited by the Particle Beam
   LANL, Los Alamos, USA: 02.07.2007

8. Dietrich, J.
   COSY — Status and Future
   LANL, Los Alamos, USA: 02.07.2007

9. Dietrich, J.
   Beam Profile Measurements Based on Beam Interaction with Residual Gas
   8th International Topical Meeting on Nuclear Applications and Utilization of Accelerators (ACCAPP'07)
   Pocatello, Id., USA: 29.07.2007 – 02.08.2007

10. Dietrich, J.
    Beam Profile Measurements Based on Light Radiation of Atoms Excited by the Particle Beam
    HIPPI 07
    Orsay, France: 26.09.2007 – 28.09.2007

11. Dietrich, J.
    Tune Measurements at COSY with Noise Excitation
    CARE-N3 networking for HHH
    Chamonix, France: 11.12.2007 – 13.12.2007

12. Dietrich, J.
    Beam Profile Measurements Based on Light Radiation of Atoms Excited by the Particle Beam
    COSY FFE Workshop
    Bad Honnef, Germany: 18.12.2007 – 19.12.2007

13. Dzyuba, A.
Study of kaon anti-kaon pair production at the ANKE spectrometer (COSY)
Seminar talk, PNPI
Gatchina, Russia: 09.01.2007

14. Dzyuba, A.
Kaon-Pair Production in Hadron-Induced Reactions at ANKE
11th International Conference on Meson-Nucleon Physics and the Structure of the Nucleon (MENU2007)
Jülich, Germany: 10.09.2007 – 14.09.2007

15. Dzyuba, A.
$K\bar{K}$-pair production near threshold in nucleon-nucleon scattering at the ANKE spectrometer
Seminar talk, PNPI
Gatchina, Russia: 23.10.2007

16. Engels, R.
The Lamb-shift Polarimeter for the polarized Fusion Experiment
Workshop on Polarized Fusion
Gatchina, Russia: 02.10.2007 – 06.10.2007

17. Engels, R.
First Experiments with the Polarized Internal Gas Target (PIT) at ANKE/COSY
12th International Workshop on Polarized Sources, Targets and Polarimeter (PSTP2007)
Brookhaven, NY, USA: 10.09.2007 – 14.09.2007

18. Engels, R.
A New Application of a Lamb-shift Polarimeter
12th International Workshop on Polarized Sources, Targets and Polarimeter (PSTP2007)
Brookhaven, NY, USA: 10.09.2007 – 14.09.2007

19. Epelbaum, E.
Subleading $3N$ interactions in chiral EFT
Workshop on Three-Nucleon Interactions from Few- to Many-Body Systems, TRIUMF
Vancouver, Canada: 12.03.2007 – 16.03.2007

20. Epelbaum, E.
Δ-resonance contributions to the nuclear force
Workshop on Effective Field Theories and Few-Nucleon Systems
Okayama, Japan: 01.06.2007 – 02.06.2007

21. Epelbaum, E.
Effective Field Theories in Nuclear Physics
Okayama University of Science, Invited lecture
Okayama, Japan: 02.06.2007

22. Epelbaum, E.
Chiral dynamics of two- and three-body systems
ECT* Workshop on Advanced Many-body Methods for Nuclear Physics
Trento, Italy: 02.06.2007 – 06.06.2007

23. Epelbaum, E.
Chiral dynamics of few-nucleon system
International Nuclear Physics Conference
Tokyo, Japan: 03.06.2007 – 08.06.2007

24. Epelbaum, E.
Chiral effective potential with Delta degrees of freedom
20th European Conference on Few-Body Problems in Physics
Pisa, Italy: 10.09.2007 – 14.09.2007

25. Epelbaum, E.
Δ-resonance contributions to the nuclear force
International Symposium on Meson-Nucleon Physics and the Structure of Hadrons
Jülich, Germany: 10.09.2007 – 14.09.2007

26. Epelbaum, E.
Few-nucleon forces and systems in chiral effective field theory
20th European Conference on Few-Body Problems in Physics
Pisa, Italy: 10.09.2007 – 14.09.2007

27. Epelbaum, E.
Effective field theory and nuclear forces
Jahrestagung des Komitees für Hadronen- und Kernphysik
Darmstadt, Germany: 25.10.2007 – 26.10.2007

28. Epelbaum, E.
Chiral dynamics in few-nucleon systems: current status and future perspectives
Bonn, Germany: 08.11.2007

29. Fedorets, P.
Droplet production from thin cryogenic jets with the Moscow-Jülich Pellet Target
Frühjahrstagung der Deutschen Physikalischen Gesellschaft
Gießen, Germany: 12.03.2007 – 16.03.2007

30. Fedorets, P.
A Frozen Pellet Target for PANDA
11th International Conference on Meson-Nucleon Physics and the Structure of the Nucleon (MENU2007)
Jülich, Germany: 10.09.2007 – 14.09.2007

31. Fedorets, P.
Presentation of MPEI and ITEP
PANDA Coordination Board Meeting, XXII. Collaboration Meeting
Darmstadt, Germany: 17.09.2007 – 19.09.2007

32. Fedorets, P.
Development of a Pellet Target for Internal Experiments
COSY-FFE Workshop and CANU Meeting
Bad Honnef, Germany: 17.12.2007 – 19.12.2007

33. Fröhlich, I.
Pluto: A Monte Carlo Simulation Tool for Hadronic Physics
XI International Workshop on Advanced Computing and Analysis Techniques in Physics Research
Amsterdam, The Netherlands: 23.04.2007 – 27.04.2007

34. Gebel, R.
Operation of the injector cyclotron JULIC for the Cooler Synchrotron COSY/Jülich
International Conference for Cyclotrons and their Applications, Cyclotrons 2007
Giardini-Naxos: 01.10.2007 – 05.10.2007

35. Gebel, R.
Polarized H^- and D^- Beams at COSY/Jülich
Polarized Sources, Targets and Polarimetry (PSTP 2007)
Brookhaven, NY, USA: 10.09.2007 – 14.09.2007

36. Goldenbaum, F.
Cosmic Rays Nucleosynthesis and Spallation Processes in the Early Galaxy
School on Pulsed Neutrons: Characterization of Materials
Trieste, Italy: 17.10.2007

37. Goldenbaum, F.
Spallation Physics and Computer Modeling
School on pulsed neutrons: Characterization of Materials (lecture, Invited by IAEA)
ICTP, Miramare, Trieste, Italy: 15.10.2007 – 26.10.2007

38. Goldenbaum, F.
Evaporation and pre-equilibrium emission and fission time scale in GeV proton-induced spallation reactions
International Conference on Nuclear Fragmentation; From basic Research to Applications (NUFRA2007)
Kemer/Antalya, Turkey: 24.09.2007 – 01.10.2007

39. Goldenbaum, F.
Evaporation, fission and pre-equilibrium emission in GeV proton-induced spallation reactions
GSI-Colloquium Talk
Darmstadt, Germany: 23.05.2007

40. Goldenbaum, F.
Progress in nuclear data for accelerator applications in Europe
International Conference on Nuclear Data for Science and Technology (ND2007)
Nice, France: 22.04.2007 – 27.04.2007

41. Gotta, D.
Pionic *NN* interactions at Threshold πN and π Atoms
Workshop on Precision Measurements at Low Energy, Paul Scherrer Institut
Villigen, Switzerland: 17.01.2007 – 18.01.2007

42. Gotta, D.
Prospects of Exotic-Atom Bragg Spectroscopy
International Workshop SPARC
Paris, France: 12.02.2007 – 15.02.2007

43. Gotta, D.
X-rays from Pionic and Antiprotonic Atoms
Atomphysik-Seminar, GSI
Darmstadt: 13.06.2007

44. Grigoryev, K.
The Polarized Internal gas Target at ANKE: a first double-polarized experiment
Frühjahrstagung der Deutschen Physikalischen Gesellschaft
Gießen, Germany: 12.03.2007 – 16.03.2007

45. Grigoryev, K.
The Polarized Internal gas Target at ANKE: a first double-polarized experiment
ANKE/PAX Workshop on SPIN PHYSICS
Ferrara, Italy: 29.06.2007 – 01.06.2007

46. Haidenbauer, J.
Hyperon-nucleon interaction
Symposium on Meson Physics at COSY-11 and WASA-at-COSY
Cracow, Poland: 17.06.2007 – 22.06.2007

47. Haidenbauer, J.
Meson production in nucleon-nucleon collisions
The 20th European Conference on Few-Body Problems in Physics
Pisa, Italy: 10.09.2007 – 14.09.2007

48. Hanhart, C.
How and when can one identify hadronic molecules in the baryon spectrum
International Conference on Baryon Spectroscopy (NSTAR2007)
Bonn, Germany: 05.09.2007 - 08.09.2007

49. Hanhart, C.
How to identify hadronic molecules
Universität Bern, seminar talk
Bern, Switzerland: 04.04.2007

50. Hanhart, C.
How to identify hadronic molecules
Universita Autonoma de Barcelona, seminar talk
Barcelona, Spain: 09.05.2007

51. Hanhart, C.
On the nature of light scalar mesons
International Workshop on Production and Decay of η and η' Mesons (Eta07)
Peniscola, Spain: 10.05.2007

52. Hanhart, C.
Reconciling the X(3872) with the near-threshold enhancement in the $D_0\,\bar{D}_0^*$ final state
International Workshop on Heavy Quarkonium 2007, DESY
Hamburg, Germany: 17.10.2007 – 20.10.2007

53. Hanhart, C.
The effect of isospin violation on scalar meson production
XII International Conference on Hadron Spectroscopy (HADRON07)
Frascati, Rome: 08.10.2007 – 13.10.2007

54. Hanhart, C.
Towards an understanding of the hadron spectrum
Universität Tübingen, seminar talk
Tübingen, Germany: 26.01.2007

55. Hanhart, C.
What we can learn from spectroscopy — and what not
BRAG2007
Bonn, Germany: 04.09.2007

56. Hügging, F.; Mertens, M.; Ritman, J.; Stockmanns, T.
Development of a Versatile Readout System for High Rate Detector Electronics 11th International Conference on Meson-Nucleon Physics and the Structure of the Nucleon (MENU2007)
Jülich, Germany: 10.09.2007 – 14.09.2007

57. Janusz, M.; Yurev, L.
From Charged tracks to the ChPT anomalies
11th International Conference on Meson-Nucleon Physics and the Structure of the Nucleon (MENU2007)
Jülich, Germany: 10.09.2007 – 14.09.2007

58. Jany, B.R.
η' Decays with WASA-at-COSY
11th International Conference on Meson-Nucleon Physics and the Structure of the Nucleon (MENU2007)
Jülich, Germany: 10.09.2007 – 14.09.2007

59. Kleines, H.; Zwoll, K.; Wüstner, P.; Erven, W.; Kämmerling, P.; Kemmerling, G.; Loevenich, H.; Ackens, A.; Wolke, M.; Hejny, V.; Ohm, H.; Sefzick, T.; Nellen, R.; Marciniewski, P.; Fransson, K.; Gustafsson, L.; Kupsc, A.; Calen, H.
Performance Issues of the New DAQ System for WASA at COSY
15th IEEE Real Time Conference 2007 (RT 07)
Batavia, Ill., USA: 29.04.2007 – 04.05.2007

60. Krewald, S.
Baryon resonance analysis with the Jülich meson exchange model
Workshop on the Physics of Excited Nucleons (NSTAR2007)
Bonn, Germany: 05.09.2007 – 08.09.2007

61. Krewald, S.
Extendend Theory of Finite Fermi Systems
The 3rd Japanese-German EFES(JSPS)-DFG/GSI Workshop on Nuclear Structure and Astrophysics
Frauenwoerth, Germany: 29.09.2007 – 02.10.2007

62. Lehrach, A.
General Design Criteria, Lattice Concepts and Structures for HESR
Review Meeting MiniTAC Lattice for the FAIR Project
Darmstadt, Germany: 5.6.2007

63. Lehrach, A.
HESR Design
Review Meeting TAC for the FAIR Project
Darmstadt, Germany: 11. – 13.06.2007

64. Lehrach, A.
Fixed Target and Collider Options for HESR at FAIR
Hard QCD with Antiprotons at GSI FAIR
Trento, Italy: 16. – 20.07.2007

65. Lehrach, A.
High-Energy Storage Ring (HESR)
11th International Conference on Meson-Nucleon Physics and the Structure of the Nucleon (MENU2007)
Jülich, Germany: 10.09.2007 – 14.09.2007

66. Lehrach, A.
Relevant storage ring properties and limitations
Workshop on Polarized Antiproton Beams — How?
Daresbury, England: 29. – 31.08.2007

67. Meißner, U.-G.
On the low-energy constants of the chiral effective pion-nucleon Lagrangian
Workshop on Three-Nucleon Interactions from Few- to Many-Body Systems
TRIUMF, Vancouver, Canada: 12.03.2007 – 16.03.2007

68. Meißner, U.-G.
HadronTH: Structure and dynamics of hadrons
I3HP Collaboration Committee Meeting
Frascati, Italy: 20.05.2007

69. Meißner, U.-G.
Nucleon from factors from dispersion theory
Jefferson Lab User Group Meeting 2007
Newport News, USA: 18.06.2007 – 20.06.2007

70. Meißner, U.-G.
Hadronic atoms
International Conference on Hadron Physics TROIA'07
Canakkale, Spain: 30.08.2007 – 01.09.2007

71. Meißner, U.-G.
QCDnet: Hadron physics with light and heavy quarks
I3 HadronPhysics2 Opening Meeting
Frascati, Italy: 28.09.2007 – 29.09.2007

72. Meißner, U.-G.
Quark mass dependence of baryons
HadronTHÂ´07 Workshop
Barcelona, Spain: 01.10.2007 – 05.10.2007

73. Meißner, U.-G.
Three-nucleon forces from effective field theory: Why Fujita and Miyazawa were not just lucky
International Symposium on New Facet of Three Nucleon Force — 50 years of Fujita-Miyazawa Three Nucleon Force (FM50)
Tokyo, Japan: 29.10.2007 – 31.10.2007

74. Nekipelov, M.
Present Understanding of Spin-Filtering Experiments
11th International Conference on Meson-Nucleon Physics and the Structure of the Nucleon (MENU2007)
Jülich, Germany: 10.09.2007 – 14.09.2007

75. Nogga, A.
Approaching light nuclei and hypernuclei based on chiral interactions
20. European Conference on Few-Body Problems in Physics (EFB20)
Pisa, Italy: 10.09.2007

76. Nogga, A.
Correlations in few-nucleon systems
Workshop on Dense and Cold Nuclear Matter and Hard Exclusive Processes
Ghent, Belgium: 20.08.2007 – 24.08.2007

77. Nogga, A.
Understanding light nuclei based on simulations
VSR-Seminar
Jülich, Germany: 12.12.2007

78. Oelert, W.
Antimaterie — 10 Jahre danach
Haus Overbach
Jülich, Germany: 19.01.2007

79. Oelert, W.
AD-Physics 2007 and Beyond
Workshop AB-Division, CERN
Geneva, Switzerland: 23.01.2007

80. Oelert, W.
Antimaterie — die gespiegelte Welt — die geheimnisvolle Materie aus Antiteilchen - I
Seminar für Schüler des Ansbachgymnasiums
Jülich, Germany: 13.03.2007

81. Oelert, W.
Antimaterie — die gespiegelte Welt — die geheimnisvolle Materie aus Antiteilchen - II Seminar für Schüler des Ansbachgymnasiums
Jülich, Germany: 15.03.2007

82. Oelert, W.
Antimatter — the mirrored world of matter
Polish Academy of Art and Sciences
Cracow, Poland: 29.05.2007

83. Oelert, W.
Production of Antihydrogen
Jagellonian University, Physics Institute
Cracow, Poland: 30.05.2007

84. Polinder, H.
Hyperon-nucleon interactions in effective field theory
Workshop on Hadron Physics with COSY-TOF
Jülich, Germany: 20.03.2007 – 21.03.2007

85. Polinder, H.
$S = -1, -2$ baryon-baryon interactions in chiral effective field theory
International Nuclear Physics Conference (INPC2007)
Tokyo, Japan: 03.06.2007 – 08.06.2007

86. Polinder, H.
Strange two-baryon interactions using chiral effective field theory
20th European Conference on Few-Body Problems in Physics (EFB20)
Pisa, Italy: 10.09.2007 – 14.09.2007

87. Redmer, C.F.
In search of the box anomaly with the WASA-at-COSY facility
Symposium on Meson Physics at COSY-11 and WASA-at-COSY
Cracow, Poland: 17.06.2007 – 22.06.2007

88. Redmer, C.F.
In search of the box anomaly with the WASA-at-COSY facility
11th International Conference on Meson-Nucleon Physics and the Structure of the Nucleon (MENU2007)
Jülich, Germany: 10.08.2007 – 14.08.2007

89. Ritman, J.
Investigations of fundamental Symmetries in Hadronic Systems — Start of WASA-at-COSY
International Workshop XXXV on Gross Properties of Nuclei and Nuclear Excitations
Hirschegg, Austria: 14.01.2007 – 20.01.2007

90. Ritman, J.
WASA-at-COSY
Internationales Graduierten-Kolleg, Universität Giessen
Giessen, Germany: 24.05.2007

91. Ritman, J.
FAIR: a Horizon for Future Charming Physics
Symposium on Meson Physics at COSY11 and WASA-at-COSY
Cracow, Poland: 19.06.2007 – 20.06.2007

92. Ritman, J.
Hadron Physics Experiments at the COSY Facility
XII International Conference on Hadron Spectroscopy (HADRON07)
Frascati, Italy: 08.10.2007 – 10.10.2007

93. Ritman, J.
Perspektiven Hadronischer Sonden
Jahrestreffen des Komittee Hadronen- und Kernphysik
Darmstadt, Germany: 25.10.2007 – 26.10.2007

94. Senichev, Y.
The advanced HESR lattice for improved stochastic cooling
COOL 2007
Bad Kreuznach, Germany: 10.09.2007 – 14.09.2007

95. Senichev, Y.
Possible lattices with imaginary gamma-transition for PS2: why and how?
BEAM 2007, CERN
Geneva, Switzerland: 01.10.2007 – 05.10.2007

96. Stockhorst, H.; Stassen, R.; Katayama, T.; Thorndahl, L.
Experimental Test of Momentum Cooling Model Predictions at COSY and Conclusions for WASA and HESR
Symposium on Meson Physics at COSY-11 and WASA-at-COSY
Cracow, Poland: 17.06.2007 – 22.06.2007

97. Stockhorst, H.; Stassen, R.; Katayama, T.; Thorndahl, L.
Theory of Stochastic Momentum Cooling
Symposium on Meson Physics at COSY-11 and WASA-at-COSY
Cracow, Poland: 17.06.2007 – 22.06.2007

98. Stockhorst, H.; Stassen, R.; Maier, R.; Prasuhn, D.; Katayama, T.; Thorndahl, L.
Stochastic Cooling for the HESR at FAIR
Workshop on Beam Cooling and Related Topics (COOL07)
Bad Kreuznach, Germany: 10.09.2007 – 14.09.2007

99. Stockmanns, T.; Hügging, F.; Mertens, M.; Ritman, J.
A high rate, high resolution Micro-Vertex-Detector for the PANDA-Experiment
11th International Conference on Meson-Nucleon Physics and the Structure of the Nucleon (MENU2007)
Jülich, Germany: 10.09.2007 – 14.09.2007

100. Stockmanns, T.
Open and hidden charm at PANDA
XII International Conference on Hadron Spectroscopy (HADRON07)
Frascati, Italy: 08.10.2007 – 13.10.2007

101. Strauch, T.
Pionic Deuterium
Frühjahrstagung der Deutschen Physikalischen Gesellschaft
Gießen, Germany: 12.03.2007 – 16.03.2007

102. Strauch, T.
Pionic Deuterium
11th International Conference on Meson-Nucleon Physics and the Structure of the Nucleon (MENU2007)
Jülich, Germany: 10.09.2007 – 14.09.2007

103. Ströher, H.
How to polarize antiprotons and what to do with it?
Hirschegg 2007: Structure and Dynamics of Hadrons
Hirschegg, Austria: 17.01.2007

104. Ströher, H.
Programm Physik der Hadronen
Helmholtz Forschungsbereich Struktur der Materie
Berlin, Germany: 03.04.2007

105. Ströher, H.
From ANKE/COSY to PAX/FAIR
ANKE-PAX Collaboration Meeting/Workshop on Spin Physics
Ferrara, Italy: 30.04.2007

106. Ströher, H.
Workshop Summary
ANKE-PAX Collaboration Meeting/Workshop on Spin Physics
Ferrara, Italy: 01.05.2007

107. Wirzba, A.
The Casimir effect as scattering problem
Workshop on Quantum Field Theory under the Influence of External Conditions (QFEXT07)
Leipzig, Germany: 16.09.2007 – 21.09.2007

108. Wolke, M.
WASA-at-COSY — Symmetries and Symmetry Breaking
Kernphysikalisches Kolloquium, Universität Bonn
Bonn, Germany: 25.01.2007

109. Wolke, M.
Status report on the experiments with WASA-at-COSY
2nd International EtaMesonNet Workshop (ETA07)
Peniscola, Spain: 10.05.2007 – 11.05.2007

110. Wolke, M.
From the candle COSY-11 to the flambeau (fackla) of WASA-at-COSY: a ship we entered to study symmetries in nature
Symposium on Meson Physics at COSY-11 and WASA-at-COSY
Cracow, Polen: 17.06.2007 – 22.06.2007

111. Wolke, M.
η Meson Decays with WASA-at-COSY
11th International Conference on Meson-Nucleon Physics and the Structure of the Nucleon (MENU2007)
Jülich, Germany: 10.09.2007 – 14.09.2007

112. Wolke, M.
Hadronenphysik an COSY
KHuK Jahrestreffen
Darmstadt, Germany: 26.10.2007 – 27.10.2007

113. Yuan, X.
Measurement of the reaction $dd \to \alpha K^+ K^-$ with ANKE/COSY
Frühjahrstagung der Deutschen Physikalischen Gesellschaft
Gießen, Germany: 12.03.2007 – 16.03.2007

114. Yuan, X.
Measurement of the reaction $dd \to \alpha K^+K^-$ with ANKE/COSY
11th International Conference on Meson-Nucleon Physics and the Structure of the Nucleon (MENU2007)
Jülich, Germany: 10.09.2007 – 14.09.2007

115. Zychor, I.
Studies of $\Lambda(1405)$ in pp Collisions with ANKE at COSY-Jülich
11th International Conference on Meson-Nucleon Physics and the Structure of the Nucleon (MENU2007)
Jülich, Germany: 10.09.2007 – 14.09.2007

E Funded Projects

Project	Responsible	Partner Institute	Funded by
Virtual Institute Spin and Strong QCD	U.-G. Meißner	GSI, Univ.'s Bern, Bonn, Ferrara, Cracow, Torino	HGF
CARE	R. Tölle		EU/FP6
TA-COSY	D. Grzonka		EU/FP6
Hadron Physics Theory Netzwerk	U.-G. Meißner	Network	EU/FP6
EtaMesonNet	W. Oelert	Network	EU/FP6
Pellet Target	M. Büscher	ITEP, MPEI Moscow (Russia)	EU/FP6
EURONS/EXL	D. Grzonka		EU/FP6
EUROTRANS/NUDATRA	F. Goldenbaum		EU/FP6
DIRAC Secondary Beams	R. Tölle		EU/FP6
DIRAC Phase 1	R. Tölle		EU/FP6
DIRAC Secondary Beams PANDA-4	J. Ritman		EU/FP6
DIRAC Second. Beams PANDA-2	J. Ritman		EU/FP6
Advanced Residual Gas Profile Monitor	J. Dietrich	GSI	EU/FP6
Design Study for Pick-up Electronic Development	J. Dietrich	GSI	EU/FP6
Strange and Charmed Scalar Mesonss	M. Büscher	ITEP, INR Moscow (Russia)	DFG
Light Scalar Resonances $a_0/f_0(980)$	M. Büscher	ITEP, MPEI Moscow (Russia)	DFG
Scalar Mesons	M. Büscher	ITEP, INR Moscow (Russia)	DFG
Pellet Target	M. Büscher	ITEP, MPEI Moscow (Russia)	DFG
K^- Production in Nuclei	M. Hartmann	ITEP Moscow (Russia)	DFG
Isospin Violation	M. Büscher	IMP Lanzhou (China)	DFG
Jets in Hard Processes	N.N. Nikolaev	Landau Inst., ITEP Moscow (Russia)	DFG
Properties of Unstable Nuclei	S. Krewald	Petersburg State Univ., IPPE Obninsk (Russia)	DFG
Pion Reactions on Few Nucleon Systems	C. Hanhart	ITEP Moscow (Russia)	DFG
Quark-gluon degrees of freedom in the confinement region of QCD	J. Haidenbauer	UNESP Sao Paulo (Brasil)	DFG
ATRAP	W. Oelert	Univ. Mainz	DFG
Fundamental Research with Hadrons	W. Oelert	Jagellinian Univ. Cracow (Poland)	DFG
Broken Symmetries	H. Machner	Univ. Helsinki (Finland)	DAAD
PPP Poland	P.v. Rossen		DAAD
Rare Decays of η and η' Mesons	S. Schadmand	Indian Inst. of Technology Bombay	DAAD/DST India
Spin observables in $\vec{d}\vec{p}\to\{pN\}N$ at low transferred momenta	J. Haidenbauer	JINR Dubna (Russia)	Heisenberg-Landau Program
Eta-Meson Physics	H. Machner	BARC Mumbai (India)	Int. Büro BMBF
Target Development for nuclear physics experiments at COSY and AEA cyclotron	J. Ritman	AEA Cairo (Egypt)	Int. Büro BMBF
Medical Applications of Accelerators	J. Dietrich	iThemba LABS (South Africa)	Int. Büro BMBF
A Pellet Target for PANDA	M. Büscher	ITEP, MPEI Moscow (Russia) Uppsala Univ. (Sweden), GSI	INTAS
Advanced Beam Dynamic for Storage Rings	A. Lehrach		INTAS
EM-processes in the peripheral collisions of relativistic and ultrarelativistic heavy ions	G. Baur	Belfast, Tashkent, Arkhangelsk	GSI-INTAS
Projectile Electron Losses in the Collisions of Fast and Relativistic Low Charged Ions	G. Baur	GSI, Stockholm, Tashkent, Moscow, Arkhangelsk	GSI-INTAS
Polarized Target	F. Rathmann	PNPI Gatchina (Russia)	ISTC
Few Nucleon Systems in χEFT	E. Epelbaum	Univ. Bonn	HGF
Baryon Resonance Analysis	U.-G. Meißner	JLAB (U.S.A.)	JLAB

F COSY-FFE Projects

Project	Responsible	Institute
Θ^+ und Anti-decuplet	Prof. K. Goeke	Univ. Bochum
Frozen Spin Target	Prof. W. Meyer	Univ. Bochum
Entwicklung von Software zur Teilchenidentifikation und Erkennung von split-offs im el.-magn. Kalorimeter des WASA-Experiments	Prof. U. Wiedner	Univ. Bochum
Zusammenarbeit von HISKP-Bonn an internen Experimenten an COSY	Prof. J. Bisplinghoff	Univ. Bonn
Polarisiertes Target für TOF	Dr. H. Dutz	Univ. Bonn
Theorectical studies of strangeness and charm production at COSY and PANDA/FAIR	Prof. H.-W. Hammer	Univ. Bonn
Entwicklung eines Partialwellenprogrammes für die Analyse von Daten von WASA	Prof. E. Klempt	Univ. Bonn
Zusammenarbeit an COSY H-Strahl Laserdiagnose	Prof. T. Weis	Univ. Dortmund
COSY-TOF detector	Prof. H. Freiesleben	TU Dresden
Bau von Detektoren für ANKE und K^--Nachweis	Prof. B. Kämpfer	FZ Dresden-Rossendorf
Measurement of the degree of polarisation of laser accelerated protons	Prof. O. Willi	Univ. Düsseldorf
Theoretische Untersuchungen zur künftigen COSY-Physik	Prof. M. Dillig	Univ. Erlangen-Nürnberg
Bau eines Cherenkovdetektors für WASA at COSY	Prof. W. Eyrich	Univ. Erlangen-Nürnberg
Experimente mit COSY-TOF	Prof. W. Eyrich	Univ. Erlangen-Nürnberg
Polarization experiments with ANKE at COSY	Prof. E. Steffens	Univ. Erlangen-Nürnberg
Meson production and resonance properties in the coupled channel K-Matix approach	Prof. U. Mosel	Univ. Gießen
ANKE Experiment und Auswertung $pp \to dK^+\bar{K}^0$	Prof. H. Paetz gen. Schieck	Univ. Köln
Schwellenexperimente an COSY-11 und ANKE	Dr. A. Khoukaz	Univ. Münster
Installation und Inbetriebnahme des WASA-Detektors am COSY-Ring und Durchführung von Experimenten an WASA at COSY	Prof. H. Clement	Univ. Tübingen
Experimente an COSY-TOF	Prof. H. Clement	Univ. Tübingen
Polarized internal target for ANKE at COSY	Prof. M. Nioradze	Tbilisi State Univ. (Georgia)
Spin dependence in *pd* interactions	Prof. P. Dalpiaz	Univ. Ferrara (Italy)
Photonendetektor an ANKE	Prof. A. Magiera	Jagellinian Univ. Cracow (Poland)
WASA at COSY	Prof. M. Jezabek	INP Crakow (Poland)
Strange Baryon Produktion at ANKE	Prof. Z. Sujkowski	IPJ Otwock-Swierk (Poland)
Neutron tagging and strangeness production at ANKE	Dr. V. Koptev	PNPI Gatchina (Russia)
Set-up and research with the spectator/vertex detection system at ANKE-COSY	Prof. V. Kulikov	JINR Dubna (Russia)
Investigation of scalar meson production in *pp*, *pd* and *dd* collisions	Prof. L. Kondratyuk	ITEP Moscow (Russia)
Development of a frozen-pellet target	Dr. A. Gerasimov	ITEP Moscow (Russia)
Development, commissioning and operation of components for the COSY experiments WASA and ANKE and spin-filtering studies at COSY as preparation of the PAX experiment in the framework of the FAIR project at GSI	Dr. A. Vasilyev	PNPI Gatchina (Russia)
Development of online software tools for COSY-TOF	Prof. V.N. Afanasiev	MIEM Moscow (Russia)
Cooperation COSY-WASA for $pp \to pp\eta$ and $pp \to pp\eta\pi^0$	Prof. T. Johansson	Uppsala Univ. (Sweden)
Search for mixing between light mesons	Prof. A. Rudchik	INR Kiev (Ukraine)
Unified analysis of meson production in hadronic reactions	Prof. K. Nakayama	Univ. of Georgia (U.S.A.)
SPIN@COSY: Spin-Manipulating Polarized Deuterons and Protons	Prof. A. Krisch	Univ. of Michigan (U.S.A.)

G Conferences (co-)organized by the IKP

G.1 The 11th International Conference on Meson-Nucleon Physics and the Structure of the Nucleon, MENU2007

The common aspects in both the charmed quark sector and in the light quark sector were the major reason to bring together 354 experts from high-energy physics and nuclear physics to the 11th International Conference on Meson-Nucleon Physics and the Structure of the Nucleon, which took place on 10–14 September at the FZJ.

The plenary talks summarized the progress in light quark physics, such as in studies of η and η' decay, exotic atoms, three-nucleon forces, and lattice methods and recent discoveries of particles both with open and hidden charm, and the opportunities opened by studying the decays of those particles. The progress at the new Japanese facility JPARC, the European FAIR project, and the 12 GeV upgrade at the Thomas Jefferson Laboratory were presented in detail. There were five parallel sessions covering special topics such as spin physics, meson and baryon spectroscopy, lattice calculations and in-medium physics. Willem Van Oers, Manitoba University, spoke as the representative of the International Union of Pure and Applied Physics who together with FZJ, Deutsche Forschungsgemeinschaft, Jefferson Lab, and the Hadron Physics I3 FP6 European Community Programme made this conference possible. The next MENU conference will be held in Newport News, Virginia, in 2010. Reports about the conference can be found in the March issue of the CERN courier, http://cerncourier.com/cws/latest/cern, and in the Nuclear Physics News International, http://www.nupecc.org/nupecc. Proceedings are on the econf archive at SLAC. For slides of the talks, see www.fz-juelich.de/ikp/menu2007.

G.2 Symposium on Meson Physics at COSY-11 and WASA-at-COSY, Cracow (Poland)

The international Symposium on Meson Physics at COSY-11 and WASA-at-COSY was held in Cracow from June 17–22 on the occasion of the completion of the COSY-11 experiment. It also coincided with the beginning of the experimentation with the WASA apparatus which was successfully transferred from CELSIUS facility in Uppsala to the cooler synchrotron COSY.
Since the core of the COSY-11 group is based on an exemplary German-Polish collaboration, the main sessions took place in Libraria of the Collegium Maius at Jagellonian University. This location has great significance as it is where Nicolaus Copernicus learned astronomy.

Fig. 2: Participants of the symposium on Meson Physics at COSY-11 and WASA-at-COSY in the medieval courtyard of the Collegium Maius of the Jagellonian University.

In the first part of the meeting the scientific achievements of the COSY-11 group were summarized and the status on the ongoing data evaluation for more than ten projects was reported. The second part of the symposium was devoted to the prospects for studies of the fundamental symmetries by means of the η and η' decays with the newly commissioned WASA-at-COSY facility.

Fig. 1: MENU2007 participants in front of the lecture hall of FZJ

Fig. 3: Participants of the WASA-at-COSY analysis meeting in front of the main building of the Institute of Nuclear Physics in Cracow.

The physics of the η and η' mesons receives increasing interest with complementary experimental programmes planned at DAΦNE-2 and MAMI-C facilities. The plans were presented by invited guests from these laboratories. The symposium continued at the Institute of Nuclear Physics in Cracow where the participants met to discuss the status of the simulations and the data analysis from the first WASA-at-COSY production run in April 2007. Written contributions have been published in volume 950 of the International Conference Proceedings Series of the American Institute of Physics. The symposium was jointly organized by the Jagellonian University, Institute of Nuclear Physics PAN, IKP of the Research Center Jülich and the University of Silesia. More information regarding the meeting is available via http://confer.uj.edu.pl/COSY-11/07/.

G.3 INTAS Meeting Pellet Targets, Moscow (Russia)

The preparation of the pellet target for PANDA is supported by an INTAS project (06-1000012-8787). The consortium comprises the IKP/FZJ, ITEP and MPEI (both Moscow), Uppsala University and GSI-Darmstadt. On June 29 representatives of all institutes met at ITEP for a project kick-off meeting.

Fig. 4: Participants of the first INTAS consortium meeting on pellet targets at ITEP.

Within the INTAS consortium the IKP is in charge of the project coordination and of the tests with the target prototype which is located in the COSY accelerator hall.

G.4 The Workshop on the Physics of Excited Nucleon, NSTAR2007

The excitation spectrum of the nucleon promises to offer important insights into the non-perturbative regime of QCD. Dedicated experimental programs at various laboratories exist to perform accurate measurements of the meson photo- and electroproduction off the nucleon, studying the excitation of the nucleon. This workshop is the 6th in a series of meetings since 2000 (Co-organizer U.-G. Meißner).

H Teaching Positions

Institute	Name	University
IKP-1	PD Dr. A. Gillitzer	Bonn
	PD Dr. F. Goldenbaum	Wuppertal
	Prof. Dr. H. Machner	Duisburg-Essen
	Prof. Dr. W. Oelert	Bochum
	Prof. Dr. J. Ritman	Bochum
	PD Dr. S. Schadmand	Gießen
IKP-2	PD Dr. M. Büscher	Köln
	PD Dr. D. Gotta	Köln
	PD Dr. F. Rathmann	Erlangen-Nürnberg
	Prof. Dr. H. Ströher	Köln
	Dr. M. Wolke	Bochum
IKP-3	Prof. Dr. G. Baur	Basel
	Prof. Dr. E. Epelbaum	Bonn
	Univ. Doz. Dr. J. Haidenbauer	Graz
	PD Dr. C. Hanhart	Bonn
	Prof. Dr. S. Krewald	Bonn
	Prof. Dr. U.-G. Meißner	Bonn
	Prof. Dr. N.N. Nikolaev	Moscow
	Dr. A. Nogga	Bonn
	PD Dr. A. Wirzba	Bonn
IKP-4	Prof. Dr. Dr. h.c. J. Dietrich	Dortmund
	Dr. A. Lehrach	Bonn
	Prof. Dr. R. Maier	Bonn

I Beam Time at COSY 2007

Date	Experiment	Duration	Reaction
12.01.07–22.01.07	ANKE	1 week	pol.deuterons, 146.2+159
22.01.–29.01.	ANKE	1 week	$\vec{d}\vec{p} \to ppn$, 172
02.02.–12.02.	GEM	1 week	$\vec{d}p \to ppn$, 148.1
16.02.–21.03.	ANKE	5 weeks	$pA \to \alpha K^+K^-X$, 147.2
06.04.–07.05.	WASA	4 weeks	$pp \to pp\eta(\to 3\pi)$, 167
11.05.–21.05.	SPIN@COSY	1 week	$\vec{d}$ beam, 170
25.05.–04.06.	TOF	1 week	$\vec{p}p \to pp\omega$, 129.2
04.06.–11.06.	TOF	1 week	$\vec{p}p \to pK^0\Sigma^+$, 141.3
11.06.–18.06.	TOF	1 week	$\vec{p}d \to pK^0\Lambda p$,141.3
18.06.–02.07.	ANKE-PAX	2 weeks	$\vec{p}$ beam, 169
07.09.–17.09.	ANKE	1 week	$pp \to K^+\Sigma^+n$, 171.1
21.09.–08.10.	WASA	2 weeks	commissioning, 136.5
12.10.–22.10.	ANKE	1 week	$\vec{d}p \to {}^3\mathrm{He}\,\eta$, 157.1
26.10.–05.11.	ANKE	1 week	$\vec{p}p \to (pp)_s\pi^0$, 158.1
09.11.–19.11.	ANKE-PAX	1 week	pol.lifetime, 169.1
20.11.–26.11.	WASA	1 week	$pd \to Scalars$, 174
27.11.–04.12.	WASA	1 week	$dd \to {}^3\mathrm{He}\,n\pi^0$, 173
04.12.–19.12.	WASA	2 weeks	$dd \to \alpha 2\pi$, 174
Total ’07		28 weeks	

J Personnel

J.1 Scientific Staff

F. Ballout (IKP-3) (until 31 May, 2007)

Prof. Dr. G. Baur (IKP-3)

Dr. U. Bechstedt (IKP-4)

Dr. K. Bongardt (IKP-4)

DI N. Bongers (IKP-4)

DI W. Borgs (IKP-2) (until 30 April, 2007)

DI R. Brings (IKP-4)

PD Dr. M. Büscher (IKP-2)

DP A. Chechenin (IKP-4)

DP A. Chechenin (IKP-4)

DP E. Czerwinski (IKP-1) (since 1 October, 2007)

DP D. Chiladze (IKP-2)

Prof. Dr.Dr.h.c. J. Dietrich (IKP-4)

Dr. A. Djalois (IKP-1)

Dr. M. Döring (IKP-3) (since 1 October, 2007)

Dr. R. Engels (IKP-2)

Prof. Dr. E. Epelbaum (IKP-3)

DI F.-J. Etzkorn (IKP-4)

Dr. P. Fedorets (IKP-2)

Dr. O. Felden (IKP-TA)

M. Freunek (IKP-3) (until 15 May, 2007)

Dr. W. Gast (IKP-1)

Dr. R. Gebel (IKP-4)

Dr. M. George (IKP-1) (since 1 April 2007)

PD Dr. A. Gillitzer (IKP-1)

PD Dr. F. Goldenbaum (IKP-1)

PD Dr. D. Gotta (IKP-2)

DI R. Greven (IKP-4) (since 1 January, 2007)

Dr. F. Grümmer (IKP-3)

Dr. D. Grzonka (IKP-1)

DI W. Günther (IKP-4)

Dr. F.-K. Guo (IKP-3) (since 1 October, 2007)

Univ. Doz. Dr. J. Haidenbauer (IKP-3)

PD Dr. C. Hanhart (IKP-3)

Dr. M. Hartmann (IKP-2)

M. Hausner (IKP-3) (since 1 August 2007)

Dr. V. Hejny (IKP-2)

DI K. Henn (IKP-4)

DP M. Hodana (IKP-1) (since 1 November, 2007)

Dr. F. Hügging (IKP-1)

Dr. V. Kamerdjiev (IKP-4)

D. Khaneft (IKP-2) (since 21 June 2007)

DP D. Kirillov (IKP-4) (until 18 December 2007)

DP P. Klaja (IKP-1)

A. Klingler (IKP-2)

St. Kölling (IKP-3) (since 16 April, 2007)

DP A. Kowalczyk (IKP-1) (until 28 February, 2007)

Dr. H. Krebs (IKP-3)

Prof. Dr. S. Krewald (IKP-3)

DI K. Kruck (IKP-4)

Dr. A. Lehrach (IKP-4)

DP V. Lensky (IKP-3) (until 7 June, 2007)

Dr. B. Lorentz (IKP-4)

Prof. Dr. H. Machner (IKP-1)

Prof. Dr. R. Maier (IKP-4)

Prof. Dr. U.-G. Meißner (IKP-3)

DP M. Mertens (IKP-1)

D. Minossi (IKP-3) (since 16 April, 2007)

DI I. Mohos (IKP-4)

Dr. M. Nekipelov (IKP-2)

Prof. Dr. N.N. Nikolaev (IKP-3)

Dr. A. Nogga (IKP-3)

Prof. Dr. W. Oelert (IKP-1)

DP D. Oellers (IKP-2)

Dr. H. Ohm (IKP-2)

DI N. Paul (IKP-1)

Dr. C. Pauly (IKP-1)

Dr. M. Pavon-Valderrama (IKP-3) (since 1 June 2007)

Dr. H. Polinder (IKP-3) (until 30 September, 2007)

Dr. D. Prasuhn (IKP-4)

DP D. Protic (IKP-TA)

DP J. Przerwa (IKP-1)

PD Dr. F. Rathmann (IKP-2)

DP Ch.F. Redmer (IKP-1)

DI A. Richert (IKP-4)
Prof. Dr. J. Ritman (IKP-1)
Dr. E. Roderburg (IKP-1)
DI J. Sarkadi (IKP-TA)
DP P. Saviankou (IKP-3)
Dr. H. Schaal (IKP-1)
PD Dr. S. Schadmand (IKP-1)
E. Schlauch (IKP-3) (until 14 January, 2007)
Dr. R. Schleichert (IKP-2)
DI M. Schmitt (IKP-4) (since 1 May, 2007)
DI H. Schneider (IKP-4) (until 30 September 2007)
DI G. Schug (IKP-4)
Dr. Th. Sefzick (IKP-TA)
DI E. Senicheva (IKP-4)
Dr. Y. Senichev (IKP-4)
DI M. Simon (IKP-4)
Dr. A. Sokolov (IKP-1)
Dr. R. Stassen (IKP-4)
Dr. H. Stockhorst (IKP-4)
Dr. T. Stockmanns (IKP-1)
DP Th. Strauch (IKP-2)
Prof. Dr. H. Ströher (IKP-2)
T. Tolba (IKP-1)
Dr. R. Tölle (IKP-4)
DI T. Vashegyi (IKP-4)
Dr. N. Vasiukhin (IKP-4)
DP P. Vlasov (IKP-1)
Chr. Weidemann (IKP-2)
DP D. Welsch (IKP-4)
M. P. Westig (IKP-2) (since 15 June 2007)
Dr. P. Wintz (IKP-1)
PD Dr. A. Wirzba (IKP-3)
DI J.-D. Witt (IKP-4)
Dr. M. Wolke (IKP-2)
Dr. E. Zaplatin (IKP-4)
F. Zarife (IKP-4) (since 15 March 2007)
DP D. Z. Zhang (IKP-1)

J.2 Technical and Administrative Staff

J. Ahlschläger (IKP-4) (since 1 March, 2007)

C. Berchem (IKP-TA)

P. Birx (IKP-4)

M. Böhnke (IKP-4)

H. Bongen (IKP-1)

J. Borsch (IKP-TA)

P. Brittner (IKP-4)

J. But (IKP-TA)

M. Comuth-Werner (IKP-TA)

B. Dahmen (IKP-4)

C. Deliege (IKP-4)

W. Derissen (IKP-TA)

N. Dolfus (IKP-TA)

G. D'Orsaneo (IKP-2)

R. Dosdall (IKP-1)

R. Enge (IKP-4)

B. Erkes (IKP-4)

W. Ernst (IKP-TA)

K. Esser (IKP-TA)

H.-P. Faber (IKP-4)

G. Fiori (IKP-TA)

H.-W. Firmenich (IKP-TA)

J. Göbbels (IKP-TA)

H. Hadamek (IKP-TA)

R. Hecker (IKP-4)

E. Heßler (IKP-TA)

M. Holona (IKP-TA)

H.-M. Jäger (IKP-1)

H. J. Jansen (IKP-TA)

M. Karnadi (IKP-2)

A. Kieven (IKP-4)

Ch. Krahe (IKP-TA)

M. Kremer (IKP-TA)

Th. Krings (IKP-TA)

G. Krol (IKP-4)

M. Küven (IKP-TA)

K.-G. Langenberg (IKP-4)

H. Metz-Nellen (IKP-TA)

S. Müller (IKP-TA)

R. Nellen (IKP-TA)

St. Nießen (IKP-TA)

H. Pütz (IKP-4)

G. Roes (IKP-TA)

N. Rotert (IKP-4)

D. Ruhrig (IKP-4)

T. Sagefka (IKP-4)

F. Scheiba (IKP-4)

H. Schiffer (IKP-TA)

J. Schmitz (IKP-4)

F. Schultheiß (IKP-TA)

H. Singer (IKP-4)

D. Spölgen (IKP-2)

G. Sterzenbach (IKP-1)

J. Strehl (IKP-TA)

J. Uehlemann (IKP-1)

P. Wieder (IKP-2)

J. Wimmer (IKP-1)

H. Zens (IKP-4)

IKP-1 = Experimental Hadron Structure
IKP-2 = Experimental Hadron Dynamics
IKP-3 = Theoretical Nuclear Physics
IKP-4 = Large-Scale Nuclear Physics Equipment
IKP-TA = Technical Services and Administration

K List of Authors